# Mathematical methods and terminology in geology 2020 : proceedings of reviewed papers / 3rd Croatian scientific congress [on] geomathematics and terminology in geology

**Edited book / Urednička knjiga**

*Publication status / Verzija rada:* **Published version / Objavljena verzija rada (izdavačev PDF)**

*Publication year / Godina izdavanja:* **2020**

*Permanent link / Trajna poveznica:* https://urn.nsk.hr/urn:nbn:hr:169:850350

*Rights / Prava:* Attribution 4.0 International/Imenovanje 4.0 međunarodna

*Download date / Datum preuzimanja:* **2024-11-29**

*Conference proceedings*

"Mathematical methods and terminology in geology 2020"

3rd Croatian scientific congress about geomathematics and terminology in geology

# Matematičke metode i nazivlje u geologiji 2020

III. hrvatski znanstveni skup iz geomatematike i nazivlja u geologiji
održan na Rudarsko-geološko-naftnom fakultetu
Sveučilišta u Zagrebu

10. listopada 2020. godine

Skup su priredili:

Rudarsko-geološko-naftni fakultet
Sveučilišta u Zagrebu

Geomatematički odsjek
Hrvatskoga geološkog društva

# Mathematical methods and terminology in geology 2020

3rd Croatian scientific congress from geomathematics and
terminology in geology
held on Faculty of Mining, Geology and Petroleum Engineering,
University of Zagreb

10th October 2020

Organised by:



Facuty of Mining, Geology and
Petroleum Engineering of the
University of Zagreb

Geomathematical Section
of the
Croatian Geological Society

Matematičke metode i nazivlje u geologiji 2020

# ZBORNIK RECENZIRANIH RADOVA

**IZDAVAČ:**



Sveučilište u Zagrebu



Rudarsko-geološko-naftni fakultet

Zagreb, 2020.

Mathematical methods and terminology in geology 2020

# PROCEEDINGS OF REVIEWED

# PAPERS

**PUBLISHER:**

University of Zagreb

## RGNF

Faculty of Mining, Geology and Petroleum Engineering

Zagreb, 2020

# SADRŽAJ / CONTENT

# Modal composition and morphometric characteristics of gravels in exploration field "Abesinija" (Otok Svibovski; SE from Zagreb, Croatia)

**Jasenka Sremac[1]; Josipa Velić[2]; Marija Bošnjak[3]; Ivo Velić[4]; Tomislav Malvić[2]; Daniel Fotović[5]; Renato Drempetić[6]**

[1] Faculty of Science, Department of Geology, University of Zagreb, 10000 Zagreb, Croatia; http://orcid.org/0000-0002-4736-7497
[2] Faculty of Mining, Geology and Petroleum Engineering, University of Zagreb, 10000 Zagreb, Croatia; http://orcid.org/0000-0002-5810-2187; http://orcid.org/0000-0003-2072-9539
[3] Croatian Natural History Museum, 10000 Zagreb, Croatia; http://orcid.org/0000-0002-1851-1031
[4] Croatian Summer School, Pančićeva 5, 10000 Zagreb, Croatia
[5] IGM šljunčara Trstenik d.o.o., 10370 Dugo Selo, Croatia
[6] 10000 Dalmatinska 12, 10000 Zagreb, Croatia

**Abstract**

Gravels exploited from the gravel pit in Trstenik area, in the Sava River floodplain SE from Zagreb, are variegated and of complex composition. All together 1399 clasts from the bulk (gross sample) and 606 from the fraction >32 mm were measured (x, y and z axes) and their lithology, shape and roundness were carefully studied. Numerical analyses were done through the Microsoft Excel program. The Zingg-shape analyses and flatness calculations were also applied. Gravels proved to be polymictic, composed of carbonate, clastic, igneous and metamorphic rocks. Size of measured clasts in bulk sample varies from 6.8 till 110.25 mm along the longest axis (x) and such value exhibits normal distribution. Carbonate, well rounded, disc-shaped clasts prevail. Sporadically, cross sections of red and green algae and macrofossils are visible on pebble surfaces, enabling the determination of stratigraphic age of some pebbles/source rocks. The second abundant group is composed of variegated sandstones, of red, green, grey, brown and yellow colour. Coarse-grained clastic rocks form less rounded clasts, similarly as green diabases. Angular quartz and chert clasts appear in all fractions, but they are more common among small-sized clasts. Modal composition, size and shape point to the important transport route from the Medvednica Mt., by combination of glacial, alluvial and lacustrine processes.

**Keywords**: gravels, lithology, morphometrics, Sava River, Croatia

## 1. Introduction

Polymictic gravels occur all along the River Sava Valley, attracting attention of several authors (e.g., **Marić et al., 1954**; **Crnković and Bušić, 1970**; **Šimunić and Basch, 1975**; **Velić and Saftić, 1996**; **Velić et al., 1999**; **Barudžija et al., 2020**, and references therein). They are exploited for various construction and industrial purposes. During this study, geological investigations were carried out at a gravel exploration field "Abesinija", between Otok Svibovski and Strugara (SE from Zagreb) (**Figure 1**), carried out by the Company IGM šljunčara Trstenik. Research area is presented on the Basic Geological Map, sheet L 33-81, Ivanić-Grad (**Basch, 1983 a,b**). The main goal of the research team was to recognize the lithotypes, morphometric characteristics and clast shape, in order to find out the possible source of gravel material and presume the most probable transport processes.

Jasenka Sremac
*jsremac@geol.pmf.hr*
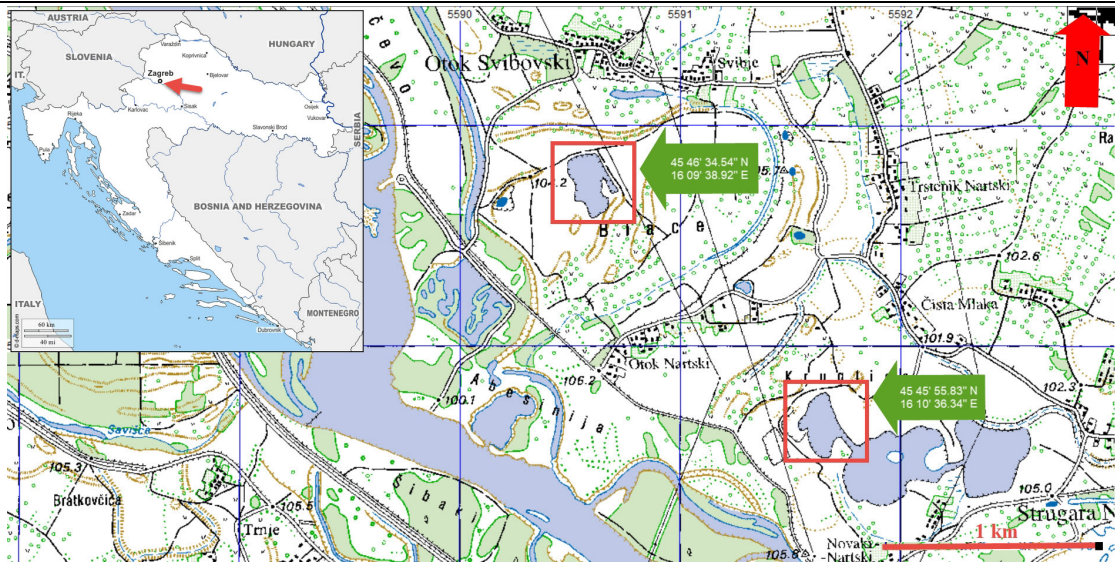
**Figure 1:** Geographic position of the research areas "Abesinija" (SE from Otok Svibovski) and "Trstenik" (ESE from Otok Nartski, marked by red rectangles (Map of Croatia from **d-maps.com**, assessed in August 2020)

## 2. Materials and methods

This study was performed on gravels from the gravel pit "Abesinija" by complex study methods, partly in the field and partly in laboratory and in cabinets.

### 2.1. Field work

Field work took place from March to July 2020 in gravel pit "Abesinija" (**Figures 1** and **2**). Fraction > 32 mm was collected at the position: 45°46'34.54"N; 16° 09'38.92. It was first sorted by colour (**Figure 3**), and then according to the lithology into limestones, sandstones, breccias/conglomerates, diabases, pyroclastics and quartz/chert grains. 22 subcategories were further distinguished by using field magnifier 10 x (**Figure 3; Table I**). All together 606 clasts were measured in the field by a digital caliper, taking care that at least 30 clasts of each category are measured (**Figure 3**).



**Figure 2:** Sampling and measuring in gravel pit "Abesinija" in March 2020

**Figure 3:** Bulk sample of gravels (a) and clast sorted into categories: (b) – carbonates; (c) – red sandstones; d) – green sandstones; (e) – quartz(ites) and cherts. Collected in gravel pit "Abesinija" in March 2020.

**Table I**: Initial classification of clast categories distinguished in the field

| FIELD MARK | LITHOLOGY |
|---|---|
| Z | GREEN, VARIOUS LITHOLOGIES |
| $Z_1$ | Fine-grained sandstone |
| $Z_2$ | Laminated micaceous sandstone |
| $Z_3$ | Dark green siltite |
| $Z_4$ | *Pietra verde* pyroclastite |
| $Z_5$ | Strongly laminated sandstone |
| $Z_6$ | Green microbreccia |
| $Z_7$ | Coarse-grained sandstones with diabase fragments |
| | RED TO BROWN, CLASTITES |
| $C_1$ | Coarse grained sandstone/microbreccia |
| $C_2$ | Vine-red sandstone |
| $C_3$ | Rusty sandstone |
| $C_4$ | Siltite |
| | GREYISH SANDSTONES |
| $P_1$ | Micaceous, laminated |
| $P_2$ | Coarse-grained |
| $P_3$ | Light grey, perforated |
| $P_4$ | Yellowish-grey |
| $P_5$ | Dark grey |
| | CARBONATES |
| $V_1$ | Grey limestone |
| $V_2$ | White dolostone |
| $V_3$ | Black calcarenite |
| BKG | BRECCIA, CONGLOMERATE |
| E | EFFUSIVE/DIABASE |
| Q | QUARTZ(ITE) |
| R | CHERT |
| O | OTHER/UNCLASSIFIED |

Gross gravelly material was collected at 45°46'31.74"N; 16°10'1.58"E and taken to the laboratory to be sorted and measured. Additional material for further study was collected at the nearby pit "Trstenik", at the position 44°45'55.83"N; 16°10'36.34"E (**Figure 1**).

## 2.2. Laboratory preparations and photography

Gross gravel sample weighing ca. 5 kilograms was taken to the laboratory. Pebbles/clasts (1399 in number) were separated into categories, clasts larger than 5 mm (371 clasts) counted and measured (longest: x, intermediate: y, shortest: z axes) by a digital caliper. Thin sections were prepared from pebbles of different lithologies in the Wet laboratory of the Department of Geology, Faculty of Science.

Field photographs and macrophotographs of pebbles were taken by a Cannon COOLPIX P900 V1.5 camera.

## 2.3. Numerical analyses

### 2.3.1. Excel sheets and graphics

All measured dimensions (axes x, y and z) were presented in Microsoft Excel sheets, enabling the graphic presentation of their relations in form of different diagrams. Relations between the axes are presented as pies and line-charts.

### 2.3.2. Zingg diagrams

To define a shape classification form, **Zingg (1935)** developed a classification scheme using the relation of the measures of the three orthogonal axes. We calculated relations between the shortest and intermediate axis (z/y or c/b) and the relation between the intermediate and the longest axis (y/x or b/a) for the Zingg diagram, and graphically defined the distribution of the four form pebbles categories for each lithotype and sublithotype: spheroids, discoids, rods and blades (**Table II**).

**Table II:** Pebble shape categories according to **Zingg (1935)**

| Category | b/a (=y/x) | c/b (=z/y) | Shape |
|----------|-----------|-----------|-------|
| I | > 2/3 | < 2/3 | disc |
| II | > 2/3 | > 2/3 | sphere |
| III | < 2/3 | < 2/3 | blade |
| IV | < 2/3 | > 2/3 | rod |

### 2.3.3. Granulometric analyses

Granulometric analyses were done for the purposes of regular material control for the Company IGM Šljunčara Trstenik in their own laboratory using sieve sizes set shown on **Figure 11**.

The grading of the aggregate was determined in accordance with the Croatian Standards Institute, document EN 933-1 (Tests for geometrical properties of aggregates — Part 1: Determination of particle size distribution — Sieving method).

### 2.3.4. Gaussian curves

Distribution of frequencies $(f_i)$ of most of the natural, technical and social categories can be represented by a continuous curve. Curve height is controlled by the concentration of data in each point. Curve *f(x)* appears in a typical bell-shaped form (**Figure 4**):
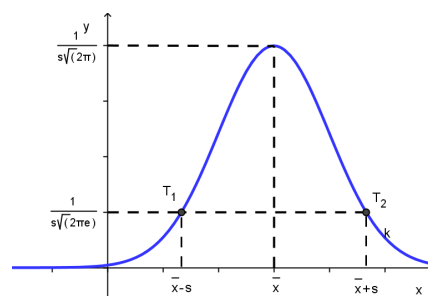


**Figure 4**: Theoretical bell-shaped Gaussian Curve representing normal distribution

Theoretical normal distribution represents a base of the applied statistics, especially parametric. In geology, the many phenomenon and belonging variables could be mostly described with Gaussian (normal) distribution (e.g., **Malvić and Medunić, 2015**)

*2.3.5. Flatness*

We calculated the flatness ratio of the pebbles to assume the original sedimentary environments of the pebbles. The flatness ratio is defined by Equation **(1)**:

$$F = (a + b)/2c \tag{1}$$

Where:
*F = flatness ratio;*
*a = the longest axis;*
*b = the intermediate axis and*
*c = the shortest axis.*

The flatness ratio for each lithotype was defined and compared to the possible environment origin according to the **Table III**.

**Table III:** Flatness in different sedimentary environments (after: **Cailleux, 1952** and **Müller, 1967**, from **Barudžija et al., 2020**)

| Depositional environment | Flatness |
|---|---|
| Potholes in river channels | 1.2 – 1.6 |
| Ground moraine | 1.6 – 1-8 |
| Fluvioglacial | 1.7 – 2.0 |
| Beach (marine) | 2.3 – 3.8 |
| Beach (lacustrine) | 2.3 – 4-4 |
| Frost river | 2.0 – 3.1 |
| Rivers in moderately warm climate | 2.5 – 3.5 |

# 3. Results

Results of analyses have shown the size span and size distribution of clasts, abundance of different lithologies, shape and sphericity through lithological classes. Lithological features and fossils in limestone pebbles indicate the age and the probable source of clasts.

## 3.1. Clast number and modal composition

Clasts number and size were studied from fractions larger than 32 mm and 16-32 mm for comparison, but clasts were particularly detailed measured and counted in a gross sample. Size and shape vary within various lithological categories (**Tables II** and **IV**). Clasts from the gross sample were taken to the laboratory and visually separated in a coarse- and fine-grained fraction. Clasts with x-axis smaller than 5 mm were divided into lithological categories and counted (**Table IV**). Coarse-grained pebbles, larger than 5 mm along the longest axis, were also sorted by lithology, and their dimensions (x, y, z) were measured by a digital caliper (**Tables V–VII**). The most abundant in both categories are calcareous pebbles, particularly white and grey micritic carbonate rocks (**Figure 3b; Table IV; Figure 5; Figure 6a,b**).

Coralgal and marly limestones appear in a small number of pebbles (**Tables IV** and **V, Figures 5** and **6c**). Among sandstones, green sandstone (**Figure 3d**) prevails in fine fraction, while red sandstone (**Figures 3c** and **6d**) is the most abundant in coarse fraction (**Table IV**). Silicate rocks (quartz grains, cherts) (**Figures 3e** and **6 h,i**) and volcanic diabases are far more abundant in a fine-grained fraction, than among larger clasts (**Table IV**), and they can be clearly recognized by their sharply-rectangular shape (**Figures 3e** and **6h**). Pyroclastites of *pietra verde* type can be easily recognized for their bluish-green colour, but they are rather scarce (**Table IV**). Quite a large number of small clasts remained unclassified (**Tables II** and **IV**).

**Table IV:** Number of clasts of different lithologies in bulk sample

| ROUNDNESS | LITHOLOGY | FIELD MARK | LITHOL. CATEGORY | BULKSAMPLE-COARSE FRACTION CLAST NUMBER | | BULK SAMPLE-FINE FRACTION CLAST NUMBER | |
|---|---|---|---|---|---|---|---|
| ANGULAR | QUARTZITE | Q | SILICATE ROCKS | 28 | 44 | 93 | 124 |
| | CHERT | R | | 16 | | 31 | |
| | DIABASE | E | VOLCANICS | 15 | 19 | 144 | 147 |
| ROUNDED | PYROCLASTIC | Z 4 | | 4 | | 3 | |
| | GREEN SANDSTONE/SILTITE | Z 1, Z 2, Z 3, Z 5 Z6, Z7 | SANDSTONES/SILTITES | 34 | 76 | 44 | 124 |
| | RED SANDSTONE/SILTITE | C 1, C 2, C 4 | | 12 | | 57 | |
| | BROWN SANDSTONE | C 3 | | 7 | | 2 | |
| | YELLOW SANDSTONE | P 4 | | 15 | | 21 | |
| | GREY SANDSTONE | P 1, P 2, P 3, P 5 | | 8 | | 0 | |
| | CORALGAL BIOCLASTIC LIMESTONE | | CARBONATES | 12 | 173 | 28 | 309 |
| | WHITE MICRITIC LIMESTONE | V 2 | | 75 | | 181 | |
| | GREY MICRITIC LIMESTONE | V 1 | | 52 | | 66 | |
| | DARK-GREY CALCARENITE | V 3 | | 28 | | 34 | |
| | MARLY LIMESTONE | | | 6 | | 0 | |
| INTERMEDIATE | BRECCIA/CONGLOMERATE | BKG | OTHER | 12 | 67 | 316 | 316 |
| | UNCLASSIFIED / OTHER | O | | 55 | | | |
| | | | | 379 | 379 | 1020 | 1020 |

BULK SAMPLE, CLASTS >5 MM



BULK SAMPLE, CLASTS <5 MM
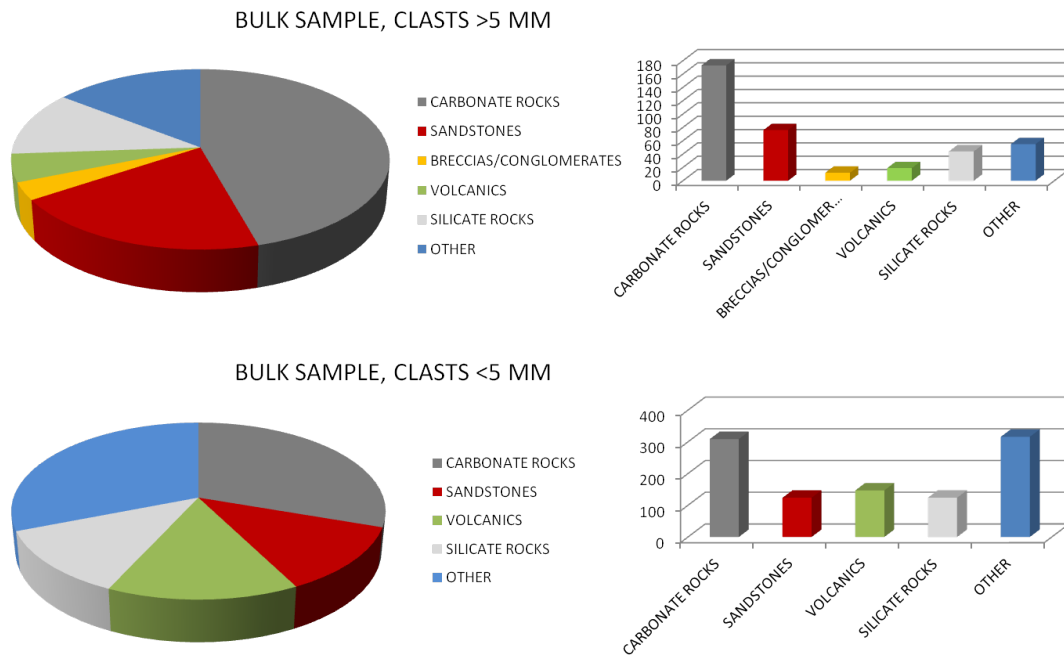


**Figure 5:** Modal composition and distribution of main clast groups from a bulk sample collected in gravel pit "Abesinija" in March 2020, divided in two size groups (larger and smaller than 5 mm) and presented as pies and histograms (Microsoft Excel Program)
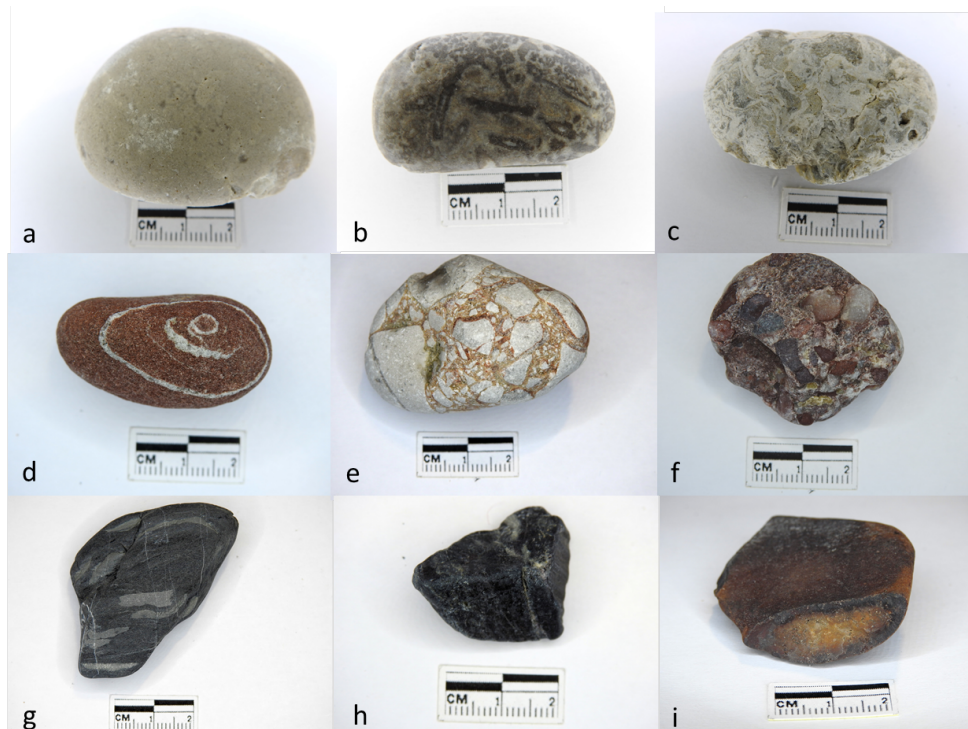


**Figure 6:** Common types of pebbles from "Abesinija" Gravel Pit: (a) – white micritic limestone; (b) – grey micritic limestone with dasyclad algae; (c) –bioclastic limestone with coralline algae; (d) – red laminated sandstone; (e) – carbonate breccias; (f) – polymictic conglomerate; (g) – bioturbated grey sandstone; (h) – black chert; (i) – chert nodule

## 3.2. Clast size, shape and distribution

Carbonate clasts are the most common both in gross sample and in fraction larger than 16 mm (**Tables IV** and **V**). Their size is variable, and, among the measured clasts, varies between 6.8 and 62.1 mm along the longest (x) axis.

**Table V:** Dimensions of measured carbonate pebbles from the bulk sample

| WHITE CARBONATES | | |
|---|---|---|
| x | y | z |
| 10,0 | 7.9 | 5.1 |
| 12.5 | 13.9 | 8.2 |
| 14.0 | 9.0 | 6.3 |
| 15.0 | 10.6 | 5.2 |
| 15.0 | 12.9 | 9.0 |
| 15.1 | 14.1 | 7.1 |
| 15.5 | 11.5 | 5.5 |
| 15.6 | 12.7 | 6.9 |
| 15.8 | 13.9 | 6.9 |
| 16.1 | 11.9 | 7.3 |
| 16.7 | 14.1 | 11.0 |
| 17.0 | 13.6 | 10.2 |
| 17.2 | 15.9 | 7.8 |
| 17.3 | 9.5 | 5.9 |
| 17.9 | 13.6 | 9.8 |
| 17.9 | 15.8 | 10.1 |
| 18.0 | 11.1 | 6.4 |
| 18.2 | 17.9 | 16.5 |
| 18.3 | 14.3 | 12.9 |
| 19.3 | 16.0 | 12.5 |
| 19.5 | 16.2 | 10.4 |
| 19.9 | 14.3 | 6.9 |
| 20.2 | 15.2 | 14.1 |
| 21.3 | 15.1 | 11.3 |
| 21.5 | 14.9 | 11.0 |
| 21.6 | 11.4 | 9.5 |
| 22.5 | 15.5 | 13.5 |
| 22.6 | 15.0 | 8.6 |
| 22.6 | 18.2 | 9.7 |
| 22.8 | 19.1 | 17.3 |
| 22.9 | 14.2 | 12.2 |
| 22.9 | 18.5 | 6.5 |
| 23.0 | 15.2 | 9.0 |
| 23.2 | 9.5 | 8.5 |
| 23.5 | 20.0 | 11.6 |
| 24.2 | 14.9 | 10.1 |
| 25.2 | 17.2 | 10.5 |
| 25.8 | 15.9 | 11.8 |
| 26.1 | 20.4 | 12.8 |
| 26.1 | 22.5 | 12.0 |
| 27.0 | 19.1 | 7.5 |
| 27.0 | 19.3 | 13.4 |
| 27.4 | 18.2 | 17.9 |
| 27.6 | 17.3 | 17.0 |
| 28.1 | 24.5 | 13.6 |
| 28.3 | 22.9 | 13.5 |
| 28.4 | 18.7 | 12.9 |
| 29.4 | 28.3 | 10.2 |
| 31.1 | 20.2 | 8.7 |
|  |  |  |
| 31.1 | 22.8 | 14.2 |
| 33.3 | 22.4 | 12.6 |
| 33.5 | 22.2 | 13.5 |
| 34.1 | 25.0 | 11.7 |

| GREY CARBONATES | | |
|---|---|---|
| x | y | z |
| 12.2 | 11.0 | 6.5 |
| 12.4 | 11.2 | 8.5 |
| 14.7 | 10.2 | 4.1 |
| 15.0 | 8.5 | 4.1 |
| 16.5 | 12.7 | 7.1 |
| 18.0 | 11.9 | 9.2 |
| 18.4 | 12.0 | 7.8 |
| 18.7 | 16.3 | 7.6 |
| 19.1 | 17.2 | 13.1 |
| 19.2 | 15.7 | 9.4 |
| 19.4 | 17.1 | 6.0 |
| 19.6 | 20.4 | 7.7 |
| 19.9 | 15.4 | 10.2 |
| 20.0 | 13.3 | 4.4 |
| 20.1 | 11.8 | 6.4 |
| 21.5 | 16.4 | 13.4 |
| 23.2 | 17.2 | 12.1 |
| 23.2 | 18.5 | 11.5 |
| 23.2 | 19.9 | 8.8 |
| 24.2 | 21.2 | 12.4 |
| 24.3 | 18.1 | 10.2 |
| 25.5 | 21.8 | 15.5 |
| 25.8 | 22.1 | 9.7 |
| 26.1 | 23.8 | 16.6 |
| 26.6 | 17.6 | 8.4 |
| 27.2 | 15.2 | 15.1 |
| 27.3 | 23.0 | 12.2 |
| 28.2 | 18.8 | 9.4 |
| 28.8 | 20.4 | 11.5 |
| 29.3 | 26.3 | 15.2 |
| 30.2 | 18.7 | 11.8 |
| 30.4 | 25.3 | 18.6 |
| 30.5 | 15.6 | 9.7 |
| 31.2 | 31.0 | 11.5 |
| 32.0 | 27.5 | 11.6 |
| 32.4 | 26.7 | 11.5 |
| 35.3 | 21.6 | 15.1 |
| 36.6 | 28.7 | 18.7 |
| 37.7 | 31.2 | 12.4 |
| 38.1 | 26.6 | 18.3 |
| 40.0 | 27.3 | 19.1 |
| 40.7 | 22.2 | 17.5 |
| 41.4 | 26.3 | 20.0 |

| BLACK CALCARENITES | | |
|---|---|---|
| x | y | z |
| 15.4 | 13.0 | 10.0 |
| 17.5 | 16.3 | 10.9 |
| 17.7 | 12.0 | 7.3 |
| 18.3 | 14.0 | 8.6 |
| 18.6 | 14.8 | 7.8 |
| 20.1 | 11.2 | 9.6 |
| 21.7 | 21.5 | 11.0 |
| 23.2 | 23.2 | 17.4 |
| 23.4 | 18.0 | 7.6 |
| 24.5 | 17.3 | 5.7 |
| 25.3 | 20.9 | 11.1 |
| 27.2 | 16.6 | 14.2 |
| 28.4 | 18.8 | 11.5 |
| 28.4 | 22.0 | 10.2 |
| 31.9 | 20.4 | 20.1 |
| 32.2 | 25.0 | 9.4 |
| 32.3 | 16.4 | 15.5 |
| 32.5 | 26.7 | 20.3 |
| 33.8 | 22.7 | 11.5 |
| 35.4 | 15.0 | 9.3 |
| 36.5 | 25.2 | 18.0 |
| 38.2 | 27.8 | 19.1 |
| 38.4 | 18.4 | 11.3 |
| 41.5 | 31.8 | 17.4 |
| 41.5 | 33.7 | 12.4 |
| 43.1 | 33.1 | 27.5 |
| 46.4 | 33.5 | 19.5 |
| 50.3 | 33.7 | 27.4 |

| MARLY LIMESTONES | | |
|---|---|---|
| x | y | z |
| 15.2 | 12.2 | 8.1 |
| 19.7 | 9.4 | 9.2 |
| 25.8 | 16.3 | 13.3 |
| 27.8 | 25.3 | 7.4 |
| 35.1 | 15.3 | 12.8 |
| 38.1 | 20.6 | 12.1 |
| 38.2 | 29.2 | 23.1 |
| 46.3 | 27.7 | 19.2 |

| BIOCALCARENITES | | |
|---|---|---|
| x | y | z |
| 6.8 | 5.0 | 3.5 |
| 11.2 | 8.9 | 4.9 |
| 15.0 | 11.5 | 4.7 |
| 23.8 | 11.5 | 9.6 |
| 25.4 | 17.0 | 16.0 |
| 43.5 | 24.8 | 20.0 |

| OTHER CARBONATES | | |
|---|---|---|
| x | y | z |
| 41.4 | 37.9 | 23.2 |
| 47.3 | 34.2 | 26.5 |

| | | |
|---|---|---|
| 34.3 | 33.7 | 14.2 |
| 34.8 | 16.2 | 13.5 |
| 36.8 | 24.4 | 17.4 |
| 36.8 | 25.5 | 12.3 |
| 36.9 | 34.3 | 8.3 |
| 37.4 | 32.7 | 12.5 |
| 38.5 | 33.6 | 12.5 |
| 40.5 | 36.2 | 15.3 |
| 41.6 | 25.5 | 20.7 |
| 42.4 | 33.5 | 16.4 |
| 42.9 | 30.0 | 14.8 |
| 44.3 | 30.7 | 20.4 |
| 44.5 | 28.2 | 20.6 |
| 62.1 | 30.4 | 21.7 |

| | | |
|---|---|---|
| 51.3 | 26.2 | 20.8 |

Relationship between the measured x, y and z axes of carbonate clasts from the bulk gravel sample are presented on **Figure 7**.
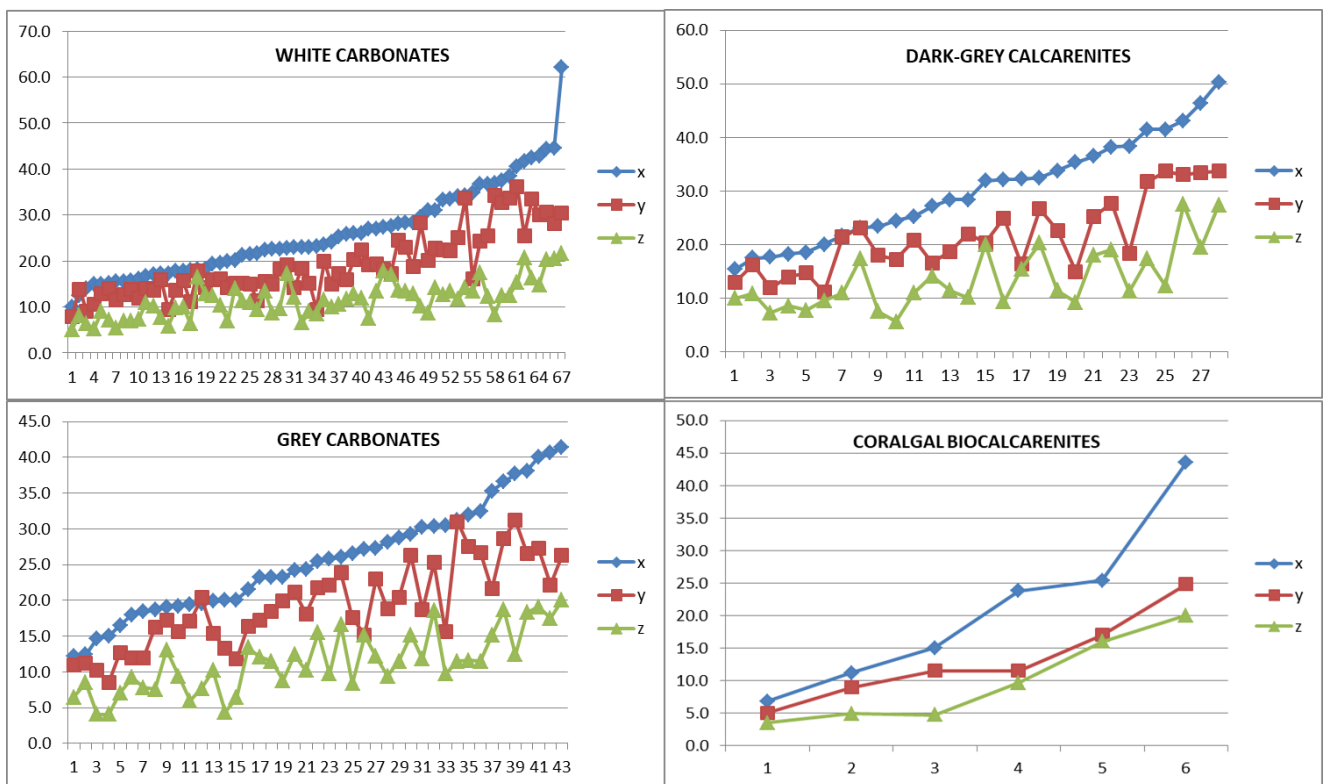


**Figure 7:** Size distribution of different types of carbonate pebbles obtained from the Microsoft Excel Programme

Sandstone pebbles are clearly visible in the field, very common in bulk and fractionated gravels (**Figure 3a**), and often present in striking colours. Green and red sandstones are equally abundant (**Tables IV** and **V**), while grey (**Figure 6g**) and brown sandstone clasts occur in small numbers (**Tables IV** and **V**). Lamination occurs in all sandstone categories (**Table I, Figures 6 d,g**).

**Table VI:** Dimensions of measured sandstone pebbles from the bulk gravel sample

| GREEN SANDSTONES | | | RED SANDSTONES | | | YELLOW SANDSTONES | | | GREY SANDSTONES | | |
|---|---|---|---|---|---|---|---|---|---|---|---|
| x | y | z | x | y | z | x | y | z | x | y | z |
| 12.8 | 8.4 | 6.0 | 9.0 | 5.2 | 3.0 | 15.5 | 12.5 | 8.6 | 8.2 | 4.2 | 4.0 |
| 16.0 | 12.9 | 11.0 | 12.5 | 8.4 | 6.5 | 16.6 | 15.2 | 4.2 | 15.5 | 11.9 | 6.5 |
| 16.5 | 13.3 | 8.9 | 26.5 | 12.2 | 11.7 | 17.4 | 14.0 | 12.0 | 17.4 | 11.0 | 7.9 |
| 17.9 | 15.5 | 5.8 | 27.2 | 22.9 | 9.1 | 18.9 | 13.1 | 9.5 | 21.6 | 14.2 | 7.9 |
| 18.5 | 10.9 | 8.9 | 27.3 | 20.9 | 15.5 | 20.2 | 14.7 | 17.9 | 22.5 | 17.4 | 13.5 |

| | | | | | | | | | | | | |
|---|---|---|---|---|---|---|---|---|---|---|---|---|
| 19.6 | 12.2 | 4.1 | | 27.5 | 17.9 | 8.0 | | 20.5 | 17.1 | 7.2 | | 25.1 | 13.3 | 8.0 |

Green sandstones:

| | | |
|---|---|---|
| 19.6 | 12.2 | 4.1 |
| 20.0 | 15.9 | 13.6 |
| 21.4 | 19.1 | 6.3 |
| 22.6 | 14.6 | 10.1 |
| 23.4 | 16.5 | 7.4 |
| 25.0 | 17.4 | 14.1 |
| 25.6 | 13.5 | 9.1 |
| 25.8 | 15.8 | 9.9 |
| 26.5 | 14.2 | 12.0 |
| 27.9 | 18.6 | 11.9 |
| 27.9 | 23.5 | 12.9 |
| 29.0 | 23.5 | 8.3 |
| 30.0 | 24.8 | 17.2 |
| 30.5 | 17.5 | 13.5 |
| 30.6 | 26.4 | 13.3 |
| 30.8 | 21.3 | 10.0 |
| 36.8 | 23.1 | 16.0 |
| 36.8 | 25.7 | 14.9 |
| 37.2 | 32.6 | 19.0 |
| 40.8 | 15.0 | 14.9 |
| 41.2 | 24.5 | 16.9 |

| | | |
|---|---|---|
| 27.5 | 17.9 | 8.0 |
| 29.0 | 20.5 | 11.2 |
| 29.2 | 20.9 | 18.0 |
| 29.4 | 20.6 | 18.4 |
| 30.0 | 28.8 | 14.0 |
| 36.6 | 31.2 | 18.8 |
| 38.5 | 20.5 | 10.2 |
| 42.3 | 23.7 | 12.7 |
| 43.1 | 21.4 | 13.5 |
| 45.5 | 23.0 | 15.5 |
| 46.0 | 24.1 | 14.6 |

RED COARSE SANDSTONES

| x | y | z |
|---|---|---|
| 18.1 | 12.8 | 11.0 |
| 19.4 | 14.8 | 10.0 |
| 22.5 | 14.1 | 12.4 |
| 26.5 | 12.3 | 11.9 |
| 28.9 | 22.5 | 18.4 |
| 32.4 | 25.6 | 25.3 |
| 39.0 | 19.5 | 10.6 |
| 50.1 | 35.5 | 24.8 |

| | | |
|---|---|---|
| 20.5 | 17.1 | 7.2 |
| 21.5 | 15.9 | 5.5 |
| 22.8 | 16.5 | 9.4 |
| 28.9 | 19.1 | 14.1 |
| 29.5 | 24.0 | 13.5 |
| 31.3 | 22.8 | 16.4 |
| 32.5 | 16.2 | 6.9 |
| 50.8 | 25.1 | 10.0 |

BROWN SANDSTONES

| x | y | z |
|---|---|---|
| 25.5 | 21,2 | 12.4 |
| 31.9 | 24.4 | 18.8 |
| 32.1 | 22.1 | 20.5 |
| 33.2 | 24.0 | 16.2 |
| 33.2 | 26.4 | 16.4 |
| 45.8 | 30.7 | 15.8 |

| | | |
|---|---|---|
| 25.1 | 13.3 | 8.0 |
| 47.5 | 28.9 | 13.1 |
| 53.0 | 35.5 | 21.2 |

Relationships between the measured x, y and z axes of sandstone clasts from the bulk gravel sample are presented on **Figure 8**. They are rather homogenized in yellow and brown sandstones (**Figure 8**), although they are represented by rather small numbers (**Table VI**). Green micaceous sandstones are of variable shape and red micaceous sandstones present a different pattern (**Figure 8**). Medium-sized clasts seem to be unified, while larger clasts show somewhat different pattern (**Figure 8**).
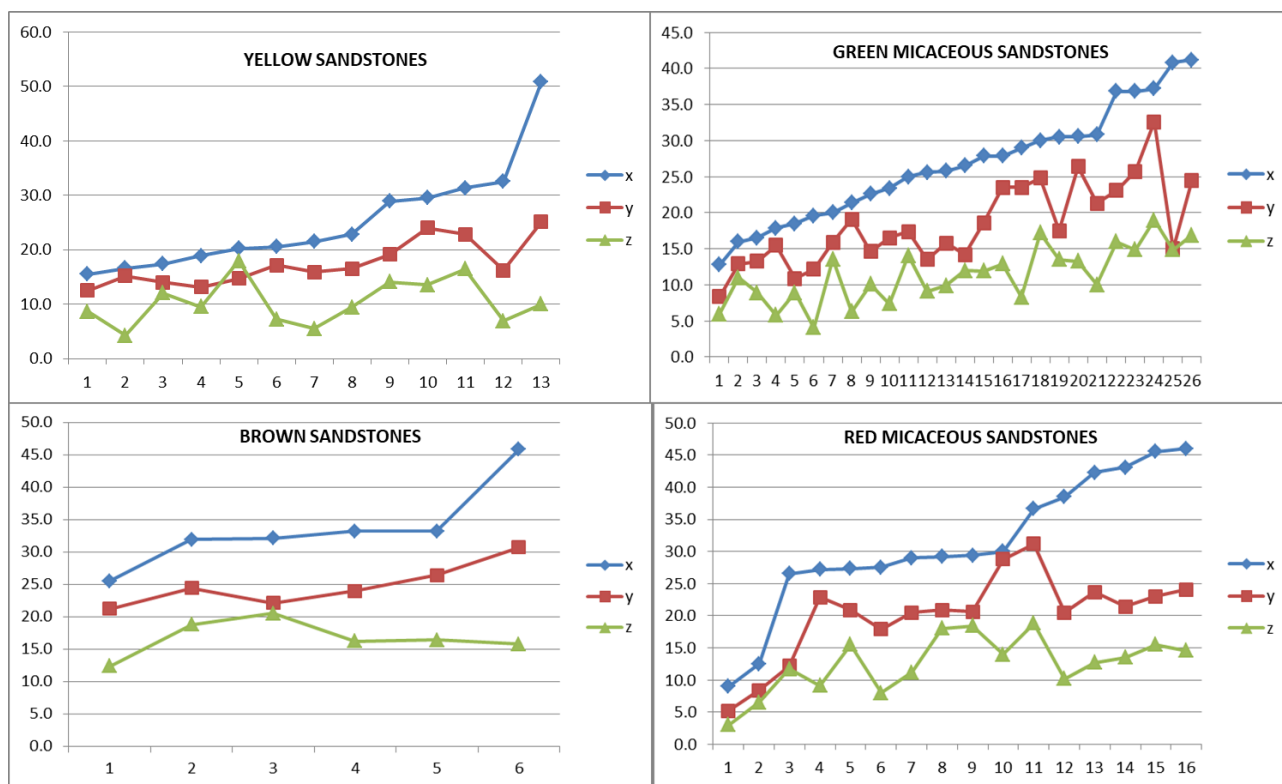


**Figure 8:** Size distribution of sandstones obtained from the Microsoft Excel Programme

**Table VII:** Dimensions of measured other pebbles from the bulk gravel sample

| QUARTZ(ITE) | | |
|---|---|---|
| **x** | **y** | **z** |
| 9.8 | 6.6 | 4.5 |
| 11.5 | 8.0 | 7.5 |
| 12.8 | 11.2 | 6.2 |
| 13.5 | 8.6 | 8.5 |
| 14.0 | 9.5 | 7.1 |
| 15.0 | 12.0 | 8.5 |
| 15.0 | 12.0 | 10.0 |
| 15.3 | 8.3 | 8.2 |
| 15.9 | 8.5 | 5.5 |
| 16.1 | 11.4 | 8.0 |
| 16.1 | 11.5 | 10.1 |
| 16.4 | 11.4 | 10.6 |
| 16.5 | 12.9 | 6.2 |
| 18.2 | 13.4 | 11.8 |
| 18.4 | 13.9 | 12.4 |
| 18.5 | 13.9 | 9.3 |
| 19.6 | 10.3 | 9.9 |
| 19.6 | 13.8 | 11.9 |
| 21.3 | 18.3 | 9.0 |
| 21.9 | 17.2 | 15.1 |
| 22.4 | 15.4 | 15.2 |
| 23.2 | 19.3 | 18.0 |
| 24.2 | 16.7 | 10.0 |
| 24.5 | 22.5 | 12.0 |
| 25.5 | 19.3 | 11.3 |
| 26.5 | 16.9 | 15.5 |
| 27.5 | 20.5 | 18.2 |
| 30.5 | 21.5 | 16.3 |
| 31.0 | 19.9 | 17.3 |
| 32.3 | 31.7 | 15.5 |
| 33.4 | 17.8 | 11.0 |
| 34.8 | 23.1 | 16.5 |
| 39.8 | 15.0 | 9.8 |

| CHERT | | |
|---|---|---|
| **x** | **y** | **z** |
| 14.4 | 10.2 | 7.0 |
| 15.0 | 14.0 | 8.2 |
| 18.0 | 12.0 | 7.3 |
| 18.7 | 14.5 | 8.4 |
| 20.2 | 12.5 | 6.8 |
| 20.5 | 14.0 | 7.5 |
| 20.7 | 17.9 | 10.5 |
| 22.9 | 14.7 | 13.5 |
| 24.5 | 12.0 | 10.4 |
| 25.0 | 14.1 | 10.5 |
| 25.0 | 15.0 | 11.5 |
| 25.0 | 20.2 | 17.7 |
| 25.7 | 12.2 | 9.6 |
| 29.8 | 20.1 | 12.8 |

| EFFUSIVES | | |
|---|---|---|
| **x** | **y** | **z** |
| 12.2 | 10.5 | 7.2 |
| 19.3 | 13.6 | 10.0 |
| 21.3 | 14.7 | 14.5 |
| 29.2 | 28.4 | 15.1 |
| 35.8 | 33.9 | 13.8 |
| 53.8 | 43.2 | 16.8 |
| 61.1 | 38.3 | 13.8 |

Breccias and conglomerates occur in small numbers, but they can be easily spotted for their colourful appearance, both in breccias with reddish matrix (e.g., **Figure 6e**), or polymodal conglomerates with clasts of different colours (e.g., **Figure 6f**). Their shape and roundness depend on the hardness, structure and texture of clasts (**Figure 9**).

Quartz(ite), chert and diabase clasts differ from carbonate and sandstone pebbles in size (they are generally smaller) and angular shape (**Figures 3e** and **6h**). They are more common in finer, than in coarser fractions (**Table IV**). Their size distribution is presented on **Figure 9**. Quartz grains are white in colour, while quartzites and cherts display different colours, usually brownish to black. Some chert grains are angular (e.g., **Figure 6h**), while others, lense-shaped, represent nodules extracted from sedimentary rocks (e.g., **Figure 6i**). The **Figure 10** clearly showed that Gaussian distribution can be obtained for number of samples data measured for all three analysed axes (x, y, z, **Figure 10a-c**). Also, if the samples are grouped according the length of the x axis, the same curve could be approximated over the histogram with classes wide 6.3 mm (automatically selected by software algorithm).

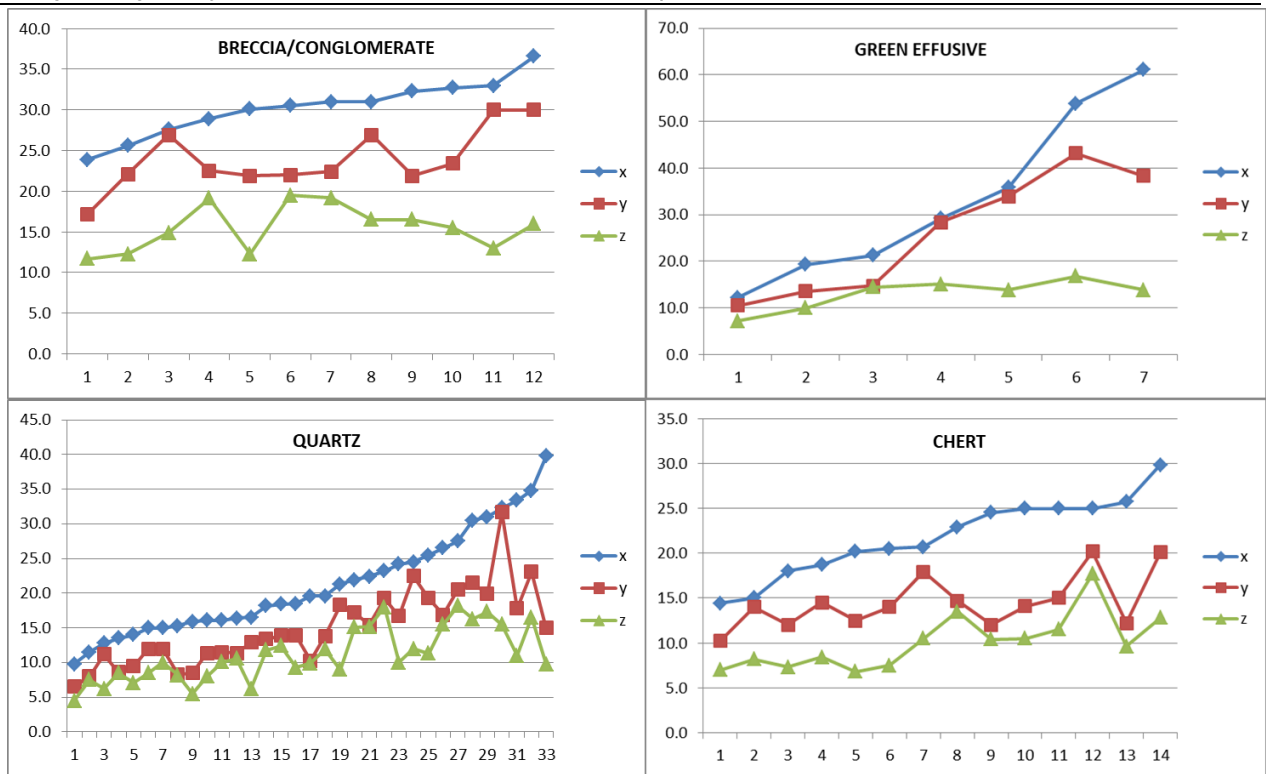**Figure 9:** Size distribution of coarse-grained clastites, diabases, quartz and chert grains obtained from the Microsoft Excel Programme
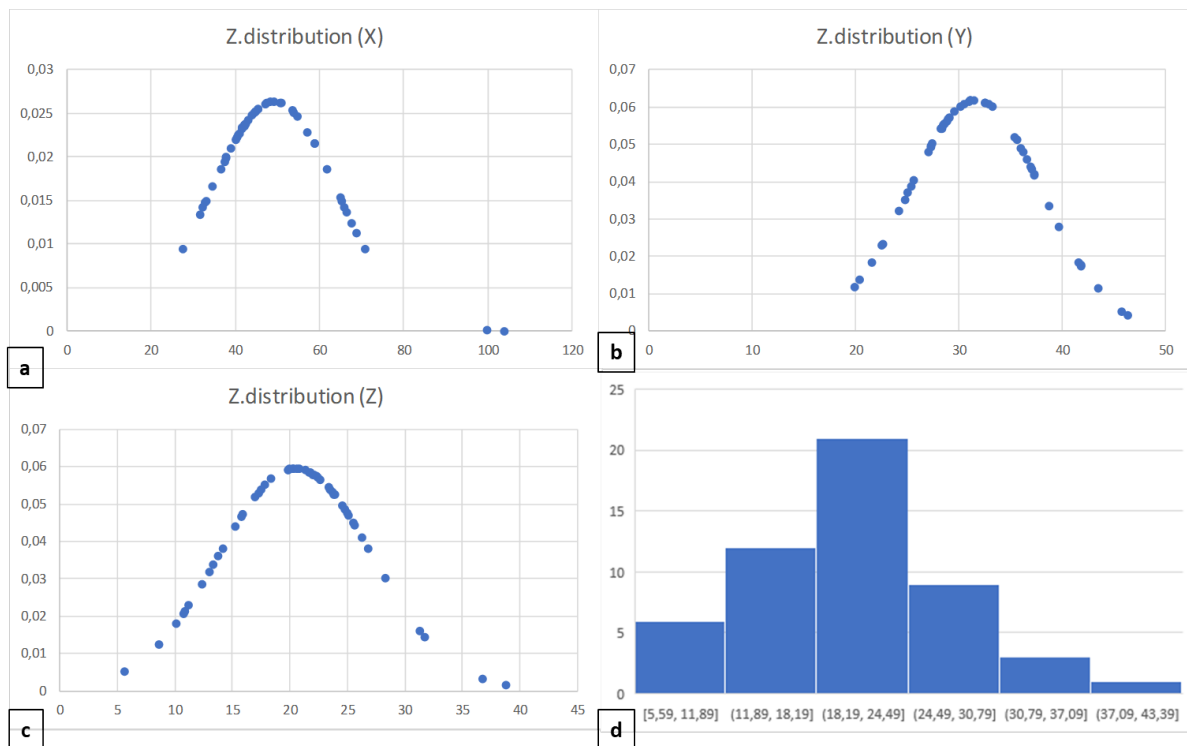


**Figure 10:** Normal distribution of size of bulk pebbles (x, y and z axes) in a Gaussian curve and histogram

**CUMMULATIVE PASSAGE OF CLASTS THROUGH THE SIEVE, 1ST LAYER**

| SIEVE (mm) | 0,063 | 1 | 2 | 4 | 5,6 | 8 | 11,2 | 16 | 22,4 | 31,5 | 45 | 63 | 90 |
|---|---|---|---|---|---|---|---|---|---|---|---|---|---|
| PASSAGE (%) | 0,80 | 17 | 20 | 26 | 34 | 46 | 60 | 75 | 87 | 94 | 98 | 100 | 100 |



**CUMMULATIVE PASSAGE OF CLASTS THROUGH THE SIEVE, 2ND LAYER**

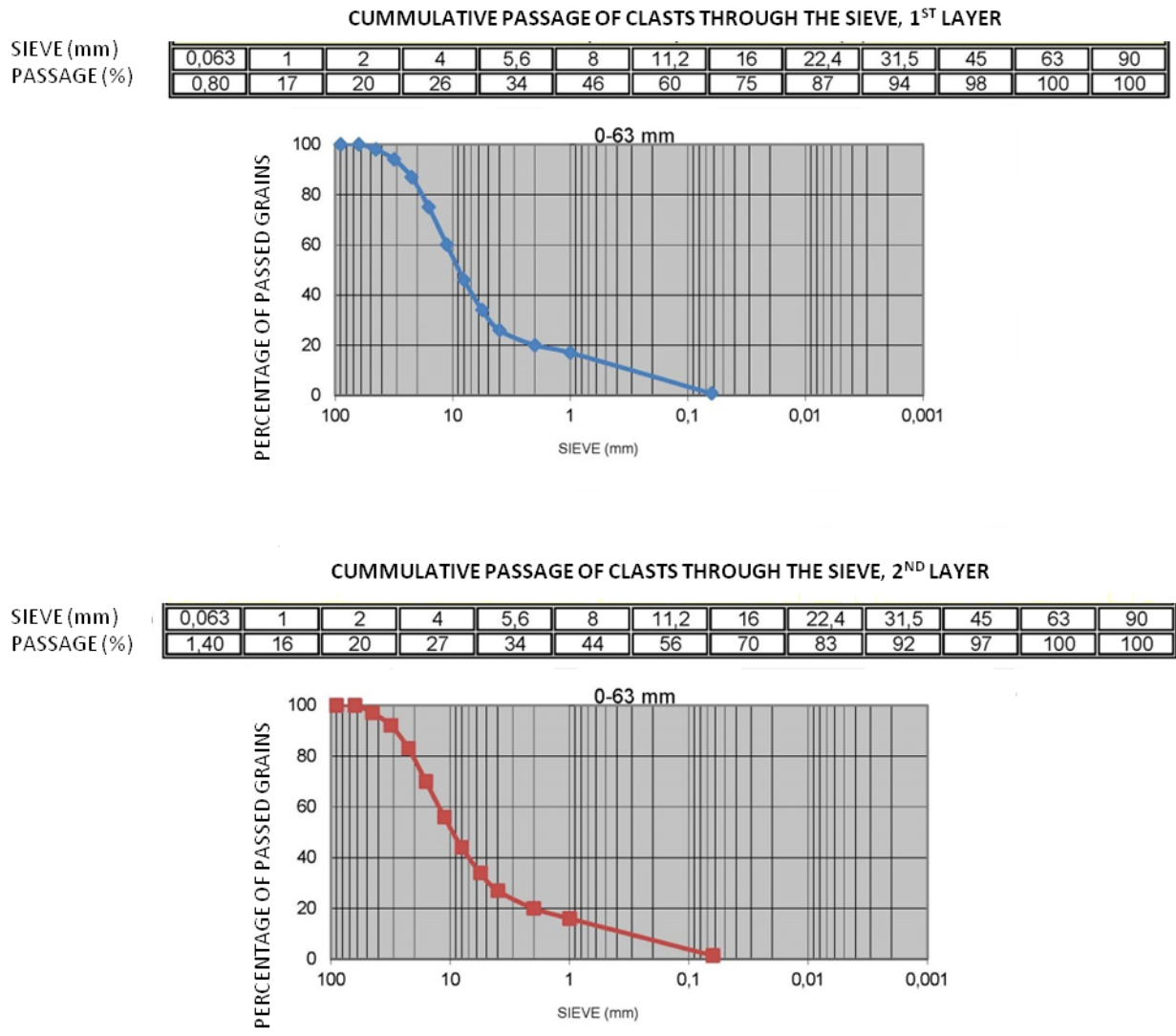| SIEVE (mm) | 0,063 | 1 | 2 | 4 | 5,6 | 8 | 11,2 | 16 | 22,4 | 31,5 | 45 | 63 | 90 |
|---|---|---|---|---|---|---|---|---|---|---|---|---|---|
| PASSAGE (%) | 1,40 | 16 | 20 | 27 | 34 | 44 | 56 | 70 | 83 | 92 | 97 | 100 | 100 |



**Figure 11:** Results of granulometric analyses of pebbles from younger (1st layer, Trstenik) and older (2nd layer, Abesinija) stratigraphic horizons (February, 2020)

Granulometric analyses, done in IGM Šljuncara Trstenik laboratory for the purposes of regular material control of gravels, gave us insight into slight differences between the younger 1st layer, 5-10 m thick (exploited in "Trstenik" pit, **Figure 1**, **Figure 11**, blue curve) and older, 2nd layer, >20 m thick which is now under exploitation in the "Abesinija" Pit (**Figure 1, Figure 11**, red curve). Gravel layers are separated by a 2.5-4.5 m thick argillaceous-peat coal layer. Curves support the normal distribution, as seen in **Figure 10**, with minor deviation in the finest fraction of the younger, 1st horizon (**Figure 11**, blue curve). Comparison between the two layers is in our plan for further research.

Shape analyses of fractioned and bulk gravel sample were done in order to recognize the shape characteristic for different types of clasts, and, if possible presume the modes of their transport, according to **Zingg (1935)**. Results are presented in form of diagrams (**Figures 12, 13, 15, 16, 18** and **20**), while the comparison of Zingg data for pebbles from bulk and fractioned gravels (fraction > 32 mm) are shown on **Figures 17, 19** and **21**. Among the most common white and grey limestones, discoidal pebbles prevail both in bulk and fractioned gravels (**Figures 12, 13** and **14**). Distribution of blade and rod shapes seems similar, with slight differences in percentage of rod-shaped clasts. The most pronounced difference is in percentage of spheroidal clasts, which occur in much larger numbers in the bulk gravel sample (**Figure 14b**).
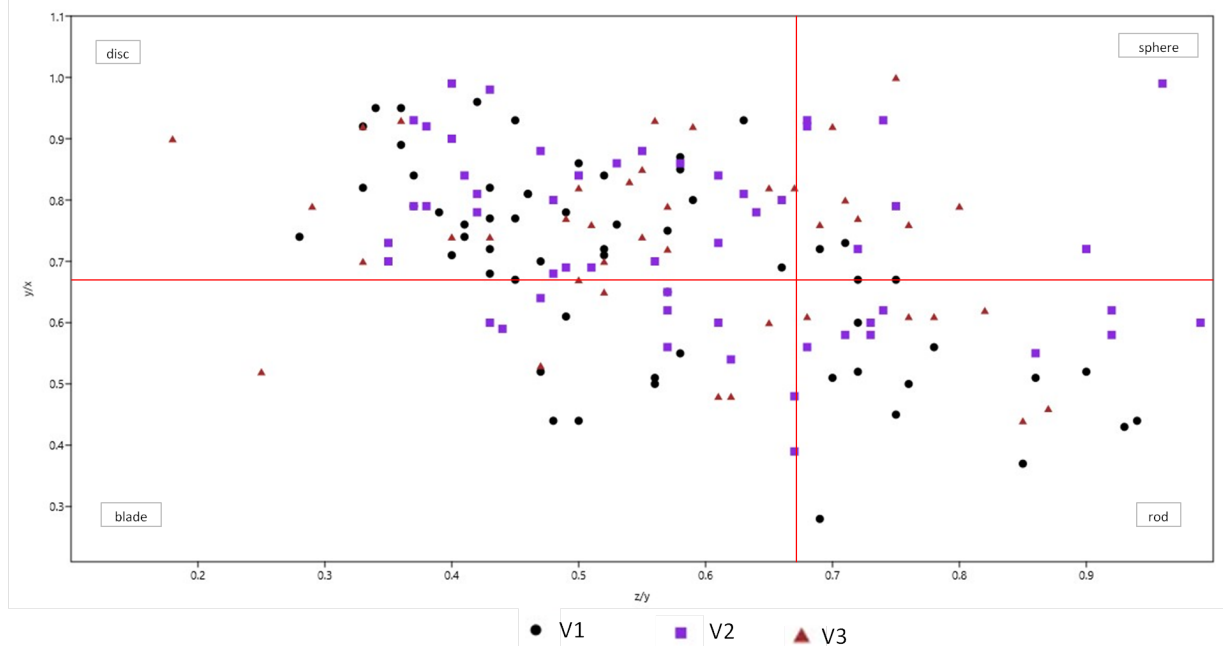
**Figure 12:** Zingg's diagrams for 146 measured carbonate pebbles from the gravel fraction > 32 mm: (a) the most common carbonate pebbles (white and grey micritic carbonates, black calcarenites). V1 – grey limestone; v2 – white limestone; v3 – black calcarenite.
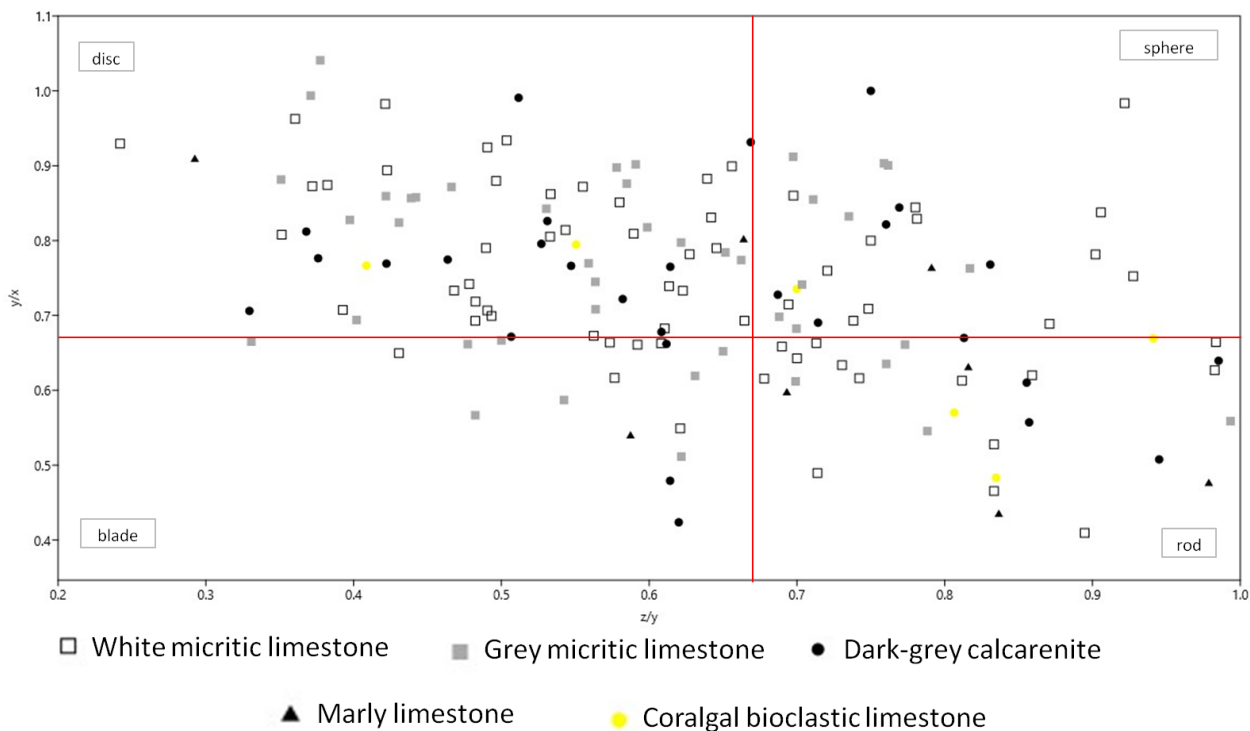


**Figure 13:** Zingg's diagram for carbonate pebbles from the bulk gravel sample, with *x*-axis larger than 5 mm
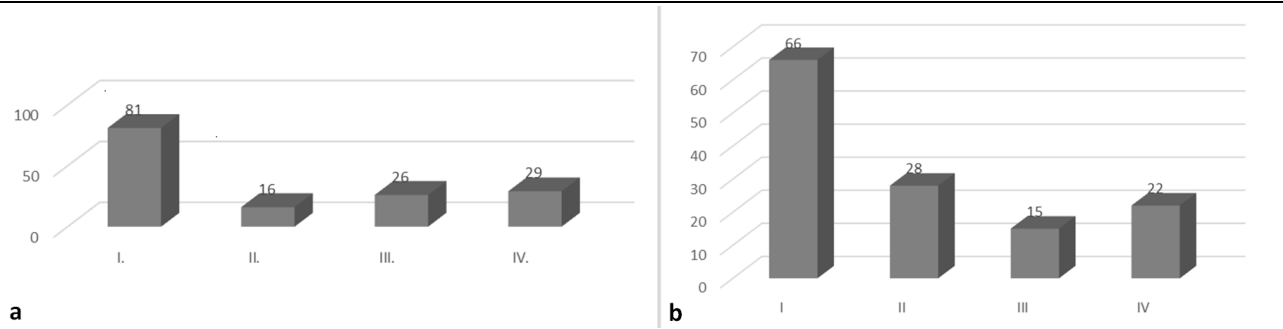
**Figure 14:** Comparison of Zingg's data for the most abundant carbonate pebbles (v1, v2, v3) from the: (a) fraction >32 mm and (b) bulk sample, without pebbles with 0.67 ratio. Categories: I. disc; II. sphere; III. blade; IV. rod.

Study of sandstone pebbles shows a variety of results, again with slight domination of discoidal pebbles in bulk sample (**Figure 15**).
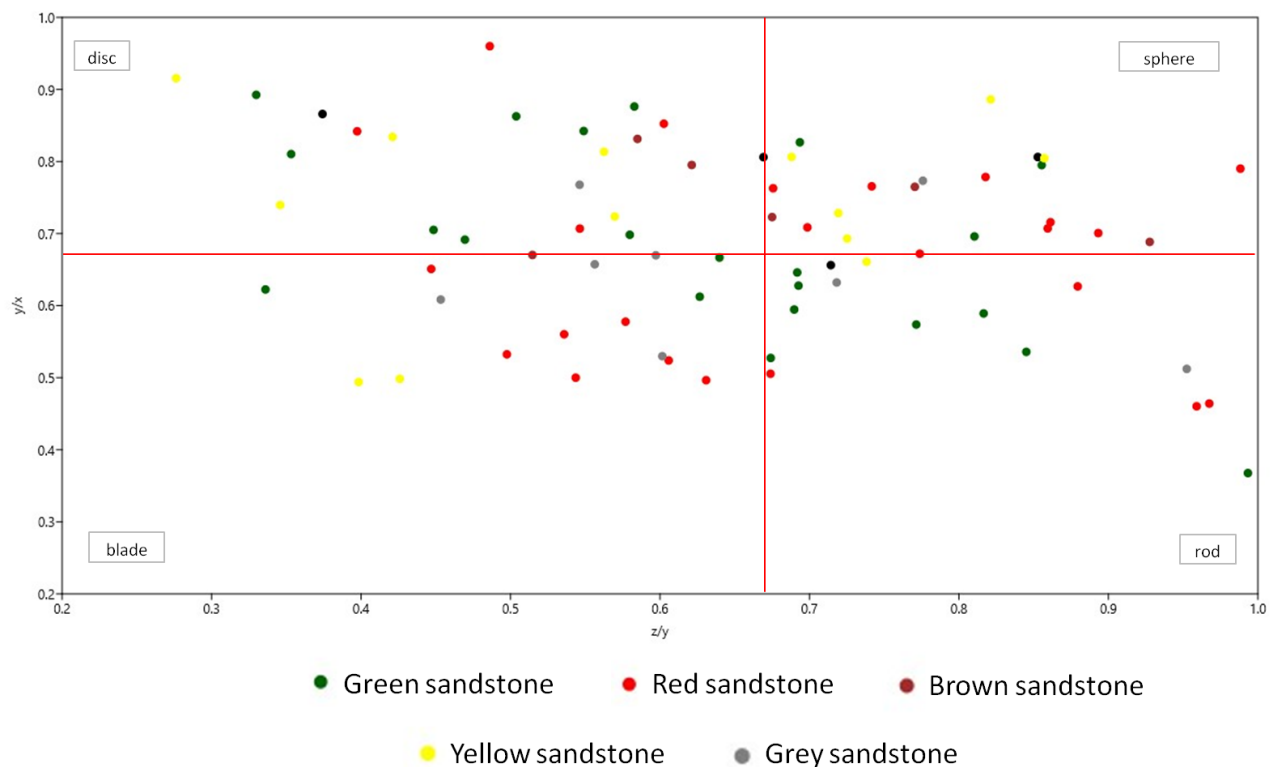


**Figure 15:** Zingg's diagram for 76 sandstone pebbles with *x*-axis larger than 5 mm, from the bulk gravel sample

Results are slightly different, when different types of sandstones are studied separately from the fractioned gravel larger than 32 mm (**Figures 16, 18** and **20**). Green sandstones are the most common both in bulk and sieved groups (**Tables IV** and **VI, Figure 5**). Their Zingg diagram looks extremely dispersed (**Figure 16**). Comparison of a fraction larger than 32 mm with bulk sample shows significant differences (**Figure 17**). In fractionated material almost all shapes are equally abundant, except blades (**Figure 17a**), while in the bulk gravel discoidal and rod-shaped clasts prevail (**Figure 17b**).

**Figure 16:** Zingg's diagram for green sandstone pebbles from the gravel fraction > 32 mm (See **Table I** for explanation of categories)
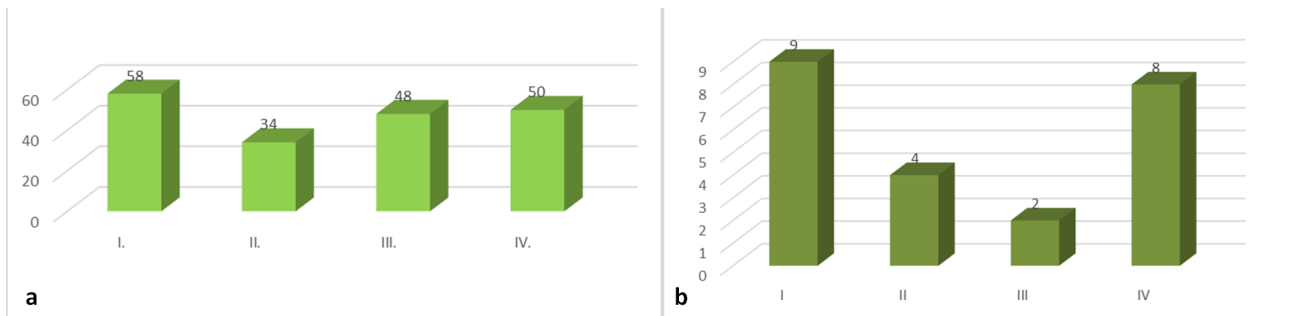


**Figure 17:** Comparison of Zingg's data for green sandstone pebbles from the: (a) fraction >32 mm and (b) bulk gravel sample, without pebbles with 0.67 ratio. Categories: I. disc; II. sphere; III. blade; IV. rod.

Within the red sandstones, discoidal shapes are the most common (**Figure 18**). In fractionated coarse material almost all shapes are equally abundant, except blades (**Figure 17a**), while in the bulk gravel discoidal and rod-shaped clasts dominate (**Figure 17b**), which is very different than in green sandstone group.
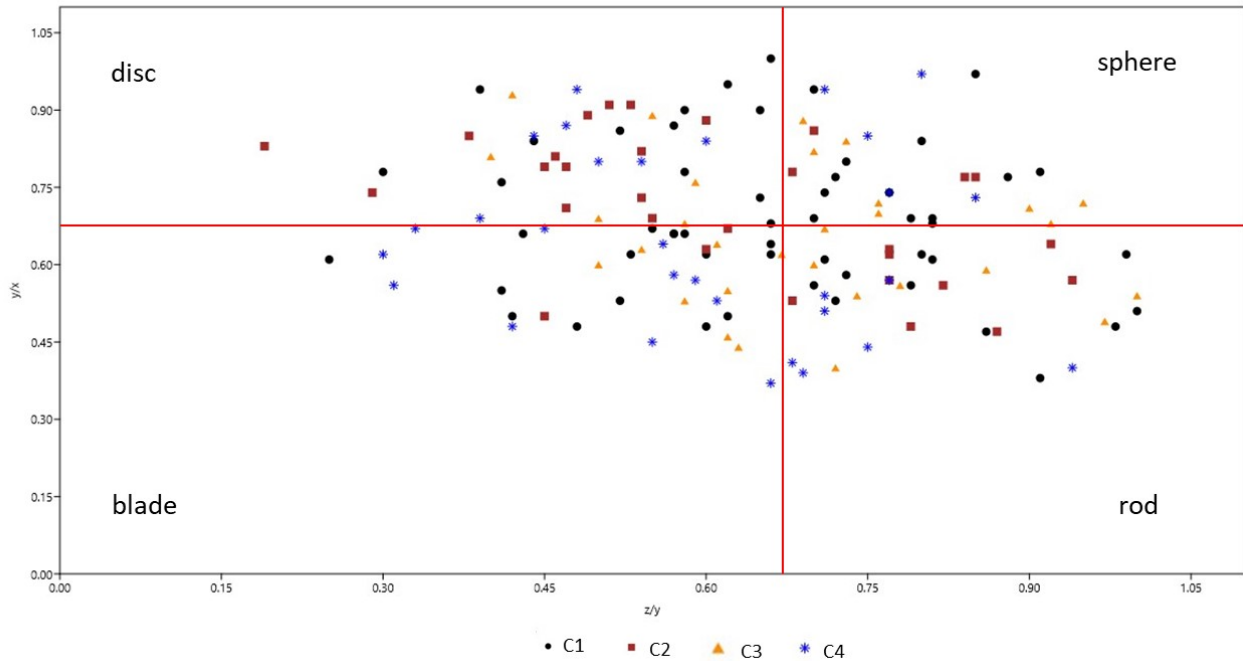
**Figure 18:** Zingg's diagram for red sandstone pebbles from the gravel fraction > 32 mm (See **Table I** for explanation of categories). C1 – coarse-grained sandstones; C2 – vine-red sandstone; C3 – rusty-coloured sandstone; C4 – fine-grained sandstone/siltite.
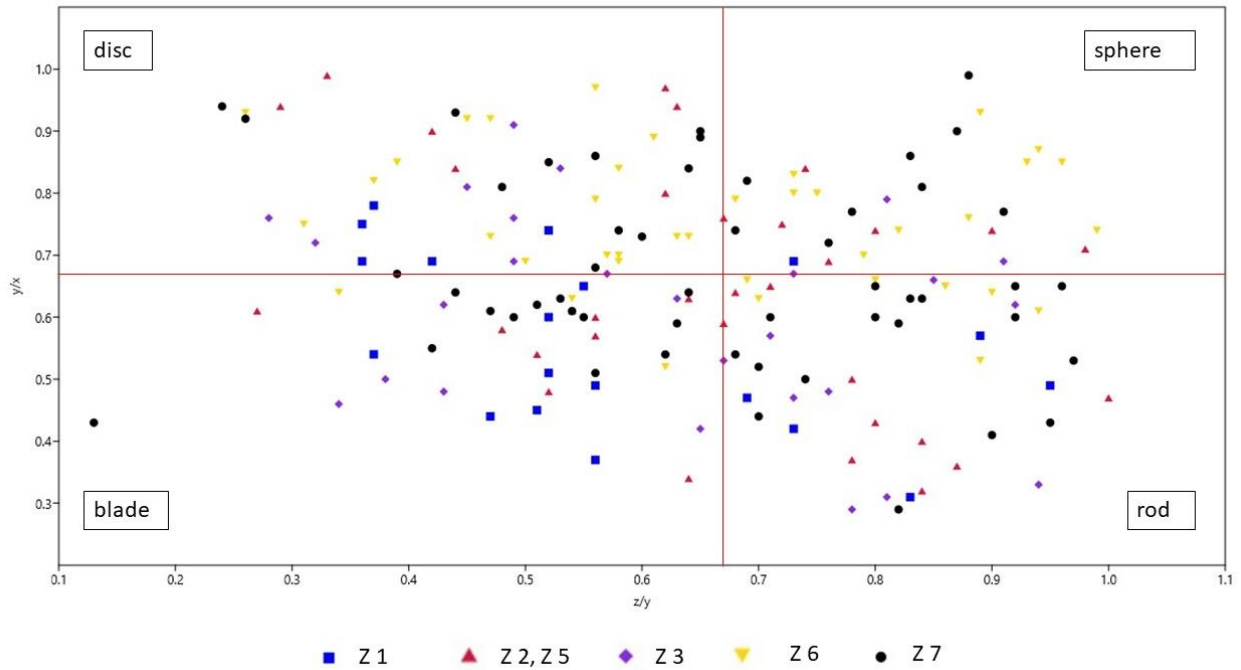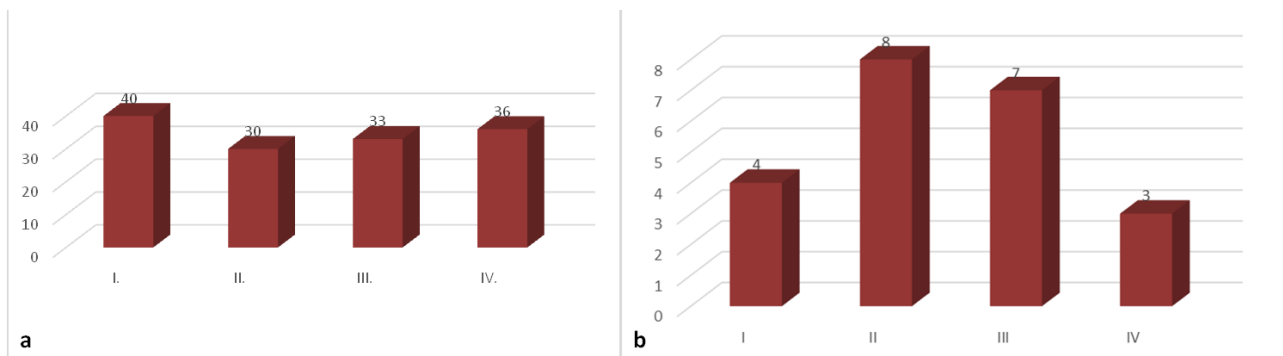


**Figure 19:** Comparison of Zingg's data for the red sandstone pebbles (C1, C2, C4) from the: (a) fraction >32 mm and (b) bulk gravel sample, without pebbles with 0.67 ratio. Categories: I. disc; II. sphere; III. blade; IV. rod.

Conglomerates and breccias are the only group of clastic rocks clasts with high percentage of spheroidal forms (**Figures 20** and **21**). They are represented with smaller number in gross sample, and their shape analyses were only done on coarse fractions.

Eruptives are represented with tuffs and diabases, also too scarce in bulk sample, and presented only from the coarse fraction (**Figures 20** and **21**). In both groups discoidal forms slightly prevail, while blades are very rare (**Figures 20** and **21**). Group of angular quartz grains and quartzites are present in all forms except blades. They are much more common in fine fractions of the bulk sample, but only small number was counted from the fraction larger than 5 mm.
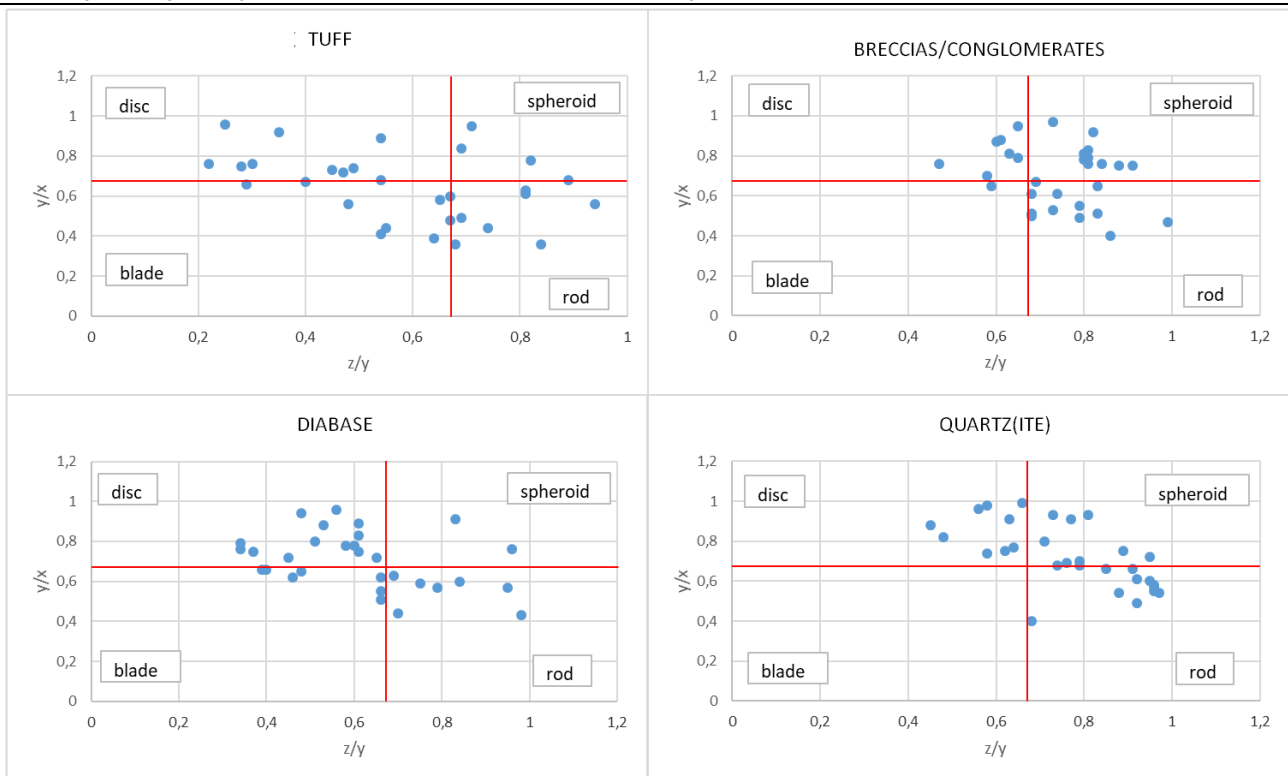
**Figure 20:** Zingg's diagram for less common pebbles from the gravel fraction >32 mm. These pebbles were not represented with statistically satisfactory numbers in bulk sample.
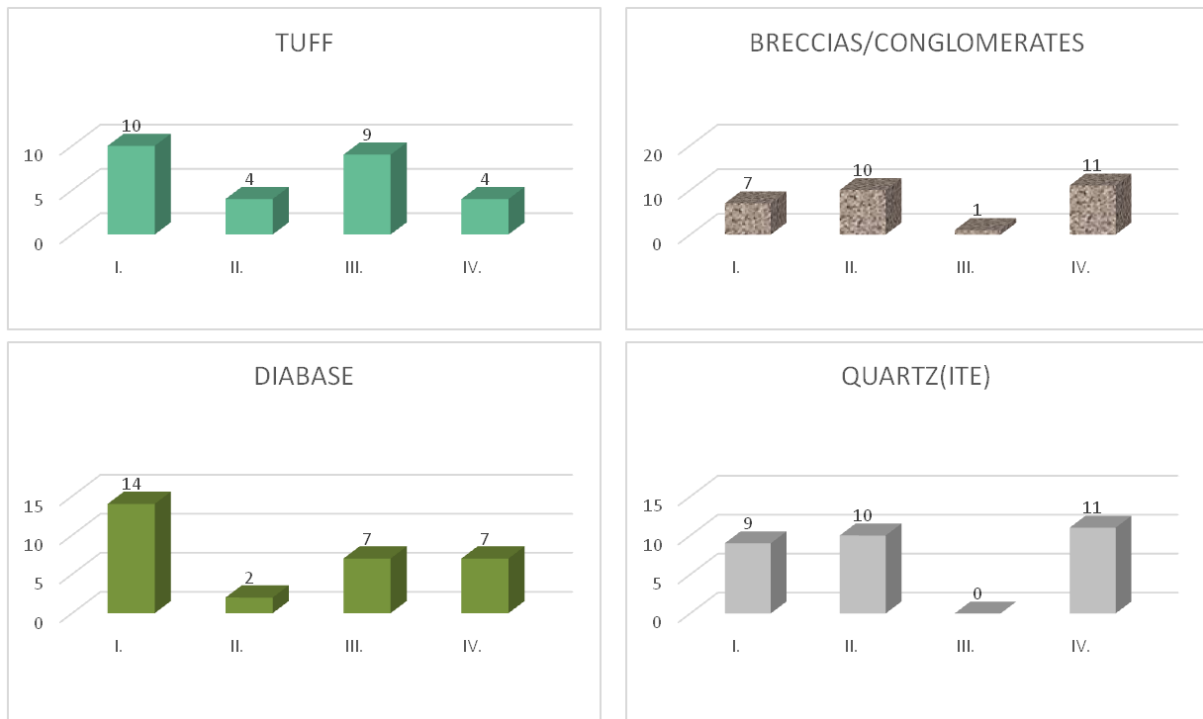


**Figure 21:** Histograms presenting Zingg's data for less common pebbles from the gravel fraction >32 mm, without pebbles with 0.67 ratio. These clasts were not represented with statistically satisfactory numbers in bulk sample larger than 5 mm. Categories: I. disc; II. sphere; III. blade; IV. rod.

Flatness ratio (after **Cailleux, 1952** and **Müller, 1967**) for all measured clasts from the bulk sample varies between 1.6 and 2.1 (**Table VIII**). The most common clasts, carbonates and sandstones, have flatness ratio of 1.9.

**Table VIII:** Flatness ratio for pebbles of different lithologies in a bulk gravel sample (calculated after: **Cailleux, 1952** and **Müller, 1967**)

| LITHOTYPE | FLATNESS RATIO |
|---|---|
| SANDSTONE | 1.9 |
| LIMESTONE | 1.9 |
| BRECCIA/CONGLOMERATE | 1.7 |
| DIABASE | 2.1 |
| QUARTZ(ITE) | 1.6 |
| CHERT | 1.7 |

# 4. Discussion

Since the beginning of this research, we were focused on two main goals: recognizing the source rocks contributing to the formation of gravels and trying to understand the mode of their transport. This study offers some interesting initial results and represents a good foundation for further research of these topics.

## 4.1. Modal composition of "Abesinija" pit gravels and possible source area(s)

Study of the coarse-grained gravels (clasts larger than 32 mm) from gravel pit "Abesinija" enabled the first insight in different lithologies present in the studied gravels. Results could be well compared with published data from the neighbouring areas (**Marić et al., 1954; Crnković and Bušić, 1970; Šimunić et al., 1975; Velić and Saftić. 1996; Velić et al., 1999; Barudžija et al., 2020, and references therein**).

Carbonate and sandstone clasts predominate in the studied samples. The most expressed difference between the fraction > 5 mm and finer fraction of the bulk gravel sample is the amount of silicate clasts of quartz(ites) and cherts, which are far more abundant in finer fractions, similar to the samples analysed by **Crnković and Bušić (1970)**. Similar distribution has been observed for the diabase clasts (**Table IV, Figure 5**). Such modal distribution points to the two possible reasons: either these smaller clasts were transported from more distant source rocks, or they were eroded from older rocks in the wider area. Amount of clasts with sharp edges within this lithological group is very high, therefore the long transport is not likely, and extraction from older clastic rocks, not very far from the depositional basin, seems more probable. Shape of carbonate clasts is dominantly discoidal, but shape charts for grey micritic limestones and dark-grey calcarenites (**Figure 7**) leave the possibility of existence of more than one source area, or different transport mechanisms. Distribution of green and red clastic rocks (microbreccias, sandstones and siltstones) display rather scattered shape data (**Figure 8**), which depends on lithological varieties within this category. Nevertheless, it is interesting that green clastites are more common in the finer fraction, while red-coloured clastic rocks are more abundant in the coarser fraction, when counted in the bulk sample (**Table IV**). The explanation can be like in quartz, chert and diabase clasts. It is possible that red clasts originate from a source area closer to the depositional basin, or green sandstones passed through more than one cycle of redeposition.

Carbonate clasts rarely comprise cross sections of macrofossils, which can hardly be determined. In some pebbles foraminiferal remnants are visible, and they will be further studied to determine the age of source rocks. Axial sections of diploporacean dasyclad algae can be recognized in several grey limestone pebbles (e.g., **Figure 5b**), pointing to the middle Triassic age. Coralline algae are visible in some bioclastic limestone pebbles (**Figure 5c**). The most probable age of these clasts is the Middle Miocene (Badenian). Red sandstones, particularly those with micas, are the typical lithotype of the Early Triassic. Green sandstones seem to be the product of weathering of diabases, which point to the Upper Jurassic to earliest Cretaceous melange on the Medvednica Mt. Scarce *pietra verde* clasts could have also been derived from the northern slopes of the Medvednica Mt. A more detailed study of clasts is necessary for further discussions and conclusions.

## 4.2. Morphometric features and transport mechanisms

Shapes calculated from three pebble axes by **Zingg (1935)** method exhibit some interesting patterns (**Figures 12-21**). In some cases they are influenced by rock textures (e.g., lamination in sandstones, character of lithoclasts in

breccias/conglomerates), but in many cases they reflect the principal mode of transport. Discoidal shape seems to prevail in all sedimentary rocks categories. Among the most common white and grey limestones (**Figures 12, 13** and **14**), distribution of blade and rod shapes seem similar, while some differences appear in percentage of rod-shaped clasts. Spheroidal clasts occur in much larger numbers in the gross sample, than in selected coarse fraction (**Figure 14b**). The Zingg diagram of sandstones is much more dispersed (**Figure 16**), due to the various lithological subcategories included in this group. In coarse fraction (>32 mm) of the fractioned material almost all shapes are equally abundant, except blades (**Figure 17a**), while in the gross sample discoidal and rod-shaped clasts prevail (**Figure 17b**), which might simply be the result of separation processes. In fractioned coarse material almost all shapes of red sandstones are equally represented, except blades (**Figure 19a**), while in the gross sample discoidal and rod-shaped clasts dominate (**Figure 19b**), which is very different pattern than in green sandstone group. The difference between the fractioned and bulk sample, can be again explained by separation processes, during which blade- and rod-shaped clasts are partly crushed. The flatness ratio for the most abundant pebbles of sedimentary rocks, sandstones and carbonates (1.9, **Table VIII**) points to the fluvio-glacial transport (**Table III**) (**Cailleux, 1952** and **Müller, 1967**, from **Barudžija et al., 2020**). Other lithological categories also fit into glacial/periglacial transport patterns, e.g., coarse-grained clasts (breccias, conglomerates), with flatness 1.7 (**Table VIII**) can be also the product of fluvio-glacial transport. Flatness result for quartz/quartzite grains of 1.6 fits into the ground moraine category (**Tables III** and **VIII**). Diabases have the highest value of 2.1, which can relate to a frost river (**Tables III** and **VIII**). Final touch in formation of these gravels might relate to a paleo-lake formed in this area after the melting of ice at the end of the Ice age. Further research will be focused on main transport modes and routes, taking into the consideration the different weathering rates for various clast categories.

## 5. Conclusions

- Gravels exploited from the gravel pits "Abesinija" and "Trstenik" in the Sava River flood-plain are polymictic and composed of dominantly carbonate pebbles, with rather common sandstones and less abundant quartz, quartzite, chert, diabase and coarse-grained clastic rocks.
- Carbonate and sandstone pebbles are dominantly discoidal in shape, with well-rounded surfaces. Quartz(ite) and chert clasts are often sharp-edged and much more abundant in smaller than in coarser fractions, as well as the semi-angular diabase clasts.
- Clast sizes indicate a normal distribution, while their shape and flatness ratio point to the important role of fluvio-glacial processes in their formation.
- The first results indicate the Medvednica Mt. as the possible important source area, and further research will be focused to reveal the source rocks and their transport routes.

## 6. References

Barudžija, U., Velić, J., Malvić, T., Trenc, N. and Matovinović-Božinović, N. (2020): Morphometric Characteristics, Shapes and Provenance of Holocene Pebbles from the Sava River Gravels (Zagreb, Croatia). Geosciences 2020, 10, 92; doi:10.3390/geosciences10030092

Basch, O. (1983a): Osnovna geološka karta SFRJ (*Basic Geological Map of SFR Yugoslavia*), 1:100000, Ivanić-Grad sheet, L33-81; Federal Geol. Institute: Belgrade, Serbia, 1983.

Basch, O. (1983b): Osnovna geološka karta SFRJ (*Basic Geological Map of SFR Yugoslavia*) 1:100000, Explanatory notes for sheet Ivanić-Grad, L33-81; Federal Geol. Institute: Belgrade, Serbia, 1983; pp. 66. (*in Croatian*)

Cailleux, A. (1952): Morphoskopische Analyse der Geschiebe und Sandkörner und Ihre Bedeutung für die Paläoklimatologie. Acta Diabetol., 40, 11–19.

Crnković, B. and Bušić, M. (1970): Mineraloško-petrografski sastav nanosa rijeke Save (*Mineralogical-petrological composition of the Sava River sediment*). Proceedings of 30th anniversary of the RGN Faculty (1939–1969*)*, Zagreb, Croatia, pp. 133–140. (*in Croatian*)

Malvić, T. and Medunić, G. (2015): Statistika u geologiji (*Statistics in Geology*), Sveučilište u Zagrebu, Rudarsko-geološko-naftni fakultet, Prirodoslovno-matematički fakultet, 88+VI str. (*in Croatian*)

Marić, L., Bogojević, D. and Majer, V. (1954): Petrografski spektar vučenog nanosa u koritu rijeke Save (*Petrographic spectrum of dragged sediment in the Sava riverbed*). Građevinar, VI/6, 201/5. (*in Croatian*)

Müller, G. (1967): Methods in Sedimentary Petrology. Schweizerbart: Stuttgart, Germany, 283 p.

Šimunić, A., and Basch, O. (1975): Stratigrafija kvartarnih sedimenata Zagrebačkog Posavlja (*The stratigraphy of Quaternary sediments in the Zagrebačko Posavlje – in Croatian with French summary*). Geološki vjesnik, 28, 153–164.

Velić, J. and Saftić, T. (1996): Dubinskogeološki odnosi područja smetlišta "Jakuševec"–čimbenik sanacije (*Deep geological relations of the "Jakuševec" Waste Depository area – remediation factor*). ZGO Gospodarenje otpadom IVth International symposium, Zagreb, 197-205. (*in Croatian*)

Velić, J., Saftić, B. and Malvić, T. (1999): Lithologic Composition and Stratigraphy of Quaternary Sediments in the Area of the "Jakuševec" Waste Depository (Zagreb, Northern Croatia). Geologia Croatica, 52, 2, 119-130.

Zingg, Th. (1935): Beiträge zur Schotteranalyse. Min. Petrog. Mitt. Schweiz., 15, 39-140.

**Internet sources:**

URL 1: d-maps.com
URL 2: McLeod, S. A. (2019): Introduction to the normal distribution (bell curve). Simply psychology: https://www.simplypsychology.org/normal-distribution.html

## SAŽETAK

**Modalni sastav i morfometrijske značajke šljunka iz eksploatacijskog polja „Abesinija" (Otok Svibovski; JI od Zagreba, Hrvatska)**

Šljunci koji se eksploatiraju u šljunčarama na širem području Trstenika u poplavnoj ravnici rijeke Save jugoistočno od Zagreba, već su na prvi pogled šaroliki i različitoga litološkog sastava. Ukupno je proučen 1399 klast iz prirodnog (nesortiranog) uzorka i 302 klasta iz krupne prosijane frakcije, veće od 32 mm. Mjerene su najduža (x), srednja (y) i najkraća (z) os, valutice su sortirane po litotipovima te je proučen njihov oblik i stupanj zaobljenosti. Numeričke analize načinjene su uz pomoć Microsoft Excel programa, a primijenjene su i Zinggove analize oblika klasta te izračuni plosnatosti. Šljunci su polimiktni i sastoje se od valutica/klasta sedimentnih (karbonatne stijene, pješčenjaci, breče i konglomerati), eruptivnih (dijabazi), piroklastičnih (tufovi) i metamorfnih (kvarciti) stijena, a dobro su zastupljena i kvarcna zrna te rožnjaci. Veličina mjerenih klasta po dužoj osi varira između 6,8 i 110,25 mm, a klasti pokazuju normalnu distribuciju. Dominiraju dobro zaobljene, diskoidalne karbonatne valutice. U nekima od njih vidljivi su presjeci zelenih i crvenih algi i makrofosila. Sljedeću najbrojniju litološku skupinu čine pješčenjaci različitih boja (zeleni, crveni, sivi, smeđi i žućkasti). Krupnozrnasti klastiti i dijabazi slabije su zaobljeni, dok su zrna kvarca i klasti kvarcita i rožnjaka često uglati i češći su u sitnijoj frakciji, nego među krupnijim šljuncima. Modalni sastav, veličina i oblik klasta upućuju na razmjerno kratak transport, vjerojatno s padina Medvednice, kombinacijom glacijalnih, fluvijalnih i lakustričkih procesa.

**Ključne riječi**: šljunci, litologija, morfometrija, rijeka Sava, Hrvatska

## Acknowledgment

## Author's contribution

**Jasenka Sremac (1)** (Dr.sc., Full Professor, geology, palaeontology, palaeoenvironment) provided the field work, palaeontological analyses, palaeoenvironmental interpretations and presentation of the results. **Josipa Velić (2)** (Dr.sc., Professor Emerita, Quaternary geology, petroleum geology, geomathematics) provided the field work, analyses of statistics results, geological settings and comparison and interpretation with the surrounding Quaternary deposits. **Marija Bošnjak (3)** (Dr.sc., senior curator, palaeontology, geomathematics) provided the field work, numerical analyses and methodological data. **Ivo Velić (4)** (Dr.sc., Meritorious Scientist, geology, stratigraphy) participated in field work, collected and determined Mesozoic microfossils from pebbles. **Tomislav Malvić (5)** (Dr.sc., Full Professor, geology, geomathematics) contributed with geomathematical methods and presentation of results. **Daniel Fotović (6)** (mining engineer), contributed with field work and provided relevant analytical data on exploited gravels for comparison. **Renato Drempetić (7)** (electrotechnics engineer), contributed with field work, field- and macrophotography, measuring pebbles from bulk sample and preparation of computer tables and graphics.

# Calculation of risk-neutral value for future exploration in the western part of the Sava Depression

**Josip Ivšinović[1]**
[1] INA-Industry of Oil Plc., Avenija Većeslava Holjevca 10, 10000 Zagreb, Croatia;
http://orcid.org/0000-0002-7451-1677

## Abstract

Risk management is an integral part of business policy of a company engaged in the exploration and production of hydrocarbons. In order to be able to numerically present and analyse the risk of investment in individual geological areas, it is necessary to calculate the risk-neutral value. The calculation of the risk-neutral value of monetary units applied to investigate additional amounts of hydrocarbons in the existing structures of the western part of the Sava Depression. The calculated value of $2.32 \cdot 10^6$ risk-neutral USD (United States Dollar) for the exploration geological probability value (500 000 m3 of geological reserves of hydrocarbons) is the investment maximum in the western Sava Depression exploration area for the company's 50 million USD hydrocarbon exploration budget.

**Keywords:** Sava Depression; Probability of Success (POS); Risk Neutral Value (RNV); risk management

## 1. Introduction

Projects aimed at hydrocarbon exploration at existing or new locations is a very risky activity of companies whose main activity is exploration and production of hydrocarbons. A feature of research projects is the overestimation of the monetary value of hydrocarbon reserves in the event of non-consideration of possible risk in the project. To avoid such a case, it is necessary to calculate a Risk Neutral Value (RNV).

Risk management is a fundamental task of any company engaged in hydrocarbon exploration and production. **Cozzolino (1977)** applied risk to basic economic calculations when deciding to invest in hydrocarbon exploration and production. **Rose (1987)** was the first to use an approximation of the utility function in calculating a risk-adjusted value. **Malvić et al. (2007)** described the calculation for the calculation of the neutral value and the application of the algorithm in the JAVATM package for examples in the Drava Depression. The first application of the calculation of RNV in Croatian part of Pannonian Basin System (CPBS) and is made in the example of Bjelovar Subdepression (**Rusan and Malvić, 2009**). By applying the method of RNV and probability of success (POS) for the area of Bjelovar Subdepression, economic and geological indicators for possible sustainable development of hydrocarbon exploration in that area obtained, and standards for such analysis set in other parts of CPBS. **Malvić et al. (2020)** are applied modification POS and calculate the risk-neutral value for future water injection on reservoir "L" of field "A" in Sava Depression. A relatively small number of literature citations used in this type of paper, due to the confidentiality of data of companies engaged in production and exploration of hydrocarbons. These papers were used as a theoretical basis for calculating the risk-neutral value.

## 2. Methods

### 2.1. Research area (western part of the Sava Depression)

The Sava Depression is in the southwestern part of the Pannonian Basin System. The area of the western part of the Sava Depression (**Figure 1**) is about 8000 km$^2$, while the area of vertical projections of hydrocarbon reservoirs discovered so far is about 930 km$^2$ (**Ivšinović, 2019**).

Corresponding author: Josip Ivšinović
*josip.ivsinovic@ina.hr*
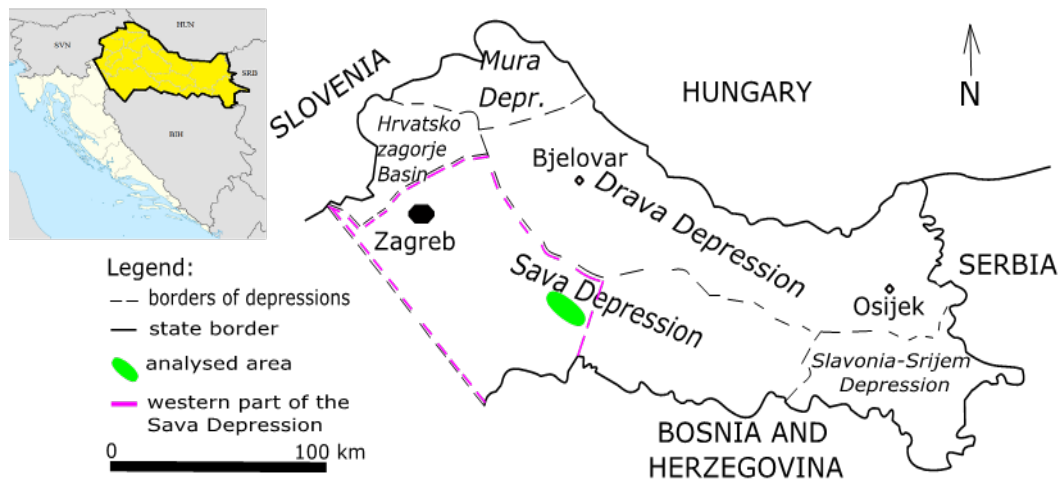
**Figure 1:** Geographical position of the western part of the Sava Depression (**Malvić et al., 2020**)

Hydrocarbon reservoirs have been proven in all formations except in the youngest Lonja Formation. A typical geological column of the western part of the Sava Depression is shown in **Figure 2**.
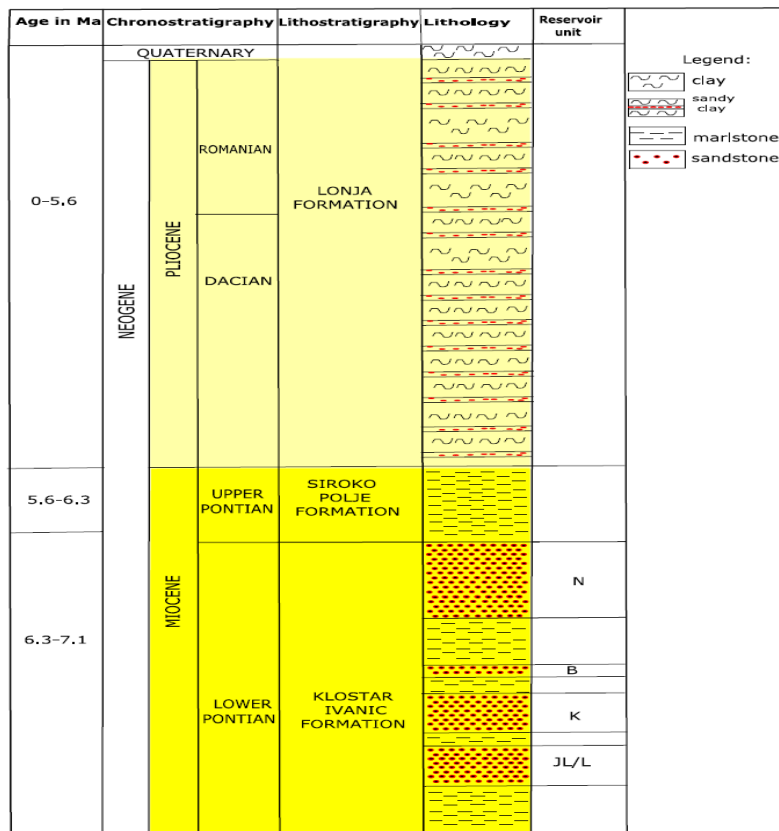


**Figure 2:** Typical geological column of the investigated area (**Ivšinović and Malvić, 2020**)

The original value of POS for possible new hydrocarbon discoveries within the Upper Miocene deposits (the Kloštar Ivanić Formation) is 42.18% (**Ivšinović et al., 2020**).

## 2.2. Risky neutral value of possible discoveries

The risk-adjusted value is derived from the utility function with respect to the level of investment and the level of acceptable risk. The derived value depends on the size of the investment, the level of risk and the investor's profit, and for the risk-adjusted value is **Equation 1**:

$$RAV = -\frac{1}{r(u)} \cdot \ln\left[ POS \cdot e^{-r(u)(R-C)} + (1-POS) \cdot e^{r(u) \cdot C} \right] \tag{1}$$

Where are:
*RAV*     *- risk-adjusted value,*
*R*         *- total profit (million USD),*
*C*         *- cost (million USD),*
*POS*     *- geological probability of success,*
*e*         *- mathematical constant, Euler's number,*
*r(u)*      *- first approximation of the utility function.*

The risk-averse function (rtc) is a value that is usually taken 1/5 and 1/6 of the total annual budget for hydrocarbon exploration (**Malvić and Rusan, 2009**). Different authors describe the calculation methodology: **Cozzolino (1977), Rose (1987), Malvić et al. (2007), Malvić and Rusan (2009) and Ivšinović (2019)**. Below are the mathematical **Equations 1 to 7** contained in the calculation methodology of RNV for the western part of the Sava Depression.

Net present value is the value obtained by discounting the difference between income and investment for each year over the observed period. When calculating the net present value, a fixed discount rate less the value of the invested capital is assumed **(2)**:

$$NPV = \frac{NT}{(1+i)^k} \tag{2}$$

Where are:
*NPV*     *- net present value of potential reserves,*
*NT*      *- cash flow (USD),*
*i*         *- discount rate,*
*k*        *- number of years.*

Expected monetary value is the profit that an investor makes by investing in oil and gas exploration projects **(3)**:

$$EMV = NPV \cdot (1-POS) \tag{3}$$

Where are:
*EMV*     *- expected monetary value (USD),*
*NPV*     *- net present value of potential reserves,*
*POS*     *- geological probability of success.*

The first approximation of the utility function is the company's annual investment in research and development of a particular area, and is calculated according to **Equation 4**:

$$r(u) = \frac{1}{GU} \tag{4}$$

Where are:

*GU*      - *annual investment (million USD),*
*r(u)*      - *first approximation of the utility function.*

Risk-neutral dollars are calculated from an exponential function that decreases with respect to risk, and expression **(5)** for converting real dollars into risk-neutral dollars is:

$$U(x) = rtc \cdot \left( 1 - e^{\frac{-NPV}{rtc}} \right)$$

(5)

Where are:
*U*      - *useful units in millions of neutral dollars,*
*NPV*      - *net present value of potential reserves,*
*e*      - *mathematical constant, Euler's number,*
*rtc*      - *risk-averse function.*

Expected utility units adjusted for values taking into account geological probability, and expected utility units are calculated according to relating **Equation 6:**

$$EU = U(x) \cdot POS - RAV \cdot (1 - POS)$$

(6)

Where are:
*EU*      - *expected utility units,*
*U*      - *useful units in millions of risk-neutral dollars,*
*POS*      - *geological probability of success,*
*RAV*      - *risk-adjusted value.*

The corresponding equivalents are a variable value that describes the utility in terms of potential return on investment, and relating **Equation 7** is:

$$CE = -rtc \cdot \ln \left( 1 - \frac{EU}{rtc} \right)$$

(7)

Where are:
*CE*      - *appropriate cash equivalents in millions of risk-neutral dollars,*
*rtc*      - *risk-averse function,*
*EU*      - *expected utility units.*

## 3. Results and Discussion

An example of the calculation is in area of the western part of the Sava Depression (**Figure 1**) is the Lower Pontian sandstone reservoir of the Klostar Ivanic Formation, which have total geological oil reserves of 556,000 m³. The predicted hydrocarbon recovery assumed 30% (primary and applied secondary production methods). The average oil price was taken at 390 USD/m³ (for 2019). Revenues from the sale of hydrocarbons were generated during 10, 15 and 20 years of production. The cost of drilling two vertical wells (one research and one confirmatory) is $6.6 \cdot 10^6$ USD. The future net value of the quantities of hydrocarbons produced, which is used to calculate the neutral value, is $59.0 \cdot 10^6$ USD. In **Table 1**, the values from **Equation 1-7** are calculated.

**Table 1:** Calculated risk-neutral monetary risk values for multiple scenarios for the western part of the Sava Depression

| | | | |
|---|---|---|---|
| Hydrocarbon production period (years) | 10 | 15 | 20 |
| Discount rate (%) | 10 | 10 | 10 |
| Net present value ($10^6$ USD) | 22.74 | 14.12 | 8.77 |
| Geological probability of success (POS) | 0.42 | 0.42 | 0.42 |
| Expected monetary value ($10^6$ USD) | 13.19 | 8.19 | 5.09 |
| CAPEX for hydrocarbon exploration ($10^6$ USD) | 50 | 50 | 50 |
| Risk-averse function | 10 | 10 | 10 |
| Useful units ($10^6$ USD) | 8.97 | 7.56 | 5.84 |
| The first approximation of the utility function | 0.02 | 0.02 | 0.02 |
| Well drilling costs ($10^6$ USD) | 6.61 | 6.61 | 6.61 |
| Risk-adjusted value (USD) | 5.87 | 2.75 | 0.65 |
| Expected utility units (USD) | 0.35 | 1.57 | 2.07 |
| Appropriate cash equivalents (RNUSD) | 0.36 | 1.71 | 2.32 |

The calculation was made for three cases of production: 10, 15 and 20 years; with a discount rate of 10% per annum. Risk averse function is calculated as 1/5 of Capital expenses (CAPEX) investments in research and is $10.0 \cdot 10^6$ US dollars. The first approximation of the utility function for investment research and according to **Malvić and Rusan (2009)** for the value of annual investment in research of 50 million USD for the area of Bjelovar Subdepression and is 0.02. Due to the similarity of the area of Bjelovar Subdepression and the western part of the Sava depression in the case of calculation (RNV), the same value of the first approximation of the utility function of 0.02 will be used. To ensure the expected 30% recovery, a longer period of hydrocarbon production is required, so the values for 10 and 15 years of hydrocarbon production will be taken for comparison data (**Table 1**). For a geological reserve of 556,000 m³, a POS value of 0.42 for the western part of the Sava Depression and a hydrocarbon production time of 20 years, the expected monetary value is $8.77 \cdot 10^6$ USD. The value of $2.32 \cdot 10^6$ dollar corresponding equivalents is the investment maximum in the explored area of the western part of the Sava Depression (**Figure 1**) considering the annual budget of the hydrocarbon exploration company of $50.0 \cdot 10^6$ USD with a risk-adjusted value of 42.4%.

The period observed in calculating the corresponding equivalents for the value of exploratory POS is 10, 15, and 20 years of hydrocarbon production from the reservoir. The best case is the one whose value of the corresponding equivalents is the largest. In the case of calculating the corresponding equivalents (**Table 1**) for the POS exploration area of the western part of the Sava Depression, 20 years of hydrocarbon production were taken with 2.32 million risk-neutral dollars and the expected monetary value of 5.09 million USD. Hydrocarbon exploration under these conditions is cost-effective given the expected risk. The calculation of the risk-neutral value on the example of exploration and adjusted POS for the area of the Western Sava Depression indicates a large impact of risk on hydrocarbon exploration and production. The results showed that in the investigated area it is possible to estimate the annual amount for research and development of 50 million USD is sufficient for work in the western part of the Sava Depression. Risk be reduced by merging two or more companies in project, because then the total risk is shared.

## 4. Conclusions

To calculate the risk-neutral monetary value of the investment for the exploratory regional POS, three cases of hydrocarbon production period of 10, 15, and 20 years used for calculation. The highest value of the corresponding monetary equivalents was obtained in the case of 20 years of hydrocarbon production and amounts to $2.32 \cdot 10^6$ USD as the investment maximum in the investigated area of the western part of the Sava Depression for the discovery of reservoirs with geological reserves of 500,000 m³ of hydrocarbons. This implies that the company dispose of a budget for exploration of hydrocarbons in the completely western part of Sava Depression of 50 million USD. In the case of risk sharing between two or more companies, the risk-neutral value of each of them is reduced, but the expected monetary value must then be divided.

## 5. References

Cozzolino, J. M. (1977): A simplified utility framework for the analysis of financial risk. Economics and Evaluation Symposium of the Society of Petroleum engineers, Dallas, U.S.A., SPE no. 6359, February 21-26, 1977, 10 p. https://doi.org/10.2118/6359-MS

Ivšinović, J. (2019): Odabir i geomatematička obradba varijabli za skupove manje od 50 podataka pri kreiranju poboljšanoga dubinskogeološkoga modela na primjeru iz zapadnoga dijela Savske depresije (*Selection and geomathematical calculation of*

*variables for sets with less than 50 data regarding the creation of an improved subsurface model, case study from the western part of the Sava Depression*). Ph.D. Thesis, University of Zagreb, Zagreb, Croatia, 129 p. (*in Croatian –English abstract*)

Ivšinović, J. and Malvić, T. (2020): Application of the radial basis function interpolation method in selected reservoirs of the Croatian part of the Pannonian Basin System. Mining of mineral deposits, 14 (3), 37-42. https://doi.org/10.33271/mining14.03.037

Ivšinović, J., Malvić, T., Velić, J. and Sremac, J. (2020): Geological Probability of Success (POS), case study in the Late Miocene structures of the western part of the Sava Depression, Croatia. Arabian Journal of Geosciences, 13 (714), 1-12. https://doi.org/10.1007/s12517-020-05640-z

Malvić, T. and Rusan, I. (2009): Investment risk assessment of potential hydrocarbon discoveries in a mature basin. Case study from the Bjelovar Sub-Basin, Croatia. Oil, gas - European Magazine (Hamburg), 35, 67-72.

Malvić, T., Ivšinović, J., Velić, J., Sremac, J. and Barudžija, U. (2020): Increasing Efficiency of Field Water Re-Injection during Water-Flooding in Mature Hydrocarbon Reservoirs: A Case Study from the Sava Depression, Northern Croatia. Sustainability 12, 786. https://doi.org/10.3390/su12030786

Malvić, T., Rusan, I. and Curi, M. (2007): Using of exponential function in risk assessment for investment in potential hydrocarbon discovery. Naftaplin-izvanredni broj, 27, 4, 33-42.

Rose, P.R. (1987): Dealing with Risk and Uncertainty in Exploration: How can we improve? AAPG Bulletin, 71, 1, 1-16. https://doi.org/10.1306/94886D30-1704-11D7-8645000102C1865D

# SAŽETAK

**Izračun rizično neutralne vrijednosti za buduće istraživanje u prostoru zapadnoga dijela Savske depresije**

Rizik i upravljanje rizikom je sastavni dio poslovnih politika tvrtki koje se bave istraživanjem i pridobivanjem ugljikovodika. Kako bi se rizik ulaganja u pojedine geološke prostore moglo numerički prikazati i analizirati, potrebno je izračunati rizično neutralnu vrijednost. Izračun rizično neutralne vrijednosti novčanih jedinica je primijenjen za istraživanje dodatnih količina ugljikovodika u postojećim strukturama zapadnog dijela Savske depresije. Izračunata vrijednost od $2,32 \cdot 10^6$ neutralnih USD (500 000 m$^3$ geoloških rezervi ugljikovodika) za vrijednost istražne geološke izglednosti je maksimalno ulaganje u istražno područje zapadnog dijela Savske depresije za proračun tvrtke od 50 milijuna USD namijenjenih za  istraživanje ugljikovodika.

**Ključne riječi**: Savska depresija; POS; rizično neutralna vrijednost; upravljanje rizicima

## Author's contribution

**Josip Ivšinović** (PhD, Field Development Project Expert) completed the entire research and publishing process.

# Geological model of the A field in the Sava Depression

**Kristina Novak Zelenika[1]; Ana Majstorović Bušić [1]**
[1] INA-Oil Industry Plc., Av. V. Holjevca 10, Zagreb, Croatia,
[1]http://orcid.org/0000-0002-0090-6879

## Abstract

The oil field A is situated about 50 km to the southeast from Zagreb, in the Sava depression. The seismic attributes analyses allowed the revision of whole depositional concept. The previously drilled wells (A-1, A-2, A-2Al) defined this area as non-commercially saturated with hydrocarbons due to very small thickness or even complete absence of the sandstones (A-2 well). The interpretation of seismic attributes, primarily amplitude anomalies reveals the existence of distinct depositional unit with depositional direction different from the regional. It is as typical stratigraphic trap, and represents sandstone series with dominant local source of material (transport direction NE-SW). The sandstones of local source supposed to have a short transport from the northeast direction and they are considered independently as isolated sandstone bodies. The reservoirs belong to Miocene period (Upper Pannonian) and consist of sandstone bodies interbedded with sandy marls and marls. X reservoir is proved as the most productive and it is the target of this paper.

Geological model was constructed in Petrel$^{TM}$ software. Structural model was built using a simple grid (cell dimension 50x50 m). Laterally, seismic anomaly and oil/water contact represent reservoir borders. Vertically, five reservoir zones were established by the well to well correlation. Porosity in the model was distributed by Moving Average method using seismic attribute as trend. OHIP was estimated in two ways; deterministic (volumetric method) and probabilistic. P50 realization of the probabilistic estimation confirmed deterministically calculated OHIP with difference of approximately 1%.

**Keywords:** geological model; stratigraphic trap; sandstone reservoir; Upper Pannonian; Sava Depression

## 1. Introduction

The oil field A is situated about 50 km to the southeast from Zagreb, in the Sava depression within boundary of B exploitation field (**Figure 1**). Exploitation license was awarded to INA in 1967, license is renewed in 2015. First wells (A-1, A-2,2Al) were drilled before seismic acquisitions.

Gravimetric measurements as well as 2D seismic data were used to determine structures B and C. Between these larger structures, the smaller traps have been discovered earlier by some delineation wells. The better visualization came after 3D seismic acquisition (1998) and its reinterpretation, done in 2009, when A structure, as independent exploitation object was defined (**Figure 2**).

A-3 well, drilled in 2012, confirmed X oil reservoir. During the same year A-1 well was put into the production. Production from the A-3 and A-4 wells started in 2017.
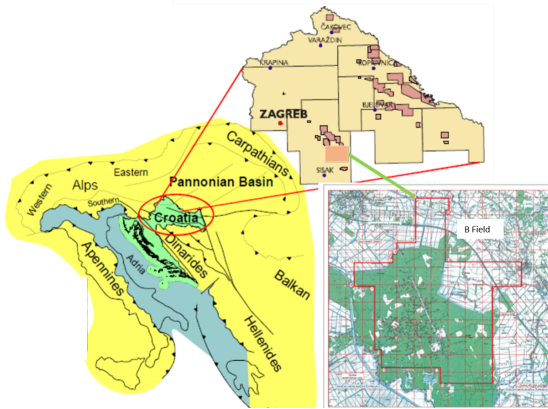
Corresponding author: Kristina Novak Zelenika
*kristina.novakzelenika@ina.hr*

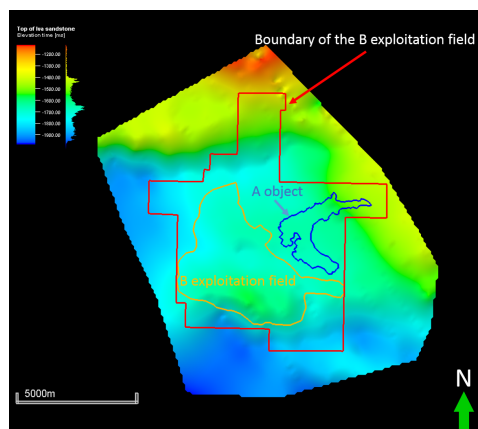**Figure 1:** B exploitation field, situation map



**Figure 2:** Exploitation object A

## 2. Geological overview

The Late Pannonian belongs to the 2nd trans-tensional phase, when thermal subsidence generally re-opened depositional space (depressions) along Pannonian Basin System, so that huge rate of sandy material could be accommodated (**Malvić and Velić, 2011**). During mentioned period the turbidite currents had been dominant clastic transport mechanism in the Croatian part of the Pannonian Basin System with a rock source in the Eastern Alps and due to gravitational instability, several times re-deposited before suspended materials finally entered in the Sava Depression (e.g., **Rögl and Steininger, 1984; Rögl, 1996, 1998**). The main direction of turbidite currents in Late Pannonian was northwest-southeast. Large quantities of sands and silts had been periodically deposited during activity of turbidite currents. Among those events, depression had been filled with mud and clay material, later compacted to marls (e.g., **Royden, 1988; Velić et al., 2002; Malvić et al., 2005; Ćorić et al., 2009; Vrbanac et al., 2010; Malvić and Velić, 2011; Novak Zelenika et al., 2013**). Upper Pannonian schematic depositional model is shown in **Figure 3**.

In the A field, beside turbidites, most of material has local origin, due to the proximity of the Moslavačka gora Mt., which was minor, but active, local source of detritus **(Novak Zelenika et al., 2013)**. Since the Moslavačka gora Mt. was island in the Pannonian Lake, eroded material has been transported to depression in form of smaller inland alluvial fans. So, northeast-southwest trend in all related reservoir parameters should be recognized **(Novak Zelenika et al., 2013)**. It indirectly describes the current direction into depositional environment. Interpretation of sedimentation conditions and sedimentary environments was based on well data and laboratory analyses. It was established that sedimentation proceeded in brackish to fresh water environments.
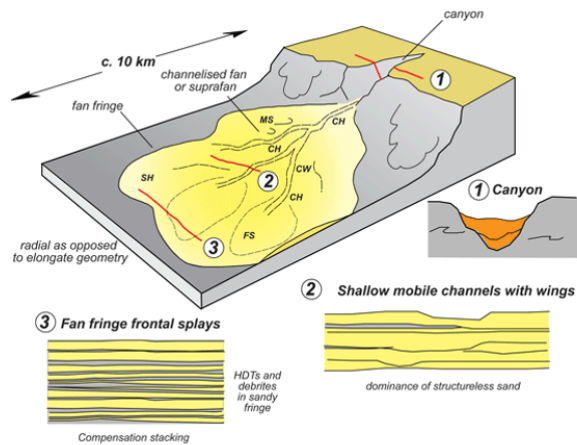
**Figure 3:** Schematic depositional model during Upper Pannonian ([http://www.sepmstrata.org/page.aspx?pageid=259](http://www.sepmstrata.org/page.aspx?pageid=259))

## 2.1. Field overview

The seismic attributes analyses allowed the revision of whole depositional concept. The previously drilled wells (A-1, A-2, A-2Al) defined this area as non-commercially saturated with hydrocarbons due to very small thickness or even complete absence of the sandstones (A-2). The interpretation of seismic attributes, primarily amplitude anomalies reveals the existence of distinct depositional unit with depositional direction different from regional depositional directions. It looks as typical stratigraphic trap, a shallow submarine flow of channel type and represents the second generation Iva sandstone series. The first generation of sandstones had the depositional direction mainly from the northwest with long transport distance resulted with relatively fine-grained particles.

The second generation of sandstones supposed to have a short transport from the northeast direction resulted with more coarse-grained particles. Those sandstones are almost not correlative with sandstones of the first generation. The both generations are considered as a single package called Iva sandstone associated with marl lateral equivalents as barriers. Now the sandstones of the second generation are considered independently as isolated sandstone bodies (**Figure 4**).

In geometry definition of the sandstone bodies, a specific approach of seismic attribute analysis was carried out in form of amplitude anomaly maps. According to average absolute amplitude it has been possible to follow lithological variations and to define an irregular geometry of the sandstone bodies. Finally, an oil reservoir in deeper part of Iva sandstones with very good reservoir quality has been confirmed by well A-3.
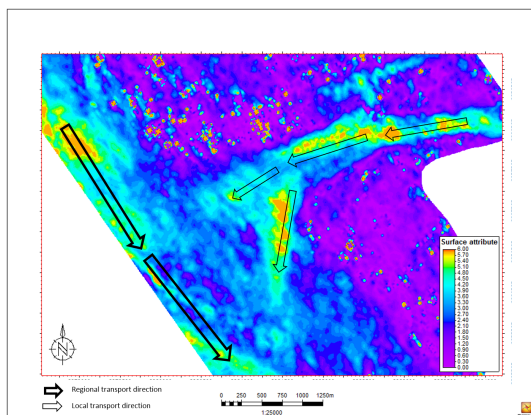


**Figure 4:** Seismic anomaly of the A field with material transport directions

A structure is located SW from major regional strike-slip fault. It is divided from B field by the system of normal faults (throw 30 m) and reverse faults (throw 40 m).

The reservoirs belong to Miocene period (Upper Pannonian) and consist of sandstone bodies interbedded with sandy marls and marls (**Figure 5**). The sandstone series, known also as Iva sandstone is composed of three reservoirs. According to core analyses from A-3 well, there are two types of sandstone bodies: subarkose sandstones with primary intergranular porosity and greywacke type of sandstones interbedded with shales. Seal rocks are Upper Pannonian marls. X reservoir is proved as the most productive and it is the target of this paper.
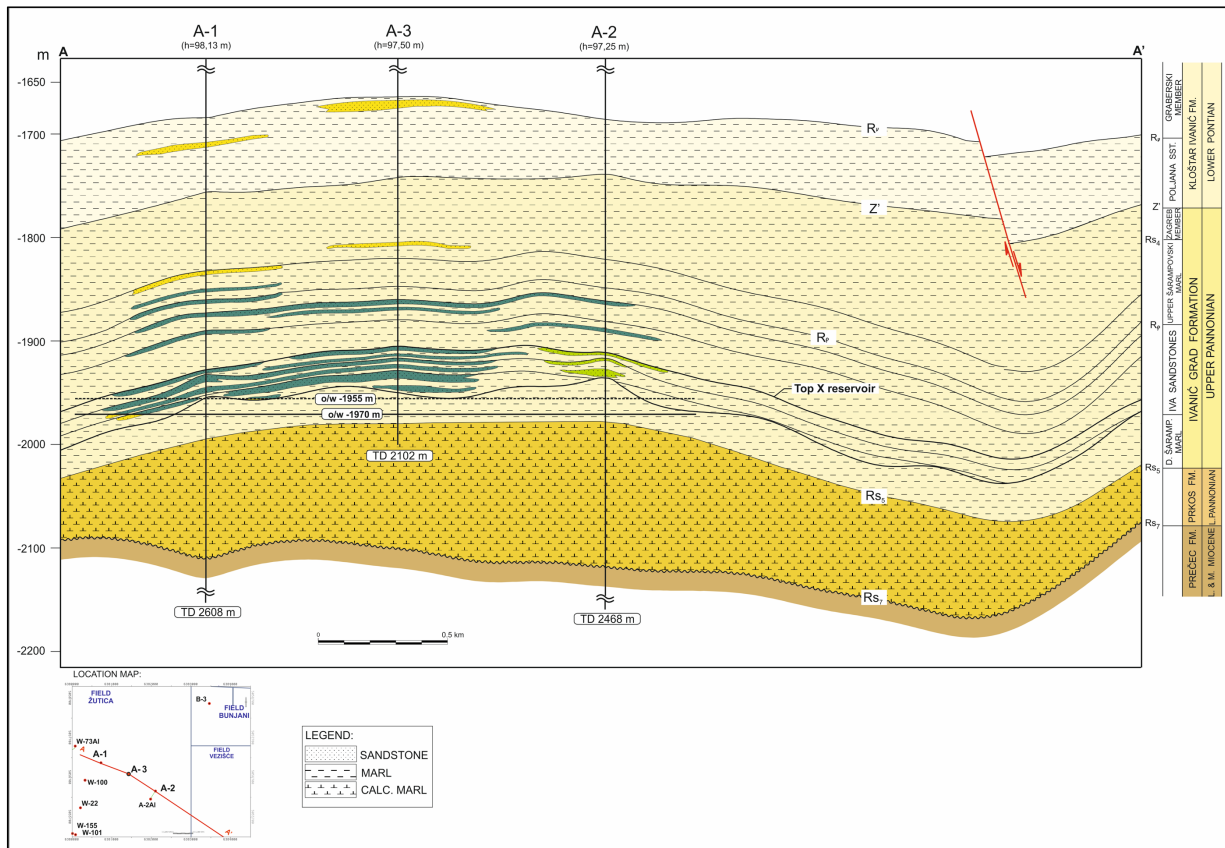


**Figure 5:** A field, geological cross section

## 3. Geological model

Geological model was constructed in Petrel^TM software. Input data set used for geological model construction comprised of:

- ➢ seismic data:
  - ○ seismic attribute (sweetness),
  - ○ top and base horizons of the X reservoir,
  - ○ seismic polygon as border of the anomaly,
- ➢ well log data,
- ➢ quantitative log analysis,
- ➢ core data,
- ➢ previous geological model.

### 3.1. Structural model

Structural model was built using a simple grid (cell dimension 50x50 m). Two horizons (X top and X base) represented the input for 3D structural model construction. Seismic polygon was used as the boundary of the X reservoir (**Figure 6**). East and west boundaries were represented as seismic anomaly borders, north boundary was a margin of soft seismic anomaly recognized after A-5 and -5Al dry wells and south boundary was represented as closure

with oil/water contact, defined on A-4 well. Vertically, five reservoir zones were established by the well correlation (**Figure 7**). Each zone consists of two to ten proportional layers, depending on zone thickness. Common oil/water contact was defined on A-4 well at -1968.5 m as the bottom of transitional zone of 60% of water saturation.
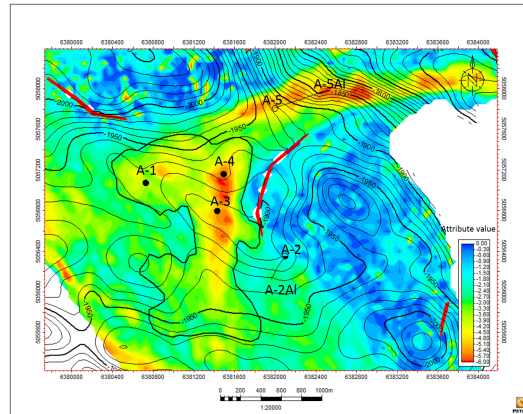


**Figure 6:** Structural top map with sweetness seismic attribute and polygon as reservoir boundary
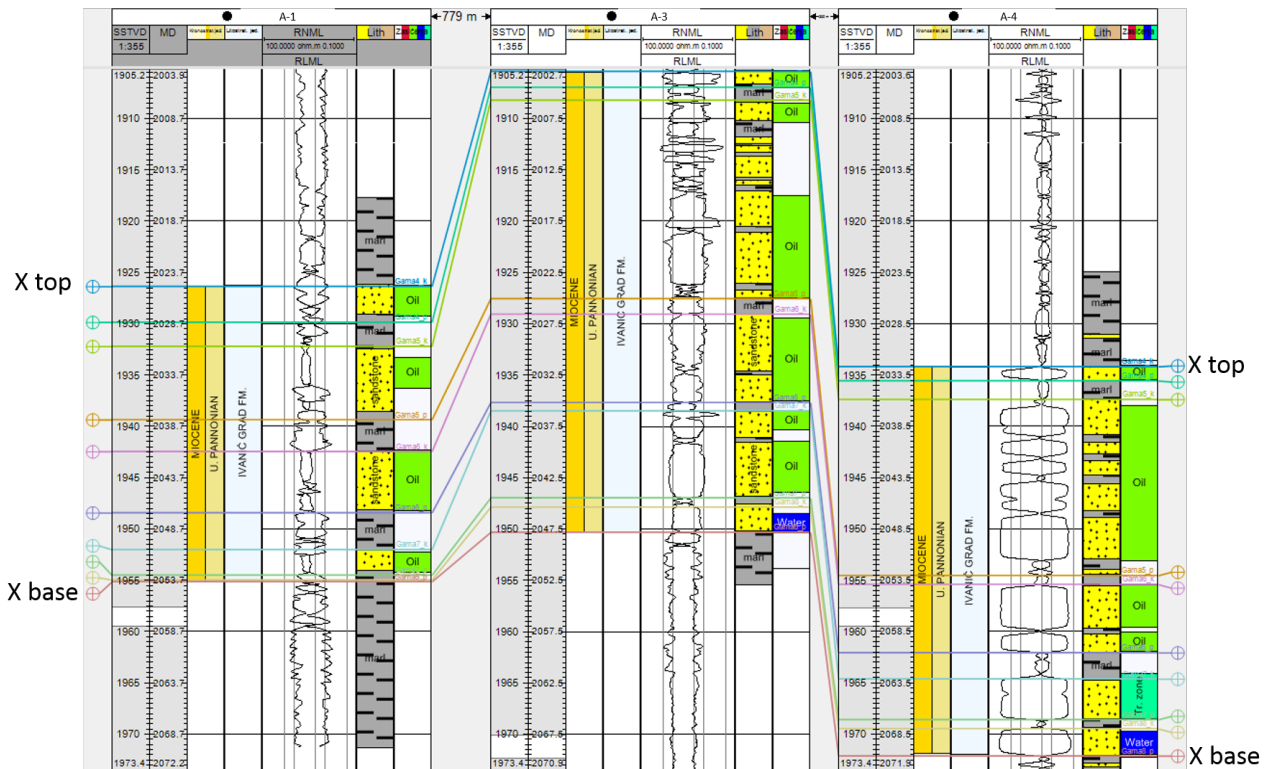


**Figure 7:** X reservoir: Well-to-well correlation

### 3.2. Petrophysical model

Net reservoir was defined by synthetic net-sand log using two criteria:
cut-off 7% of porosity (based on k-Por correlation),
cut-off 60% of shale volume (based on Por-Vsh correlation on X reservoir of the A field).
According to the analogy with other fields in the area, permeability lower than $1 \cdot 10^{-3} \mu m^2$ can be considered as impermeable for fluid flow. It is clearly visible that $1 \cdot 10^{-3} \mu m^2$ (1mD) on the diagram (**Figure 8**) corresponds to the

porosity value of 7%. Based on permeability - porosity ratio, cut-off of 7% on porosity has been used as criteria for net reservoir distribution.
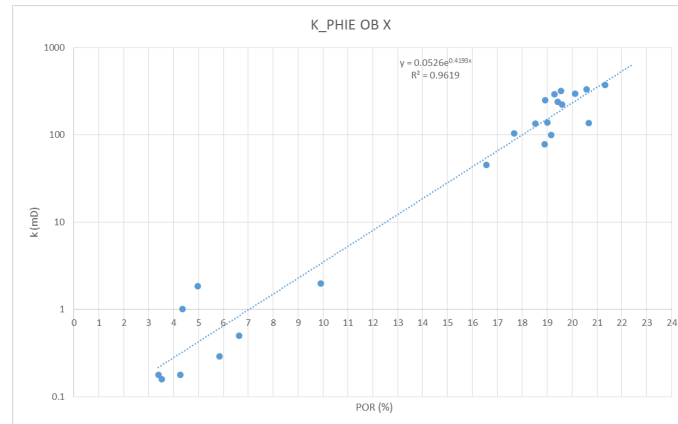


**Figure 8:** Cross plot diagram $k_{hor}$ (core) vs. porosity (core)

Cross plot diagram Por vs. Vsh of the X reservoir confirmed used criteria, showing that 7% of porosity corresponds to 56% of shale volume (**Figure 9**).
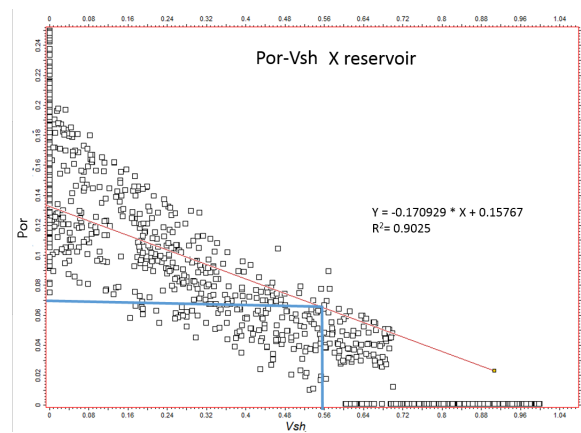


**Figure 9:** Cross plot diagram Vsh vs. porosity (X reservoir of the A field)

Input data for porosity model were porosity logs derived from quantitative log analysis and porosity measurements on core at standard conditions and corrected for overburden pressure. Corrected porosity logs were upscaled in the model representing input for porosity modeling. Upscaling method was average. Upscaled values were distributed by Moving average method using seismic attribute as trend (**Figure 10**).
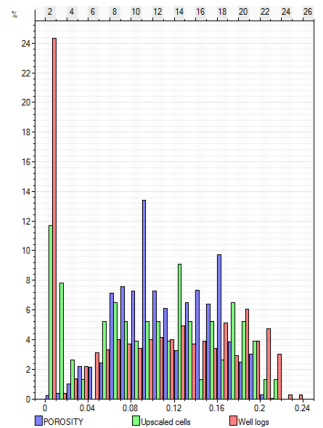
**Figure 10:** Histogram of the well logs, upscaled and distributed porosity (X reservoir of the A field)

Generally, water saturation coming from quantitative log analysis is considered overestimated. In heterogeneous reservoirs upscaled data are usually influenced by vertical anisotropy, showing significantly higher SW values especially in the lithologically heterogeneous parts of reservoir. For that reason, water saturation was estimated by using Por-Sw approximation curve obtained by sampling the lowest Sw values for respective porosity. Sw model was created by applying established Por-Sw relation on porosity model.

Final volumetric hydrocarbon reserves have been estimated based on petrophysical model and oil/water contact. Probabilistic method was used as an additional tool of the estimated OHIP revision. Probabilistic resource distributions were estimated by using excel-based MMRA (Multi-Method Risk Analysis) program. Applied estimation method was Net Rock Volume, which use Gross Rock Volume, Percent Volumetric Fill and Net to Gross Ratio. Varied parameters were gross reservoir volume (from seismic), net to gross ratio (from petrophysics), porosity (from log analysis) and hydrocarbon saturation (between the values of the defined oil/water contact and $Sw_{ir}$). Based on the input varied parameters calculation defines key values (P90, P50, Mean, P10) of the resource distribution. P50 realization confirmed deterministically estimated OHIP. Difference between OHIP estimated by probabilistic (P50) and deterministic method was only 1%.

## 4. Conclusions

Definition of the A structure, as independent exploitation object come after the 3D seismic acquisition in 1998 and its reinterpretation in 2009. The X oil reservoir has been confirmed in 2012, after A-3 well was drilled.

The whole depositional concept has been revised based on the seismic attributes analyses. A reservoir is typical stratigraphic trap, a shallow submarine flow of channel type. In A field, beside turbidites, most of material has local origin, which probably derived from the Moslavačka gora Mt. (transport direction NE-SW). The reservoir belongs to Miocene period (Upper Pannonian) and consist of sandstone bodies with primary intergranular porosity, interbeded with sandy marls and marls. Seal rocks are Upper Pannonian marls.

Geological model was constructed in Petrel™ software. Structural model was built using a simple grid (cell dimension 50x50 m). Laterally, seismic anomaly and oil/water contact represent reservoir borders. Vertically, five reservoir zones were established by the well to well correlation. Porosity in the model was distributed by Moving Average method using seismic attribute as trend. Water saturation model was created by applying established Por-Sw relation on porosity model. OHIP was estimated in two ways; deterministic (volumetric method) and probabilistic (using MMRA). P50 realization of the probabilistic estimation confirmed deterministically calculated OHIP with difference of 1%.

## 5. References

Ćorić, S., Pavelić, D., Rögl, F., Mandić, O., Vrabac, S., Avanić, R., Jerković, L. and Vranjković, A. (2009): Revised Middle Miocene datum for initial marine flooding of North Croatian Basins (Pannonian Basin System, Central Paratethys). Geologia Croatica, 62, 31-43.

Malvić, T. and Velić, J. (2011): Neogene tectonics in Croatian Part of the Pannonian Basin and reflectance in hydrocarbon accumulations. In: Schattner, U. (ed.): New frontiers in tectonic research: At the midst of plate convergence. – InTech, 215-238.

Malvić, T., Velić, J. and Peh, Z. (2005): Qualitative-quantitative analyses of the influence of depth and lithological composition on Lower Pontian sandstone porosity in the central part of Bjelovar Sag (Croatia). Geologia Croatica, 58, 73-85.

Novak Zelenika, K., Velić, J. and Malvić, T. (2013): Local sediment sources and palaeoflow directions in Upper Miocene turbidites of the Pannonian Basin System (Croatian part), based on mapping of reservoir properties. Geological Quarterly, 57, 17-30.

Rögl, F. (1996): Stratigraphic correlation of the Paratethys Oligocene and Miocene. Mitt. Ges. Geol. Bergbaust. Österr., 41, 65-73.

Rögl, F. (1998): Palaeographic consideration for Mediterranean and Paratethys seaways (Oligocene to Miocene). Ann. Naturhist. Mus. Wien, 99A, 279-310.

Rögl, F. and Steininger, F. (1984): Neogene Paratethys, Mediterranean and Indo-Pacific seaways. Geol. Jour., Spec. issue, 11, 171-200.

Royden, L.H. (1988): Late Cenozoic tectonics of the Pannonian Basin System. AAPG Mem., 45, 27-48.

Velić, J., Weisser, M., Saftić, B., Vrbanac, B. and Iković, Ž. (2002): Petroleum-geological characteristics and exploration level of the three Neogene depositional megacycles in the Croatian part of the Pannonian Basin. Nafta, 53, 239-249.

Vrbanac, B., Velić, J. and Malvić, T. (2010): Sedimentation of deep-water turbidites in main and marginal basins in the SW part of the Pannonian Basin. Geol. Carpath., 61, 55-69.

**Internet sources:**

URL: http://www.sepmstrata.org/page.aspx?pageid=259 (accessed August 2020)

## SAŽETAK

### Geološki model A ležišta u Savskoj depresiji

Naftno polje A nalazi se oko 50 km jugoistočno od Zagreba, u području Savske depresije. Analiza seizmičkih atributa omogućila je reviziju konceptualnog taložnog modela analiziranog područja. Ranije izrađene bušotine (A-1, A-2, A-2Al) definirale su ovaj prostor kao nekomercijalni u smislu zasićenja ugljikovodicima, zbog malih debljina ili čak potpunog odsustva pješčenjaka (A-2). Interpretacijom seizmičkih atributa, posebno amplitudnih anomalija, utvrđeno je postojanje taložnog tijela, koje je imalo drugačiji smjer taloženja od regionalnog smjera. Radi se o stratigrafskoj zamci, a predstavljena je pješčenjacima nastalim dominantnim lokalnim donosom materijala (smjer donosa materijala je SI-JZ). Pješčenjaci nastali lokalnim donosom imali su kratak transport iz smjera sjeveroistoka i smatraju se odvojenim pješčenjačkim tijelima. Ležišta su miocenske starosti (gornji panon), a čine ih pješčenjaci proslojeni pjeskovitim laporima i laporima. Ležište X se smatra najproduktivnijim horizontom te je zbog toga prikazano u ovom radu.

Geološki model je napravljen u programu Petrel™. Za izradu strukturnog modela koristila se jednostavna mreža s dimenzijama ćelija 50x50 m. Lateralne granice ležišta definirane su poligonom seizmičke anomalije i kontaktom nafta/voda. Vertikalno, bušotinskom korelacijom definirano je pet zona. Šupljikavost je u modelu distribuirana metodom pokretne sredine, a seizmička anomalija korištena je kao trend. Ukupni volumeni otkrivenih ugljikovodika procijenjeni su na dva načina; deterministički (volumetrijskom metodom) i probabilistički (MMRA). Realizacija P50 dobivena probabilističkom metodom, potvrdila je ukupne volumene otkrivenih ugljikovodika dobivenih determinističkom volumetrijskom metodom s razlikom od oko 1%.

**Ključne riječi**: geološki model; stratigrafska zamka; pješčenjačko ležište; gornji panon; Savska depresija

## Author's contribution

**Kristina Novak Zelenika (1)** (PhD, Reservoir modelling expert) provided the geological model and deterministic OHIP estimation. **Ana Majstorović Bušić (2)** (PhD, Geological expert**)** provided the probabilistic MMRA analysis.

# Biometric analysis of the Eocene Lucinidae shells from Croatia

**Marija Bošnjak[1]; Nediljka Prlj Šimić [1]; Jasenka Sremac[2]**

[1] Croatian Natural History Museum, Demetrova 1, 10000 Zagreb, Croatia;
http://orcid.org/0000-0002-1851-1031; https://orcid.org/0000-0002-5862-5965
[2] Faculty of Science, Department of Geology, University of Zagreb, 10000 Zagreb, Croatia; http://orcid.org/0000-0002-4736-7497

## Abstract

Numerous marine bivalves of the family Lucinidae were collected from the Eocene localities at the Promina Mt. and Imotski area (Lažete) in Croatia. The specimens are today housed in the Croatian Natural History Museum in Zagreb. The Lucinidae shells were measured and the biometric analysis was performed to compare morphometric characteristics of the height, length and width of the shells between the localities in Croatia, and the comparative specimens from the Paris Basin housed in the Museum. Morphometric analyses showed differences between the lucinid samples in Croatia, also between the samples from Croatia and specimens from the Paris Basin. Lucinidae samples from Croatia have higher morphometric values and indicate the possible favourable paleoecological conditions for the growth of the bigger shells. This study is the first step in the further biometric research on the Eocene malacofauna from Croatia and its comparison with the neighbouring contemporaneous localities.

**Keywords:** Biometry, Lucinidae, Eocene, Croatia

## 1. Introduction

Lucinidae are a family of marine bivalves known in the fossil record from Paleozoic to today, especially from the Paleogene and Neogene periods. In Croatia, numerous specimens of lucinids are recorded in the Eocene sediments in Dalmatia (for references see next chapter). Part of the Eocene lucinids from Croatia are housed in the Croatian Natural History Museum (abbr. CNHM) in Zagreb. Here presented specimens are part of the five collections which are result of the long year's field- and cabinet work of the museum curators, as well as international cooperation with other Museums. The lucinids were mostly collected and determined during the second half of the 20th century by the curators Ante Milan and Krešimir Sakač, who were investigating Eocene localities with lucinids in Lika (Bunić-Kozijan), Dalmatia (Ostrovica-Benkovac, Otres-Ostrovica, Dubravica-Skradin, Kosavin-Bribir, Promina and Imotski – Lažete, Borak, Mamutovo brdo, Podgradina, Suvaja and Ćosići localities) and Herzegovina (Vir). Professor Gjuro Pilar, who was also a curator in the CNHM, enriched the Museum fundus with the comparative collection "Tertiary fauna of the Paris basin", containing lucinids among other fauna.

In this paper authors presented the biometric analysis on part of the lucinids from the Museum collections. Biometrical analysis included comparison of measured parameters of the lucinid shells (height, length and width) (e.g., **Malvić et al., 2020 and references therein**) to study differences between the morphometry of the lucinid shells from the two localities in Croatia (Promina and Imotski area), and to compare samples from Croatia with the lucinids from the Paris Basin present in the Museum comparative collection (**Figure 1**). This paper is part of the research started on Eocene localities in Imotski area and Herzegovina (**Sremac et al., 2014, 2015**), and represents a baseline study on the morphometry of the Lucinidae, as a first step in the biometrical analysis of the Eocene macrofauna from the Museum collections and specimens collected during the field work in Imotski area.

Corresponding author: Marija Bošnjak
*marija.bosnjak@hpm.hr*

**Figure 1:** Geographical location of the localities with Eocene Lucinidae presented in this paper (**Google Earth Pro, https://earth.google.com/web/**)

## 2. Historical background on the Eocene lucinids from the Museum collections

**Milan (1956)** described various Eocene fossil fauna, including Lucinidae, collected from the yellowish marls and sandstones in Dalmatia, in the area between Otres and Ostrovica. According to **Dainelli (1905)**, **Schubert (1905)** and **Kochansky (1947)** the deposits with lucinids are of the Middle Eocene, Upper Lutetian age.

**Dainelli (1905)** compared Eocene fauna from the several localities in Dalmatia with the other known Eocene fossil fauna, concluding that the fauna from Croatia corresponds to the fauna from the localities San Giovanni and Ronca in Italy.

Part of the lucinids in the Museum collections is collected at the Promina Mt. **Kühn (1946)** gave historical review of geological research on Promina Mt. He determined the Upper Eocene age of the sediments, and the deposits with fossils as the lowest part of the Upper Eocene.

**Sakač (1965)** described Cretaceous and Lower Paleogene sediments from the Imotski area. According to him the lower Paleogene deposits of Imotski area are rich with fossil molluscs, and cosmopolitic species recorded in the Middle- and Upper Eocene deposits, also mentioning the species *Lucina dalmatina* characteristic for the Upper Eocene. Sakač concluded that the Eocene molluscs correspond to the other fauna in the Dinarides, especially to the fauna of the Promina Mt.

**Sakač et al. (1984)** continued the research of the Imotski area and collected fossil macrofauna with numerous lucinids from different localities of the Imotski area and Herzegovina. Among the collected lucinids there are gigantic specimens, what was later confirmed by **Sremac et al. (2014, 2015)**.

Lucinid specimens from the comparative Museum collection from the Paris Basin are very well preserved, diversified and collected at various localities in the Paris Basin. The Paris Basin is an area of a typical development of Paleocene and Eocene deposits, with a clear boundary between Paleogene and Neogene marked by a marine regression.

First description of the Eocene deposits comes from the Paris and London basins by C. Lyell. From the fossil record of the Paris Basin, the main contributions in paleontology are made on the molluscan fauna from Eocene and Oligocene deposits described by Jean-Baptiste Pierre Antoine de Monet, chevalier de Lamarck, and Gérard-Paul Deshayes (e.g., **Lozouet, 2014 and references therein**). Geology of this basin has been intensively analysed, and the synthesis of the results is presented in **Mégnien and Mégnien (1980)**. The Paris Basin is considered as one of the best researched Eocene sites in the stratigraphic and paleontological sense (e.g., **Čvorović, 2000**).

## 3. Methods

We analyzed 204 Lucinidae shell from the following CNHM collections: "Fauna of the Eocene deposits of Croatia and Dalmatia" (in Croatian, "*Fauna eocenskih naslaga Hrvatske i Dalmacije*"; 5 specimens, inventory numbers: 1996, $1998_{1-2}$, $1999_{1-2}$), "Molluscan fauna of the Middle Eocene of the northern Dalmatia" (in Croatian, "*Fauna molusaka srednjeg eocena sjeverne Dalmacije*", 4 specimens, inventory numbers: 20, $21_{1-2}$, $22_3$), two Professor Sakač's

collections (77 specimens, temporary inventory numbers: 1L-5L, 8L-14L, 17L-19L, 21L, 24L-27L, 29L, 32L-41L, 43L, 45L-47L, 50L-54L, 1KS-29KS, 32KS-39KS), and "Tertiary fauna of the Paris Basin" (in Croatian, "*Zbirka tercijarne faune Pariške kotline*", 118 specimens, inventory numbers: 113, 113bb, 114$_{1-4}$, 115$_{1-3}$, 116$_{1-5}$, 117$_{1-2}$, 118$_{1-10}$, 119$_{1-5}$, 119bb, 120, 121$_{1-3}$, 122$_{1-3}$, 123$_{1-4}$, 124$_{1-6}$, 128$_{1,3,4}$, 129$_{1-6}$, 130$_{1-3}$, 131$_{1-3}$, 132$_{1-6}$, 133$_{1-7}$, 134$_{2,3}$, 135, 136$_{1-7}$, 139, 142$_{1-4}$, 143$_{1-10}$, 144$_{1-2}$, 145$_{1-3}$, 146$_{1,2,4-8,10-13}$).

There are various sizes of lucinid specimens present in the Museum collections, therefore we analysed the specimens by biometrical analyses. Using the digital caliper, we measured the height (H), length (L) and width or thickness (W) of the shell (**Figure 2**). Height (H) is the largest measurement perpendicular to the length. Length (L) is the largest measurement in the anterio-posterior axis. The width or thickness of the shell (W) is the maximum thickness of two joined valves. Measurements are presented in **Tables 1, 2, 3** and **4**. We also calculated morphometric indices of the shell showing elongation (H/L ratio), compactness or roundness (E/L ratio) and convexity (E/H ratio) of the shell (e.g., **Modestin 2017 and references therein**).

The measured lucinid shells had a complete valve and we did not include the specimens representing the lucinid fragmented shells. As mentioned above, the width or thickness of the shell is measured as a thickness of two valves. This was not possible to perform in here presented analysis on all the specimens, due to the fossil preservation of lucinids having mostly only one valve preserved. Thickness is therefore here presented as the width of only one valve for part of the measured specimens.

Descriptive analysis of the morphometric relations between measured lucinid shells was carried out using the XY graphs and histograms in the PAST (PAleontological STatistics) Program (**Hammer et al., 2001**).

Authors also revised the determinations of Lucinidae species names according to the fossil databases „Paleobiology Database. Fossilworks." (**fossilworks.org**) and „World Register of Marine Species (WORMS, **www.marinespecies.org**) to compare similarities of the findings from Croatia with the ones from the Paris Basin collection. The revised names are shown in **Table 5**.
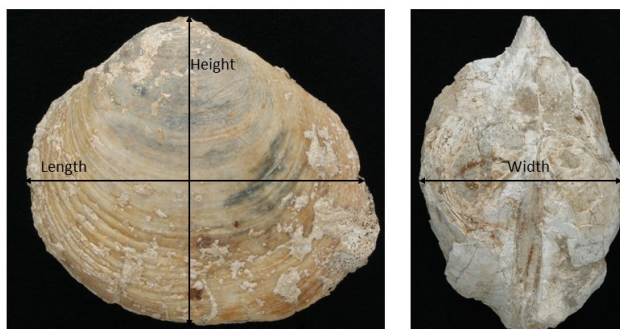


**Figure 2:** Measured elements height, length and width of the Lucinidae shells

**Table 1:** Measured Lucinidae shells from the CNHM collection "Fauna of the Eocene deposits of Croatia and Dalmatia". Revised names are presented in **Table 5**.

| Inventory number | Species name | Height, H (mm) | Length, L (mm) | Width, W (mm) |
|---|---|---|---|---|
| 1996. | *Lucina gigantea* Deshayes | 79.9 | 88.5 | 30.7 |
| 1998.$_1$ | *Lucina zignoi* Oppenheim | 49.9 | 56.2 | 28 |
| 1998.$_2$ | *Lucina zignoi* Oppenheim | 32.8 | 33 | 19.2 |
| 1999.$_1$ | *Lucina* sp. | 32.9 | 25.9 | 15.6 |
| 1999.$_2$ | *Lucina* sp. | 33.1 | 31.5 | 20.4 |

**Table 2:** Measured Lucinidae shells from the CNHM collection "Molluscan fauna of the Middle Eocene of the northern Dalmatia". Revised names are presented in **Table 5**.

| Inventory number | Species name | Height, H (mm) | Length, L (mm) | Width, W (mm) |
|---|---|---|---|---|
| 20. | *Lucina escheri* Mayer | 37.2 | 42.1 | 10 |
| 21.$_1$ | *Lucina dalmatina* Oppenheim | 18.1 | 22.3 | 11.4 |
| 21.$_2$ | *Lucina dalmatina* Oppenheim | 14.4 | 18.7 | 7.8 |
| 22.$_3$ | *Lucina saxorum* Lamarck | 44.6 | 50 | 27.3 |

**Table 3:** Measured Lucinidae shells from the Professor Sakač's collections. a) Lucinidae from Lažete locality near Imotski. b) Lucinidae from Promina Mt. Revised names are presented in **Table 5.**

a) Lucinidae from Lažete locality near Imotski.

| Temporary inventory number | Species name | Height, H (mm) | Length, L (mm) | Width, W (mm) |
|---|---|---|---|---|
| 1 L | *Lucina* sp. | 138.7 | 170.2 | 80.5 |
| 2 L | *Lucina* sp. | 162.3 | 170.2 | 75.8 |
| 3 L | *Lucina* sp. | 157.9 | 172.9 | 75.5 |
| 4 L | *Lucina* sp. | 171 | 188.5 | 44.3 |
| 5 L | *Lucina* sp. | 144.2 | 145.3 | 66.2 |
| 8 L | *Lucina* sp. | 137.1 | 164.6 | 45.7 |
| 9 L | *Lucina* sp. | 126.8 | 148.5 | 64.4 |
| 10 L | *Lucina* sp. | 138.6 | 141.1 | 46.5 |
| 11 L | *Lucina* sp. | 106.6 | 115 | 61.9 |
| 12 L | *Lucina* sp. | 94.1 | 129 | 51.5 |
| 13 L | *Lucina* sp. | 132.1 | 129.9 | 46.2 |
| 14 L | *Lucina* sp. | 106.5 | 125.8 | 57.5 |
| 17 L | *Lucina* sp. | 126.7 | 87.8 | 70.9 |
| 18 L | *Lucina* sp. | 106.3 | 114.5 | 57.9 |
| 19 L | *Lucina* sp. | 120.1 | 116.9 | 51.9 |
| 21 L | *Lucina* sp. | 104.9 | 83.2 | 75 |
| 24 L | *Lucina* sp. | 77.2 | 74.6 | 40.4 |
| 25 L | *Lucina* sp. | 89.6 | 91.2 | 47.6 |
| 26 L | *Lucina* sp. | 100.5 | 93.5 | 31.7 |
| 27 L | *Lucina* sp. | 88.5 | 91.9 | 27.1 |
| 29 L | *Lucina* sp. | 72 | 87.8 | 24.4 |
| 32 L | *Lucina illyrica* Oppenheim | 103.6 | 118.2 | 52.3 |
| 33 L | *Lucina* sp. | 89.9 | 91.4 | 43.2 |
| 34 L | *Lucina* sp. | 47 | 58.7 | 8.3 |
| 35 L | *Lucina* sp. | 95.7 | 107.4 | 19.4 |
| 36 L | *Lucina* sp. | 45.5 | 64.8 | 23.3 |
| 37 L | *Lucina* sp. | 52.1 | 53.3 | 13.6 |
| 38 L | *Lucina prominensis* Oppenheim | 69.7 | 65 | 32.1 |
| 39 L | *Phacoides* (*Lucinoma*) *dinarii* Kühn | 27.6 | 26 | 13.8 |
| 40 L | *Lucina* sp. | 73.1 | 68.3 | 25.2 |
| 41 L | *Lucina* sp. | 64.4 | 75.6 | 30.5 |
| 43 L | *Lucina* sp. | 83 | 68.4 | 14.9 |
| 45 L | *Lucina* sp. | 66.2 | 70.1 | 44.2 |
| 46 L | *Lucina* sp. | 45.7 | 72.4 | 22.4 |
| 47 L | *Lucina* sp. | 48 | 35.5 | 27.3 |
| 50 L | *Lucina* cf. *escheri* Mayer 1870 | 50.2 | 68 | 13.4 |
| 51 L | *Lucina saxorum* Lamarck | 24.5 | 26.6 | 14.1 |
| 52 L | *Lucina saxorum* Lamarck | 22.2 | 20.1 | 12.7 |
| 53 L | *Lucina* sp. | 42.3 | 44.6 | 18.2 |
| 54 L | *Lucina* sp. | 40.1 | 44.4 | 8.6 |

b) Lucinidae from Promina Mt.

| Temporary inventory number | Species name | Height, H (mm) | Length, L (mm) | Width, W (mm) |
|---|---|---|---|---|
| 1 KS | *Lucina prominensis* Oppenheim | 54.1 | 61.6 | 25.2 |
| 2 KS | *Lucina prominensis* Oppenheim | 57.3 | 62.9 | 25.6 |
| 3 KS | *Lucina prominensis* Oppenheim | 19.7 | 23.2 | 5.4 |
| 4 KS | *Lucina prominensis* Oppenheim | 64.6 | 66.6 | 25.3 |
| 5 KS | *Lucina prominensis* Oppenheim | 48.2 | 69.6 | 20.2 |
| 6 KS | *Lucina dalmatina* Oppenheim | 18.9 | 24.8 | 11.2 |
| 7 KS | *Lucina dalmatina* Oppenheim | 18.4 | 22.3 | 11.9 |
| 8 KS | *Lucina saxorum* Lamarck | 40.4 | 37.4 | 19.1 |
| 9 KS | *Lucina saxorum* Lamarck | 40 | 44.1 | 19.2 |
| 10 KS | *Lucina saxorum* Lamarck | 38.3 | 47.9 | 21.7 |
| 11 KS | *Lucina saxorum* Lamarck | 45.6 | 49.9 | 27.4 |
| 12 KS | *Lucina saxorum* Lamarck | 48.6 | 44.2 | 25.8 |
| 13 KS | *Lucina saxorum* Lamarck | 51.2 | 55.8 | 28.3 |
| 14 KS | *Lucina saxorum* Lamarck | 46.1 | 49 | 24.4 |
| 15 KS | *Lucina saxorum* Lamarck | 59.2 | 58.4 | 31 |
| 16 KS | *Lucina saxorum* Lamarck | 51.9 | 55.2 | 27.3 |
| 17 KS | *Lucina saxorum* Lamarck | 22.1 | 19.2 | 12.8 |
| 18 KS | *Lucina saxorum* Lamarck | 21.2 | 18.5 | 7.7 |
| 19 KS | *Lucina saxorum* Lamarck | 16.2 | 14.4 | 8.4 |
| 20 KS | *Lucina saxorum* Lamarck | 18.3 | 18.1 | 12.6 |
| 21 KS | *Phacoides* (*Lucinoma*) *dinarii* Kühn | 35.7 | 34.2 | 21.1 |
| 22 KS | *Phacoides* (*Lucinoma*) *dinarii* Kühn | 38.6 | 41.3 | 24.4 |
| 23 KS | *Phacoides* (*Lucinoma*) *dinarii* Kühn | 22.2 | 19.2 | 7.9 |
| 24 KS | *Lucina dalmatina* Oppenheim | 20.3 | 25 | 13.3 |
| 25 KS | *Lucina dalmatina* Oppenheim | 21.6 | 24.9 | 12.8 |
| 26 KS | *Lucina dalmatina* Oppenheim | 16.9 | 22.6 | 12.6 |
| 27 KS | *Lucina* cf. *dalmatina* Oppenheim | 16.8 | 20.1 | 11.6 |
| 28 KS | *Lucina* cf. *dalmatina* Oppenheim | 18.5 | 21 | 14.1 |
| 29 KS | *Lucina* cf. *dalmatina* Oppenheim | 16.1 | 20.6 | 10.4 |
| 32 KS | *Lucina* cf. *dalmatina* Oppenheim | 38.5 | 36.9 | 17.4 |
| 33 KS | *Lucina dalmatina* Oppenheim | 17.9 | 20.4 | 13.6 |
| 34 KS | *Lucina dalmatina* Oppenheim | 18.6 | 24.2 | 8.7 |
| 35 KS | *Lucina prominensis* Oppenheim | 27.6 | 18.4 | 16 |
| 36 KS | *Lucina prominensis* Oppenheim | 23.5 | 20.1 | 12.1 |
| 37 KS | *Lucina prominensis* Oppenheim | 18 | 21.4 | 12.1 |
| 38 KS | *Lucina prominensis* Oppenheim | 18.3 | 21.6 | 13.3 |
| 39 KS | *Lucina prominensis* Oppenheim | 17 | 17.9 | 7.3 |

**Table 4:** Measured Lucinidae shells from the CNHM collection "Tertiary fauna of the Paris Basin". Revised names are presented in **Table 5**.

| Inventory number | Species name | Height, H (mm) | Length, L (mm) | Width, W (mm) |
|---|---|---|---|---|
| 113 | *Lucina columbella* Lamarck | 16.9 | 16.4 | 6.9 |
| 113 bb | *Lucina columbella* Lamarck | 15.4 | 15.6 | 6.9 |
| 114.$_1$ | *Lucina heberti* Deshays | 15.7 | 16.1 | 4.3 |
| 114.$_2$ | *Lucina heberti* Deshays | 14 | 15.4 | 3.9 |
| 114.$_3$ | *Lucina heberti* Deshays | 14.2 | 15.1 | 3.4 |
| 114.$_4$ | *Lucina heberti* Deshays | 14.6 | 15.8 | 3.3 |
| 115.$_1$ | *Lucina elegans* Deshayes | 22.2 | 24.4 | 4.4 |
| 115.$_2$ | *Lucina elegans* Deshayes | 14.8 | 16 | 3.5 |
| 115.$_3$ | *Lucina elegans* Deshayes | 10.9 | 11.2 | 2.6 |
| 116.$_1$ | *Lucina elegans* Deshayes | 14.7 | 15.9 | 3.6 |
| 116.$_2$ | *Lucina elegans* Deshayes | 14.4 | 15.7 | 2.4 |
| 116.$_3$ | *Lucina elegans* Deshayes | 12.8 | 13.4 | 2.5 |
| 116.$_4$ | *Lucina elegans* Deshayes | 11.9 | 13 | 3.5 |
| 116.$_5$ | *Lucina elegans* Deshayes | 8.4 | 10.5 | 1.9 |
| 117.$_1$ | Lucina pulchella Lamarck | 13.2 | 15.3 | 4 |
| 117.$_2$ | Lucina pulchella Lamarck | 12.8 | 13.9 | 3.6 |
| 118.$_1$ | *Lucina saxorum* Deshayes | 21.3 | 20.3 | 4.5 |
| 118.$_2$ | *Lucina saxorum* Deshayes | 17.9 | 18.4 | 4.3 |
| 118.$_3$ | *Lucina saxorum* Deshayes | 17.7 | 17.9 | 4.3 |
| 118.$_4$ | *Lucina saxorum* Deshayes | 15.7 | 16.3 | 3.6 |
| 118.$_5$ | *Lucina saxorum* Deshayes | 16 | 16.8 | 2.9 |
| 118.$_6$ | *Lucina saxorum* Deshayes | 15.8 | 16.4 | 3.8 |
| 118.$_7$ | *Lucina saxorum* Deshayes | 14.8 | 15.6 | 2.9 |
| 118.$_8$ | *Lucina saxorum* Deshayes | 14.1 | 14.5 | 2.5 |
| 118.$_9$ | *Lucina saxorum* Deshayes | 16.3 | 16.5 | 2.9 |
| 118.$_{10}$ | *Lucina saxorum* Deshayes | 13.8 | 13.7 | 2.8 |
| 119.$_1$ | *Lucina scalaris* Deshayes | 17.8 | 17.4 | 4.9 |
| 119.$_2$ | *Lucina scalaris* Deshayes | 13.1 | 13.2 | 3.1 |
| 119.$_3$ | *Lucina scalaris* Deshayes | 13.5 | 12.8 | 3.7 |
| 119.$_4$ | *Lucina scalaris* Deshayes | 10.4 | 11.1 | 2.2 |
| 119.$_5$ | *Lucina scalaris* Deshayes | 9.6 | 10.5 | 2.2 |
| 119.bb | *Lucina scalaris* Deshayes | 8.5 | 8.4 | 2.3 |
| 120. | *Lucina unicata* Defrance | 19.5 | 20.3 | 2.1 |
| 121.$_1$ | *Lucina sulcata* Lamarck | 12.5 | 12.9 | 3.7 |
| 121.$_2$ | *Lucina sulcata* Lamarck | 10.9 | 11.4 | 2.9 |
| 121.$_3$ | *Lucina sulcata* Lamarck | 4.5 | 5.1 | 1.5 |
| 122.$_1$ | *Lucina sulcata* Lamarck | 12.2 | 12.5 | 3.6 |
| 122.$_2$ | *Lucina sulcata* Lamarck | 11.8 | 11.5 | 3.1 |
| 122.$_3$ | *Lucina sulcata* Lamarck | 5.9 | 6.8 | 1.3 |
| 123.$_1$ | *Lucina squammula* Deshayes | 12.5 | 13.1 | 2.9 |
| 123.$_2$ | *Lucina squammula* Deshayes | 10.1 | 10.2 | 2.6 |
| 123.$_3$ | *Lucina squammula* Deshayes | 11 | 10.1 | 3.1 |
| 123.$_4$ | *Lucina squammula* Deshayes | 8.6 | 8.8 | 2.1 |
| 124.$_1$ | *Lucina saxorum* Lamarck | 19 | 19.3 | 4.9 |
| 124.$_2$ | *Lucina saxorum* Lamarck | 14.2 | 14.6 | 5.9 |
| 124.$_3$ | *Lucina saxorum* Lamarck | 12.6 | 12.8 | 5.4 |
| 124.$_4$ | *Lucina saxorum* Lamarck | 17.7 | 19.2 | 4.2 |
| 124.$_5$ | *Lucina saxorum* Lamarck | 16.3 | 16.5 | 3.6 |
| 124.$_6$ | *Lucina saxorum* Lamarck | 13.9 | 14.1 | 3.4 |
| 128.$_1$ | *Lucina contorta* Defrance | 20.5 | 34.8 | 3.6 |
| 128.$_3$ | *Lucina contorta* Defrance | 20.7 | 21.8 | 3.9 |
| 128.$_4$ | *Lucina contorta* Defrance | 17.6 | 21.5 | 4 |
| 129.$_1$ | *Lucina gibbosula* Lamarck | 19.1 | 19.7 | 4.8 |
| 129.$_2$ | *Lucina gibbosula* Lamarck | 17.8 | 20.1 | 4.6 |
| 129.$_3$ | *Lucina gibbosula* Lamarck | 16.1 | 19.5 | 4.1 |
| 129.$_4$ | *Lucina gibbosula* Lamarck | 14.5 | 15.6 | 6.2 |
| 129.$_5$ | *Lucina gibbosula* Lamarck | 14 | 15.5 | 4 |
| 129.$_6$ | *Lucina gibbosula* Lamarck | 14.5 | 15.9 | 4.1 |

| Inventory number | Species name | Height, H (mm) | Length, L (mm) | Width, W (mm) |
|---|---|---|---|---|
| 130.$_1$ | *Lucina connubrica* Lamarck | 33.7 | 34.9 | 8.9 |
| 130.$_2$ | *Lucina connubrica* Lamarck | 30.1 | 31.8 | 6.9 |
| 130.$_3$ | *Lucina connubrica* Lamarck | 22.9 | 25.3 | 4.3 |
| 131.$_1$ | *Lucina callosa* Deshayes | 11.1 | 11.6 | 3.1 |
| 131.$_2$ | *Lucina callosa* Deshayes | 10.9 | 11.9 | 2.8 |
| 131.$_3$ | *Lucina callosa* Deshayes | 9.7 | 10.3 | 3.4 |
| 132.$_1$ | *Lucina rigaulti* Deshayes | 13.4 | 15.1 | 3.7 |
| 132.$_2$ | *Lucina rigaulti* Deshayes | 10.4 | 10.7 | 3.6 |
| 132.$_3$ | *Lucina rigaulti* Deshayes | 10.3 | 10.6 | 3.4 |
| 132.$_4$ | *Lucina rigaulti* Deshayes | 10.1 | 10.4 | 3.4 |
| 132.$_5$ | *Lucina rigaulti* Deshayes | 9.2 | 9.4 | 3.3 |
| 132.$_6$ | *Lucina rigaulti* Deshayes | 8.6 | 8.8 | 3.2 |
| 133.$_1$ | *Lucina concentrica* Lamarck | 33.2 | 34.7 | 7.5 |
| 133.$_2$ | *Lucina concentrica* Lamarck | 28.3 | 32.6 | 6.2 |
| 133.$_3$ | *Lucina concentrica* Lamarck | 30.5 | 33.6 | 6.3 |
| 133.$_4$ | *Lucina concentrica* Lamarck | 29.8 | 30.5 | 6.9 |
| 133.$_5$ | *Lucina concentrica* Lamarck | 31.9 | 32.9 | 6.7 |
| 133.$_6$ | *Lucina concentrica* Lamarck | 29.3 | 31.2 | 5.8 |
| 133.$_7$ | *Lucina concentrica* Lamarck | 20.9 | 24.6 | 4 |
| 134.$_2$ | *Lucina gigantea* Deshayes | 44.4 | 51.5 | 7.2 |
| 134.$_3$ | *Lucina gigantea* Deshayes | 37.2 | 43.5 | 8.8 |
| 135. | *Lucina gigantea* Deshayes | 71.1 | 76.8 | 9.3 |
| 136.$_1$ | *Lucina gibbosula* Lamarck | 16.9 | 18.6 | 5.1 |
| 136.$_2$ | *Lucina gibbosula* Lamarck | 16 | 18.3 | 4.7 |
| 136.$_3$ | *Lucina gibbosula* Lamarck | 16.6 | 18.2 | 4.8 |
| 136.$_4$ | *Lucina gibbosula* Lamarck | 16.7 | 17.3 | 4.1 |
| 136.$_5$ | *Lucina gibbosula* Lamarck | 15.8 | 16.9 | 3.9 |
| 136.$_6$ | *Lucina gibbosula* Lamarck | 13.5 | 14.5 | 3.7 |
| 136.$_7$ | *Lucina gibbosula* Lamarck | 7.2 | 8.3 | 2.4 |
| 139. | *Lucina albella* Lamarck | 12.2 | 12.1 | 5.5 |
| 142.$_1$ | *Lucina saxorum* Lamarck | 13.2 | 14.3 | 3.2 |
| 142.$_2$ | *Lucina saxorum* Lamarck | 13.7 | 14.2 | 3.3 |
| 142.$_3$ | *Lucina saxorum* Lamarck | 11.2 | 11.5 | 2.8 |
| 142.$_4$ | *Lucina saxorum* Lamarck | 7.7 | 8.3 | 2.4 |
| 143.$_1$ | *Lucina circinaria* Lamarck | 18.2 | 16.8 | 4.3 |
| 143.$_2$ | *Lucina circinaria* Lamarck | 17.2 | 18.1 | 3.7 |
| 143.$_3$ | *Lucina circinaria* Lamarck | 16.7 | 17.8 | 4.1 |
| 143.$_4$ | *Lucina circinaria* Lamarck | 14.8 | 15.3 | 3.3 |
| 143.$_5$ | *Lucina circinaria* Lamarck | 15.7 | 16.7 | 3.3 |
| 143.$_6$ | *Lucina circinaria* Lamarck | 15.1 | 16.5 | 3.3 |
| 143.$_7$ | *Lucina circinaria* Lamarck | 14.8 | 15.9 | 3.5 |
| 143.$_8$ | *Lucina circinaria* Lamarck | 13.7 | 14.7 | 2.7 |
| 143.$_9$ | *Lucina circinaria* Lamarck | 11.4 | 11.8 | 2.8 |
| 143.$_{10}$ | *Lucina circinaria* Lamarck | 9.1 | 10.3 | 2.2 |
| 144.$_1$ | *Lucina concentrica* Lamarck | 24.3 | 26.3 | 5.5 |
| 144.$_2$ | *Lucina concentrica* Lamarck | 23.2 | 25.4 | 6.4 |
| 145.$_1$ | *Lucina lapidum* Lamarck | 18.4 | 19.5 | 4 |
| 145.$_2$ | *Lucina lapidum* Lamarck | 18.8 | 18 | 4.8 |
| 145.$_3$ | *Lucina lapidum* Lamarck | 18.9 | 19.6 | 4.1 |
| 146.$_1$ | *Lucina proxima* Deshayes | 17.5 | 18 | 3.9 |
| 146.$_2$ | *Lucina proxima* Deshayes | 16.1 | 15.7 | 4.3 |
| 146.$_4$ | *Lucina proxima* Deshayes | 14.5 | 14.7 | 3.7 |
| 146.$_5$ | *Lucina proxima* Deshayes | 13.7 | 13.5 | 3.2 |
| 146.$_6$ | *Lucina proxima* Deshayes | 13.8 | 12.6 | 2.3 |
| 146.$_7$ | *Lucina proxima* Deshayes | 11.8 | 11.6 | 3.1 |
| 146.$_8$ | *Lucina proxima* Deshayes | 11.7 | 11.6 | 2.5 |
| 146.$_{10}$ | *Lucina proxima* Deshayes | 11.3 | 12.1 | 2.5 |
| 146.$_{11}$ | *Lucina proxima* Deshayes | 10.1 | 10.5 | 2 |
| 146.$_{12}$ | *Lucina proxima* Deshayes | 11.7 | 11.9 | 3.6 |
| 146.$_{13}$ | *Lucina proxima* Deshayes | 10.4 | 10.7 | 2.6 |

**Table 5:** Revision of the Lucinidae species names and comparison between the findings from Croatia and Paris Basin. Light orange rows represent the specimens present in Croatia and in the Paris Basin. [1] „Paleobiology Database. Fossilworks.“ (**fossilworks.org**), [2] „World Register of Marine Species (**WORMS, www.marinespecies.org**).

| Species name | | Number of specimens | Croatia (Dalmatia) | Paris Basin |
|---|---|---|---|---|
| CNHM Inventory book | Revised name | | | |
| *Lucina gigantea* Deshayes | *Pseudomiltha gigantea* (Deshayes, 1825)[1] | 4 | 1 | 3 |
| *Lucina zignoi* Oppenheim | *Saxolucina saxorum* Lamarck 1806[1] | 2 | 2 | / |
| *Lucina escheri* Mayer | no available data[1,2] | 2 | 2 | / |
| *Lucina dalmatina* Oppenheim | no available data[1,2] | 11 | 11 | / |
| *Lucina saxorum* Lamarck | *Saxolucina saxorum* Lamarck 1806[1] | 36 | 16 | 20 |
| *Lucina prominensis* Oppenheim | no available data[1,2] | 10 | 10 | / |
| *Lucina illyrica* Oppenheim | no available data[1,2] | 1 | 1 | / |
| *Phacoides (Lucinoma) dinarii* Kühn | no available data[1,2] | 3 | 3 | / |
| *Lucina columbella* Lamarck | *Lucina (Linga) columbella* Lamarck 1818[1] | 2 | / | 2 |
| *Lucina heberti* Deshays | no available data[1,2] | 4 | / | 4 |
| *Lucina elegans* Deshayes | *Monitilora (Monitilora) elegans* Defrance 1823[1] | 8 | / | 8 |
| *Lucina pulchella* Lamarck | *Boeuvia pulchella* Agassiz 1845[1]; *Liralucina lyngei* M. Huber, 2015[2] | 2 | / | 2 |
| *Lucina scalaris* Deshayes | no available data[1,2] | 6 | / | 6 |
| *Lucina unicata* Defrance | no available data[1,2] | 1 | / | 1 |
| *Lucina sulcata* Lamarck | *Cavilucina (Cavilucina) sulcata* Lamarck 1806[1] | 6 | / | 6 |
| *Lucina squammula* Deshayes | no available data[1,2] | 4 | / | 4 |
| *Lucina contorta* Defrance | *Miltha (Eomiltha) contorta* Defrance 1823[1] | 3 | / | 3 |
| *Lucina gibbosula* Lamarck | *Gibbolucina (Gibbolucina) gibbosula* Lamarck 1806[1] | 13 | / | 13 |
| *Lucina connubrica* Lamarck | no available data[1,2] | 3 | / | 3 |
| *Lucina callosa* Deshayes | no available data[1,2] | 3 | / | 3 |
| *Lucina rigaulti* Deshayes | no available data[1,2] | 6 | / | 6 |
| *Lucina concentrica* Deshayes | *Codakia (Epilucina) concentrica* Lamarck 1806[1] | 9 | / | 9 |
| *Lucina albella* Lamarck | *Parvilucina (Callucinella) albella* Lamarck 1806[1] | 1 | / | 1 |
| *Lucina circinaria* Lamarck | no available data[1,2] | 10 | / | 10 |
| *Lucina lapidum* Lamarck | no available data[1,2] | 3 | / | 3 |
| *Lucina proxima* Deshayes | no available data[1,2] | 11 | / | 11 |

## 4. Results

The descriptive biometric analysis of the measured elements of the height, length and width of the lucinid shells and their morphometric indices can be seen on **Figure 3**.

As presented on **Figure 3**, three groupings can be distinguished: first group make the specimens from the Paris Basin (black dots), second group the specimens from the Imotski-Lažete area (violet rectangulars), and to the third group belong the Lucinidae from Promina Mt. (blue diamonds and red rectangular). Lucinidae from the Paris Basin are smaller in size than the specimens from Croatia, and in size they are similar to the specimens from the Promina Mt. than Imotski area. Lucinidae from Imotski-Lažete are more scattered, bigger in size and less comparable with the samples from the Promina Mt. and the Paris Basin. Specimens from Paris Basin are in all graphs more or less homogenous, and the most scattered are the samples from Imotski-Lažete. As the elongation grows, roundness and convexity have lower values in Lucinidae from Paris Basin, and the samples from Croatia are dispersed. Convexity and roundness are proportional in all specimens, showing higher values in specimens from Croatia (**Figure 3**).

Differences between samples from Croatia (Promina Mt. area and Imotski-Lažete) are visible on **Figure 3** by grouping of those samples, and Imotski-Lažete specimens being more scattered and of bigger dimensions. On **Figure 4** we show the relations between height, length and width of the lucinid shells from Promina Mt. and Imotski-Lažete.
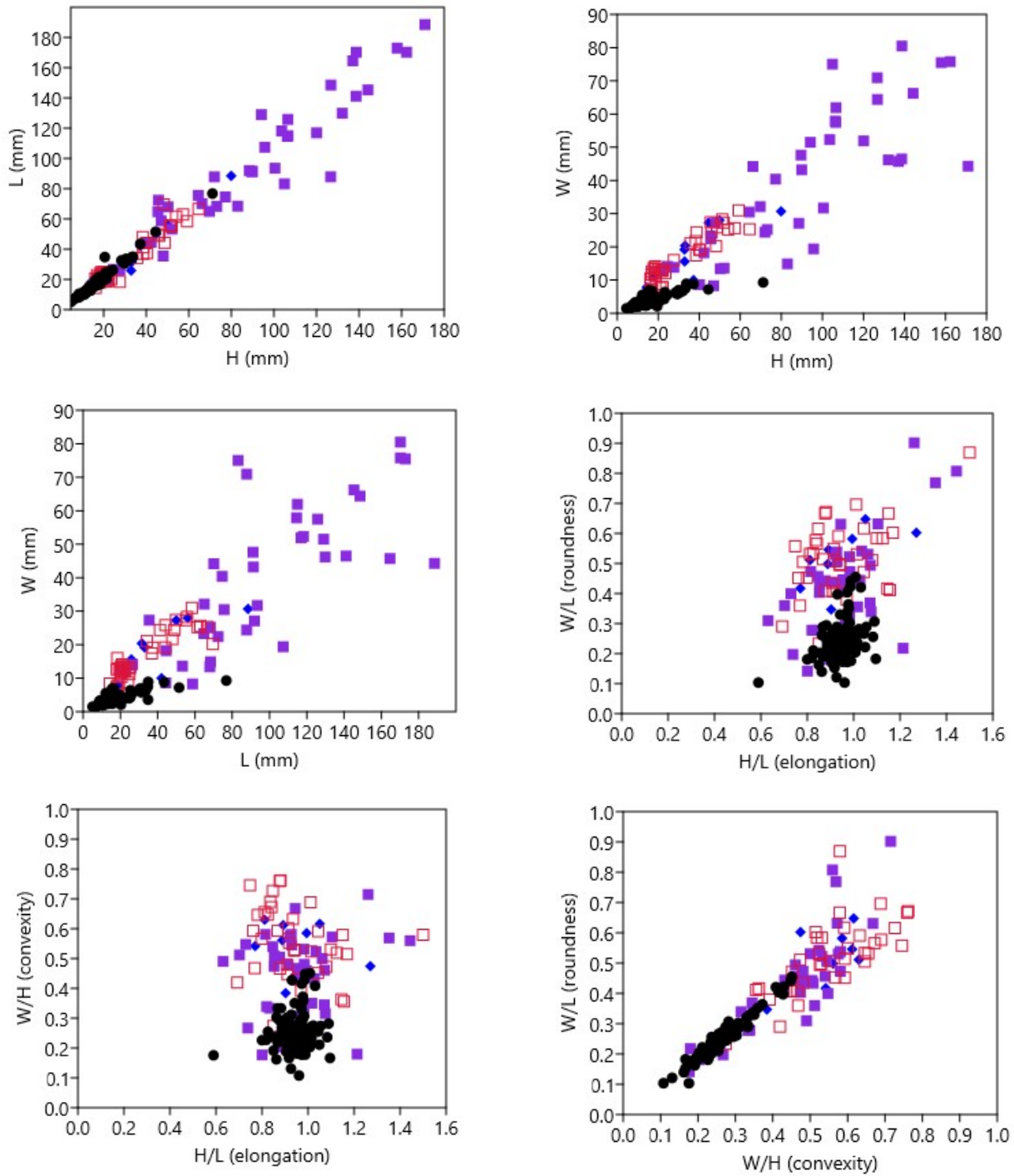
**Figure 3:** Relations of the measured elements of height (H), length (L) and width (L) of the Lucinidae shells from Promina Mt. (blue diamond, red rectangular; each sign representing one Museum collections), Imotski-Lažete (violet rectangular) and Paris Basin (black dots)
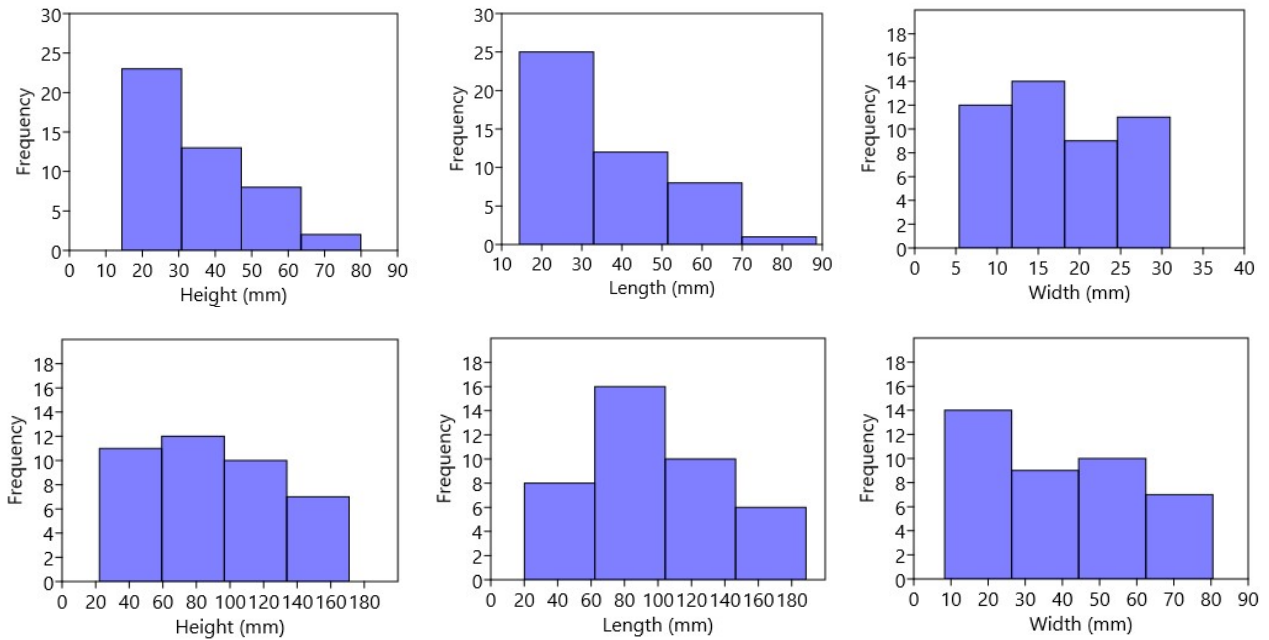
**Figure 4:** Histograms of height, length and width of the shells of Lucinidae from Promina Mt. (upper row) and Imotski-Lažete (bottom row)

**Figure 4** shows differences between the specimens from Croatia. Smaller height range values of Lucinidae show the specimens from Promina Mt., and Lucinidae from Imotski-Lažete have wider range value and they are more or less evenly distributed. The length values of Promina Mt. specimens are similar as the one regarding the height of the shell. Lucinidae from Imotski-Lažete again have wider lenght value range, but they are not so evenly distributed as in height histogram, here we see more middle values. Value range of the shell width is again narrower for the samples from Promina Mt., but here samples from both localities are more or less evenly distributed, with prevailing smaller values of shell thickness.

The comparison between Lucinidae species present in the Paris Basin and Croatia based on the revision of the names from the Museum inventory book and the fossil databases is shown in **Table 5**. Only two species are mutual to the localities, *Pseudomiltha gigantea* and *Saxolucina saxorum*, two extinct species of the family Lucinidae. To see differences in the sizes of the mutual species, we present the histograms of the *Saxolucina saxorum* shell specimens from Croatia and Paris Basin on **Figure 5**. Since there is only one specimen of *P. gigantea* present in Croatia, the sample size is not sufficient for the histogram plotting.

As presented on **Figure 5**, *S. saxorum* shells from Croatia have a smaller range of height and length values than the specimens from Paris Basin. Looking at the height, they are more or less equally distributed in those ranges, and comparing to the shell length, the specimens are either smaller or bigger. Lucinidae from the Paris Basin have a bigger range of shell height and length values, and they are more homogenously distributed in the smaller specimens, with a few of them larger. Range of shell width values is higher in lucinids from Croatia, but again the specimens from Paris Basin are more homogenous and show lower values.
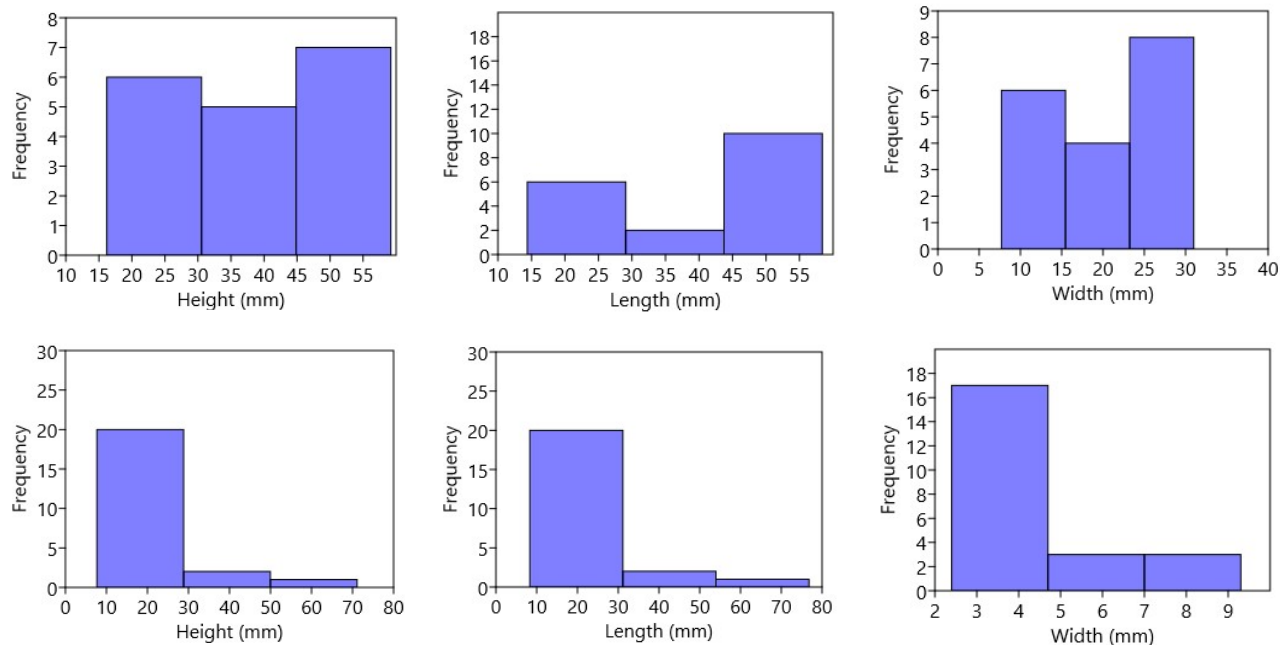
**Figure 5:** Histograms of height, length and width of the shells of the *Saxolucina saxorum* specimens from Croatia (upper row) and Paris Basin (bottom row)

## 5. Discussion and Conclusions

Bivalves Lucinidae are today widely distributed in various marine habitats, from the intertidal zone to bathyal depths of over 2100 m, over a broad geographical range (60°N−55°S). As **Taylor and Glover (2006, and references therein)** describe, Lucinidae occur in mangrove muds, intertidal and offshore muds, offshore locations where sunken vegetation accumulates, cold seeps and mud oxygen minimum zones (some species) and a single species from a hydrothermal vent. Lucinidae are very diversified group of bivalves with more than 400 living species, and usually are considered as a shallow water group with recent greatest species richness in the coral reef and seagrass environments of the tropical Atlantic and Indo-West Pacific (**Taylor et al., 2014**). In several families of bivalves, including Lucinidae, the nutritional strategy of chemosymbiosis with sulphide-oxidizing and less commonly methane-oxidizing bacteria is recognized, and the widespread sulphide-rich habitats with chemosymbiotic organisms are the suboxic zones of the marine sediments, where most of the lucinids live (e.g., **Taylor and Glover, 2006; Taylor et al., 2014**).

As presented in chapter Results, there are differences in shell morphology regarding its size between Eocene Lucinidae from Croatia (Promina Mt. and Imotski-Lažete), and from the comparative specimens of the Paris Basin. Samples from Croatian localities have higher height, length and width values, and the samples from Paris Basin showed better grouping in the descriptive analyses being more homogenous in size. Higher values of the measured shell parameters (height, length, width) seen on the samples from Croatia could indicate the more favourable paleoecological conditions that result in the bigger size of the Lucinidae shell. However, more samples are required to get a more precise conclusion. Generally, morphology of a species shell depends on various abiotic and biotic factors, for example latitude, depth, shore level, tidal level, currents, water turbulences, wave exposure, type of bottom, type of sediment, characteristics of the seagrass bed, the density of the population, predation, trophic conditions, burrowing behaviour etc. (e.g., **Derbali et al., 2018 and references therein; Modestin, 2017 and references therein**).

Localities of Promina Mt. and Lažete near Imotski are rich in Lucinidae findings, which are also the most numerous bivalves here recorded. At Lažete locality, near Imotski, „gigantic" dimensions of Lucinidae shells are recognized, as well as at the nearby Eocene localities (**Sremac et al., 2015**). This big shell sizes are indicative for the period of the Paleocene/Eocene thermal maximum, and Eocene climatic events (**Figure 6**). Eocene malacofauna represented in this paper and previous research by **Sremac et al. (2014, 2015)** is of the Middle and Upper Eocene age (see references in chapter 2). The numerous molluscs recorded in the Eocene deposits of the Promina Mt. and Imotski-

Lažete, including the localities in **Sremac et al. (2014, 2015)**, correspond to the global biodiversity of molluscs during the Eocene (**Figure 6**).
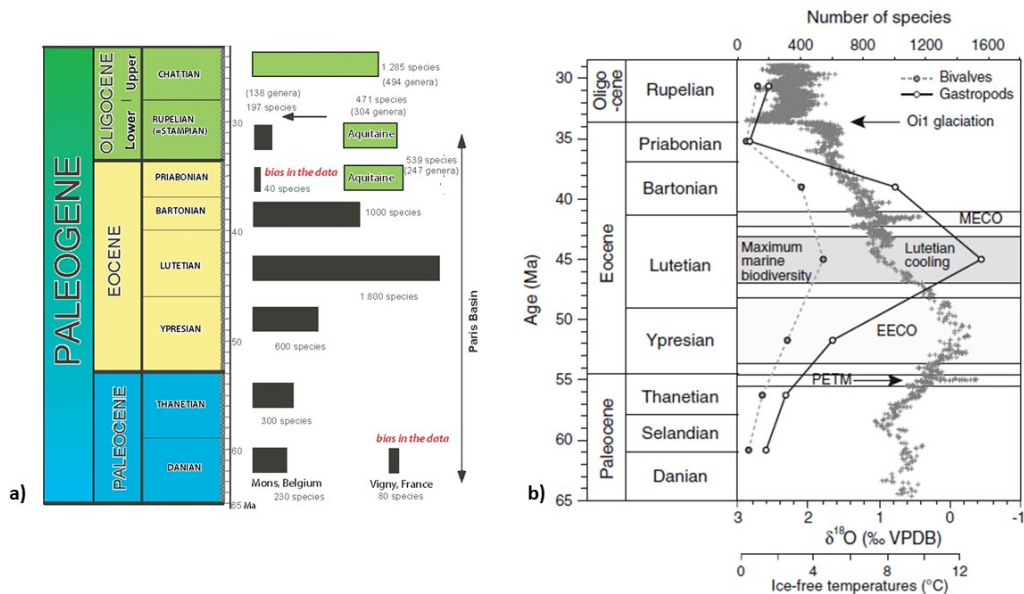


**Figure 6:** Richness of molluscan fauna during the Eocene compared to the climatic conditions on the example of Paris Basin. a) Gastropods biodiversity after **Lozouet (2014)**; b) Climate events and molluscs species richness during the Eocene after **Huyghe et al. (2012)**.

According to the published papers (e.g., **Sakač, 1965; Sakač et al., 1984; Sremac et al., 2014, 2015**) we can see that the rich lucinids of the Western Tethys bioprovince findings possibly correspond to the age of the Eocene „bloom" during the Lutetian, Middle Eocene climatic optimum, and gradual decrease of the molluscs biodiversity after the Lutetian (**Figure 6**). Lutetian molluscan fauna of the Paris Basin is one of the finest in the world and records the greatest Cenozoic shallow-water marine biodiversity, with around 2700 marine species, of which 1500 species belong to gastropods and 540 to bivalve species (e.g., **Lozouet, 2014; Huyghe et al., 2012**) (**Figure 6**). After **Huyghe et al. (2012)** Lutetian was a warm period in the Paris Basin, with mean annual temperatures around 20°C, maximum summer temperatures close to 30°C and mild winters, and the southern part of the Mediterranean Sea could be considered as a modern model of the Lutetian climate of the Paris Basin. To get more insight into the Eocene malacofauna and paleoecology, comparisons with other localities are necessary. For example, **Huyghe et al. (2012)** considered the island arcs of the western Tethys as the centres of a large hotspot, analogue to the today's Indo-Pacific biota, and the Lutetian malacofauna of the northern Italy as a comparison with the Paris Basin.

As we presented in this paper, Lucinidae findings in the Eocene of Croatia are rich, and the biometrical analyses showed differences in shell morphology not only among the localities in Croatia, but also among the specimens from the comparative locality of the Paris Basin. The differences can be a product of numerous factors, and for the further research of the Eocene malacofauna from Croatia the first step is the revision of the Lucinidae specimens to see the distribution of the species and the mutual records with other representative localities in Europe. The concluding step to our further work is the comparison with the molluscs from the other contemporaneous nearby Eocene localities, as it is started by **Sremac et al. (2014)**, to fulfil the current knowledge on the paleoenvironments of Croatia and paleoecological conditions during the Eocene.

# 6. References

Čvorović, B., (2000): Biostratigrafska analiza klastičnih naslaga eocena Dabrice (Hercegovina) na osnovi faune molusaca (*Biostratigraphic analysis of the Eocene clastic deposits of Dabrica, Hercegovina based on the molluscs fauna*). Prirodoslovno-matematički fakultet Sveučilišta u Zagrebu, 145 pp. (*in Croatian*)

Dainelli, G., (1905): La fauna eocenica di Bribir in Dalmazia. Parte secondo. Pal. Ital.,11, 1-92.

Derbali, A., Hadj Taieb, A., Kammoun, W., Jarboui, O. and Ghorbel, M. (2017): Shell morphometric relationships of the most common bivalve species (Mollusca: Bivalvia) in southern Tunisian waters. Cah. Biol. Mar., 59, 481–487. DOI: 10.21411/CBM.A.6C9B5600

Hammer, Ø.; Harper, D.A.T. and Ryan, P.D. (2001): PAST: Paleontological statistics software package for education and data analysis. Palaeontologia Electronica 4(1): 9pp. http://palaeo-electronica.org/2001_1/past/issue1_01.htm

Huyghe, D.; Merle, D.; Lartaud, F.; Cheype, E. and Emmanuel, L. (2012): Middle Lutetian climate in the Paris Basin: implications for a marine hotspot of paleobiodiversit. Facies, 58, 587–604. DOI 10.1007/s10347-012-0307-3

Kochansky, V. (1947): Eocenski koralji i hidrozoi Dubravice i Ostrovice u Dalmaciji (*Les coralliaires et hydrozoaires Eocenes de Dubravica et Ostrovica en Dalmatie – in Croatian with French summary*). Geološki vjesnik, 5, 48–67.

Kühn, O. (1946): Das Alter der Prominaschichten und der intereozänen Gebirgsbildung. Jahrb. Geol. Bundesanst., Bd 91/ 1- 2, 49-94.

Lozouet, P. (2014): Temporal and latitudinal trends in the biodiversity of European Atlantic Cenozoic gastropod (Mollusca) faunas. A base for the history of biogeographic provinces. Carnets de Géologie [Notebooks on Geology], 14, 14, 273–314.

Malvić, T., Bošnjak, M., Velić, J., Sremac, J., Ivšinović, J., Pimenta Dinis, M.A. and Barudžija, U. (2020): Recent Advances in Geomathematics in Croatia: Examples from Subsurface Geological Mapping and Biostatistics. Geosciences, 10, 188, 1–22. doi:10.3390/geosciences10050188

Milan, A. (1956): Prilog poznavanju eocenske faune moluska sjeverne Dalmacije (*Beiträge zur Kenntnis der Eozänfauna Mollusca Norddalmatiens – in Croatian with German summary*). Geološki vjesnik, 10, 57–69.

Mégnien, C. and Mégnien, F. (1980): Synthése gèologique du Bassin du Paris. Mèm. BRGM, 101, 1-400, Paris.

Modestin, E. (2017): Morphological variations of the shell of the bivalve Lucina pectinata (Gmelin, 1791). Journal of Advances in Biology, 10, 2, 2092–2107. DOI : 10.24297/jab.v10i2.6355

Sakač, K. (1965): O naslagama krede i mlađeg paleogena na području Imotskog u srednjoj Dalmaciji (*On Cretaceous and Late Paleogene deposits in the area of Imotski in central Dalmatia – in Croatian with English summary*). Acta geologica, 5, 331–339.

Sakač, K.; Šinkovec, B.; Jungwirth, E. and Lukšić, B. (1984): Opća obilježja geološke građe i ležišta boksita područja Imotskog (*Common Features of Geological Structure and Bauxite Deposits in the Imotski Region, Dalmatia-Hercegovina, Yugoslavia – in Croatian with English summary*). Geološki vjesnik, 37, 153–174.

Schubert, R. (1905): Zur Stratigraphie des istrisch-norddalmatinischen Mitteleocäns. Jahrb. Geol. Reichsanst., 55,153-188.

Sremac, J.; Glamuzina, G.; Prlj Šimić, N.; Bošnjak Makovec, M.; Mikulić, I. and Drempetić, R. (2015): Velike eocenske lucinide (Mollusca: Bivalvia) – indikatori postojanja podmorskih metanskih ispusta na području južne Hrvatske i Hercegovine (*Giant Eocene lucinids (Mollusca: Bivalvia) – indicators of the submarine methane vents in the area of south Croatia and Herzegovina*). Rudarsko-geološki glasnik, 18, 121–134. (*in Croatian*)

Sremac, J.; Bošnjak Makovec, M.; Prlj Šimić, N.; Glamuzina, G. and Mikulić, I. (2014): Eocenska marinska makrofauna područja Imotski–Ričice-Tribistovo: paleontoloski dragulj i geoturisticki "as u rukavu" (*Eocene marine macrofauna of Imotski-Ričice-Tribistovo area: paleontological jewel and "an ace up the sleeve"*). Rudarsko-geološki glasnik, 18, 121–134. (*in Croatian with English abstract*)

Taylor, D. and Glover, E.A. (2006): Lucinidae (Bivalvia) – the most diverse group of chemosymbiotic molluscs. Zoological Journal of the Linnean Society, 148, 421–438.

Taylor, D.; Glover, E.A. and Williams, S.T. (2014): Diversification of chemosymbiotic bivalves: origins and relationships of deeper water Lucinidae. Biological Journal of the Linnean Society, 111, 401–420.

## Internet sources:

URL 1: Google Earth Pro, https://earth.google.com/web/
URL 2: Paleobiology Database. Fossilworks. www.fossilworks.org (accessed 14 September, 2020)
URL 3: WoRMS Editorial Board (2020). World Register of Marine Species. Available from http://www.marinespecies.org at VLIZ. Accessed 2020-09-14. doi:10.14284/170

# SAŽETAK

**Biometrijska analiza eocenskih školjkaša Lucinidae iz Hrvatske**

Na eocenskim lokalitetima na području Promine i Imotskog (Lažete) u Hrvatskoj prikupljeni su brojni primjerci morskih školjkaša iz familije Lucinidae. Primjerci se danas čuvaju u Hrvatskom prirodoslovnom muzeju u Zagrebu. Na temelju mjera ljuštura lucinida napravljena je biometrijska analiza kako bi se usporedile morfometrijske karakteristike visine, širine i debljine ljuštura primjeraka na lokalitetima u Hrvatskoj, kao i komparativnih primjeraka iz Pariškog bazena koji se čuvaju u Muzeju. Morfometrijske analize pokazale su razlike između primjeraka iz Hrvatske, koji se također razlikuju i od primjeraka iz Pariškog bazena. Lucinide iz Hrvatske imaju veće morfometrijske vrijednosti i ukazuju na moguće povoljnije paleoekološke uvjete za veći rast ljuštura školjkaša. Ovaj rad predstavlja prvi korak u daljnjoj biometrijskoj analizi eocenske malakofaune prikupljene na području Hrvatske i njezine usporedbe sa susjednim istovremenim lokalitetima.

**Ključne riječi**: biometrija, Lucinidae, eocen, Hrvatska

## Acknowledgment

## Author's contribution

**Marija Bošnjak (1)** (Dr, senior curator, paleontology, geomathematics) provided the biometry analysis, preparation of computer graphs and the graphics, comparison, interpretation and presentation of the results. **Nediljka Prlj Šimić (2)** (Mr.sc., senior curator, paleontology, geomathematics) provided the measuring of 204 Lucinidae shells, revision of 26 Lucinidae species names, methodological data, comparison and presentation of the results. **Jasenka Sremac (3)** (Dr, Full Professor, geology, paleontology, paleoenvironment) provided the comparison of data, interpretation and presentation of the results.

# Morphometric characteristics and origin of Paleogene macroids from beach gravels in Stanići (vicinity of Omiš, Southern Croatia)

**Jasenka Sremac[1]; Filip Huić [2]; Marija Bošnjak[3]; Renato Drempetić[4]**

[1] Faculty of Science, Department of Geology, University of Zagreb, 10000 Zagreb, Croatia; http://orcid.org/0000-0002-4736-7497
[2] Oboj 9 D, 10000 Zagreb, Croatia
[3] Croatian Natural History Museum, 10000 Zagreb, Croatia; http://orcid.org/0000-0002-1851-1031
[4] Dalmatinska 12, 10000 Zagreb, Croatia

## Abstract

A collection comprising 322 samples of macroid pebbles was found at the beach at Stanići near Omiš (Dalmatia, southern Croatia), derived from the beach-rocks by the marine erosional processes. Macroids were measured by a digital caliper, providing information on their size and shape. Thin sections microscopy pointed to red algae as the dominant macroid builders, associated with acervulinid foraminifera and some other encrusters. Morphometric analyses of macroid shapes, together with micropaleontological analyses, enable the recognition of two macroid groups. Rhodolits and less complex macroids are dominantly spheroidal, exhibiting normal size distribution with good correlation. Multispecific macroids (composed of red algae, acervulinid foraminifera and other encrusters) exhibit a variety of shapes, mostly discoidal or elongate, with poor correlation. Rhodolits were derived from the Eocene bioclastic rocks rich in nummulitids and other benthic biota, informally known as "Nummulitic breccias". Blocks of these rocks, scattered along the beaches in the vicinity of Omiš, are a part of rockfall and avalanche deposits developed as megabeds during the collapse of Dinaride shelf margins.

**Keywords:** Macroids, measurements, bioconstructors, Eocene, Croatia

## 1. Introduction

The wider area of Omiš during the Paleogene was a part of the North Dalmatian Foreland Basin situated in front of the tectonically developed Dinaride structures. A ramp formed on its distal part was characterized by carbonate deposition until the Middle Eocene (**Ćosović et al., 2008; Babić and Zupanič, 2007, 2008, 2012; Vlahović and Velić, 2009; Španiček et al., 2017; Ćosović et al., 2018 and references therein**). The subsidence of carbonate ramp enabled the deposition of a 220 m thick carbonate succession, starting with terrestrial and marginal marine carbonates. Foraminiferal limestones are overlain with clastic/carbonate Transitional Beds and Flysch deposits, mostly deposited in the Middle and Upper Eocene. Shallowing-upward processes resulted in gradual replacement of Flysch with molasse Promina Beds, so these two types of deposits are in some places contemporaneous (**Ćosović et al., 2008**). Molasse deposition continued into the Oligocene and Miocene epochs (**Marinčić et al., 1977; Ćosović et al., 2008, Mrinjek et al., 2012; Ćosović et al., 2018 and references therein**).

During the Upper Eocene rockfall and avalanche processes lead to the formation of broadly distributed megabeds, comprising the foraminiferal packstones (also known as "Nummulite breccias") and blocks of older rocks, as described in several papers (e.g., **Marjanac, 1991, 1996; Marjanac and Ćosović, 2000**).

Paleogene fossils, particularly large benthic foraminifera extracted from megabed olistoliths, occur as bioclasts and within beach pebbles at several places along the eastern Adriatic coast, including the vicinity of Omiš in Dalmatia (**Figure 1**). Macroids, in most cases rhodolits, are also abundant, but they were not previously collected, as they look like common pebbles, except of their slightly tuberculate surface (**Figure 2c**). Such extracted macroid bioconstructions give us insight on their real shape and size, which can easily be observed and measured.

Jasenka Sremac
*jsremac@geol.pmf.hr*

**Figure 1:** Geographic position (Google Earth, accessed August 2020) and geological map of the Omiš-Stanići area (segment from the Basic Geological Map OMIŠ, K 33-22; **Marinčić et al., 1976**)

The aim of this study is to analyse the connection between the shape/size of the collected macroids with their builders and to compare them with contemporary bioconstructions in the wider region. Authors also tested some statistical tools from other geological fields in order to cross-validate the obtained geomathematical results.

## 2. Materials and methods

During the several field excursions, between June 2019 and July 2020, we randomly collected 322 samples of macroids on the beaches in the vicinity of Omiš in central Dalmatia. Most of the material was derived after the strong Jugo (south-easterly wind) storm-waves at the Stanići beach, at the position 43° 24' 45,41" N; 16° 43' 54,26" (**Figures 1 and 2**).



**Figure 2:** "Nummulitic breccia"(a) and part of the collected macroids (b) from the beach in Stanići. Macroid surface is always a bit bulbous (c).

Altogether thirty thin sections were prepared from randomly picked samples larger than 20 mm (to avoid the destruction of macroids by a saw blade during the cutting process) at the Wet laboratory, Department of Geology, Faculty of Science. Among them, nine were made from the blocks of source rocks (sample FH/M1 – one thin section; sample FH/O – five thin sections; FH/F1 and F2– three thin sections). Twenty-one preparation was made from pebbles, fifteen of which proved to be macroids (samples FH/1, 1.2,1.3,1.x,2.,3.,4.,5.,14, C1, V1a, V1b, V3, V4 and 6) .

Photomicrographs were done using the Olympus SZX10 Microscope with adjusted Canon EOS 1100D Camera at the Department of Geology, Faculty of Science.

Macroid shapes, when analysed from thin sections, were classified according to the basic rhodolith classification (**Sneed and Folk, 1958**; **Bosence, 1983**).

**Table I:** Classification of rhodoliths as proposed by **Bosence (1983)**, simplified

| No. of species | Shape (Sneed and Folk's 1958 pebble shape diagram) | Shape (Bosence, 1983) |
|---|---|---|
| Monospecific | Spheroidal (S) | Laminar (L) |
| Multispecific | Ellipsoidal (E) | |
| | Discoidal (D) | Branching (B) |
| | | |
| | | |
| | | |
| | | Columnar (C) |

Three main perpendicular axes were measured by a digital caliper: x (=a) – the longest axis, y (=b) – intermediate, z (=c) – the shortest one.

Microsoft Excel SHAPE and PAST Programmes (**Hammer et al., 2001**) were applied for morphometric and shape analyses.

Macroid shape was graphically presented by the ternary, TRI-PLOT diagrams (**Sneed and Folk, 1958**), using the Excel spreadsheet method (e.g., **Graham and Midgley, 2000**). TRI-PLOT is available from the Wiley Interscience web site (**www.interscience.wiley.com**) (after **Graham and Midgley, 2000**). To plot the ternary diagram, ratios of the three orthogonal macroid axes need to be calculated: c:a, b:a, and (a-b)/(a-c) (see **Figure 3**). The corners of the diagram are marked by blocks or spheres (upper corner, between c:a and b:a), slabs or discs (left corner, between c:a and (a-b)/(a-c)) and rods (right corner, between b:a and (a-b)/(a-c)) (see more in **Graham and Midgley, 2000** and references therein).
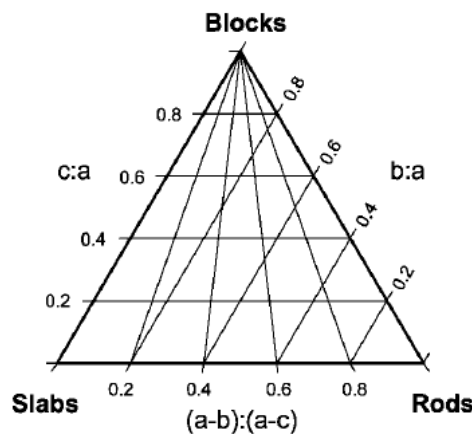


**Figure 3:** Graphic analyses of particle shape (Sneed & Folk) (from **Graham & Midgely, 2000**)

Shape classification was additionally done according to **Zingg (1935)**, taking into calculations the relations between the shortest and intermediate axis (z/y or c/b) and the relation between the intermediate and the longest axis (y/x or b/a). The results enable macroid division into the four form categories: spheroids, discoids, rods and blades.

## 3. Results

Monospecific rhodoliths may occur in a variety of growth forms and multispecific rhodoliths are even more diverse (**Lemoine 1910, Bosence, 1983; Foslie, 1984; Pejnović and Pensa, 2017 and references therein**). In such a case it is important to distinguish the rhodolith classification according to their shape from the taxonomical determinations (**Bosence, 1983**). Taxonomical analyses also underwent thorough revision, with the basic division into the geniculate/non-geniculate taxa proposed by **Rasser (2000)**.

In order to classify the macroid shapes, measurements of three axes (x,y and z) were recorded in **Table II**. It is probable that extracted macroids are smaller than the original ones, due to the wave erosion, but the relationships remain more or less similar.

**Table II:** Measurements of collected macroids

| x | y | z | | x | y | z | | x | y | z | | x | y | z |
|---|---|---|---|---|---|---|---|---|---|---|---|---|---|---|
| 11.12 | 10.05 | 8.74 | | 19.45 | 14.57 | 12.97 | | 23.49 | 17.03 | 9.38 | | 28.70 | 23.16 | 13.87 |
| 11.28 | 10.80 | 6.80 | | 19.53 | 13.01 | 6.33 | | 23.55 | 20.18 | 12.09 | | 28.72 | 17.54 | 10.23 |
| 12.11 | 11.89 | 10.91 | | 19.54 | 16.34 | 14.31 | | 23.55 | 18.73 | 14.12 | | 28.90 | 25.06 | 14.70 |
| 12.47 | 11.87 | 10.00 | | 19.56 | 18.13 | 13.34 | | 23.57 | 22.54 | 12.49 | | 29.03 | 19.46 | 10.39 |
| 12.58 | 12.49 | 10.61 | | 19.63 | 15.67 | 7.61 | | 23.57 | 18.96 | 10.28 | | 29.51 | 19.69 | 13.22 |
| 12.60 | 11.84 | 8.62 | | 19.64 | 17.71 | 12.88 | | 23.61 | 22.82 | 15.66 | | 29.59 | 21.59 | 20.07 |
| 12.84 | 12.48 | 9.48 | | 19.67 | 13.36 | 8.68 | | 23.66 | 15.56 | 12.29 | | 29.61 | 22.21 | 18.73 |
| 12.98 | 12.80 | 9.32 | | 19.71 | 11.88 | 12.90 | | 23.70 | 13.54 | 11.44 | | 29.72 | 19.87 | 17.29 |
| 13.39 | 12.28 | 9.87 | | 19.74 | 11.31 | 11.25 | | 23.75 | 19.36 | 17.26 | | 30.03 | 19.19 | 16.34 |
| 13.47 | 10.17 | 7.60 | | 19.76 | 16.71 | 10.04 | | 23.78 | 22.26 | 10.85 | | 30.10 | 18.62 | 14.34 |
| 13.86 | 11.33 | 7.37 | | 19.82 | 11.98 | 11.20 | | 23.84 | 15.70 | 13.20 | | 30.20 | 25.68 | 16.08 |
| 14.21 | 10.45 | 9.57 | | 19.90 | 17.12 | 11.37 | | 23.88 | 16.36 | 11.25 | | 30.22 | 16.45 | 12.20 |
| 14.46 | 12.12 | 6.96 | | 20.00 | 14.52 | 12.49 | | 23.97 | 16.63 | 12.06 | | 30.32 | 27.94 | 10.94 |
| 14.84 | 13.12 | 7.92 | | 20.04 | 18.17 | 10.25 | | 23.97 | 22.07 | 16.61 | | 30.32 | 20.82 | 11.05 |
| 15.00 | 12.95 | 10.25 | | 20.05 | 15.49 | 14.41 | | 23.99 | 15.46 | 10.78 | | 30.48 | 20.65 | 13.58 |
| 15.12 | 14.34 | 11.03 | | 20.16 | 13.19 | 8.00 | | 24.05 | 19.97 | 14.72 | | 30.50 | 28.36 | 16.19 |
| 15.36 | 12.35 | 11.48 | | 20.17 | 12.66 | 8.45 | | 24.10 | 14.28 | 11.04 | | 30.58 | 21.91 | 13.46 |
| 15.45 | 15.33 | 9.31 | | 20.19 | 18.57 | 6.95 | | 24.16 | 21.02 | 11.08 | | 30.62 | 16.28 | 10.12 |
| 15.50 | 11.54 | 6.29 | | 20.34 | 14.87 | 12.60 | | 24.20 | 19.86 | 17.28 | | 30.64 | 21.95 | 11.46 |
| 15.52 | 10.81 | 10.54 | | 20.34 | 18.46 | 9.12 | | 24.22 | 17.93 | 10.99 | | 30.72 | 22.62 | 18.42 |
| 15.55 | 12.28 | 11.20 | | 20.53 | 10.78 | 7.77 | | 24.23 | 18.39 | 11.36 | | 30.95 | 19.96 | 16.70 |
| 15.76 | 15.00 | 13.65 | | 20.58 | 15.63 | 8.46 | | 24.24 | 22.54 | 16.15 | | 30.96 | 26.73 | 20.18 |
| 15.97 | 14.08 | 12.41 | | 20.67 | 17.67 | 13.00 | | 24.29 | 17.18 | 10.00 | | 31.00 | 24.64 | 15.68 |
| 16.09 | 13.88 | 8.43 | | 20.68 | 15.39 | 13.34 | | 24.33 | 13.08 | 10.30 | | 31.04 | 24.83 | 14.62 |
| 16.12 | 13.14 | 9.23 | | 20.75 | 15.73 | 11.65 | | 24.35 | 17.54 | 14.61 | | 31.07 | 23.32 | 19.45 |
| 16.34 | 12.94 | 11.84 | | 20.87 | 14.16 | 10.72 | | 24.38 | 13.70 | 10.93 | | 31.11 | 26.59 | 24.06 |
| 16.35 | 15.77 | 9.74 | | 20.87 | 16.68 | 13.84 | | 24.65 | 15.02 | 7.70 | | 31.45 | 19.14 | 9.93 |
| 16.39 | 11.17 | 10.55 | | 20.89 | 15.33 | 8.64 | | 24.68 | 15.67 | 14.08 | | 31.49 | 17.57 | 7.23 |
| 16.47 | 10.99 | 8.57 | | 20.91 | 20.18 | 11.52 | | 24.69 | 20.12 | 12.26 | | 31.63 | 16.76 | 13.35 |
| 16.60 | 11.22 | 10.66 | | 20.94 | 11.63 | 7.83 | | 24.70 | 19.24 | 11.20 | | 31.72 | 27.90 | 18.51 |
| 16.64 | 12.75 | 7.71 | | 20.95 | 15.66 | 10.38 | | 24.76 | 19.40 | 6,91 | | 31.73 | 24.80 | 23.07 |
| 16.65 | 11.15 | 7.03 | | 21.02 | 13.94 | 8.22 | | 24.82 | 18.16 | 12.55 | | 31.82 | 18.03 | 16.49 |
| 16.72 | 15.77 | 11.16 | | 21.12 | 14.44 | 13.93 | | 24.97 | 13.36 | 11.52 | | 31.88 | 26.81 | 14.59 |
| 16.73 | 13.32 | 10.58 | | 21.13 | 18.88 | 9.87 | | 25.17 | 14.02 | 7.51 | | 31.88 | 21.06 | 17.62 |
| 16.78 | 16.46 | 13.79 | | 21.19 | 14.58 | 7.43 | | 25.23 | 18.35 | 15.50 | | 32.00 | 22.69 | 9.67 |
| 16.83 | 13.91 | 11.12 | | 21.19 | 18.52 | 11.00 | | 25.24 | 21.79 | 11.47 | | 32.11 | 22.18 | 15.53 |
| 16.96 | 12.63 | 8.31 | | 21.20 | 12.55 | 11.31 | | 25.29 | 22.65 | 11.24 | | 32.46 | 20.12 | 17.03 |
| 17.05 | 15.14 | 10.72 | | 21.25 | 15.22 | 8.59 | | 25.32 | 20.76 | 15.66 | | 32.61 | 24.64 | 23.18 |
| 17.09 | 14.95 | 7.86 | | 21.26 | 21.20 | 7.13 | | 25.36 | 18.36 | 10.63 | | 32.74 | 27.65 | 21.76 |

| | | | | | | | | | | | |
|---|---|---|---|---|---|---|---|---|---|---|---|
| 17.21 | 13.75 | 13.02 | 21.34 | 20.31 | 13.10 | 25.38 | 16.17 | 14.20 | 32.93 | 18.79 | 10.37 |
| 17.22 | 13.87 | 6.46 | 21.38 | 17.26 | 11.75 | 25.39 | 12.73 | 12.69 | 32.97 | 28.30 | 24.31 |
| 17.26 | 12.96 | 8.83 | 21.43 | 17.46 | 11.51 | 25.44 | 18.25 | 14.98 | 33.19 | 31.36 | 18.97 |
| 17.30 | 15.72 | 9.70 | 21.50 | 17.95 | 15.81 | 25.47 | 23.51 | 14.33 | 33.31 | 22.66 | 11.84 |
| 17.43 | 15.30 | 7.71 | 21.50 | 19.71 | 13.40 | 25.58 | 24.35 | 13.03 | 33.52 | 19.70 | 18.80 |
| 17.44 | 17.00 | 13.45 | 21.55 | 19.41 | 10.20 | 25.66 | 22.00 | 20.35 | 33.60 | 16.89 | 9.76 |
| 17.46 | 13.03 | 11.00 | 21.58 | 17.13 | 11.62 | 25.76 | 25.59 | 14.95 | 33.72 | 27.90 | 27.51 |
| 17.66 | 11.76 | 8.26 | 21.63 | 16.36 | 13.80 | 25.76 | 17.62 | 15.53 | 33.76 | 24.79 | 19.88 |
| 17.73 | 10.05 | 9.78 | 21.69 | 16.40 | 14.00 | 25.81 | 14.30 | 13.63 | 34.16 | 24.63 | 21.98 |
| 17.80 | 13.43 | 7.84 | 21.77 | 10.84 | 9.81 | 25.82 | 15.88 | 9.44 | 34.35 | 20.19 | 12.01 |
| 17.85 | 12.42 | 6.99 | 21.87 | 12.66 | 8.39 | 25.84 | 24.47 | 14.83 | 34.36 | 25.17 | 14.60 |
| 18.00 | 15.95 | 11.09 | 22.04 | 16.15 | 12.69 | 25.90 | 15.85 | 12.19 | 34.60 | 18.72 | 10.21 |
| 18.04 | 17.52 | 13.22 | 22.06 | 14.29 | 12.11 | 26.00 | 21.38 | 15.23 | 34.71 | 29.90 | 23.49 |
| 18.08 | 13.33 | 10.16 | 22.10 | 22.03 | 12.98 | 26.02 | 24.28 | 14.23 | 34.94 | 26.02 | 18.14 |
| 18.09 | 13.83 | 7.30 | 22.18 | 14.88 | 10.77 | 26.02 | 21.40 | 8.56 | 35.17 | 27.82 | 23.05 |
| 18.13 | 16.98 | 13.40 | 22.18 | 17.85 | 15.55 | 26.21 | 19.03 | 16.06 | 35.20 | 24.07 | 22.62 |
| 18.20 | 16.64 | 16.28 | 22.22 | 16.86 | 10.37 | 26.27 | 21.46 | 19.56 | 35.20 | 25.30 | 16.61 |
| 18.24 | 17.30 | 11.23 | 22.28 | 19.75 | 7.65 | 26.45 | 17.00 | 10.87 | 35.46 | 34.79 | 21.42 |
| 18.26 | 14.09 | 12.77 | 22.29 | 16.03 | 13.74 | 26.50 | 19.21 | 19.33 | 35.84 | 22.09 | 15.77 |
| 18.26 | 12.79 | 8.41 | 22.30 | 15.37 | 15.01 | 26.54 | 16.57 | 10.01 | 36.27 | 22.26 | 20.46 |
| 18.33 | 17.50 | 9.12 | 22.31 | 16.38 | 7.03 | 26.57 | 17.94 | 11.10 | 37.24 | 16.70 | 12.57 |
| 18.36 | 12.70 | 12.61 | 22.38 | 16.27 | 9.86 | 26.57 | 24.13 | 16.88 | 38.17 | 27.57 | 20.23 |
| 18.37 | 13.75 | 10.14 | 22.44 | 16.79 | 11.87 | 26.62 | 19.43 | 11.71 | 38.33 | 30.63 | 17.87 |
| 18.38 | 14.84 | 8.87 | 22.51 | 20.87 | 9.38 | 26.64 | 18.42 | 16.78 | 38.83 | 36.25 | 21.76 |
| 18.40 | 14.38 | 10.36 | 22.54 | 18.22 | 7.72 | 26.68 | 22.00 | 14.64 | 39.31 | 36.26 | 13.89 |
| 18.52 | 13.30 | 6.04 | 22.56 | 13.06 | 9.87 | 26.69 | 24.49 | 15.19 | 39.53 | 23.42 | 10.66 |
| 18.57 | 10.67 | 10.23 | 22.58 | 16.25 | 10.72 | 26.73 | 23.65 | 18.92 | 39.66 | 18.16 | 11.82 |
| 18.57 | 12.36 | 9.86 | 22.59 | 14.74 | 10.29 | 26.88 | 16.84 | 10.20 | 39.73 | 24.44 | 17.55 |
| 18.59 | 10.94 | 5.12 | 22.66 | 17.22 | 9.66 | 26.95 | 21.31 | 10.18 | 40.08 | 27.30 | 11.64 |
| 18.62 | 12.85 | 8.02 | 22.71 | 18.30 | 11.98 | 27.21 | 23.15 | 11.82 | 40.83 | 27.33 | 23.39 |
| 18.68 | 15.10 | 8.23 | 22.92 | 20.70 | 15.54 | 27.32 | 19.41 | 11.04 | 41.19 | 16.96 | 13.45 |
| 18.72 | 12.77 | 6.30 | 22.93 | 14.98 | 14.43 | 27.36 | 19.13 | 17.20 | 41.81 | 29.00 | 26.61 |
| 18.75 | 14.16 | 13.88 | 23.01 | 18.65 | 12.62 | 27.37 | 18.09 | 10.80 | 43.79 | 32.60 | 16.77 |
| 18.85 | 17.06 | 12.86 | 23.02 | 19.32 | 11.12 | 27.38 | 24.60 | 16.34 | 44.90 | 29.35 | 27.51 |
| 18.98 | 16.92 | 8.81 | 23.06 | 14.61 | 9.83 | 27.41 | 17.47 | 15.26 | 45.59 | 36.34 | 29.50 |
| 19.03 | 16.80 | 16.02 | 23.06 | 16.90 | 8.65 | 27.66 | 16.94 | 10.72 | 46.51 | 35.72 | 26.97 |
| 19.05 | 14.90 | 9.60 | 23.13 | 14.41 | 11.23 | 27.87 | 18.33 | 14.91 | 46.53 | 35.73 | 27.73 |
| 19.18 | 15.56 | 8.02 | 23.30 | 15.86 | 10.17 | 27.97 | 24.87 | 11.53 | 46.90 | 31.95 | 18.34 |
| 19.18 | 17.09 | 10.76 | 23.43 | 15.40 | 11.13 | 28.03 | 17.17 | 9.46 | 48.16 | 27.55 | 19.25 |
| 19.24 | 16.53 | 9.21 | 23.43 | 19.33 | 6.91 | 28.03 | 19.67 | 12.82 | 51.44 | 30.88 | 16.94 |
| 19.28 | 16.58 | 16.31 | 23.47 | 17.84 | 13.65 | 28.42 | 19.43 | 18.11 | | | |
| 19.41 | 13.48 | 13.61 | 23.48 | 19.98 | 7.04 | 28.42 | 20.90 | 12.38 | | | |

## 3.1. Numerical analysis of macroid measures

The measured collection comprises a variety of macroid sizes, but the longest axis lengths point to a normal distribution (**Figure 4**).
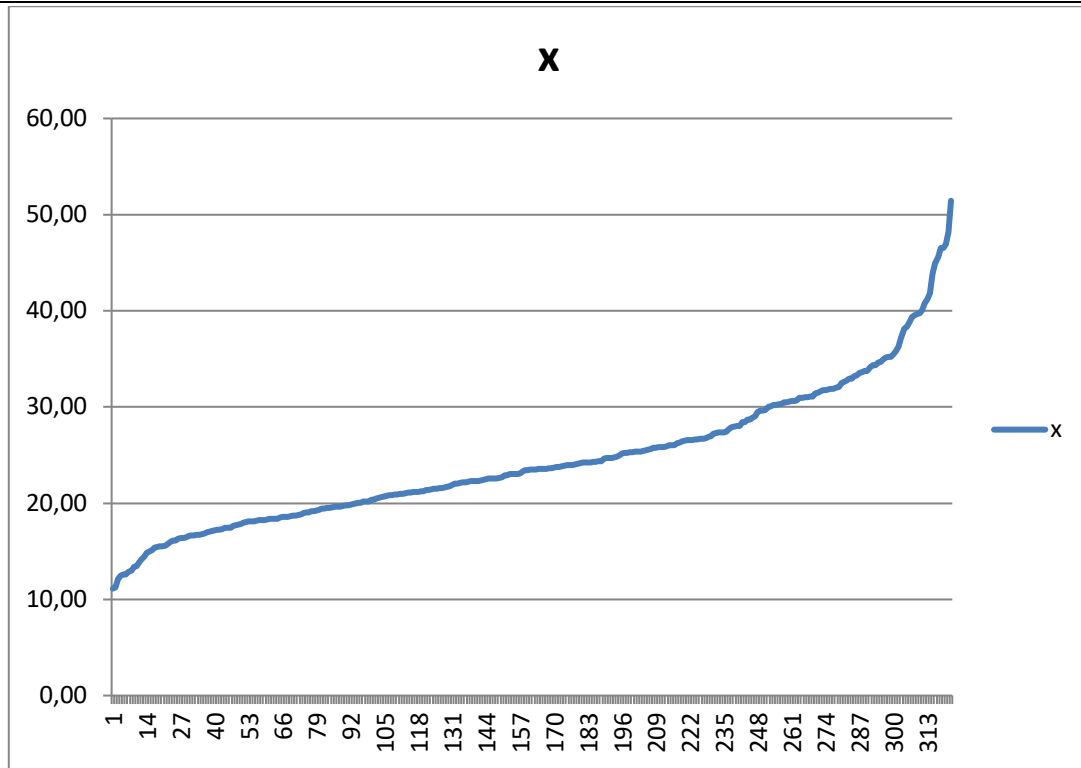
**Figure 4:** Distribution of sizes of the longest axis (x or a) of measured rhodoliths shown on the line chart (Microsoft Excel Programme), showing normal distribution

Relationship between the macroid axes reveal a variety of forms (**Figures 5, 6**), with regular spherical and subspherical shapes present mostly among the small specimens (**Figure 6**).
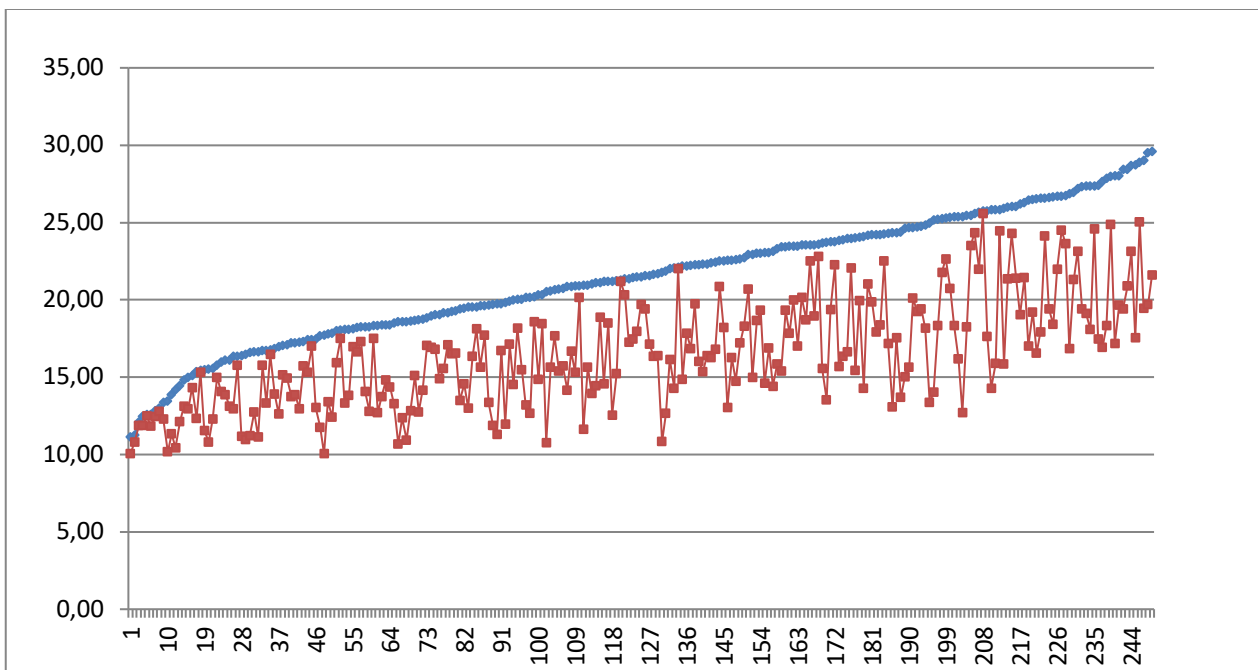


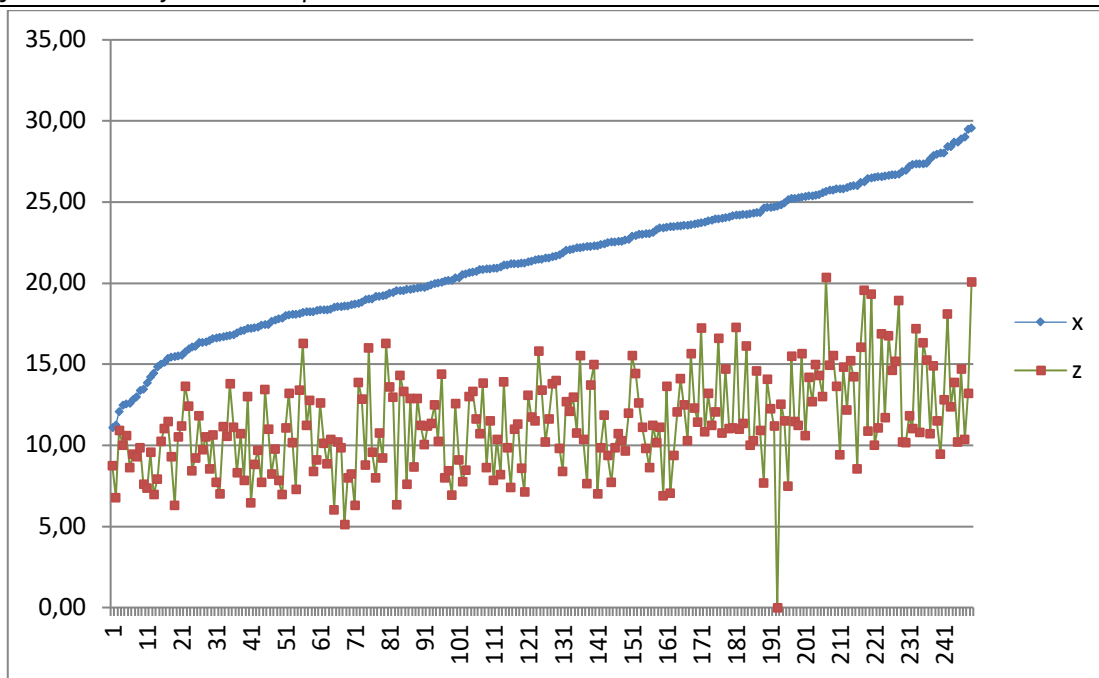**Figure 5:** Relationship between the macroid axes x (blue line) and y (red line) presenting the variety of forms. Obtained from the Microsoft Excel Programme.

**Figure 6:** Relationship between the macroid axes x (blue line) and z (green line with red peaks) presenting the discrepancy in macroid growth. Spherical and subspherical forms only occur among the small collected specimens. Obtained from the Microsoft Excel Programme.
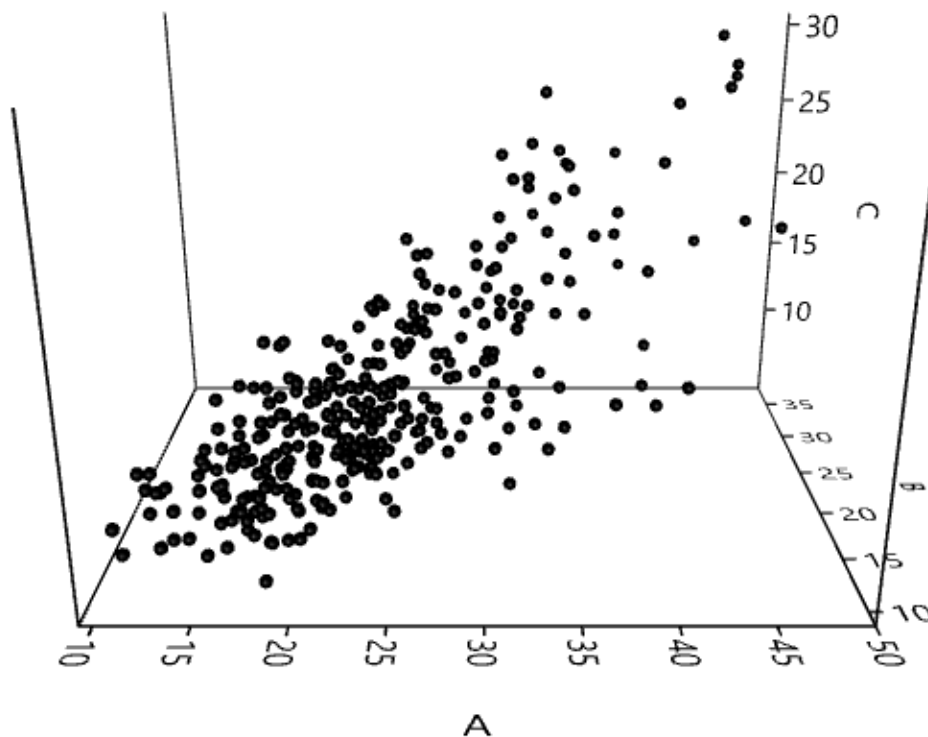


**Figure 7:** Scattered 3-D diagram presenting the relationship between the longest (x/A), intermediate (y/B) and shortest (z/C) axes of macroids. Obtained from the PAST Programme (**Hammer et al., 2001**).

Scattered 3-D diagrams drawn from the PAST program (**Hammer et al., 2001**) proved to be very useful in our analyses. They show in a simple way how smaller macroids present a more homogenous group, while those with the longest axis (x or A) form a very heterogenous group (**Figure 7**).

## 3.2. Clast shape and fossil content

Macroid shape analyses using the Zingg diagram (**Zingg, 1935**) and ternary diagram (**Sneed and Folk, 1958**) have shown that collected macroids are mostly represented by the particles of the discoidal and spheroidal shape as shown in **Figures 8, 9 and 10**. Only a small number of particles belong to the blade- and rod-shaped macroids (right corner) (see **Figures 3 and 8-10**).
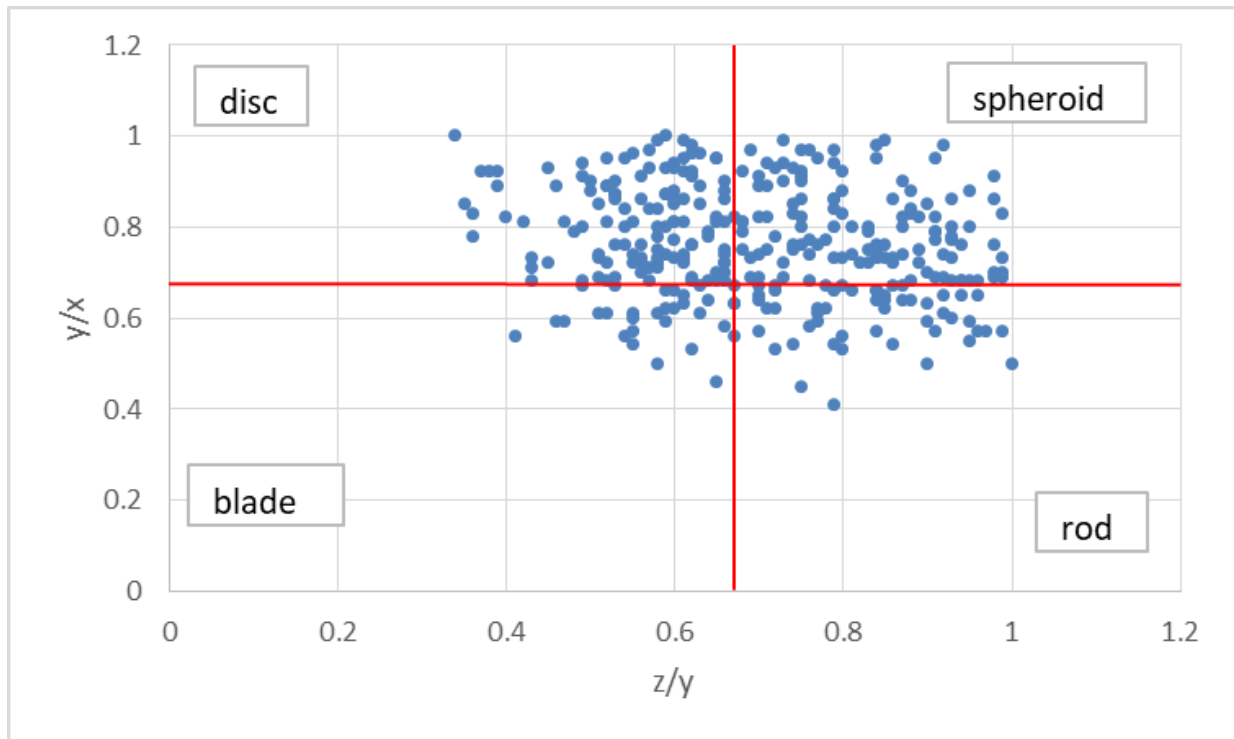


**Figure 8:** Zingg's diagrams for the measured macroids from the Stanići beach. Discoidal and spherical macroids are the most common.
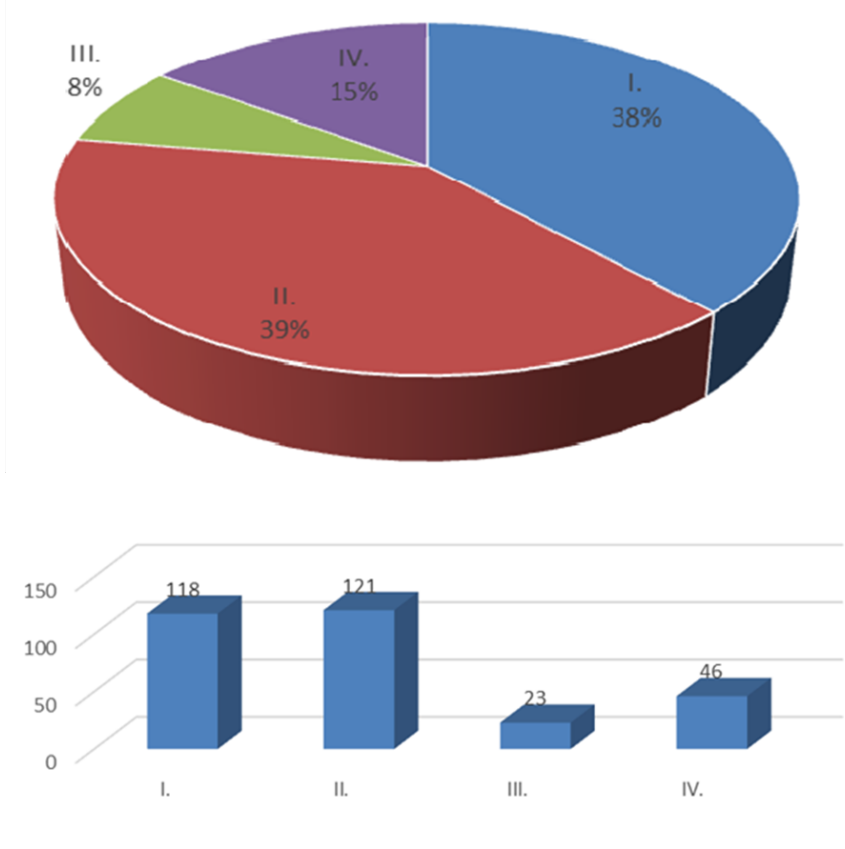
**Figure 9:** Comparison of Zingg's data for the collected macroids presented as a pie and a histogram. Categories: I. disc; II. sphere; III. blade; IV. rod. Microsoft Excel programme.
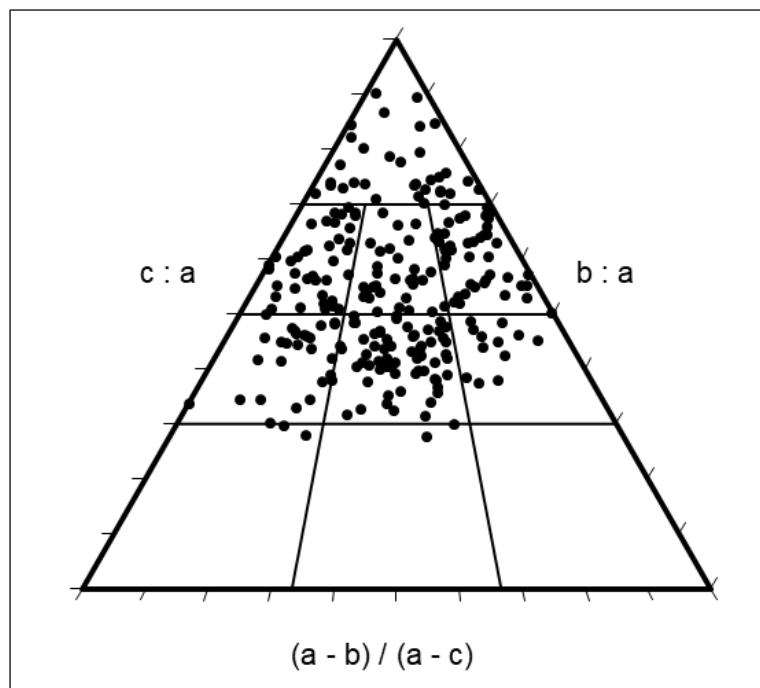


**Figure 10:** Graphic analyses of macroid shape carried out by ternary (Sneed & Folk) diagram based on measurements of long (a = x), intermediate (b = y) and short (c = z) axes (from **Graham and Midgley, 2000**)

# 4. Discussion

A hypothesis at the beginning of our research was that, according to previous studies, macroids, composed exclusively of red algae (rhodoliths), or those with a minor amount of other encrusters, will be developed in more regular shapes (subsphaeroidal, or, sometimes discoidal) (**Figure 11 a,b**) than the complex ones, composed by a variety of bioconstructors (**Figure 11 c,d**). The most expressed diversity is expected among the branching forms.
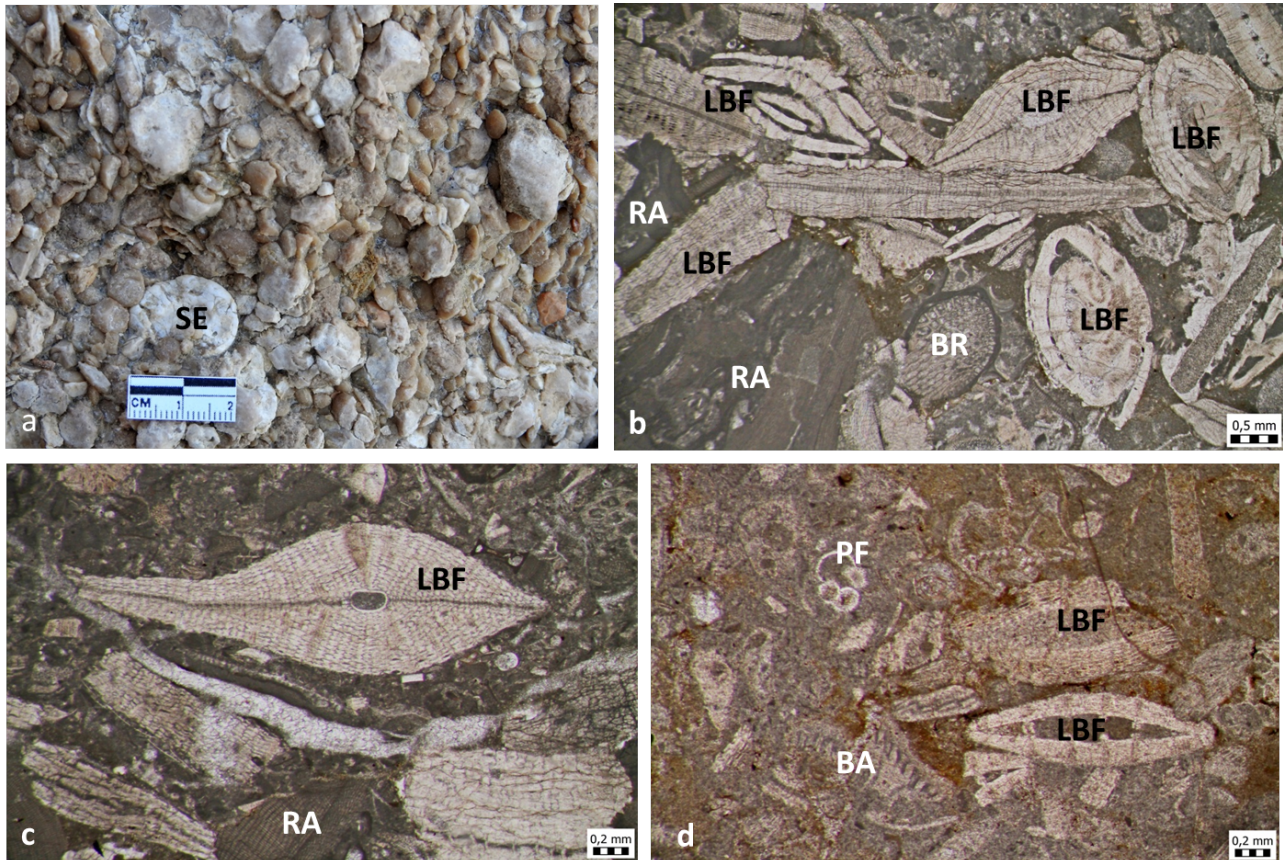


**Figure 11:** Source rock on the Stanići beach (a); photomicrographs presenting packstone-type of biocalcarenites (b-c) from the sample FH/O and wackestone, sample FH/M₁ (d). Fossils: large benthic foraminifera (LBF), planktic foraminifera (PF) red algae (RA), balanids (BA), serpulids (SE) and bryozoans (BR).

After the macroscopic analyses of source rocks (**Figure 11**), thirty thin sections with macroids (ca. 10% of the bulk sample) were studied. The results so far fit into the presumption that small and regularlly-shaped macroids are dominantly composed of red algae, while larger pebbles represent complex macroids (**Figure 12**). Rhodoliths are mostly derived from the coralline algal packstone, with bioclasts transported from the inner to mid-ramp by storms, similar to the Microfacies MF5 described by **Ćosović et al. (2018)** from the Dinaric Foreland Basin in Northern Dalmatia. Combined macroids, particularly those with large amount of acervulinid foraminifera, point to the middle to lower photic zone, moderate water energy and/or increased turbidity. They sometimes comprise planktic foraminifera (**Figure 11d**). Similar bioconstructions were described from Northern Dalmatia as foraminiferal packstone/grainstone from the middle ramp environment (Microfacies MF6 in **Ćosović et al., 2018**), but also from younger, Miocene deposits found in different regions (e.g., in Zagros, Iran; **Roozpeykar et al., 2019**). In the Dinaric Foreland Basin, the succession of Microfacies types MF5 into MF6 (in this case rhodoliths into acervulinid-rhodalgal macroids) reflects the deepening of the basin and the transition into the flysch-type deposition. Further research, with preparation of thin sections from a larger amount of macroids, is in progress.

Here presented research offered the opportunity to compare the results obtained from the different methods revealing the shape of the measured object in paleontological and geological (sedimentological) programmes. **Zingg (1935)** and **Sneed and Folk (1958)** calculations can both generate similarly valuable results, and we would recommend them as cross-validating methods in both research topics.

Furthermore, graphics presenting the relationship among the three variables (in this case macroid axes: x/a, y/b and z/c), obtained from the open-access paleontological PAST programme (**Hammer et al., 2001**), could be successfully applied to other similar cases aside from paleontology (e.g., pebble morphometry).
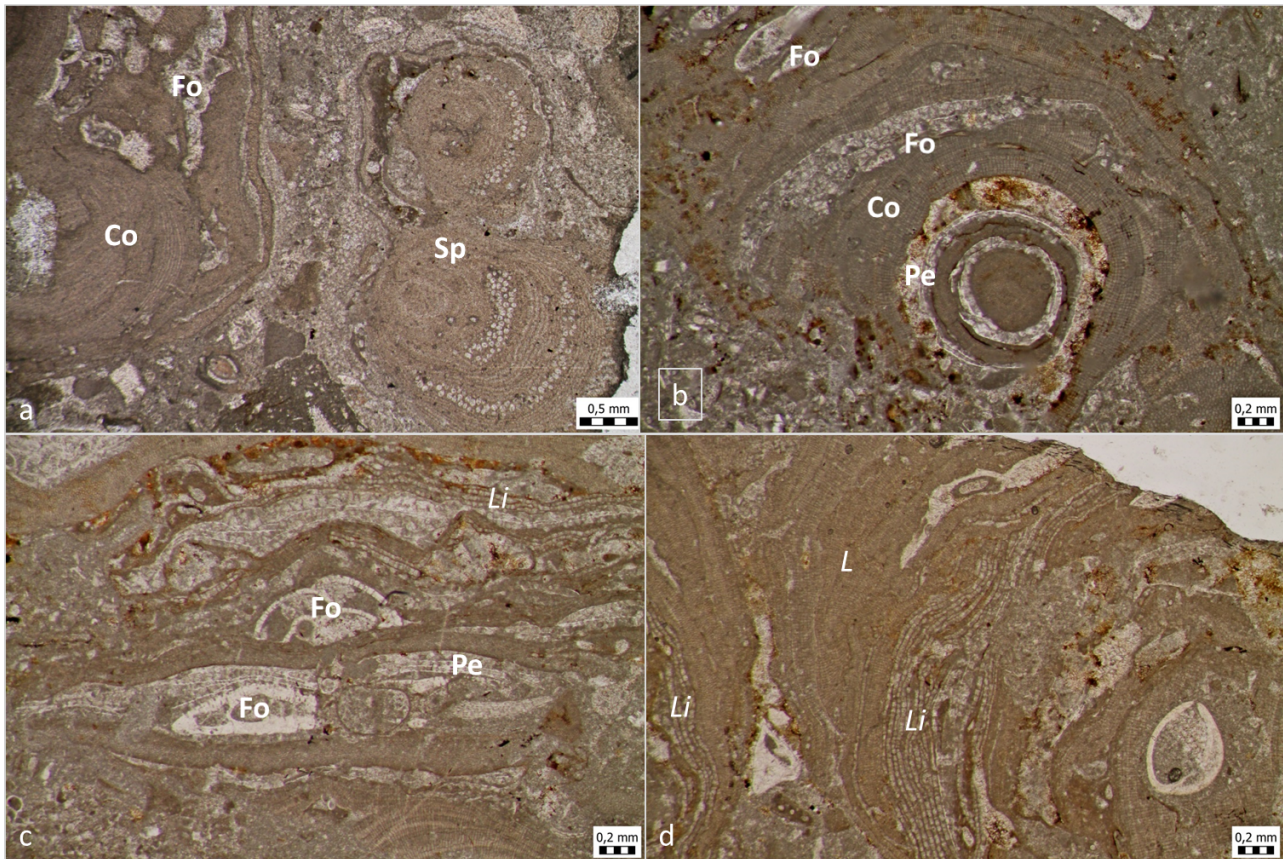


**Figure 12:** Photomicrographs of macroids from the source rock ("Nummulitic breccia") at the Stanići beach . Algal remnants: Co – Corallinales (*L – Lithothamnion?* sp.*; Li – Lithoporella*); Sp – Sporolithales; Pe - Peyssonneliales . Fo – foraminifera.
(a) Corallinales and regularly-shaped *Sporolithon* rhodoliths, with scarce foraminifera; (b) a partly crushed rhodolith composed of rhodalgal layers and encrusting foraminifera; (c) Complex laminar crusts composed of red algae and sessile foraminifera from an elongate, box-shaped pebble; (d) Crushed complex rhodoliths with dominant coralgal laminae and with sporadic layers composed of encrusting foraminifera. Cross section of a macrofossil is visible in the macroid core.

## 5. Conclusions

- Macroids collected at the Stanići beach near Omiš are of variable shape and size.
- Regularly formed, in most cases sphaeroidal macroids are rhodoliths of monospecific composition or composed from a small number of taxa. They were mostly formed in the inner ramp environment and transported into the middle ramp milieu by storms.
- Larger and less regular-shaped macroids are commonly multispecific, with a significant amount of sessile foraminifera and other bioconstructors. They originate from the middle ramp environment with increased turbidity.
- Macroids were extracted from the Eocene "Nummulitic breccias" scattered as olistolites along the beaches in this part of Dalmatia, reflecting the gradual transition from the carbonate ramp into the flysch-type deposition.
- Some of the morphometrical methods applied in paleontology can be successfully used in sedimentological research and *vice versa*.

# 6. References

Babić, Lj. and Zupanič, J. (2007): Major events and stages in the sedimentary evolution of the Paleogene Promina basin (Dinarides, Croatia). Natura Croatica, 16/4, 215–232.

Babić, Lj. and Zupanič, J. (2008): Evolution of a river-fed foreland basin fill: the North Dalmatian flysch revisited (Eocene, Outer Dinarides). Natura Croatica, 17, 357–374.

Babić, Lj. and Zupanič, J. (2012): Laterally variable development of a basin-wide transgressive unit of the North Dalmatian foreland basin (Eocene, Dinarides, Croatia). Geologia Croatica, 65, 1–27. doi: 10.4154/GC.2012.01

Bosence, D.W.J. (1983): Coralline algal reef frameworks: Cenozoic carbonates. Description and Classification of Rhodoliths (Rhodoids, Rhodolites). Journal of the Geological Society, 140, 3, 365–376. https://doi.org/10.1144/gsjgs.140.3.0365

Ćosović, V., Marjanac, T., Drobne, K. and Moro, A. (2008): Outer Dinarides: eastern Adriatic coast. Paleogene and Neogene. In: Mccann, T. (ed.): The Geology of Central Europe, Volume 2: Mesozoic and Cenozoic. The Geological Society London, London, 1031–1139.

Ćosović, V., Mrinjek, E., Nemec, W., Španiček, J. and Terzić, K. (2018): Development of transient carbonate ramps in an evolving foreland basin. Basin Research, vol 544, 30/4, 746-765, doi: 10.1111/bre.12274

Foslie, M. (1984): New or critical Norwegian algae. Kongelige Norske Videnskabers Selskabs Skrifter, 1893, 114–144.

Graham. D. J. and Midgley, N. G. (2000): Graphical representation of particle shape using triangular diagrams: an Excel spreadsheet method. Earth Surface Processes and Landforms, 25(13), 1473-1477.

Hammer,Ø., Harper, D.A.T. and Ryan, P.D. (2001): PAST: Paleontological statistics software package for education and data analysis. Palaeontologia Electronica 4(1): 9pp. http://palaeo-electronica.org/2001_1/past/issue1_01.htm

Lemoine, M. (1910): Repartition et mode de vie du maerl (*Lithothamnium calcareum*) aux environs de Concarneau (Finistére). Ann. Inst. Oceanogr. Monaco, 1, 3, 1−28.

Marinčić, S., Korolija, B. and Majcen, Ž. (1976): Osnovna geološka karta SFRJ 1:100000, list Omiš K 33-22 [*Basic Geological Map of SFRY, Omiš sheet – in Croatian*]. Geološki zavod, Zagreb, Savezni geološki zavod, Beograd.

Marinčić, S., Korolija, B., Mamužić, P., Magaš, N., Majcen, Ž., Brkić, M. and Benček, Đ. (1977): Osnovna geološka karta SFRJ 1:100000, Tumač za list Omiš [*Basic Geological Map of SFRY, Omiš sheet explanatory notes – in Croatian*]. Geološki zavod, Zagreb, Savezni geološki zavod, Beograd.

Marjanac, T. (1991): Importance of megabeds for reconstruction of Paleogene flysch basin in Split hinterland (Middle Dalmatia), Yugoslavia. Sedimentology, 37, 921−929.

Marjanac, T. (1996): Deposition of megabeds (megaturbidites) and sea-level change in a proximal part of Eocene-Miocene flysch of central Dalmatia (Croatia). Geology, 26, 6, 543−546. DOI: 10.1130/0091-7613(1996)024<0543:DOMMAS>2.3.CO;2

Marjanac, T. and Ćosović, V. (2000): Tertiary depositional history of Eastern Adriatic realm. Vijesti Hrvatskoga geološkog društva, 37/2, 93–103.

Mrinjek, E., Nemec, W., Pecinger, V., Mikša, G., Vlahović, I., Ćosović, V., Velić, I., Bergant, S. and Matičec, D. (2012): The Eocene–Oligocene Promina Beds of the Dinaric Foreland Basin in northern Dalmatia. In: Gawlick, H.J. & Lein, R. (eds.): 29th IAS Meeting of Sedimentology − Schladming 2012, Field Trip Guides. Geoaustria, Wien, 409–451.

Pejnović, I. and Pensa, T. (2017): Kako su koralinacejske alge pomogle u paleoekološkoj interpreaciji eocenskih gornjih numulitnih vapnenca sjeverno dalmatinskog predgorskog bazena (*The role of coralline red alga in paleoenvironmental interpretation of the Eocene upper nummulitic limestones in Northern Dalmatian Foreland Basin – in Croatian with English summary*). University of Zagreb, Faculty of Science, 1−24.

Rasser, M.W. (2000): Coralline red algal limestones of the Late Eocene Alpine Foreland Basin in Upper Austria: component analysis, facies and paleoecology. Facies, 42, 59–92. doi: 10.1007/BF02562567

Roozpeykar, A., Maghfouri-Moghaddam, I., Yazdi, M. and Yousefi-Yegane, B. (2019): Facies and paleoenvironmental reconstruction of Early–Middle Miocene deposits in the north-west of the Zagros Basin, Iran. Geologica Carpathica, 70, 1, 75−87. doi: 10.2478/geoca-2019-0005

Sneed E.D. and Folk R.L. (1958): Pebbles in the lower Colorado River, Texas, a study in particle morphogenesis, Journal of Geology, 66(2), 114−150.

Španiček, J., Ćosović, V., Mrinjek, E. and Vlahović, I. (2017): Early Eocene evolution of carbonate depositional environments recorded in the Čikola Canyon (North Dalmatian Foreland Basin, Croatia). Geologia Croatica, 70, 11–25. https://doi.org/10.4154/gc.2017.05

Vlahović, I. and Velić, I. (2009): Liburnijske naslage, foraminiferski vapnenci i prijelazne naslage (?gornji paleocen, donji i srednji eocen –?Pc, E1,2) [*Liburnian deposits, Foraminiferal limestones and Transitional Beds (?Upper Paleocene, Lower and Middle Eocene –?Pc, E1,2 – in Croatian*].− In: Velić, I. and Vlahović, I. (eds.): Tumač Geološke karte Republike Hrvatske 1:300000 [*Explanatory Notes of Basic Geological Map of Croatia 1:300000 – in Croatian*]. Hrvatski geološki institut, Zagreb, 76−77.

Zingg, Th. (1935): Beiträge zur Schotteranalyse. Min. Petrog. Mitt. Schweiz., 15, 39−140.

## Internet sources

URL 1: Google Earth, https://www.google.com/earth/ (accessed in September, 2020)
URL 2: Wiley Interscience Web, www.interscience.wiley.com (accessed in August, 2020)

# SAŽETAK

**Morfometrijske karakteristike i porijeklo paleogenskih makroida iz šljunaka na plaži u Stanićima (okolica Omiša, južna Hrvatska)**

Na plaži u Stanićima kraj Omiša prikupljena je zbirka od 322 makroidna klasta, koje je more ispralo iz okolnih bioklastičnih naslaga. Makroidi su mjereni digitalnim mjeračem (kaliperom) kako bi se zabilježile njihove dimenzije (najduža, srednja i najkraća os). Morfometrijske analize, zajedno s mikropaleontološkim analizama, omogućile su razlikovanje dviju skupina makroida. Jednostavni rodoliti ili makroidi složeni od malog broja inkrustanata, pretežito su sferoidnog ili diskoidalnog oblika i pokazuju normalnu raspodjelu veličina i dobru korelaciju. Multispecifički makroidi (načinjeni od lamina crvenih algi, acervulidnih foraminifera i drugih inkrustanata) pojavljuju se u raznolikim oblicima, najčešće su diskoidalni ili štapićasti i na dijagramima pokazuju slabu korelaciju. Makroidi su erodirani iz obalnih bioklastičnih stijena eocenske starosti, gdje se pojavljuju uz izobilje numulita i drugih foraminifera te fragmente skeleta makrofosila, a često ih neformalno nazivamo "Numulitnim brečama". Blokovi ovih stijena razbacani su duž plaža na cijelom širem području Omiša, a dio su megaslojeva, nastalih tijekom urušavanja rubova Dinaridskoga šelfa. Rodoliti su nastajali u okolišima unutarnje do srednje rampe, a složeni makroidi, nastali proslojavanjem crvenih algi i acervulinidnih foraminifera, upućuju na postupno produbljavanje mora, uz porast turbiditeta, koji obilježava završetak karbonatne sedimentacije i početak taloženja flišnih naslaga u Dinarskom predgorskom bazenu. Istraživanje je pokazalo da se neki sedimentološki programi i metode mogu uspješno primjenjivati u paleontologiji, dok sedimentolozima neki paleontološki morfometrijski programi mogu poslužiti za kontrolu i usporedbu njihovih rezultata.

**Ključne riječi:** makroidi, morfometrija, biokonstruktori, eocen, Hrvatska

## Acknowledgment

## Author's contribution

**Jasenka Sremac (1)** (Dr, Full Professor, geology, paleontology, paleoenvironment) provided the fieldwork, paleontological analyses, description of geological settings, interpretation and presentation of the results. **Filip Huić (2)** (student, anthropology, paleontology) provided the fieldwork, measuring, taking photomicrographs and part of preliminary fossil determinations. **Marija Bošnjak (3)** (Dr, senior curator, paleontology, geomathematics) provided the numerical analyses and methodological data. **Renato Drempetić (4)** (electrotechnics engineer), contributed with fieldwork, field- and macro-photography, measuring macroids and preparing computer tables and graphics.

# Neogene deposits of the western slopes of the Psunj Mt., Croatia: an overview of historical background and actualisation of geological research

Davor Vrsaljko[1]; Marija Bošnjak[1]; Anja Jarić[2]; Jasenka Sremac[3]; Tomislav Malvić[4]

[1] Croatian Natural History Museum, Demetrova 1, 10000 Zagreb, Croatia; http://orcid.org/0000-0002-6829-7774; http://orcid.org/0000-0002-1851-1031

[2] Tratinska 57, 10000 Zagreb, Croatia; http://orcid.org/0000-0003-3364-2280

[3] Faculty of Science, Department of Geology, University of Zagreb, 10000 Zagreb, Croatia; http://orcid.org/0000-0002-4736-7497

[4] Faculty of Mining, Geology and Petroleum Engineering, Pierottijeva 6, 10000 Zagreb, Croatia, http://orcid.org/0000-0003-2072-9539

***Dedicated to Dr. Ivan Blašković, Full Professor,***
***Antovo, Crikvenica, 18. VII. 1935. – Zagreb, 30. VIII. 2008.***
***(Faculty of Mining, Geology and Petroleum Engineering, University of Zagreb)***

## Abstract

On the crystalline rocks of the western slopes of the Psunj Mt. disconformably lie Neogene sediments with recorded deposits from the Lower Miocene to the Quaternary period. The basal Neogene sediments are in the older papers defined as "Oligomiocene" or "preTortonian", today corresponding to the Lower Miocene sediments. These freshwater and marine-brackish sediments are transgressively overlain by the marine middle Miocene sediments. Badenian deposits are distributed as a continuous belt along the western slopes of the Psunj Mt., east from Pakrac and Lipik, with various lithofacies diversity. In the wider area they are a part of the structure Bijela Stijena–Novska. Lower Sarmatian rhythmic sediments conformably lie on the Badenian sedimentary rocks. The brackish and freshwater development is marked by the continuation of the Upper Miocene sedimentation, and Pliocene sediments with complete "*Paludina* beds" development mark the end of the Neogene. Dominant is the anticlinal structure – structure nose with an axis Bijela Stijena–Novska. In the core of the structure are crystallinic rocks. Neogene sediments are periclinal and almost continued along the limbs and forehead of the structure.

Keywords: Neogene, stratigraphy, petroleum geology, Psunj Mt., Croatia

## 1. Introduction

Neogene sediments of the western slopes of the Psunj Mt. have been long-time studied by Professor Ivan Blašković and coauthors. They achieved significant results in geological research, giving the valuable overview of the geological development of the Psunj Mt. and Moslavačka gora Mt. during the Neogene, including the petroleum geology characteristics of adjacent parts of the Drava and Sava Depressions, especially the Ilova Subdepression as a marginal part between the Drava Depression toward the Sava Depression.

In this paper the authors presented an overview of the previous geological research of the Neogene deposits of the western part of the Psunj Mt., based on the dissertation of **Blašković (1975),** for which he received university award as the best composed and graphically prepared dissertation, and published papers afterwards. Contributions of Professor Blašković's dissertation was recognized by the University of Zagreb, which gave him an award for the best graphically designed dissertation. Main goal of this review is to actualize research of the Neogene sediments in the area of the Psunj Mt. and to valorize results of the previous Blašković's research. The further updates are proposed using examples of Middle Miocene outcrop analyzed in the area of Rogolji near the Psunj Mt. (**Figure 1**). That was compared to sections

Corresponding author: Davor Vrsaljko
davor.vrsaljko@hpm.hr

given in **Blašković (1975).** Their significance for the geology of this area is evaluated and compared with the recent knowledge of Neogene evolution in the Northern Croatia.

## 2. Historical background

Historical background of geological research of the Psunj Mt. is divided in two parts. The first part includes older papers, from the second half of the 19th and beginning of the 20th century, dealing with the geology of Psunj Mt. and the detailed descriptions and contributions from the dissertation of **Blašković (1975)**. Second part of historical background comprises research papers after **Blašković (1975)**.

There are several papers describing mineralogy and older, pre-Neogene rocks of the Psunj Mt., as well as non-available and non-published geological reports from a few geological institutions in Croatia. Here are included only the available and published papers about stratigraphy and paleontology of the Psunj Mt. during the Neogene period, as basic papers for the further research in selected area.

### 2.1. Research papers from the 1850's until 1975 (Blašković, 1975)

Geological records about the Slavonian Mountains, including the Psunj Mt. are described in **Stur (1861, 1862a,b)**. According to the author, the oldest Neogene deposits of the western slopes of the Psunj Mt. are located northern from Benkovac and Rogolji, and are comprised of "Lithothamnium limestone" ("*litavac*"; see more on topic "Lithothamnium limestone" and "litavac" and differences between them in e.g., **Basso et al., 2009**) and Badenian clay below, containing rich mollusc fauna, foraminifers and bryozoans.

**Paul (1870, 1872, 1874)** describes the younger Neogene deposits from Slavonia, including the Psunj Mt. area. He continues the stratigraphic research after Stur, and divides the deposits overlying the white marls on older "Congerian sediments", and younger "*Paludina* clays" or freshwater facies.

Paper by **Neumayr and Paul (1875)** is of big importance for the stratigraphy and paleontology of younger Neogene deposits in Slavonia. The authors described in detail the Pliocene of Slavonia emphasizing the "*Paludina* beds" and dividing them into the lower, middle and upper "*Paludina* beds" based on the phylogeny of the gastropod genus *Viviparus* (before known as *Paludina*).

The first detailed geological maps (M 1:75 000) of the area of Daruvar and Pakrac – Jasenovac are given by **Koch (1908a,b; 1935)**. He described the Neogene sediments as a ring around the western Slavonian Mountains. According to him, the oldest Neogene deposits are the Badenian "Lithothamnium limestone" (sometimes called "*litavac*") deposited in the shallow sea environments, and marls in the deep marine environments. The marls are older than the Badenian ("Tortonian") conglomerates near Rogolji, Trnakovac and Benkovac, described in **Stur (1861, 1862a,b)**. Koch corrected Stur's comparison of Rajić marls with the Sarmatian deposits of Radoboj and compared them with the Badenian marls. He also considers the white limy marls of the Upper Sarmatian by **Stur (1862b)** as the freshwater deposits of the Lower Pliocene, with the congerian marls and sands and "*Paludina* beds" in the top.

In the early 1940's began the more intensified geological research on oil and gas in northern Croatia. One of the most significant papers regarding the geology of Neogene deposits of northern Croatia and corresponding oil geology is **Ožegović (1944)**, in which the author describes stratigraphic relations of younger Neogene (then "Tertiary") deposits according to the data collected from the drilled cores. The research area to which belongs and here presented area, **Ožegović (1944)** describes as the valley of the river Ilova known as a "Tertiary" valley between the Moslavačka gora Mt. on the west, Psunj and Papuk Mts. on the east and Bilogora Mt. on north. Neogene basement was drilled in the wells of the Ilova River valley, i.e. the Ilova Subdepression (according to the petroleum geology division of the Croatian part of the Pannonian Basin System, abbr. CPBS), and the author concluded the existence of crystalline basement spread also in Moslavačka gora, Psunj and Papuk, Motajica and Prosara Mts. **Ožegović (1944)** mentioned Paleozoic and Mesozoic rocks of the Psunj Mt., which were most probably eroded from the crystalline basement of the drilled area, and gave the material for the Neogene sedimentation in the depressions.

The first part of the research era ends with the **Blašković (1975)** dissertation as a "path for the further research" of the Neogene sediments of the western slopes of the Psunj Mt. area. In his dissertation, **Blašković (1975)** gives special attention to the Ilova Subdepression as a connection between the Sava and Drava Depressions. He collects data on lithostratigraphic characteristics of the Neogene sediments, thickness of the deposits of the chronostratigraphic units and tectonic elements based on the field research, which he interprets together with the available geological, geophysical and deep drilling research data (**Blašković, 1975 and references therein**). **Blašković (1975)** also gives the reconstruction of the structural-tectonic and paleogeographical relations.

**2.2. Research papers after 1975 (Blašković, 1975)**

There are a few papers dealing with the Neogene sediments of the western slopes of the Psunj Mt. after the **Blašković (1975)** dissertation. The more detailed stratigraphic and paleoecological significance of the mentioned papers is given in Discussion chapter, and here are listed source selected as the most important for the further research in study area.

**Blašković et al. (1975)** described lithological and paleogeographical characteristics of the Miocene sediments at the western slopes of the Psunj Mt., between Kraguj and Šeovica, ranging from the Lower "Tortonian" (today Badenian) to the Upper Pannonian.

**Kranjec and Blašković (1976)** present the results of the detailed geological mapping of younger "Tertiary" (today Neogene) and Quaternary sediments from the western area of the Psunj Mt., i.e. Jagma – Popovac – Paklenica. The authors extended the knowledge of the stratigraphy, tectonics and structural-geomorphology of the investigated area, and emphasize the Upper Pontian (today Pannonian *sensu* **Pavelić and Kovačić, 2018** and references therein) and "*Paludina* beds" containing quartz-sands.

**Blašković et al. (1981)** described the Lower Sarmatian deposits from the southwestern slopes of the Psunj Mt., characterized by the regular rhythmic alternation distinguishing lithological sequences, and identifying the turbidity currents sedimentation caused by paleogeographic conditions between the Bijela Stijena–Novska paleostructure and Psunj Mt.

Different "Tortonian" (today Badenian) deposits from the area of Okučani, Pakrac and Novska, i.e. western slopes of the Psunj Mt., were described by **Blašković et al. (1982)**. The authors distinguished seven lithofacies, suggesting different depositional environments such as coastal, near-reef, reef, back-reef, turbidites and upper slope.

**Blašković et al. (1984)** summarize the results of the Miocene sediments research of the western slopes of the Psunj Mt., i.e., in the Lipik-Okučani-Novska region, and presented the lithofacies and sedimentological interpretation of the paleoenvironment and sedimentary conditions, particularly "pre-Tortonian" (pre-Badenian), "Tortonian" (Badenian) and Lower Sarmatian deposits.

Geology of the wider area of the western slopes of the Psunj Mt. is shown on the Basic Geological Map, sheets Nova Gradiška (**Šparica et al., 1984a**) and Daruvar (**Jamičić, 1989**), and described in the explanatory notes of the sheets (**Šparica et al., 1984b**; **Jamičić et al., 1989,** respectively).

Among the paleontological papers, **Kochansky-Devidé and Slišković (1978)** described dreisenid bivalves from the localities of the Miocene age in Croatia and Bosnia and Herzegovina, including the Rogolji locality.

**Sokač (1987)** described a new ostracod genus from the Bjelanovac section on the western slopes of the Psunj Mt., found in the pre-Badenian freshwater deposits, and indicating the Middle Miocene age.

From the recent papers, **Kruk et al. (2005)** described quartz sand deposit Jagma-6 near Lipik, explaining the paleoenvironmental conditions and genesis of the quartz sand in the Rhomboidea-beds of the upper Miocene.

**Malvić (2003)** described Neogene and Quaternary evolution of the Bjelovar Subdepression, which included also the Ilova Subdepression and western margins of the Psunj and Papuk Mts. The numerous data from deep wells are presented as well as regional structural and thickness maps using EK markers and borders, and lithostratigraphic formations or members in the Drava Depression. **Malvić (2011)** published separated and re-drawn set of such maps in the Bjelovar Subdepression.

## 3. Geological settings

The investigated area of Psunj Mt. during Neogene paleogeographically belonged to the Paratethys realm and later to consequent brackish and fresh water lakes (Pannon, Slavonia and smaller remnants) (e.g., **Rögl, 1998; Pavelić et al., 2003; Harzhauser and Piller, 2007; Kováč et al., 2007, 2017; Piller et al., 2007; Pavelić and Kovačić, 2018 and references therein; Vrsaljko et al., 2018 and references therein**). Paratethys started developing during the Oligocene, in the northern area of the former Tethys Ocean, and represented by a system of Paratethyan sedimentary basins distributed from Central Europe to Central Asia, due to tectonic changes. The connection of the Paratethys Sea with the Mediterranean and Indo-Pacific was unstable due to the constant paleogeographical changes controlled by geodynamic, climatic and glacio-eustatic fluctuations (e.g., **Rögl, 1998; Harzhauser and Piller, 2007; Piller et al., 2007; Kováč et al., 2017, 2018**), which reflected in opening and closing of the marine seaways. Due to the changes in fauna content between the Paratethys area/basins, three parts are recognized: Western, Central and Eastern Paratethys (e.g**., Rögl, 1998; Harzhauser and Piller, 2007; Kováč et al., 2007, 2017; Piller et al., 2007**). On the **Figure 1** is shown the location of the here presented area of Croatia, which belongs to the Central Paratethys area, and geotectonically to the Pannonian Basin System, bordered by the mountain chains of the Alps, Carpathians and Dinarides. The Central

Paratethys Sea persisted from the Oligocene to the Sarmatian with the open marine conditions and fully marine fauna (e.g., **Rögl, 1998; Harzhauser and Piller, 2007**; **Kováč et al., 2007; Piller et al., 2007**), and the major expansion (marine transgression) of the Central Paratethys is dated as the Middle Miocene and known as the Badenian marine flooding (e.g., **Rögl, 1998; Harzhauser and Piller, 2007**; **Kováč et al., 2007; Piller et al., 2007; Ćorić et al., 2009**; **Malvić, 2012**). During the Badenian marine connections were possibly open to the Mediterranean via the "Transtethyan Trench Corridor" (Slovenian gateway), but there is still strong debate going on about the existence of open marine connections between Paratethys and neighbouring marine areas during the Badenian stage (e.g., **Rögl, 1998; Studencka et al., 1998; Piller et al., 2007; Bartol et al., 2014**). There was also eastern connection toward Black Sea and Indopacific paleobasins. Open marine conditions persisted until ~12.6 Ma when the gradual extinction of the fully marine biota and disappearing of marine environments marks the regional Sarmatian age, being replaced by brackish, lacustrine, fluvial and terrestrial environments and living creatures (e.g., **Pavelić and Kovačić and references therein; Vrsaljko et al., 2018 and references therein**).

Here we present the general outline of the Neogene paleoenvironments of the Croatian part of the Pannonian Basin System (CPBS). The Pannonian Basin System formed in the Early Miocene due to the continental collision and subduction of the Euroasian plate beneath the Pannonian crustal fragment. CPBS is a rift-type basin. The extensional tectonics started during the Early Miocene and generated forming of the four half-grabens as the elongated subbasins as the main depocentres: Drava Depression, including the Bjelovar Subdepression, Sava Depression, including the Karlovac Subdepression, Mura Depression and Slavonija-Srijem Depression (e.g., **Pavelić and Kovačić, 2018 and references therein**; which also similar area described as the North Croatian Basins). The evolution of the basin is divided into two or four phases, synrift and postrift, during which the basin was marked by transgressive-regressive cycles (e.g., **Kováč et al., 2007, 2018; Pavelić and Kovačić and references therein**). Synrift phase lasted from the Early Miocene – Ottnangian, until the Middle Miocene – Middle Badenian, and was characterized by the continental environments changed to the marine environments. The postrift lasted from the Middle Miocene – Late Badenian to the Quaternary and was characterized by the marine environments replaced by continental environments. In later work it was improved in model with two transtensional and two transpressional phases (e.g., **Malvić and Velić, 2011**).

After the development of the Paratethys sea during the Eocene – Oligocene boundary, sedimentation continued during the Oligocene only in north-western Croatia (**Pavelić and Kovačić, 2018**; **Vrsaljko et al., 2018 and references therein**). The deposition in the CPBS started in the Ottnangian, with the formation of continental environments, with the oldest deposits being the alluvial deposits. **Pavelić and Kovačić (2018 and references therein)** assumed the existence of one large lake in the Early Badenian. Marine environments were introduced in the CPBS by one of the Middle Miocene – Badenian transgression (e.g., **Rögl, 1998**; **Kováč et al., 2007**; **Piller et al., 2007**; **Ćorić et al., 2009 and references therein**). Marine transgressions in the Paratethys area during the Early Miocene did not affect the CPBS, and the basement was unconformably overlain by deposits of different age. The full marine conditions lasted until the Sarmatian, during which the shallowing of the Central Paratethys started, and there was only a connection to the Eastern Paratethys by a narrow marine connection into the Indopacific/Black Sea (e.g., **Rögl, 1998**; **Piller et al., 2007**). The end of Sarmatian is marked by the regression caused by eustatic sea-level fall. The final isolation of the Central Paratethys Sea commenced around 11.6 Ma ago when Lake Pannon formed (e.g., **Magyar et al., 1999**; **Harzhauser and Piller, 2007**; **Piller et al., 2007**). Decreased salinity generated evolution of endemic, brackish-water fauna. The Pannonian lithology indicates that the river floodplains and delta systems already existed in CPBS by the early Pannonian and reached its eastern part in the latest Pannonian (**Pavelić and Kovačić, 2018 and references therein**). According to the recent studies (e.g., **Mandic et al., 2015**), the boundary between the Miocene and Pliocene is placed at about 4.5 Ma, marking the beginning of the Lake Slavonia. Described paleogeographical changes in the Central Paratethys resulted in the style of the development of the basin different from the Mediterranean, and evolution of endemic species, therefore the Neogene regional stages for the Central Paratethys have been introduced (**Figure 2**), which are, for the investigated area, described in the Discussion of this paper.

**Blašković (1975)** describes two geological complexes of the Ilova Subdepression area; (a) the magmatic-metamorphic complex with partially sedimentary complex of the Paleozoic and Mesozoic age, recorded on the surfaces of Papuk, Psunj and Moslavačka gora Mts., and also as the pre-Neogene basement of the wider area by drilled cores, and (b) sedimentary complex of the Neogene and Quaternary period (further in the text). The Paleozoic and Mesozoic rocks are considered the basement of the Neogene and Quaternary deposits and represent the terrestrial environments which gave the local material for the deposition of the younger sediments.

Here presented area of the western slopes of the Psunj Mt. is a part of the tectonic anticline structure, a structural nose. The axis of the nose stretches from the Bijela Stijena locality to the town of Novska (**Figure 2**) (e.g., **Blašković, 1975; Blašković et al, 1982, 1984**). Crystalline rocks are in the core of the structure, and the Neogene deposits surround the core marking the limbs and the forehead of the structure nose.

The investigated locality is located near the Rogolji locality (**Figure 2**), in the north-western part of the Bijela Stijena structure, where Middle Miocene – Badenian ("Helvetian" by **Jamičić et al., (1989)**) sediments are recorded (e.g, **Blašković, 1975; Blašković et al., 1982, 1984**).
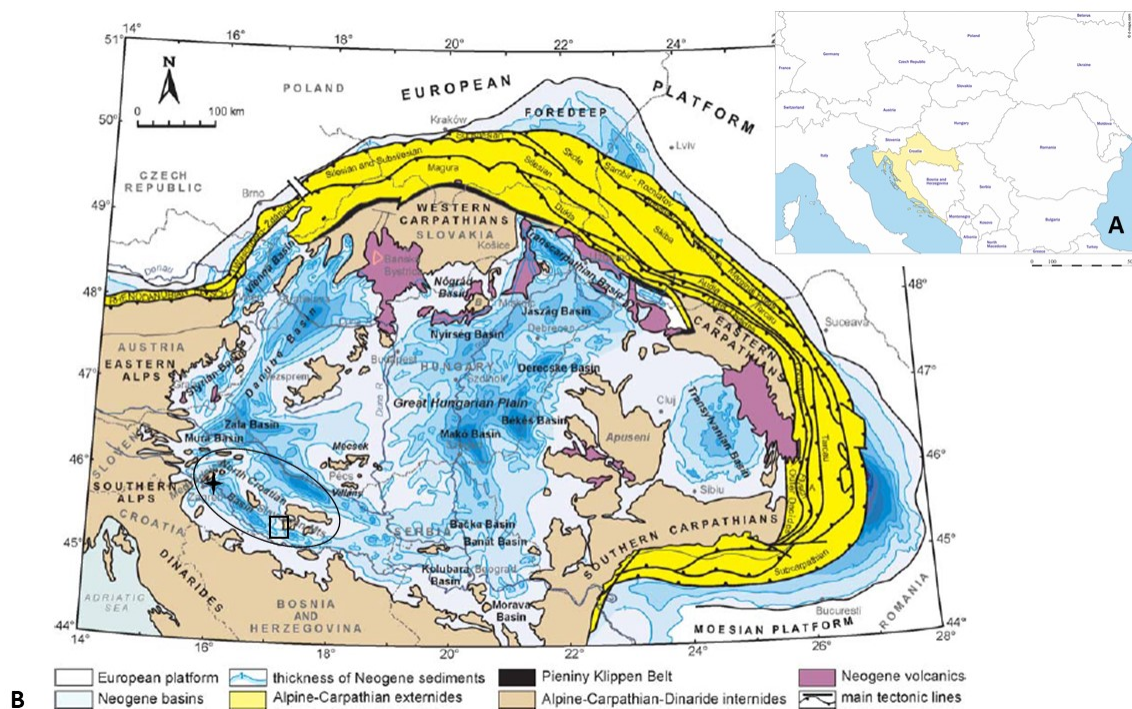


**Figure 1:** Pannonian Basin System (after **Kováč et al., 2007**). A) Geographical position of Croatia, coloured in yellow (after **https://d-maps.com/carte.php?num_car=2242&lang=en**). B) Pannonian Basin System. Marked area is the location of the Croatian part of the Pannonian Basin System. Four-point star marks the location of Zagreb, capital of Croatia. Rectangular marks the investigated area of the western slopes of the Psunj Mt.

## 4. Results

The schematic lithological column of the investigated outcrop on the Bijela Stijena structure is shown on **Figure 3**. The height of the outcrop is more than 8 meters and it is made of two sequences of the Badenian sediments. They overlay the Paleozoic Basement ("Temeljno gorje" in Croatian). The Neogene basement, in wider area, is composed of Paleozoic and Mesozoic rocks, but in both cases the top is represented by transgressive fluvial-lacustrine or marine Neogene sediments. The thickness can vary widely and sometimes cannot be determined (**Blašković, 1975**), but is measured on the here presented outcrop. The first sequence recognized at the outcrop is made of the fine-grained laminated sandstones with the thickness 3 meters or more (**Figure 3**). The sandstones contain biogenic detritus, with fragments of corals, molluscs (bivalves ostreids and pectinids), echinoid spines and possible algae, indicating the fully marine conditions with prevailing fossil echinoid spines. The second sequence of sandstones is around 5 meters or more thick. The sandstones are characterized with coarsening upward sequence and are consisted of fragments of fine-grained sandstones in a dominant conglomeratic sandstone (**Figure 3**). Fossil findings are similar as in the first sandstone sequence, but more crushed, and again with echinoid spines as the most numerous fossil findings.
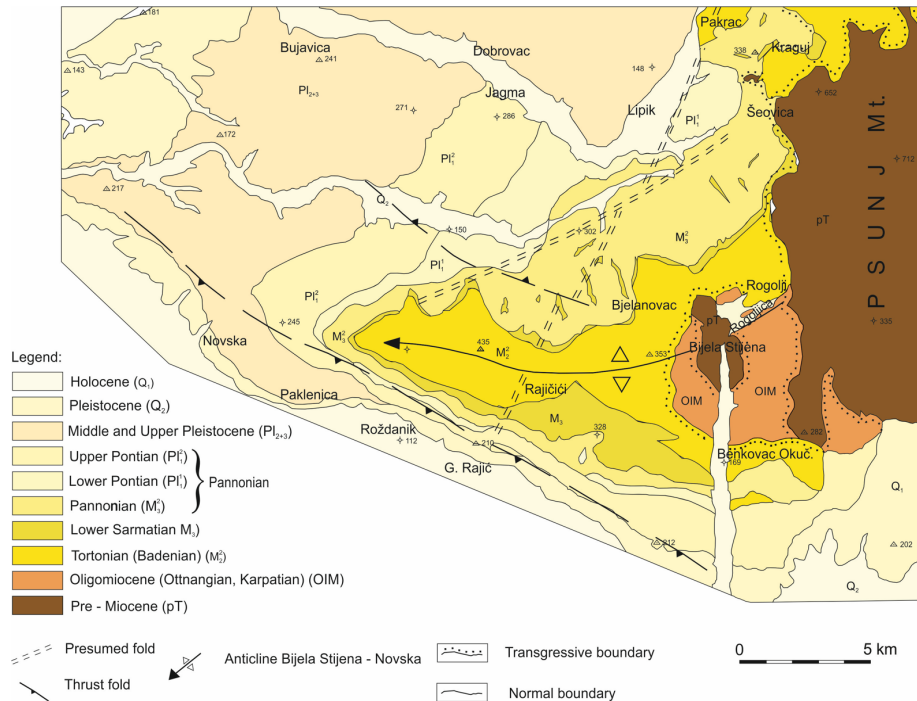
**Figure 2.** Neogene regional stages for the Central Paratethys compared to the stratigraphic units in **Blašković (1975)** and **Blašković et al. (1982, 1984)** for the area of the western slopes of the Psunj Mt. shown on the schematic geologic map (after **Blašković, 1975**). *after International Commission on Stratigraphy 2020 (**www.stratigraphy.org**); ** after **Pavelić and Kovačić (2018)** and references therein; ***after **Blašković (1975)** and **Blašković et al., (1982, 1984)**
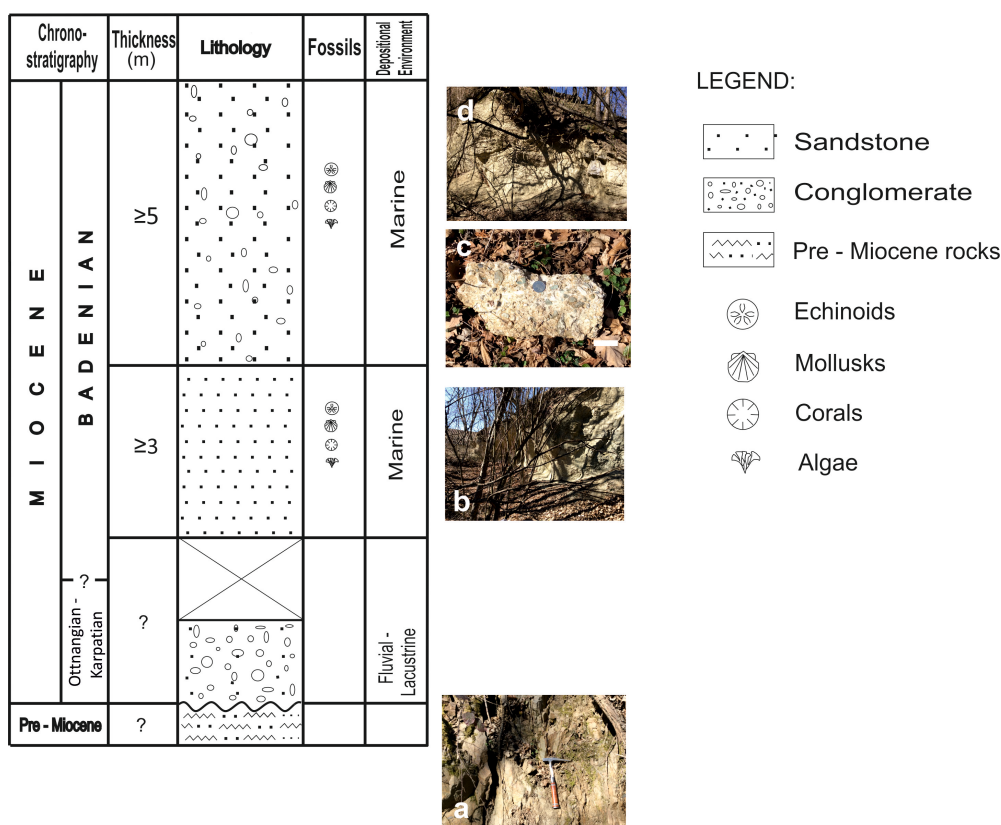
**Figure 3.** Schematic geological column of the investigated outcrop Bijela Stijena near Rogolji. a) Pre-Miocene rocks, in the wider area of Rogolji locality); b) First Badenian sandstone sequence; c and d) Second Badenian conglomeratic sandstone sequence.

## 5. Discussion and Conclusions

As can be seen in the research papers of the Neogene sediments of the western slopes of the Psunj Mt. and wider area, the Neogene deposits recognized at the area are divided in the chronostratigraphic units according to the "old chronostratigraphic unit" of the CPBS shown on the **Figure 2**. The old units are compared to the "new chronostratigraphic division" of the Central Paratethys and described in this chapter.

### 5.1. Neogene stratigraphic units of the western slopes of the Psunj Mt.

*5.1.1. Lower Miocene – Ottnangian – "Oligomiocene"*

The oldest deposits disconformably covering the pre-Miocene basement are of the "Oligomiocene" age after **Blašković (1975)** or "Pretortonian" after **Blašković et al. (1984)**, corresponding to the recent division to the Lower Miocene – Ottnangian (**Figure 2**). In the general lithology of the stratigraphic unit, dominate marls with subordinately present sands, conglomerates and gravels (**Blašković, 1975; Blašković et al., 1984**) recorded at the Rogolji and Bjelanovac locality (silty marls) and Okučanski Benkovac I, Dobrovac and Rogoljica (conglomerates, gravels, sands/sandstones) (**Figure 2**). **Blašković et al. (1984)** report fragments of bryozoans, bivalves, echinoids and planktic foraminifers found in the sandstones, and redeposited from the coastal area.

In the Lower Miocene deposits, **Blašković et al. (1984)** differentiate four lithofacies: A) low energy shallow sea or marly lithofacies; B) near coast, chaotic coarse-grained clastic sediments; C) delta fans D) fine-grained clastic-carbonate (basin) deposits.

From the investigated localities in the literature, freshwater and marine-brackish developments are distinguished. The freshwater development is present at the Rogolji and Bjelanovac localities, corresponding to the above mentioned

lithofacies A (**Figure 2 after Blašković, 1975**), supported by the present dreienids and ostracods (**Blašković, 1975**; **Blašković et al., 1984**), and **Kochansky-Devidé and Slišković (1978)** defined Rogolji locality as the Ottnangian in age according to the dreisenid fauna. Profile in the area of Okučanski Benkovac after **Blašković (1975)** (**Figure 2**) comprises marine-brackish sediments deposited in the marine environment with weak freshwater influx.

The Lower Miocene deposits of the western slopes of the Psunj Mt. were deposited in the alluvial environment in the time span from the beginning of the Ottnangian to the end of the Karpatian (e.g., **Pavelić and Kovačić, 2018 and references therein**).

### 5.1.2. Middle Miocene – Badenian– "Tortonian"

Middle Miocene, "Tortonian" (= Badenian) deposits are recorded in the area east of the Pakrac and Lipik cities (**Figure 2**). They are marked by the lithological diversity as a result of varied environmental and depositional conditions, paleorelief, and by the regularity in the lateral and vertical changes (e.g., **Blašković et al., 1982 and references therein**). The Badenian deposits of the western slopes of the Psunj Mt. are made of conglomerates, conglomeratic sands / sandstones, sands / sandstones, biocalcrudites and biocalcarenites, sandy and silty marls and clayey limestones (**Blašković, 1975; Blašković et al., 1982**).

There are seven Badenian lithofacies recognized at several localities in the western part of the Psunj Mt. according to **Blašković et al. (1982)**:

(A) coarse-grained clastic coastal (littoral) lithofacies
(B) biohermal lithofacies
(C) biocalcarenitic fore-reef lithofacies
(D) lithofacies of back-reef shoals
(E) sandy-marly lithofacies
(F) lithofacies of transitional slope
(G) turbidite lithofacies

**Blašković et al. (1982)** describe in detail the lithofacies recognized at the area of Bijela Stijena structure (localities Rogolji, Bjelanovac, Bijela Stijena), northern from the Bijela Stijena structure, in the area east from Pakrac (localities Šeovica, Omanovac, Sigovac) and west and south from the Bijela Stijena structure (localities Rajičići, Dobrovac, Okučanski Benkovac, Luka stream, Roždanik) (**Figure 2**). At the area of Bijela Stijena structure authors recognized lithofacies A, C and E, and eastern from Pakrac city the lithofacies B and D are present. Lithofacies E is present in the area of Bijela Stijena structure and eastern from Pakrac (**Figure 2**). To the west and south from the Bijela Stijena structure, lithofacies F and G are recognized.

*Lithofacies (A)* is recognized at the Rogolji, Bjelanovac and Bijela Stijena localities (**Figure 2**), and is comprised of transgressive conglomerates of the coastal environments lying on the pre-Badenian marls or directly on the crystalline rocks (**Blašković, 1975; Blašković et al., 1982**). There are differences in the fossil record between these localities: in Rogolji prevail fragments of lithothamnions (coralline algae), bivalves and bryozoans, and at the Bjelanovac and Bijela Stijena area the most numerous are fragments of echinoids and bivalves (**Blašković et al., 1982**).

The area east of Pakrac city (**Figure 2**) is covered by "Lithothamnium limestones" of *lithofacies (B)*, covering the Badenian transgressive contact with the crystalline basement (Šeovica, Omanovac, Sigovac) as described in **Blašković et al. (1982)**. Together with numerous coralline algae, there are recorded pectinid and ostreid bivalves, gastropods and bryozoans.

*Lithofacies (C)* is present at the Rogolji locality (**Figure 2**), with uniform development of biocalcarenites with well sorted fragments of lithothamnions, echinoids, bryozoans, bivalves and scarce benthic foraminifera (**Blašković et al., 1982**).

*Lithofacies (D)* is marked by the Badenian transgressive sediments with bivalve coquinas (pectinids, ostreids) in a clayey-carbonate (marly) matrix, and smaller pectinids, brachiopods and echinoid spines. At the investigated localities Sigovac and Šeovica (east from Pakrac city, **Figure 2**), the Badenian sediments are directly overlying the crystalline basement (**Blašković et al., 1982**). The authors recorded lateral transition of lithofacies (D) into lithofacies (B), covered by the sediments of the lithofacies (E).

**Blašković et al. (1982)** describe *lithofacies (E)* in the area of Bijela Stijena structure and at the localities east from the Pakrac city (**Figure 2**), as a sequence with mostly vertical exchange of sandy-marly sediments. The most numerous fossils are fragments of bryozoans, bivalves and echinoids, and less lithothamnion fragments and benthic foraminifera.

The authors also recorded bentonite layers at the Bjelanovac locality (**Figure 2**), which could indicate altered tuff and/or tuffites.

From the Bijela Stijena structure to the west, **Blašković et al. (1982)** describe the transition from the lithofacies (A), (C) to (E) and *lithofacies (F)*, which is marked by the frequent change of sand layers, sandy-silty marls and marls. Lithofacies (F) is changing to the *lithofacies (G)* in the deeper parts of the sedimentary basins, marking the turbiditic lithofacies. Lithofacies (G) is recorded also in the southern part of the Bijela Stijena structure and marked by the regular rhythmic change of sequences made of conglomeratic sand / sandstones, middle- to fine-grained sands / sandstones, sandy-silty marls, marls and sometimes marls rich in carbonate and /or clayey limestones.

The analysed outcrop near Bijela Stijena structure shown on **Figure 3**, corresponds to the lithofacies (A). The sandstone sequence with conglomerates points to the transgressive rocks of the coastal environments, and the zone of high wave energy. Fossil fragments of red algae and echinoids point to the shallow environments and reef structures. Crushing of the shells in the high energy water produced fossil detritus deposited in the interspace of coarser pebbles.

According to **Pavelić and Kovačić (2018),** Early Badenian of the Croatian part of the Pannonian Basin System is marked by the lacustrine development, with gradual replacement by the marine environments due to the marine transgression and flooding during the Middle Badenian. The end of the Badenian is also marked by the widespread transgression in the Late Badenian, which was of regional character. The marine deposits of the "Tortonian" age described in older papers correspond to the Middle and Late Badenian sediments.

### 5.1.3. Middle Miocene – Sarmatian– Lower Sarmatian

Lower Sarmatian deposits conformably overlie the Badenian sediments (**Blašković, 1975**). **Blašković et al. (1984)** describe Lower Sarmatian deposits as similar to turbiditic lithofacies (G) of the "Tortonian" (Badenian), with main characteristic of frequent and regular rhythmic change between sandy-marly-clayey-carbonate sediments, described also in **Blašković et al. (1982)**. From the investigated Lower Sarmatian profiles, **Blašković (1975)** describes redeposition of Badenian fossils in the Sarmatian, with exception of fauna adapted to the brackish Sarmatian conditions.

**Pavelić and Kovačić (2018)** describe Sarmatian deposits as overlying the Badenian in a continuous depositional succession with a transgressive-regressive cycle. The latest Badenian was marked by the sea-level fall, and the deposition of Sarmatian sediments was in a restricted marine environment of reduced salinity, with the shallowing trend in the latest Sarmatian, marking the beginning of closure of the CPBS.

### 5.1.4. Upper Miocene – Pannonian

The boundary between the Sarmatian and Pannonian is marked by a major drop in a sea-level base. During the Pannonian, area of the CPBS was isolated from the sea, forming the brackish Lake Pannon with a consequent adaptation and speciation of endemic molluscs (**Pavelić and Kovačić, 2018 and references therein; Vrsaljko et al., 2018 and references therein**). Pannonian is divided into four zones based on the present molluscs (the oldest *Croatica*, *Banatica*, *Abichi* and the youngest *Rhomboidea* beds). The *Croatica*-beds were deposited during the low-stand, as a consequence of the regression in the latest Sarmatian. *Banatica*- and *Abichi*-beds were deposited in the deeper lake environments. *Rhomboidea*-beds are characterized by delta front due to a final infilling and closing of the lake.

Until recently, Upper Miocene sediments of the CPBS were divided into the Pannonian and Pontian horizons, with the subdivision on the zones based upon molluscs: Croatica (lower Pannonian, based on the gastropod *Radix croatica*), Banatica (upper Pannonian, based on the bivalve *Congeria banatica*), Abichi (lower Pontian, based on the bivalve *Paradacna abichi*) and Rhomboidea (upper Pontian, based on the bivalve *Congeria rhomboidea*). According to the new division of the Upper Miocene in the CPBS (**Figure 2**), there is only the Pannonian stage in the Upper Miocene, and the four marker zones are considered to be of the early Pannonian (Croatica- and Banatica-beds) age and of the late Pannonian (Abichi- and Rhomboidea-beds) age (**Pavelić and Kovačić, 2018 and references therein**). The authors also mention the possibility that the upper Rhomboidea-beds were deposited during the Pliocene Epoch (Early Pliocene = Zanclean).

#### a) Lower Pannonian (Croatica beds)

Pannonian sediments *sensu stricto* are, in the wider area of Bijela Stijena structure, mostly represented by the marly limestones, calcareous marls and marls. They overlie the Lower Sarmatian, Badenian or pre-Miocene deposits (**Blašković, 1975; Blašković et al., 1975**).

The dominant member of the *Croatica* beds are the clayey limestones ("white marls"), with marls, silty and sandy marls and mostly thin layers of sand, that is, sandstones (**Blašković et al., 1984**).

**Kranjec and Blašković (1976)** describe the Upper Miocene deposits of the area between Jagma, Popovac and Paklenica (**Figure 2**). The authors describe Croatica-beds in two sequences: lower part is composed of hard, thick and thin platy white and light grey marly limestone, while in the upper part marly limestones and limy marls prevail. Fossils recorded in the *Croatica*-beds are characteristic for the Pannonian ("Lower Pannonian") deposits and comprise freshwater molluscs: gastropods *Radix croatica* (Gorjanović-Kramberger, 1890), *Radix extensa* (Gorjanović-Kramberger, 1890) (old name *Lymnaea extensa* Gorjanović-Kramberger, 1890), *Gyraulus vrapceanus* Neubauer, Harzhauser, Kroh, Georgopoulou & Mandic, 2014 (old name *Planorbis dubius* Gorjanović-Kramberger, 1890), *Gyraulus* (*Gyraulus*) *praeponticus* (Gorjanović-Kramberger, 1890), then bivalves limnocardiids, dreisenids, ostracods and fish remains (**Blašković, 1975; Kranjec and Blašković, 1976**).

*b) Upper Pannonian (*Banatica *beds)*

*Banatica*-beds overlie the *Croatica*-beds (**Figure 2**), and are lithologically similar to them, represented by the mostly grey and light grey marls with freshwater mollusc fauna (e.g., bivalve *Congeria banatica* R. Hörnes, gastropod *Gyraulus tenuistriatus* (Gorjanović-Kramberger, 1899) (old name *Planorbis tenuistriatus* Gorjanović-Kramberger, 1899) and fossil flora remains (**Blašković, 1975; Kranjec and Blašković, 1976**).

*c) Lower Pontian (*Abichi *beds)*

*Abichi*-beds (**Figure 2**) overlie the marly sediments of the *Banatica*-beds, and are represented by the light and dark grey greyish to brownish marls and clayey marls rich in macrofossils: bivalves *Paradacna abichi* R. Hörnes, *Paradacna* sp., *Congeria zagrabiensis* Brusina and gastropods *Gyraulus tenuistriatus* (Gorjanović-Kramberger, 1899) (old name *Planorbis tenuistriatus* Gorjanović-Kramberger, 1899), *Lymnaea* sp., Valenciennius reussi Neumayr in Neumayr & Paul, 1875 (old name *Valenciennesia reussi* Neumayr in Neumayr and Paul, 1875), *Valenciennesius* sp. (**Blašković, 1975; Kranjec and Blašković, 1976**).

*d) Upper Pontian (*Rhomboidea *beds)*

Rhomboidea-beds represented by marls, clay and sands concordantly come on the Abichi-beds and make the continued belt around the Bijela Stijena structure–Novska area (**Figure 2**). **Blašković (1975)** and **Kranjec and Blašković (1976)** describe two parts of the Rhomboidea-beds: marly sediments in the lower part, and sandy-clayey sediments with limy concretions in the upper part. The authors list rich fossil findings in *Rhomboidea*-beds: bivalves (e.g., *Congeria rhomboidea* M. Hörnes, *C. zagrabiensis* Brusina, *C. croatica* Brusina, *Limnocardium* (*Arpadicardium*) *mayeri* Hörnes, *Limnocardium* sp., *Paradacna okrugici* (Brusina)), gastropods (e.g., Valenciennius reussi Neumayr in Neumayr & Paul, 1875 (old name *Valenciennesia reussi* Neumayr in Neumayr & Paul, 1875), *Planorbis* sp., *Unio* sp., *Melanopsis lepavinensis* Brusina, 1897, *M. sabolici* Brusina, 1902, *Goniochilus croaticus* (Brusina, 1892) (old name *Micromelania croatica* (Brusina, 1892)), *Zagrabica ampullacea* Brusina, 1884, etc.), ostracods, redeposited foraminifers, fish remains, and freshwater gastropods viviparids in the latest Rhomboidea-beds, marking the transition to the Pliocene.

*5.1.5. Pliocene – "*Paludina *beds"*

Pliocene sediments are well distributed in the western part of the Psunj Mt. (**Figure 2**). As described by **Blašković (1975)** and **Kranjec and Blašković (1976)**, they are well defined based on the fossil content, mostly on the freshwater gastropods Viviparidae and divided into the lower, middle and upper "*Paludina* beds" (*Paludina* is the old genus name for *Viviparus*). "*Paludina* beds" are made of regular repeating of the mostly clayey and less sandy sediments, continuing on the upper part of the *Rhomboidea* beds.

**5.2. Neogene paleogeography and paleoenvironments of the western slopes of the Psunj Mt.**

Neogene stratigraphic units recorded on the western slopes of the Psunj Mt. are listed in the chapter 5.1. and described in detail in cited papers. Based on the investigated localities, **Blašković (1975), Blašković et al. (1975, 1982,**

**1984)** and **Kranjec and Blašković (1976)** gave an overview of the paleonvironmental development of the western part of the Psunj Mt. area during the Miocene.

Pre-Miocene deposits are described from the localities Rogolji and Okučanski Benkovac in the area of Bijela Stijena structure (e.g., **Blašković, 1975; Blašković et al., 1984**). Locality Rogolji is determined as a freshwater development, and Okučanski Benkovac as a brackish-marine development (**Figure 2**), indicating the existence of a land mass, that is an anticline Bijela Stijena–Novska, as a shallow barrier which divided these two areas (**Blašković, 1975**).

As described in **Blašković (1975)** and **Blašković et al. (1982)** due to the Badenian marine transgression over the pronounced paleorelief and tectonic changes in the basin, Badenian sediments ("Tortonian") in the area between Okučani, Novska and Pakrac (**Figure 2**) show different lithofacies characteristics as described in the previous chapter, pointing to the different depositional conditions and environments. Psunj Mt. crystalline massif with the Bijela Stijena structure, as the submarine reef, played the main role in the lithofacies development. Psunj Mt. represented the coastal area during the Badenian marine transgression and was a source of material for the filling of the basin due to the constant eustatic changes. Also, the rugged coast enabled the evolution of various environments and fauna. Conglomerates were developed in the coastal area due to the abrasion of the coast and influx of the eroded material in the zone of high energy waves and represent the above mentioned Badenian lithofacies (A) (coarse-grained coastal lithofacies). In the coastal area with less pronounced terrigenous influx, lithofacies (B; biohermal lithofacies) is developed. Sediments of lithofacies (E; sandy-marly lithofacies) are developed in time of more intensive terrigenous particles input. Fossil detritus produced by crushing the biogenic reefs is deposited in the near-reef environments as lithofacies (C, biocalcarenitic lithofacies), or it is deposited in the deeper part of the basin as a turbiditic lithofacies (G). Lithofacies comprised of coquinas (D) is developed in the back-reef environments with favorable ecologic conditions for molluscs, brachiopods and echinoids.

**Blašković et al. (1975)** assume the existence of land mass in the area of Lipik during the Badenian and Lower Sarmatian, which was possibly connected to the land mass of the crystalline rocks in Omanovac as a barrier of the basin south of Kraguj to the open sea (**Figure 2**). Although the Lower Sarmatian is marked by the transgression, it is of local character, and Sarmatian sediments are generally deposited in the regressive conditions (**Blašković, 1975**). The sedimentary basin is starting to close, the fossil fauna is redeposited from the Badenian and the water salinity is decreasing influencing the development of the brackish fauna. Material is in the basin transported as a turbiditic sequence as described in (e.g., **Blašković, 1975; Blašković et al., 1984**).

The beginning of the Upper Miocene is marked by the regional transgression. The deposition of the Upper Miocene sediments is similar in lithology, with marl as a dominant member with less strong tectonic activity. The transition to the Pliocene is gradual but short, and indicated by the regressive tendencies, tectonic movements, and climatic changes (e.g., **Blašković, 1975**).

### 5.3. Further actualization of Prof. Blašković's work

The analysed outcrop is only a small fragment selected to revive the researching of the Psunj Mt. area, as a heritage of perennial and fruitful work of the Dr. Ivan Blašković, Full Prof. Authors here describe all main Neogene sequences important for the regional geology of the Psunj Mt. and wider reconstruction of the Paratethys period in the CPBS. They could be correlated with lithological composition, stratigraphic position and petrophysical properties of the Neogene-Quaternary sediments and basement rocks, especially on the west, in the Bjelovar Subdepression and specially the Ilova Subdepression. Badenian deposits (the Mosti Member) are proven as a promising reservoir rocks in the northern, northeastern and central part of the subdepression.

Structural interpretation could be done using regional EK markers and borders and lithostratigraphic units, but on particular localities, like presented, the smaller units can be selected and mapped. However, regionally it was the most promising to map EK border Tg/Pt (basement/Neogene), EK marker Rs7 (Sarmatian/Pannonian) and Rs5 (Lower Pannonian/Upper Pannonian), i.e. Mosti and Križevci Members (as part of the Moslavačka gora Formation). It is sure that one of two main fault systems in the Bjelovar Subdepression play crucial tectonic role on the western margins of the Psunj Mt. It strikes approximately west/northwest-east/southeast (approximately longitudinal). Fault activity, as well as the weathering, especially of the Paleogene rocks, caused strong disintegration of the upper part of the basement rocks and sedimentation of coarse-grained deposits, mostly in the alluvial-fan environments, which are characterized by a strong and abrupt transport.

# 6. References

Bartol M., Mikuž V. and Horvat A. (2014): Palaeontological evidence of communication between the Central Paratethys and the Mediterranean in the late Badenian/early Serravalian. Palaeogeogr. Palaeoclimatol. Palaeoecol. 394, 144–157. https://doi.org/10.1016/j.palaeo.2013.12.009

Basso, D., Vrsaljko, D. and Grgasović, T. (2009): The coralline flora of a Miocene *maërl*: the Croatian "Litavac". Geologia Croatica, 61/2-3, 333–340.

Blašković, I. (1975): Geološki odnosi područja između Moslavačke gore i Psunja (Ilovska depresija) (*Geology of the area between Moslavačka gora Mt. and Psunj Mt., Ilova depression*). Rudarsko-geološko-naftni fakultet Sveučilišta u Zagrebu, Zagreb, 75 p. (*in Croatian*)

Blašković, I., Sokač, A. and Šikić, L. (1975): Biostratigrafski i paleogeografski odnosi miocenskih naslaga u području Kraguja, istočno od Pakraca (*Biostratigraphy and palaeogeography of Miocene deposits in the Kraguj area, east of Pakrac, Northern Croatia – in Croatian with English abstract*). Geološki vjesnik, 28, 25-34. 551.782:551.882(161.17.45)

Blašković, I., Tišljar, J. and Velić, J. (1981): Ritmička sedimentacija donjosarmatskih naslaga jugozapadnih obronaka Psunja (*Rhythmic sedimentation of the Lower Sarmatian deposits of the southwestern slopes of Mt. Psunj – in Croatian with English abstract*). Nafta, 32, 1, 5-14. UDK 551.782.13:552.51/.52:552.54

Blašković, I., Tišljar, J. and Velić, J. (1982): Litofacijelne značajke tortonskih naslaga u području Okučani–Pakrac–Novska (*Lithofacies characteristics of Tortonian deposits in the area of Okučani–Pakrac–Novska, Northern Croatia – in Croatian with English abstract*). Geološki vjesnik, 35, 71-86. UDK 551.782(497 .13)

Blašković, I., Tišljar, J., Dragičević, I. and Velić, J. (1984): Razvoj sedimentacijskih okoliša miocenskih naslaga na zapadnim obroncima Psunja, sjeverna Hrvatska (*Development of the Sedimentary Environments in the Miocene on the Slopes of the Psunj Mountain, North Croatia – in Croatian with English abstract*). Geološki vjesnik, 37, 11-32. UDK 551.782(497.13)

Ćorić, S., Pavelić, D., Rögl, F., Mandic, O., Vrabac, S., Avanić, R. and Vranjković, A. (2009): Revised Middle Miocene datum for initial marine flooding of North Croatian Basins (Pannonian Basin System, Central Paratethys). Geol. Croat. 62, 31–43. https://doi.org/10.4154/GC.2009.03

Harzhauser, M. and Piller, W.E. (2007): Benchmark data of a changing sea – palaeogeography, palaeobiogeography and events in the Central Paratethys during the Miocene. Palaeogeogr. Palaeoclimatol. Palaeoecol. 253, 8–31. http://dx.doi.org/10.1016/j.palaeo.2007.03.031.

Jamičić, D. (1989): Basic Geological Map 1:100 000, sheet Daruvar L 33-95. Geološki zavod Zagreb (1988), Savezni geološki zavod Beograd.

Jamičić, D., Vragović, M. and Matičec, D. (1989): Basic Geological Map 1:100 000. Explanatory notes for sheet Daruvar L 33-95. Geološki zavod Zagreb (1988), Savezni geološki zavod Beograd, 1-51 (*in Croatian*).

Koch, F. (1908a): Geologijska prijegledna karta Kraljevine Hrvatske-Slavonije, list Daruvar, 1:75 000 (*Geological map of the Kingdom Croatia-Slavonia, Daruvar sheet, 1:75 000*). Kr. hrv. slav.-dalm. vlada, Zagreb.

Koch, F. (1908b): Geologijska prijegledna karta Kraljevine Hrvatske-Slavonije, Tumač geologijske karte Daruvar (*Geological map of the Kingdom Croatia-Slavonia, explanatory notes for sheet Daruvar – in Croatian*). Kr. hrv. slav.-dalm. vlada, VI, Zagreb.

Koch, F. (1935): Geološka karta Jugoslavije, list Pakrac – Jasenovac, 1:75 000 (*Geological map of Yugoslavia, Pakrac – Jasenovac sheet, 1:75 000*). Geol. inst. Kralj. Jugosl., Beograd.

Kochansky-Devidé, V. and Slišković, T. (1978): Miocenske kongerije Hrvatske, Bosne i Hercegovine (*Miozäne Kongerien in Kroatien, Bosnien und Herzegowina – in Croatian with German summary*). Palaeontologia Jugoslavica, 19, 1-98.

Kováč, M., Andreyeva-Grigorovich, A., Bajraktarević, Z., Brzobohatý, R., Filipescu, S., Fodor, L., Harzhauser, M., Nagymarosy, A., Oszczypko, N., Pavelić, D., Rögl, F., Saftić, B., Sliva, Ľ. and Studencka, B. (2007): Badenian evolution of the Central Paratethys Sea: palaeogeography, climate and eustatic sea level changes. Geol. Carpath. 58, 579–606.

Kováč, M., Hudáčková, N., Halásová, E., Kováčová, M., Holcová, K., Oszczypko-Clowes, M., Báldi, K., Less, Gy, Nagymarosy, A., Ruman, A., Klučiar, T. and Jamrich, M. (2017): The Central Paratethys palaeoceanography: a water circulation model based on microfossil proxies, climate, and changes of depositional environment. Acta. Geol. Slovaca 9, 75–114.

Kováč, M., Halásová, E., Hudáčková, N., Holcová, K., Hyžný, M., Jamrich, M. and Ruman, A. (2018): Towards better correlation of the Central Paratethys regional time scale with the standard geological time scale of the Miocene Epoch. Geologica Carpathica, 69, 3, 283–300. doi: 10.1515/geoca-2018-0017

Kranjec, V. and Blašković, I. (1976): Geološki odnosi u području Jagma-Popovac-Paklenica (zapadna Slavonija; sjeverna Hrvatska) s osobitim obzirom na pojave kremenih pijesaka (*Geology of the Jagma-Popovac-Paklenica area (Western Slavonia; Northern*

*Croatia) as regards the occurrences of quartz-sands – in Croatian with English abstract*). Geološki vjesnik, 29, 91-123. 551.7:553.623(161.17 .45)

Kruk, B., Kastmüller, Ž., Kovačić, M., Vrsaljko, D. and Miknić, M. (2005): Točka 2: Ležište kremenog pijeska Jagma-6 kod Lipika (*Quartz Sand Deposit Jagma-6 near Lipik – in Croatian*). In: Biondić, R., Vlahović, I. and Velić, I. (eds.): Excursion Guide-Book, Third Croatian Geological Congress, Opatija, 29.9.-1.10.2005. Croatian Geological Society, Croatian Geological Survey, Faculty of Science, Faculty of Mining, Geology and Petroleum Engineering, INA-Industrija nafte d.d., 8-10.

Magyar, I., Geary, D.H. and Müller, P. (1999): Palaeogeographic evolution of the Late Miocene Lake Pannon in central Europe. Palaeogeogr. Palaeoclimatol. Palaeoecol. 147, 151–167.

Malvić, T. (2003): Naftnogeološki odnosi i vjerojatnost pronalaska novih zaliha ugljikovodika u bjelovarskoj uleknini (*Oil-Geological Relations and Probability of Discovering New Hydrocarbon Reserves in the Bjelovar Sag*). Doctoral thesis, University of Zagreb, Faculty of Mining, Geology and Petroleum Engineering, 123 p. + enclosures

Malvić, T. (2011): Geological maps of Neogene sediments in the Bjelovar Subdepression (northern Croatia). Journal of Maps, 2011, S.I., 304-317. doi:10.4113/jom.2011.1185

Malvić, T. and Velić, J. (2011): Neogene Tectonics in Croatian Part of the Pannonian Basin and Reflectance in Hydrocarbon Accumulations. In: Schattner, Uri (ed.): New Frontiers in Tectonic Research: At the Midst of Plate Convergence, InTech, 215-238, Rijeka.

Malvić, T. (2012): Review of Miocene shallow marine and lacustrine depositional environments in Northern Croatia. Geological quarterly, 56, 3, 493-504.

Mandic, O., Kurečić, T., Neubauer, T.A. and Harzhauser, M. (2015): Stratigraphic and palaeogeographic significance of lacustrine molluscs from the Pliocene *Viviparus* beds in central Croatia. Geologia Croatica, 68/3, 179–207.

Neumayr, M. and Paul, M. (1875): Die Congerien und Paludinenschichten Slavoniens und deren Faunen (*in German*). Abhandl. geol. R. A., 7, 3.

Ožegović, F. (1944): Prilog geologiji mlađeg terciara na temelju podataka iz novijih dubokih bušotina u Hrvatskoj (*Beitrag zur Geologie des jüngeren Tertiärs Kroatiens auf Grund der Ergebnisse aus neueren Tiefbohrungen – in Croatian with German summary*). Vjestnik Hrvatskog državnog geoložkog zavoda i Hrvatskog državnog geoložkog muzeja, II/III, 391-491.

Paul, C. M. (1870): Beitrage zur Kenntnis der Congerien-Schichten West-Slavoniens (*in German*). Jahrb. geol. R. A., 20.

Paul, C. M. (1872): Die Neogenablagerungen Slavoniens (*in German*). Verh. geol. R. A.

Paul, C. M. (1874): Die Braunkohlen-Ablagerungen von Croatien (*in German*). Jahrb. geol. R. A., 24, 287-324.

Pavelić, D., Avanić, R., Kovačić, M., Vrsaljko, D. and Miknić, M. (2003): An outline of the evolution of the Croatian part of the Pannonian Basin System. In: Vlahović, I. and Tišljar, J. (Eds.), Evolution of Depositional Environments from the Palaeozoic to the Quaternary in the Karst Dinarides and the Pannonian Basin. 22nd IAS Meeting of Sedimentology, Opatija – Sept. 17–19, 2003. Field Trip Guidebook, Zagreb, 155–161.

Pavelić, D. and Kovačić, M (2018): Sedimentology and stratigraphy of the Neogene rift-type North Croatian Basin (Pannonian Basin System, Croatia): A review. Marine and petroleum geology, 91, 455-469. doi: 10.1016/j.marpetgeo.2018.01.026.

Piller, W., Harzhauser, M. and Mandic, O. (2007): Miocene Central Paratethys stratigraphy – current status and future directions. Stratigraphy 4, 151–168.

Rögl, F. (1998): Palaeogeographic considerations for Mediterranean and Paratethys seaways (Oligocene to Miocene). Ann. Naturhist. Mus. Wien 99 A 279–310.

Sokač, A. (1987): *Pannoninotus* n. gen. (Crustacea, Ostracoda) from the Middle Miocene of Bjelanovac (Psunj Mountain, North Croatia). Geološki vjesnik, 40, 39-44. UDC 565.3:551.782

Studencka, B., Gontsharova, I.A. and Popov, S.V. (1998): The bivalve faunas as a basis for reconstruction of the Middle Miocene history of Paratethys. Acta Geologica Polonica, 48, 3, 285–342.

Stur, D. (1861): Erste Mitteilungen über die geologische Übersichtsaufnahme von West-Slavonien (*in German*). Verhandl. geol. R. A., 12/1, 115-118.

Stur, D. (1862a): Zweite Mitteilungen über die geologische Übersichtsaufnahme von West-Slavonien (*in German*). Verhandl. geol. R. A., 12/2 (1861-62), 200-205.

Stur, D. (1862b): Die Neogen-tertiaren Ablagerung von West-Slavonien (*in German*). Jahrb. geol. R. A., 12, 2, 285-299.

Šparica, M., Buzaljko, R. and Jovanović, Č. (1984a): Basic Geological Map 1:100 000, sheet Nova Gradiška L 33-107. Geološki zavod Zagreb and RO Geoinženjering OOUR Institut za geologiju Sarajevo (1983), Savezni geološki zavod Beograd.

Šparica, M. and Buzaljko, R. (1984b): Basic Geological Map 1:100 000. Explanatory notes for sheet Nova Gradiška L 33-107. Geološki zavod Zagreb and RO Geoinženjering OOUR Institut za geologiju Sarajevo (1983), Savezni geološki zavod Beograd, 1-50 (*in Croatian*).

Vrsaljko, D., Bošnjak, M. and Japundžić, S. (2018): Miocen sjeverne Hrvatske: od blata do zlata (*Miocene of Northern Croatia: from Mud to Gold – in Croatian with English summary*). Hrvatski prirodoslovni muzej, 90 pp.

**Internet sources:**

URL 1: International Commission on Stratigraphy, www.stratigraphy.com (accessed September 7, 2020)
URL 2: https://d-maps.com/carte.php?num_car=2242&lang=en (accessed September 6, 2020)

## SAŽETAK

**Neogenske naslage zapadnih padina Psunja, Hrvatska: pregled dosadašnjih istraživanja i aktualizacija geoloških istraživanja**

Na kristalinskoj podlozi zapadnih padina Psunja diskordantno slijede neogenske naslage starosti od donjeg miocena do kvartara. Stariji neogenski sedimenti se u ranijim radovima nazivaju "oligomiocenski" ili "predtortonski", što danas odgovara donjomiocenskim sedimentima. Preko tih slatkovodnih i morsko-bočatih sedimenata transgresivno slijede morske srednjomiocenske naslage. Badenski talozi čine kontinuirani pojas oko zapadnih padina Psunja, istočno od Pakraca i Lipika, s raznolikim litofacijesima. U širem području strukture Bijela Stijena-Novska, donjosarmatski sedimenti su diskordantni na badenske. Bočati i slatkovodni okoliši obilježeni su kontinuiranim taloženjem gornjomiocenskih sedimenata, a pliocenski sedimenti s kompletnim razvojem "paludinskih naslaga" obilježavaju kraj neogena. Dominantna je antiklinalna struktura – strukturni nos s osi Bijela Stijena-Novska. Jezgru strukture čine kristalinske stijene, a neogenski sedimenti slijede periklinalno duž krila i čela strukture.

**Ključne riječi:** neogen, stratigrafija, naftna geologija, Psunj, Hrvatska.

## Acknowledgments

## Author's contribution

**Davor Vrsaljko (1)** (Dr, senior advisor, paleontology, biostratigraphy, sedimentology, regional geology, geomathematics) provided the field work, geological setting, stratigraphic interpretation and presentation of results. **Marija Bošnjak (2)** (Dr, senior curator, paleontology, geomathematics) provided the field work, interpretation and presentation of results. **Anja Jarić (3)** (Mag. geol., curator volunteer, paleontology, geomathematics) provided the field work and the graphics. **Jasenka Sremac (4)** (Dr, Full Professor, geology, paleontology, paleoenvironment) contributed with paleoenvironmental and paleogeographic interpretation and presentation of results. **Tomislav Malvić (5)** (Dr, Full Professor, geology, geomathematics) provided the field work, interpretation and presentation of results.

# Trends of the hydrometeorological variables in the wider area of the Zagreb aquifer

**Sara Bačeković[1]; Dominik Rukavina[1]; Zoran Kovač[2]**
[1] Faculty of Mining, Geology and Petroleum Engineering, University of Zagreb,
Pierottijeva 6, 10000 Zagreb, Croatia – student
[2] Faculty of Mining, Geology and Petroleum Engineering, University of Zagreb, Pierottijeva 6, 10000 Zagreb, Croatia,
http://orcid.org/0000-0001-8091-7975

## Abstract

The aim to this paper was to estimate trends of hydrometeorological variables in a different time scales in order to see whether it will generate an indication of the impact of climate change in the wider research area. Trends were estimated on a monthly and yearly basis for precipitation, air temperature, evapotranspiration and maximum water available for infiltration at meteorological station Pleso, and for Bregana River water levels at hydrological station Koretići. Both locations are important because they can show patterns that could be characteristic for the wider Zagreb area, and are associated with Zagreb aquifer recharge. Linear regression and t-test were used for trend estimation. Monthly analysis showed ascending trends for air temperature and evapotranspiration, especially in the summer months. Descending trends for Bregana River water levels were observed when minimum and average values were considered, while statistically significant ascending trend for maximum water levels was observed only for February. Yearly trends showed similar patterns. Moreover, it was shown that evaluation of trends only on a yearly basis can sometimes hide important information. All results suggest that more dry periods should be expected, while floods could be more frequent in February. Bigger difference between high and low waters, i.e. extremes, was observed, but the results were not statistically significant. Trends showed that smaller infiltration from precipitation and reduced inflow from Bregana River to Sava River will probably result with the smaller recharge to the Zagreb aquifer, what can potentially be result of a climate change.

**Keywords:** trend; hydrometeorological variable; Zagreb aquifer; linear regression

## 1. Introduction

Trend evaluation of basic hydrometeorological variables, i.e. flow, river water level, precipitation, air temperature and evapotranspiration, is very important because it can show how human impacts and/or some natural events can influence on the availability of water in different areas. A lot of shallow alluvial aquifers are directly connected with rivers where the estimation of river water level trends can directly show which kind of groundwater level trends can be expected and estimate how will groundwater seasonal water reserves change in the future. The same situation is with observation and definition of trends. Some variables have direct influence on effective infiltration, i.e. the water that participates in the replenishment of seasonal groundwater reserves through the water percolation from the unsaturated zone into the aquifers. Also, changes in runoff, frequency and regime of flows and precipitation can present the evidence of human impact through the increase of greenhouse gases which can affect the water cycle. This can be seen in the form of flooding, droughts and heavy precipitation (**Groisman et al., 2005; Barnett et al., 2008; Murphy et al., 2013; Pavlić et al., 2017**). Furthermore, EU Water Framework Directive (2000/60/EC; WFD) and Groundwater Directive (2006/118/EC; GD) have shown that trends have to be calculated for a groundwater body or a group of bodies, where appropriate, in the procedure related with the definition of chemical and quantitative status and risk assessment. Although trends estimation can be done with different methods, the nonparametric Mann-Kendall test (**Mann, 1945; Kendall, 1975**) is maybe the most often used method in the trend estimation of hydroclimatic and water quality data series (**Gebremedhin et al., 2016; Lutz et al., 2016; Pavlić et al., 2017; Diamantini et al., 2018**). However, other methods like linear regression, piecewise regression and logistic regression can be used in the estimation of trends of hydrological and water quality time series (**Grath et al., 2001; Yue et al., 2002; Kovač et al., 2018**).

In this paper, the focus is not on the application of different statistical methods, but on the data aggregation, which was done on the monthly and yearly basis. It was tested whether the data aggregation and evaluation of data in different time intervals can generate different conclusions. Also, one of the aims was to see if there was an impact of a climate change in the wider research area. For that purpose, linear regression was used to estimate trends on meteorological variables at meteorological station Pleso in the area of Zagreb aquifer, while trends on hydrological variables were estimated on the data from hydrological station Koretići, which is located in the upstream of the Bregana River. Evaluation

Zoran Kovač
*zoran.kovac@rgn.hr*

of trends for both locations is very important, first because it can be used for the estimation of maximum values available for the effective infiltration which participates in the recharge of seasonal groundwater reserves of the Zagreb aquifer, and other due to possible flooding of inhabited areas of the Bregana River. Previous statistical studies of meteorological variables in the research area were focused on the analysis of daily, monthly and yearly values of the precipitation at meteorological station Zagreb-Grič. In that research it was concluded that precipitation trend is not the consequence of the climate change or urbanization (**Bonacci and Roje-Bonacci, 2019**). **Ivezić et al. (2019)** have done statistical analysis on the hydrological stations of the Bregana River. They investigated hydrological extremes due to more often flooding in the year 2005, 2014 and 2015. In that research trends were estimated for yearly maximum river flows. Results showed ascending trends of maximum flows, especially after year 2000. Evaluation of trends on a monthly and yearly basis for evapotranspiration and maximum water available for infiltration have not been studied before in the research area, as well as trends related to the difference between hydrological extremes.

In **Figure 1** location of meteorological station Pleso and hydrological station Koretići is shown. Both locations are located in the northwestern part of the Croatia. Meteorological station Pleso is one of the main meteorological stations in the wider area of the City of Zagreb and is located in the southeastern part of the Zagreb aquifer, which is designated as part of Country`s strategic water reserves. Hydrological station Koretići is the most upstream station of the Bregana River which in extreme hydrological conditions floods areas downstream and in the end flows into the Sava River which presents the main source of recharge for the Zagreb aquifer.

**Figure 1** was made in ArcMap 10.1., while geocoded terrain (orthophoto) image was obtained from geoportal of Croatian Geodetic Administration. All other calculations and figures were made with Microsoft© Excel and Power Point.
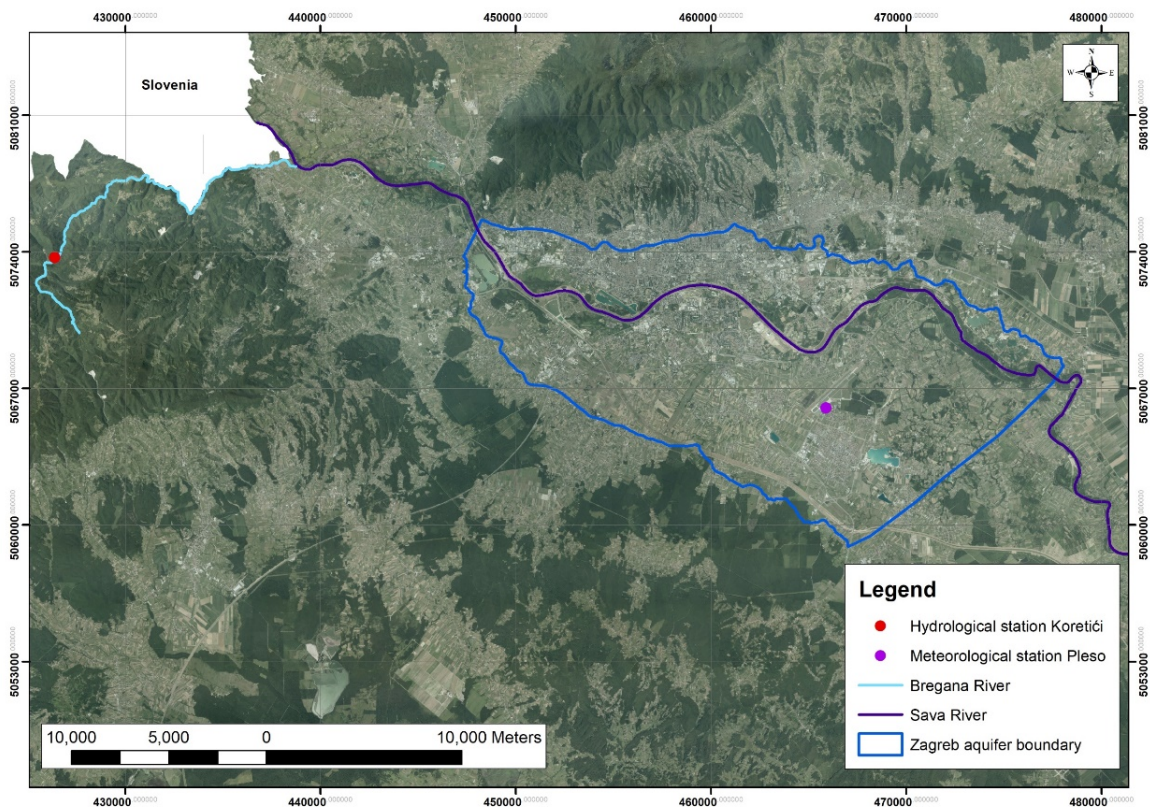


**Figure 1:** Location of meteorological station Pleso and hydrological station Koretići

## 2. Data and Methods

Meteorological and hydrological data for this research was given by Croatian Meteorological and Hydrological Service. Meteorological data consisted from daily precipitation and air temperature data for the meteorological station Pleso located in the southeastern part of the Zagreb aquifer. Daily data was aggregated (average values were calculated) on a monthly and yearly time period and were used for the calculation of evapotranspiration and maximum available water for infiltration into the Zagreb aquifer, and associated trends on monthly and yearly basis. Time period from 1981 till the end of 2019 was used. Data from September to December in year 1991 were not available which resulted in the exclusion of that year in the trend estimation on a yearly basis. Trends were estimated with linear regression using least squares approach, while t-test was used to calculate p-values and test statistical significance ($\alpha=0.05$).

All monthly and yearly average data are presented through the histograms shown in **Figures 2 to 13**. For bin estimation **Scott (1979)** equation has been used:

$$W = 3.49 \cdot \sigma \cdot N^{-1/3} \tag{1}$$

where $\sigma$ present standard deviation, while N presents number of used data.

In **Figures 2 to 6** histograms for monthly and yearly precipitation and air temperature (in °C) is presented. From these variables yearly evapotranspiration was calculated according to **Turc`s formula (1953)**:

$$E_T = \frac{P}{\sqrt{0.9 + \frac{P^2}{L^2}}} \tag{2}$$

where:
$P$ – yearly precipitation (mm);
$L = 300 + 25T + 0.05T^3$;
$T$ – average yearly air temperature (°C).

Since the data related to monthly average air temperatures and precipitation can be calculated, for the calculation of corrected evapotranspiration air temperatures were corrected according to the equation:

$$T_p = \frac{\sum(P_i T_i)}{\sum P_i} \tag{3}$$

where:
$P_i$ – monthly precipitation (mm);
$L = 300 + 25T_p + 0.05T_p^3$;
$T_i$ – average monthly air temperature (°C).

Precipitation values were reduced for the value of evapotranspiration and corrected evapotranspiration to get the estimation of maximum water available for infiltration. Yearly trends were calculated for both evapotranspiration and corrected values, while estimation of yearly trends for maximum water available for infiltration was also done with evapotranspiration and corrected evapotranspiration. It can be seen that in the study area yearly precipitation values mostly vary from 700 to 1200 mm, while average air temperature varies mostly from 10 to 12 °C.

Hydrological data consisted from river water levels (cm) for the station Koretići from the year 1980 till year 2017. Daily data was aggregated to monthly and yearly basis, while minimum, maximum and average values of river water levels were used for the trend estimation (histograms are shown at **Figures 7 to 13**). For the year 1980, only data from September to December were available. Additionally, trends for difference between extremes, i.e. difference between maximum and minimum values, were calculated. Maximum water levels at station Koretići can be more expected in the May and September and minimum in August. Yearly maximum water levels are mostly between 45 and 88 cm, minimum water levels between 19 to 26 cm, while average values vary mostly between 24 and 33 cm.
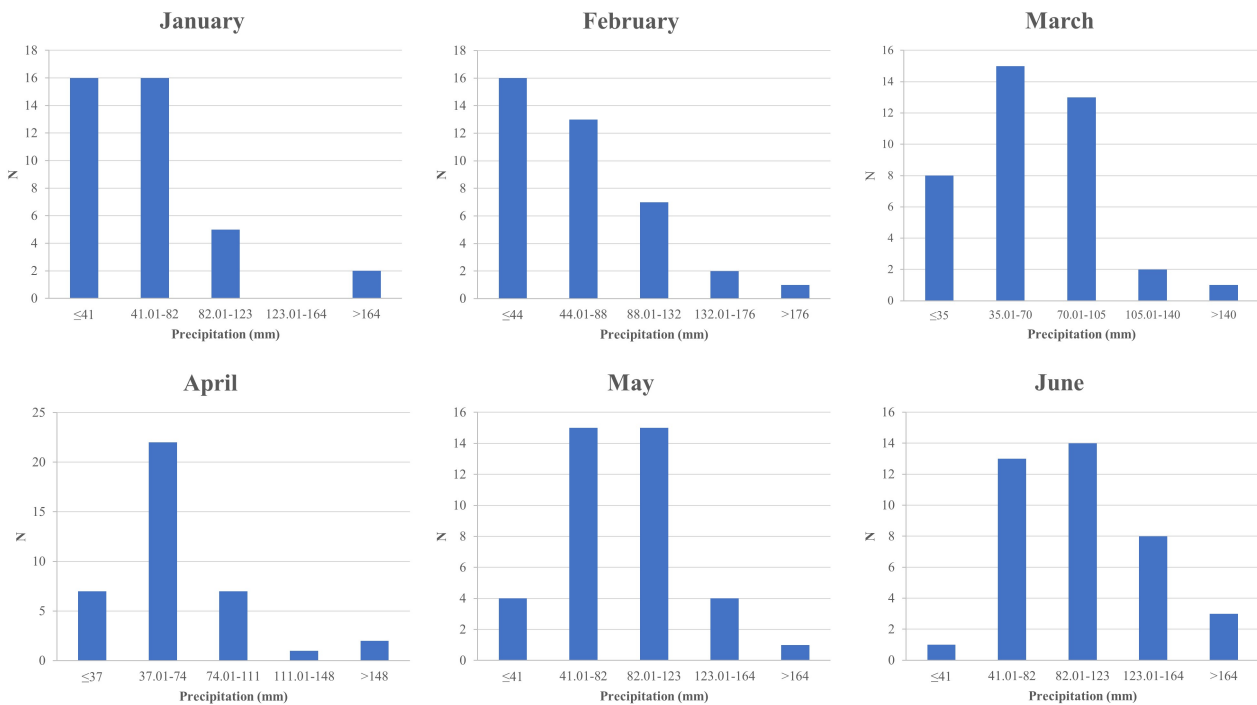
**Figure 2:** Histograms for average values of precipitation from January to June at meteorological station Pleso
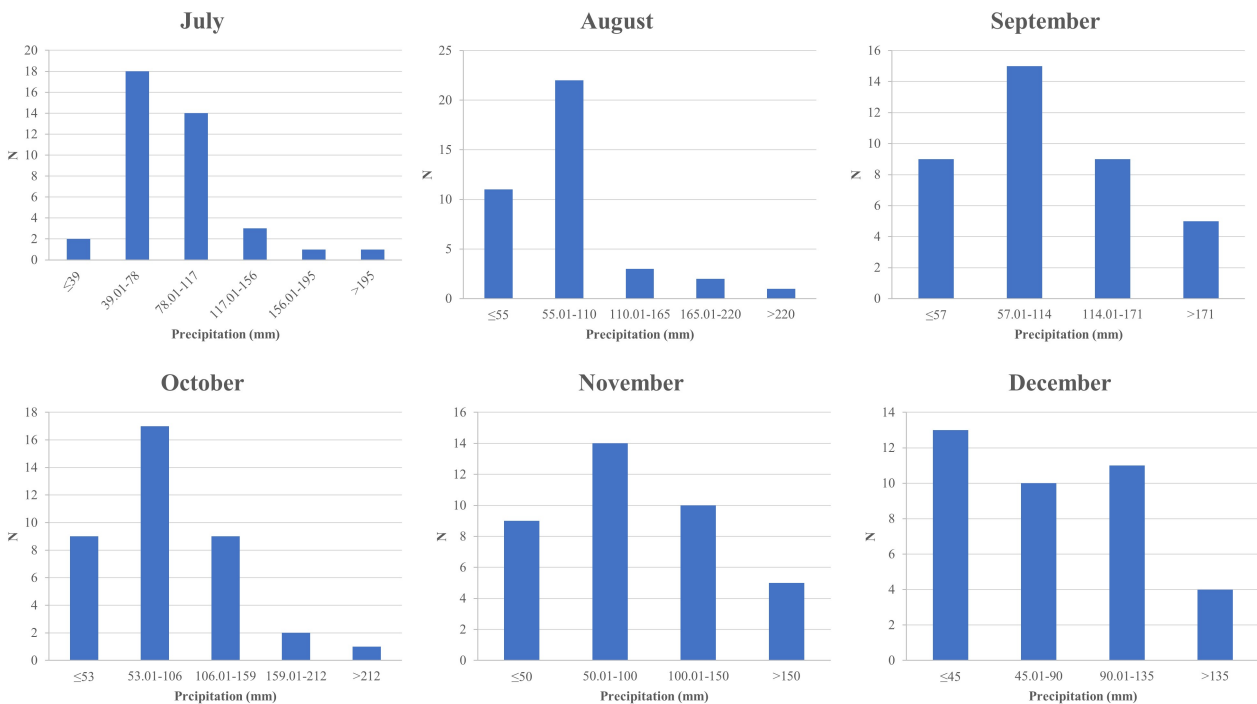


**Figure 3:** Histograms for average values of precipitation from July to December at meteorological station Pleso
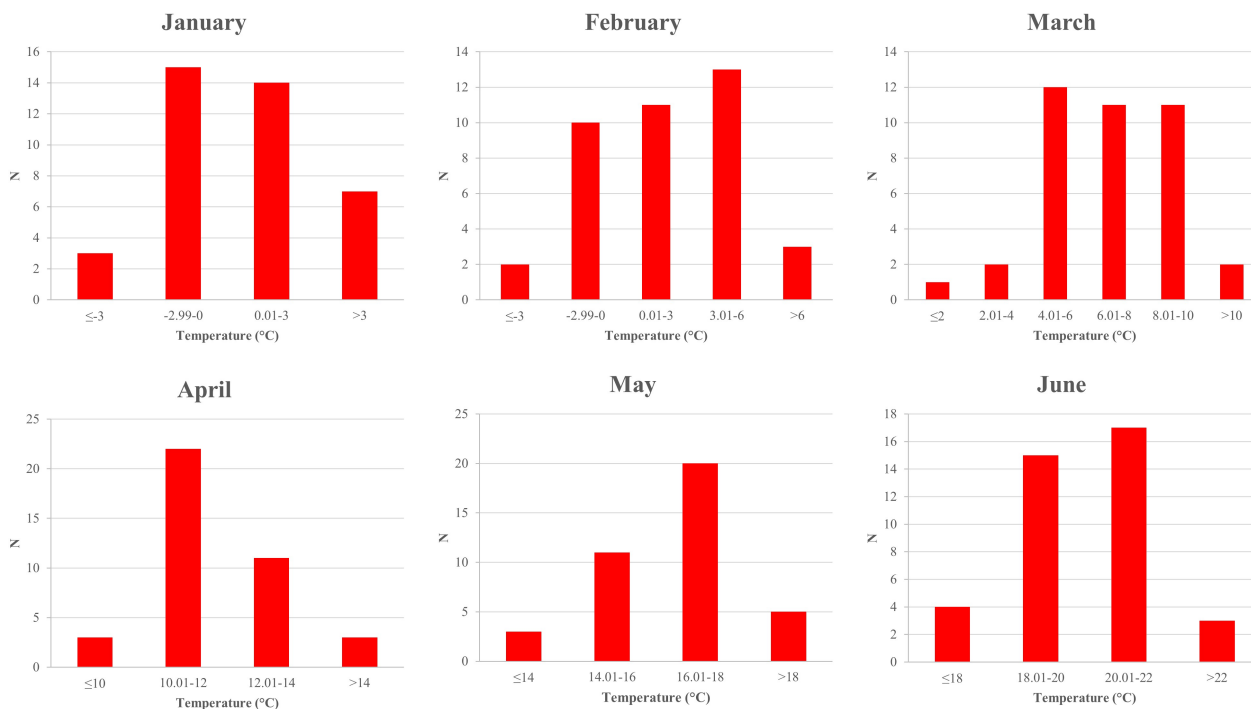
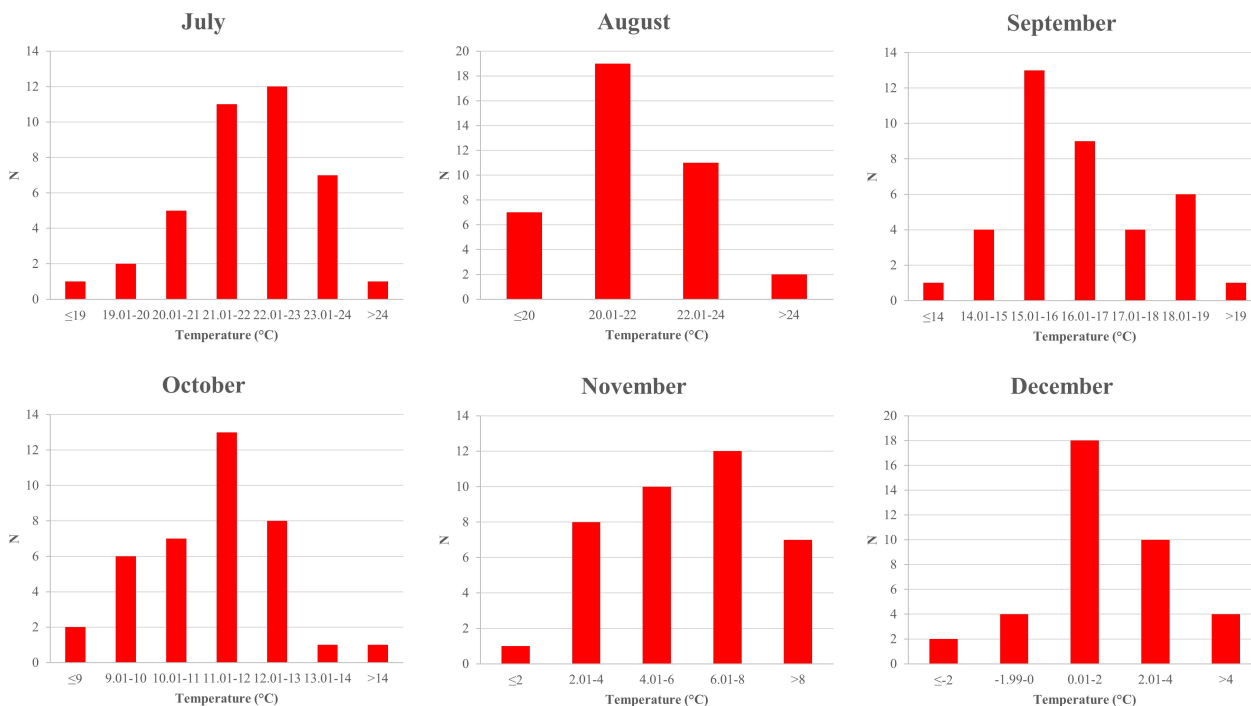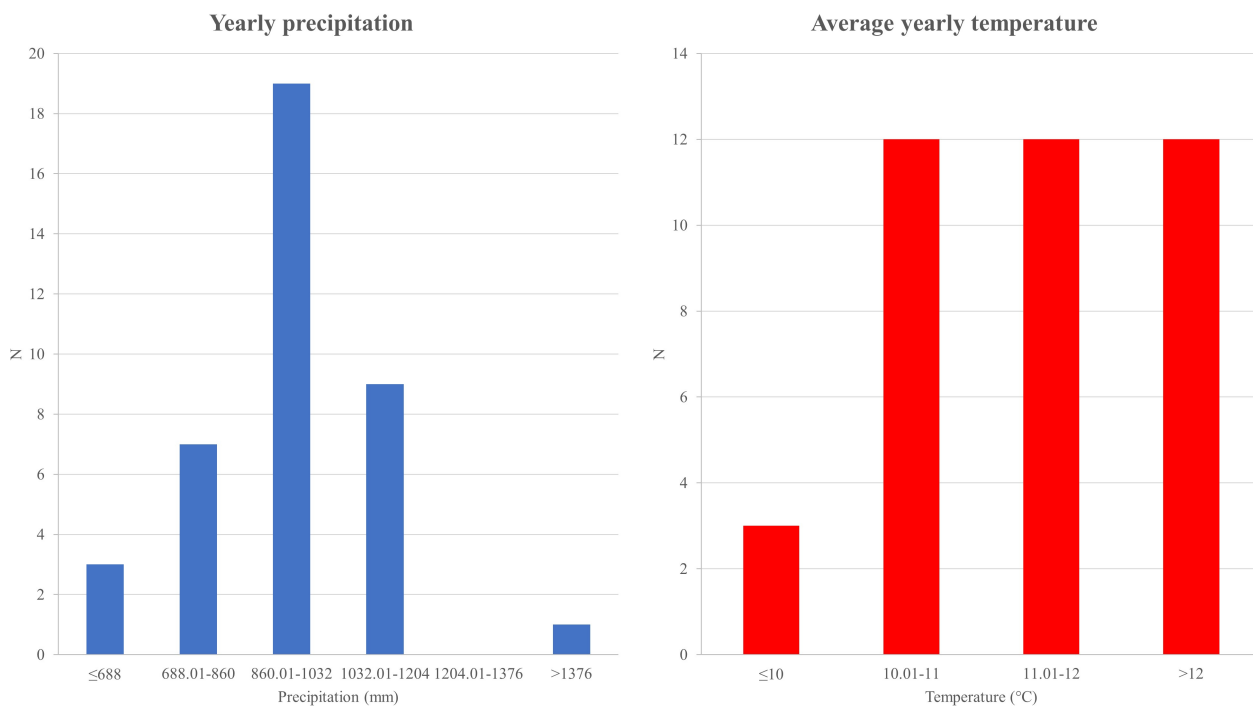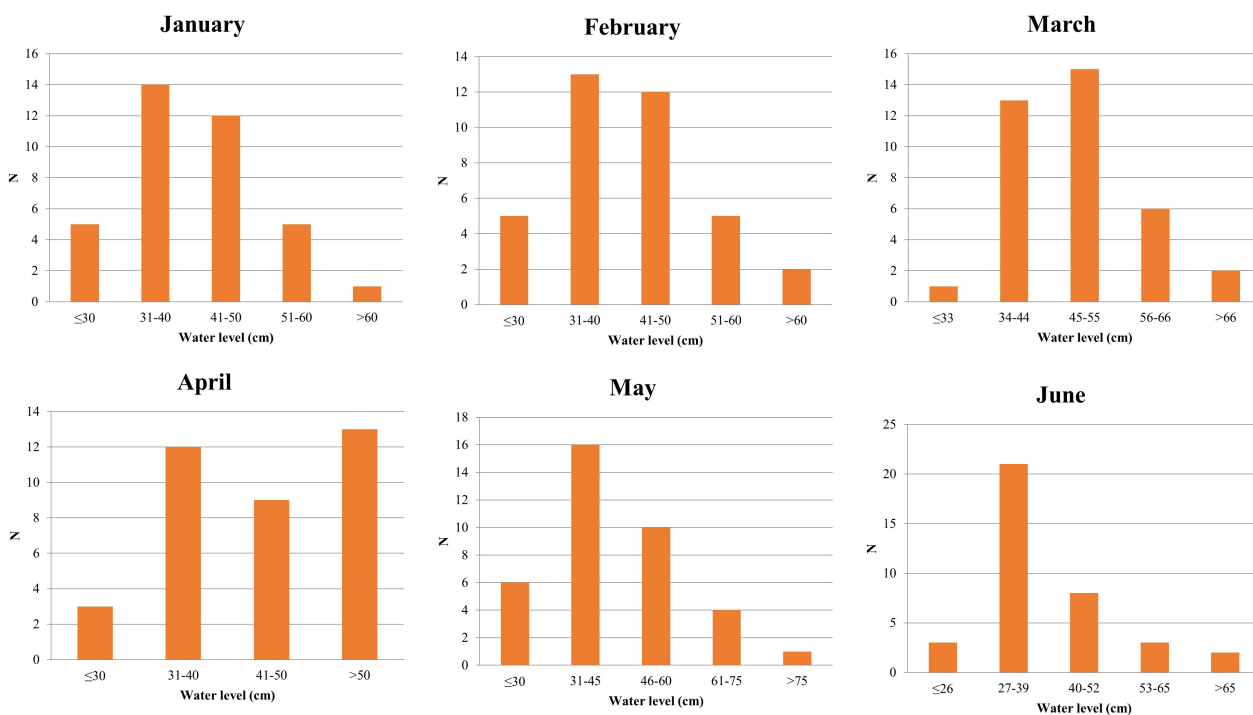**Figure 4:** Histograms for average values of air temperature from January to June at meteorological station Pleso



**Figure 5:** Histograms for average values of air temperature from July to December at meteorological station Pleso

**Figure 6:** Histograms for average yearly values of precipitation and air temperature at meteorological station Pleso



**Figure 7:** Histograms for maximum water levels from January to June at hydrological station Koretići
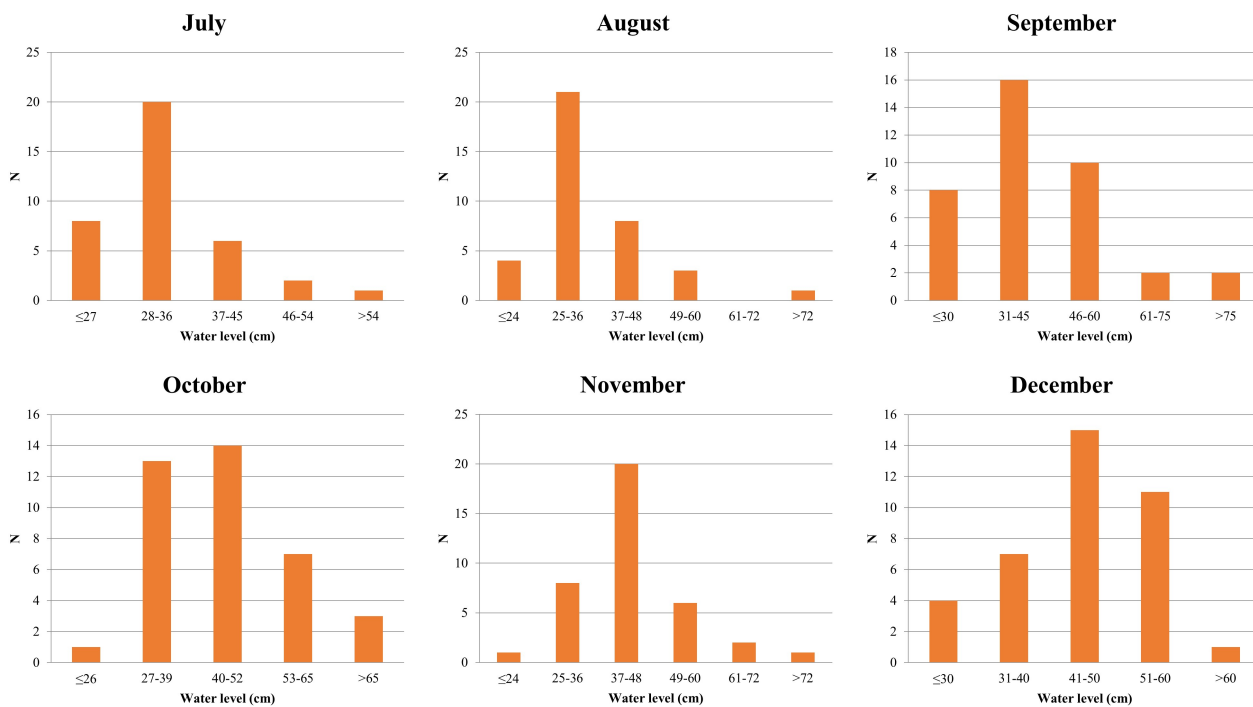
**Figure 8:** Histograms for maximum water levels from July to December at hydrological station Koretići
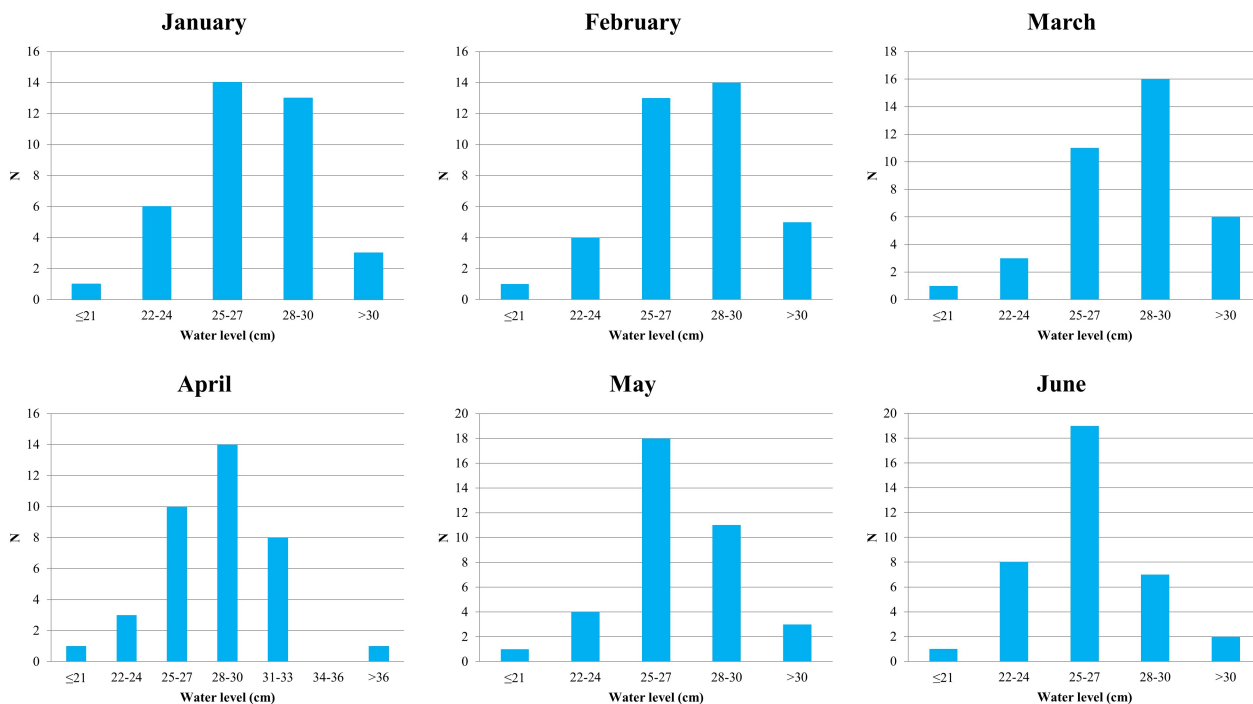


**Figure 9:** Histograms for minimum water levels from January to June at hydrological station Koretići
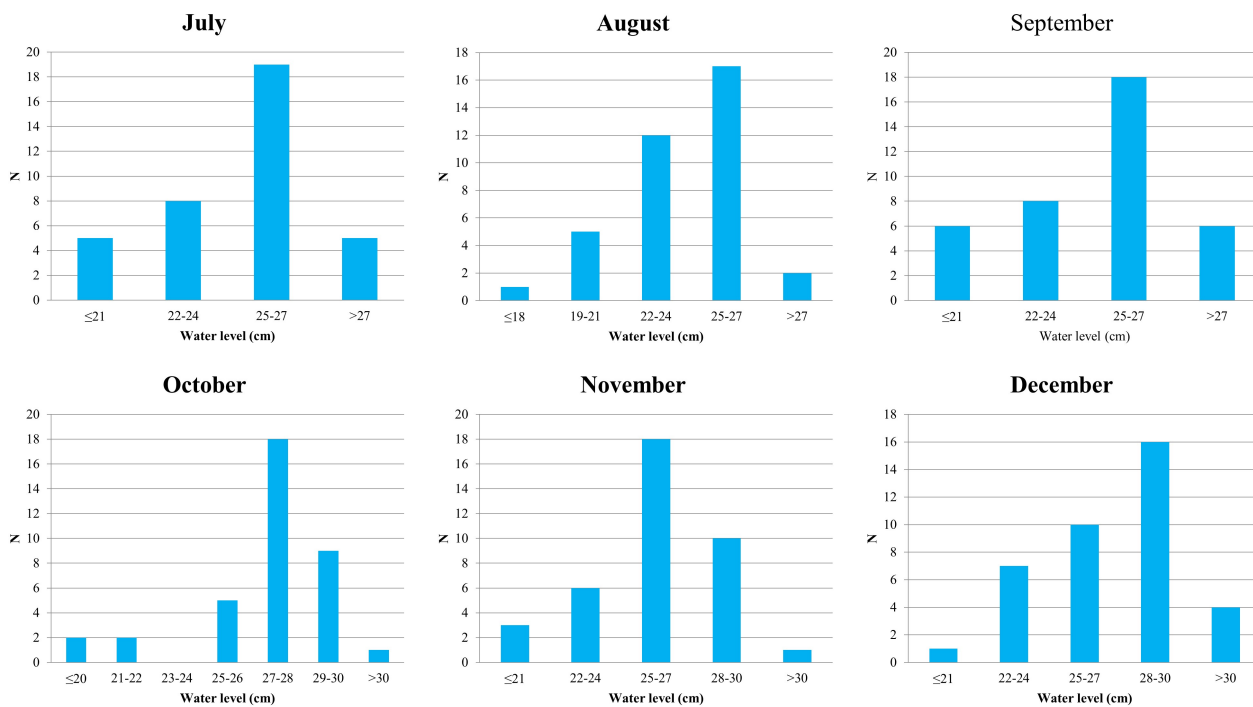
**Figure 10:** Histograms for minimum water levels from July to December at hydrological station Koretići
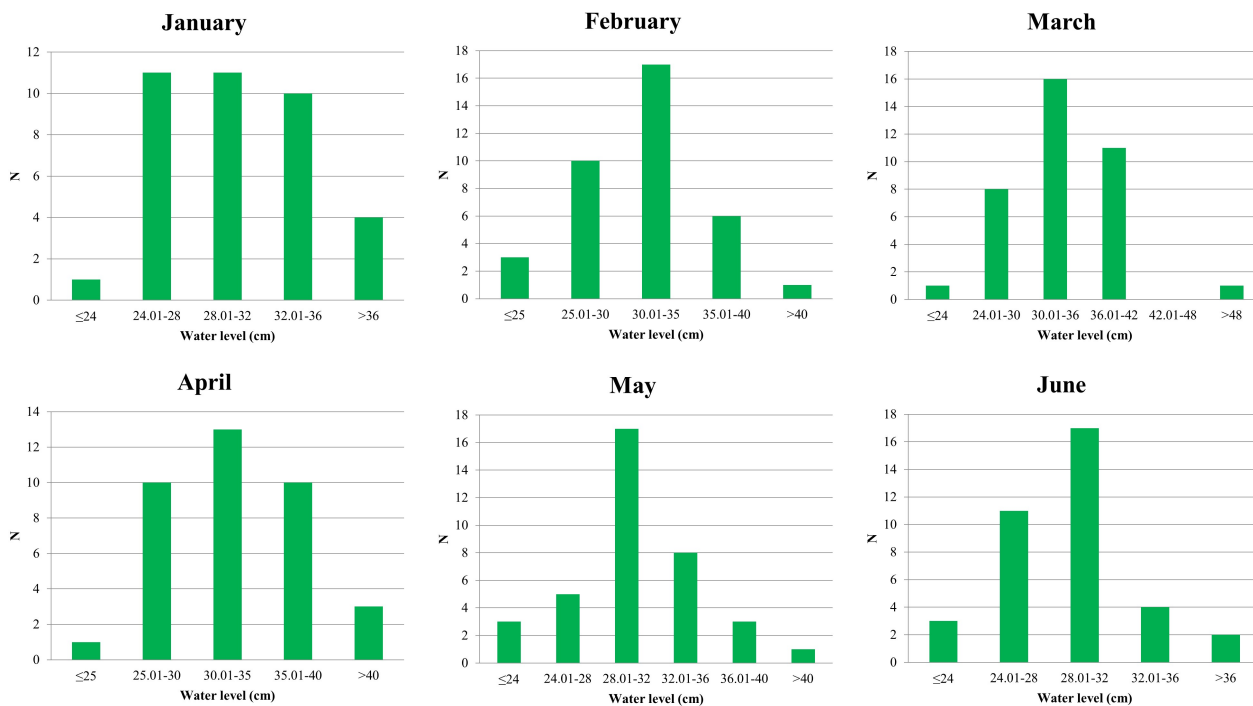


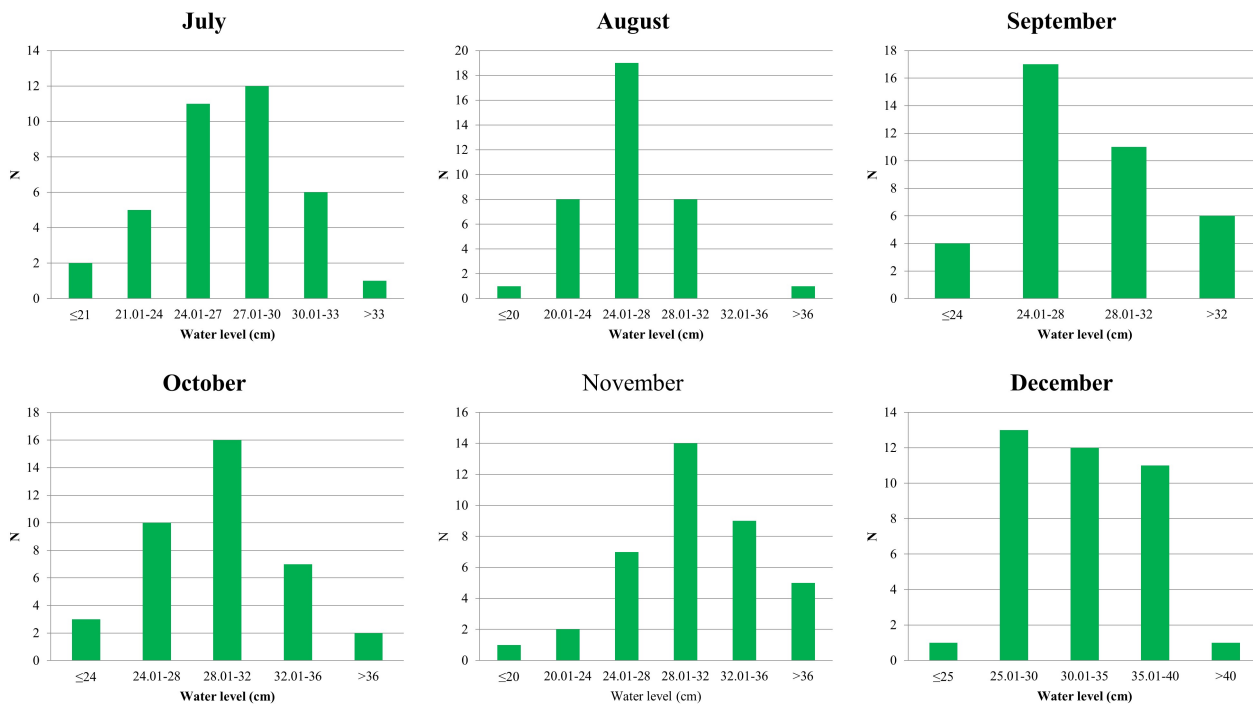**Figure 11:** Histograms for average water levels from January to June at hydrological station Koretići

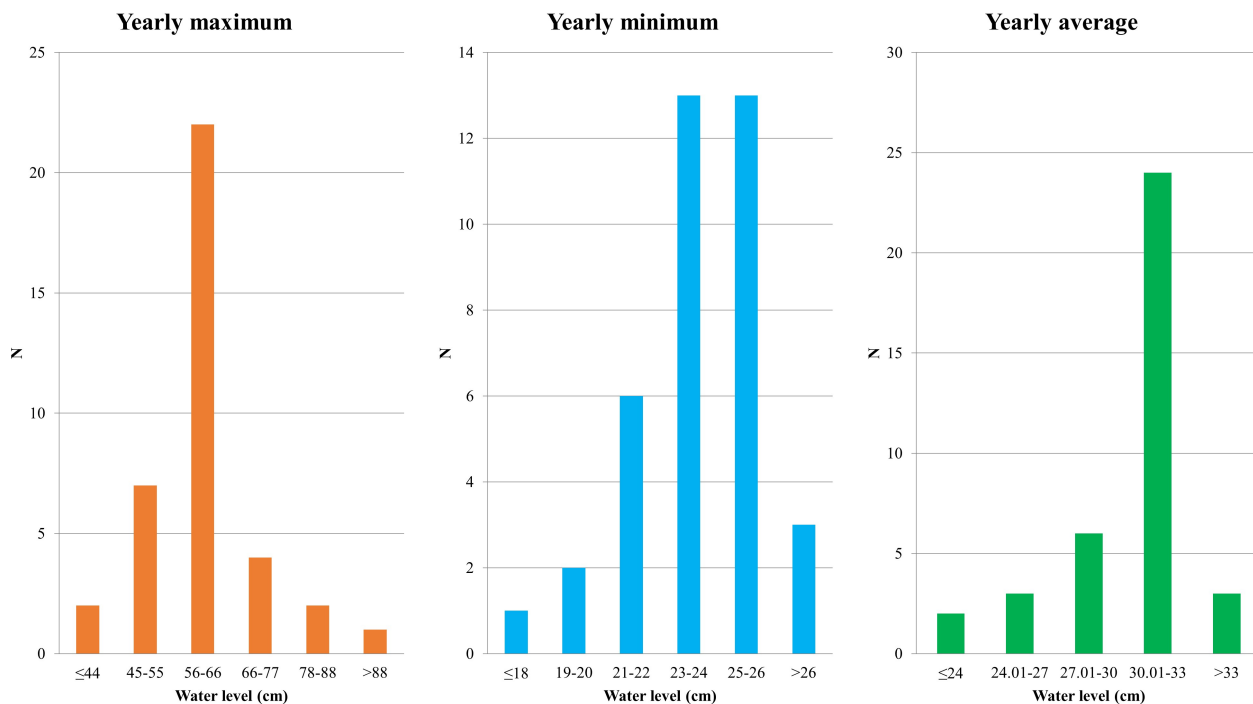**Figure 12:** Histograms for average water levels from July to December at hydrological station Koretići



**Figure 13:** Histograms for yearly maximum, minimum and average water levels at station Koretići

# 3. Results and discussion

## 3.1. Trends of meteorological variables

Meteorological data has shown that in the Zagreb aquifer area year 2014 was the year with the highest value of precipitation (**Table 1**), but also with the highest average air temperature and values of evapotranspiration and water available for infiltration. Years 2011 had the smallest values of precipitation, which is also associated with smallest values of evapotranspiration and water available for infiltration. In this year, maximum water available for infiltration was about 100 mm or less. In 2014 maximum water available for infiltration was about 800 mm which means that potential for water infiltration can vary a lot in different meteorological conditions. Evaluation of evapotranspiration and corrected evapotranspiration has showed that differences range from -9.9% to 22.9% with average of -3.3% (**Table 1**). The usage of exact variable in this case should be investigated in detail in the future research.

Monthly trend analysis has shown very interesting results. Precipitation trends resulted with no statistically significant trend, while statistically significant ascending trends for average air temperatures have been identified for February, April, June, July, August and November (**Figures 14 to 19; Table 2**).

**Table 1:** Yearly values of evapotranspiration and maximum water available for infiltration (modified according to **Bačeković, 2020**)

| Year | Precipitation | Et | Et-corrected | Difference between Et and Et corrected (%) | Maximum water available for infiltration using Et | Maximum water available for infiltration using Et-corrected |
|------|---------------|-----|-------------|---------------------------------------------|---------------------------------------------------|-------------------------------------------------------------|
| 1981 | 998.2 | 530.0 | 535.1 | 1.0 | 468.2 | 463.1 |
| 1982 | 877.8 | 518.2 | 550.8 | 6.3 | 359.6 | 327.0 |
| 1983 | 737.5 | 490.2 | 486.2 | -0.8 | 247.3 | 251.3 |
| 1984 | 981.3 | 514.0 | 512.9 | -0.2 | 467.3 | 468.4 |
| 1985 | 894.7 | 495.1 | 504.9 | 2.0 | 399.6 | 389.8 |
| 1986 | 955.4 | 511.8 | 537.7 | 5.1 | 443.6 | 417.7 |
| 1987 | 917.7 | 512.5 | 507.0 | -1.1 | 405.2 | 410.7 |
| 1988 | 847.5 | 514.3 | 528.9 | 2.8 | 333.2 | 318.6 |
| 1989 | 989.1 | 542.3 | 666.6 | 22.9 | 446.8 | 322.5 |
| 1990 | 745.2 | 501.4 | 491.3 | -2.0 | 243.8 | 253.9 |
| 1992 | 834.7 | 531.6 | 497.1 | -6.5 | 303.1 | 337.6 |
| 1993 | 1039.3 | 546.0 | 559.3 | 2.4 | 493.3 | 480.0 |
| 1994 | 938 | 567.6 | 607.8 | 7.1 | 370.4 | 330.2 |
| 1995 | 1072 | 560.9 | 589.2 | 5.0 | 511.1 | 482.8 |
| 1996 | 1062.5 | 529.7 | 555.9 | 4.9 | 532.8 | 506.6 |
| 1997 | 877.9 | 522.9 | 538.0 | 2.9 | 355.0 | 339.9 |
| 1998 | 976.8 | 543.5 | 609.0 | 12.0 | 433.3 | 367.8 |
| 1999 | 1083.7 | 566.8 | 572.2 | 1.0 | 516.9 | 511.5 |
| 2000 | 785 | 536.7 | 539.0 | 0.4 | 248.3 | 246.0 |
| 2001 | 1021.2 | 567.4 | 583.2 | 2.8 | 453.8 | 438.0 |
| 2002 | 1049.3 | 585.6 | 630.4 | 7.7 | 463.7 | 418.9 |
| 2003 | 681.6 | 489.6 | 497.8 | 1.7 | 192.0 | 183.8 |
| 2004 | 971.8 | 543.8 | 562.6 | 3.5 | 428.0 | 409.2 |
| 2005 | 1102 | 545.7 | 610.4 | 11.9 | 556.3 | 491.6 |
| 2006 | 871.4 | 538.7 | 581.9 | 8.0 | 332.7 | 289.5 |
| 2007 | 992.3 | 582.8 | 602.8 | 3.4 | 409.5 | 389.5 |
| 2008 | 805.1 | 535.0 | 570.9 | 6.7 | 270.1 | 234.2 |
| 2009 | 872 | 551.6 | 538.0 | -2.5 | 320.4 | 334.0 |
| 2010 | 1147.5 | 564.7 | 581.1 | 2.9 | 582.8 | 566.4 |

| 2011 | 560.3 | 444.4 | 471.9 | 6.2 | 115.9 | 88.4 |
| 2012 | 853.1 | 549.2 | 558.3 | 1.6 | 303.9 | 294.8 |
| 2013 | 1149.9 | 588.7 | 530.6 | -9.9 | 561.2 | 619.3 |
| 2014 | 1459.5 | 653.1 | 690.5 | 5.7 | 806.4 | 769.0 |
| 2015 | 935.1 | 575.4 | 605.2 | 5.2 | 359.7 | 329.9 |
| 2016 | 973.9 | 568.6 | 586.5 | 3.1 | 405.3 | 387.4 |
| 2017 | 922 | 568.1 | 575.8 | 1.4 | 353.9 | 346.2 |
| 2018 | 968.3 | 587.0 | 584.5 | -0.4 | 381.3 | 383.8 |
| 2019 | 1054.3 | 605.2 | 610.0 | 0.8 | 449.1 | 444.3 |
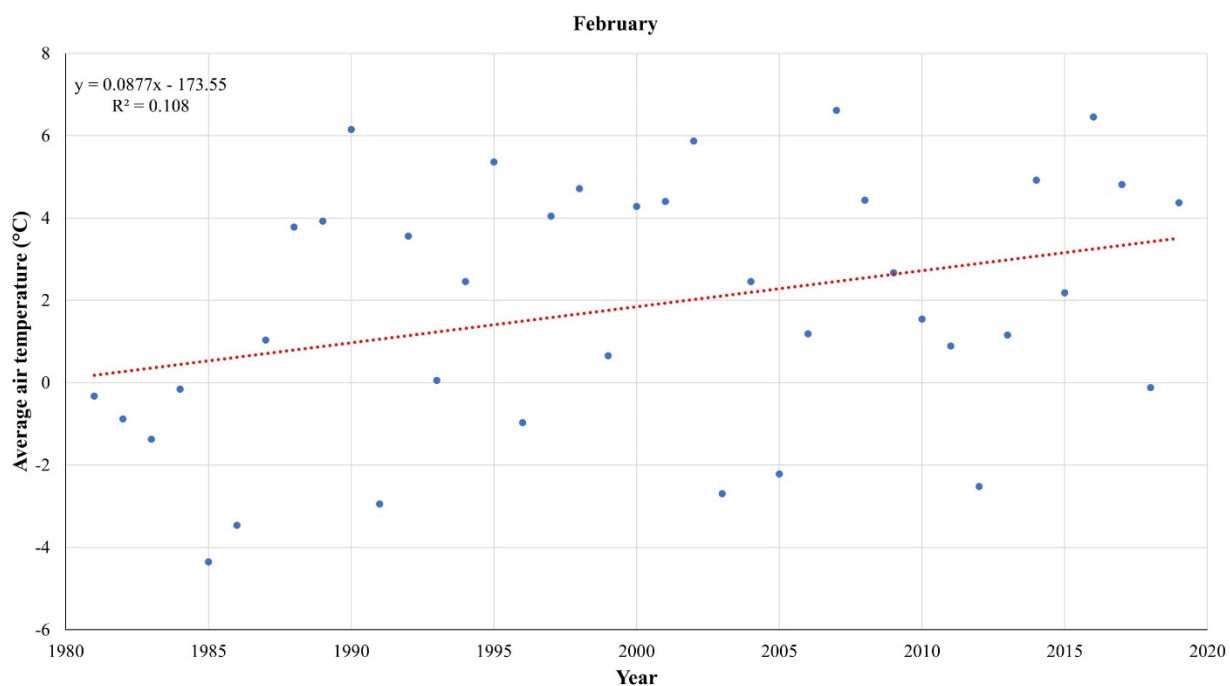


**Figure 14:** Trend of average monthly air temperature in February (modified according to **Bačeković, 2020**)

**April**



$y = 0.076x - 140.25$
$R^2 = 0.3222$
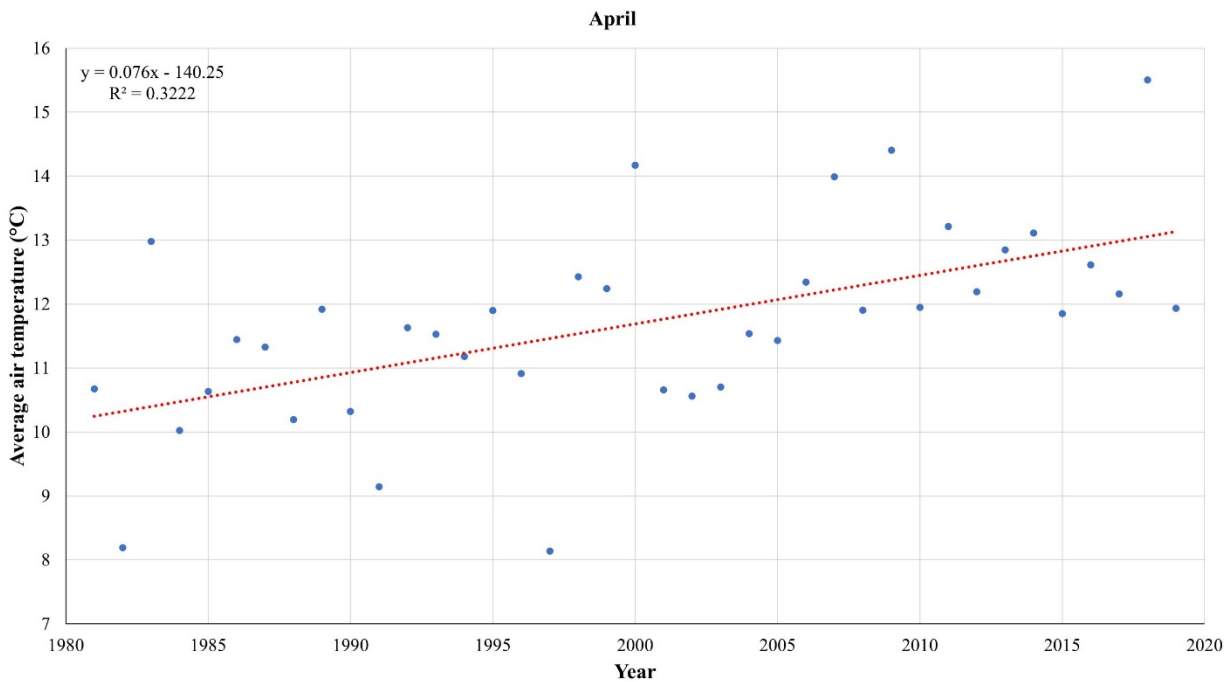
**Figure 15:** Trend of average monthly air temperature in April (modified according to **Bačeković, 2020**)

**June**



$y = 0.097x - 174.08$
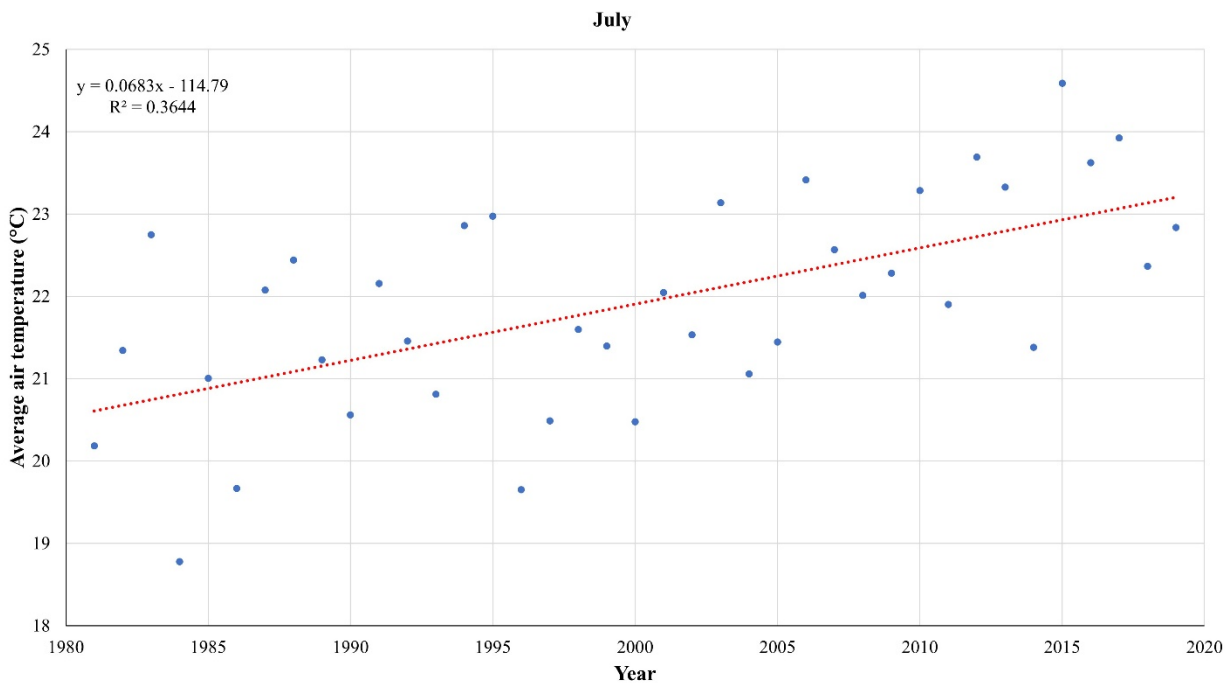$R^2 = 0.4876$
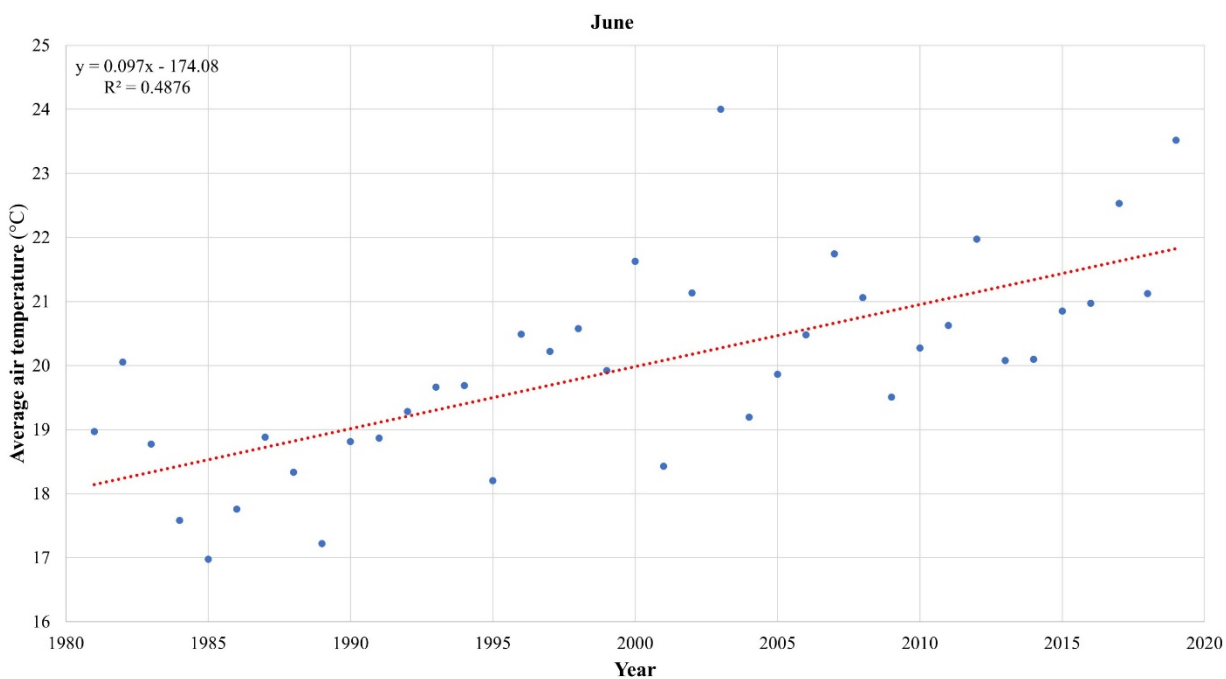
**Figure 16:** Trend of average monthly air temperature in June (modified according to **Bačeković, 2020**)

**July**



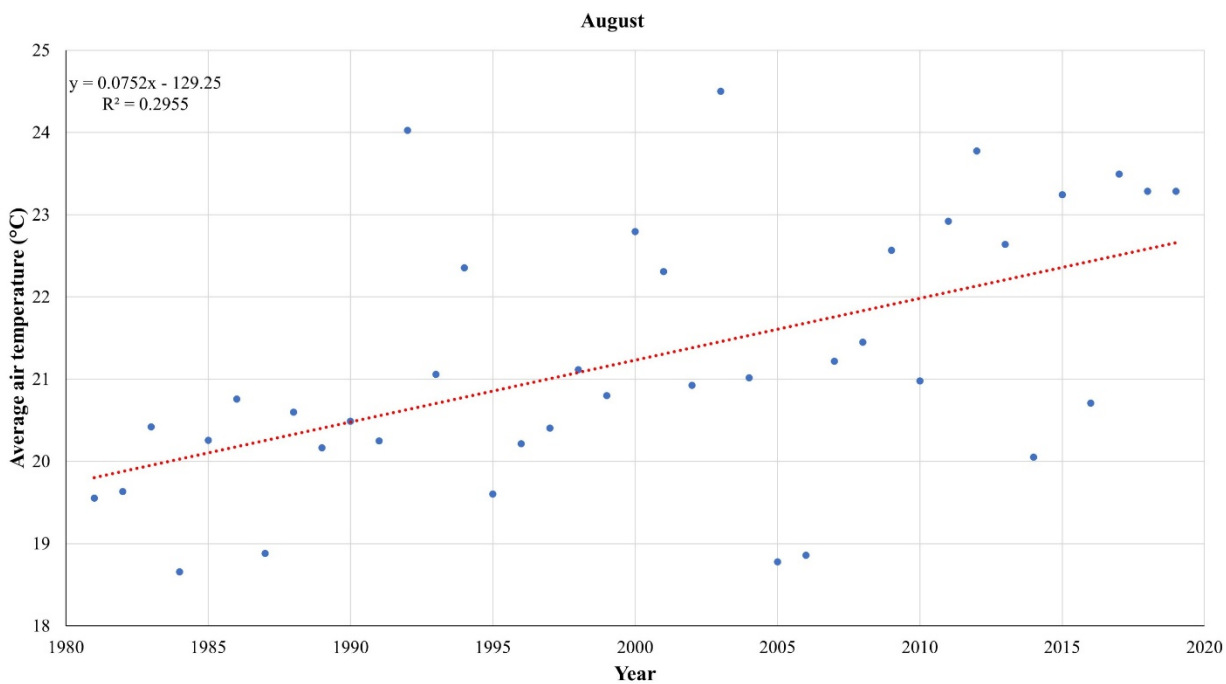**Figure 17:** Trend of average monthly air temperature in July (modified according to **Bačeković, 2020**)

**August**



**Figure 18:** Trend of average monthly air temperature in August (modified according to **Bačeković, 2020**)
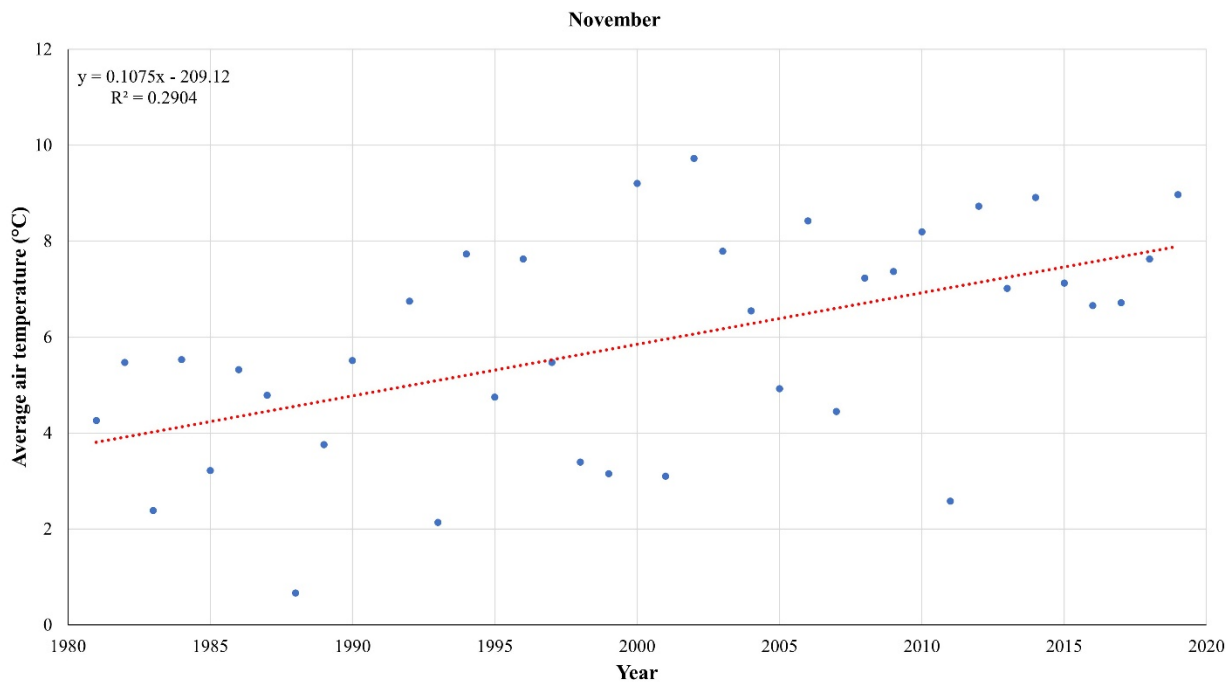
y = 0.1075x - 209.12
R² = 0.2904

**Figure 19:** Trend of average monthly air temperature in November (modified according to **Bačeković, 2020**)

**Table 2:** Results of statistical analysis for monthly trends of precipitation and average air temperature (modified according to **Bačeković, 2020**)

| Month | N | Precipitation | | | Average air temperature | | |
|---|---|---|---|---|---|---|---|
| | | p-value | statistically significant | trend | p-value | statistically significant | trend |
| **January** | 39 | 5.17E-01 | - | - | 5.28E-02 | - | - |
| **February** | 39 | 1.22E-01 | - | - | 4.11E-02 | + | ascending |
| **March** | 39 | 2.54E-01 | - | - | 7.10E-02 | - | - |
| **April** | 39 | 5.14E-01 | - | - | 1.64E-04 | + | ascending |
| **May** | 39 | 5.45E-01 | - | - | 1.48E-01 | - | - |
| **June** | 39 | 9.95E-01 | - | - | 7.71E-07 | + | ascending |
| **July** | 39 | 2.86E-01 | - | - | 4.74E-05 | + | ascending |
| **August** | 39 | 3.74E-01 | - | - | 3.49E-04 | + | ascending |
| **September** | 38 | 9.85E-02 | - | - | 4.34E-01 | - | - |
| **October** | 38 | 8.84E-01 | - | - | 1.14E-01 | - | - |
| **November** | 38 | 2.94E-01 | - | - | 4.82E-04 | + | ascending |
| **December** | 38 | 3.36E-01 | - | - | 2.88E-01 | - | - |

When evaluating trends on a yearly basis, additionally, trends for evapotranspiration, corrected evapotranspiration and maximum water available for infiltration have been calculated. Similar to the results of a monthly analysis, precipitation trend is not statistically significant. Similar results for precipitation trends in the wider research area have been observed in the previous studies (**Bonacci and Roje-Bonacci, 2019**). On the other hand, trend of average air temperature is ascending, and is statistically significant. This also resulted in the statistically significant trends of evapotranspiration and corrected evapotranspiration, while for the maximum water available for infiltration, statistically significant trends have not been observed (**Figure 20 to 22, Table 3**).
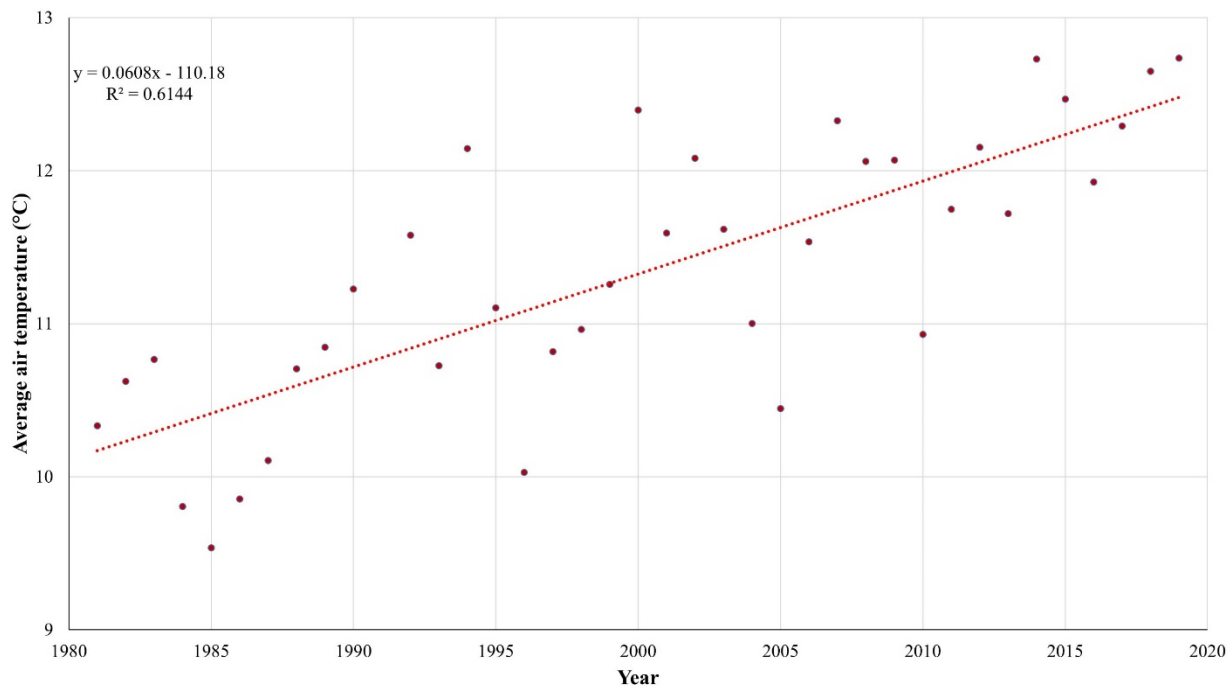


**Figure 20:** Trend of yearly average air temperature (modified according to **Bačeković, 2020**)
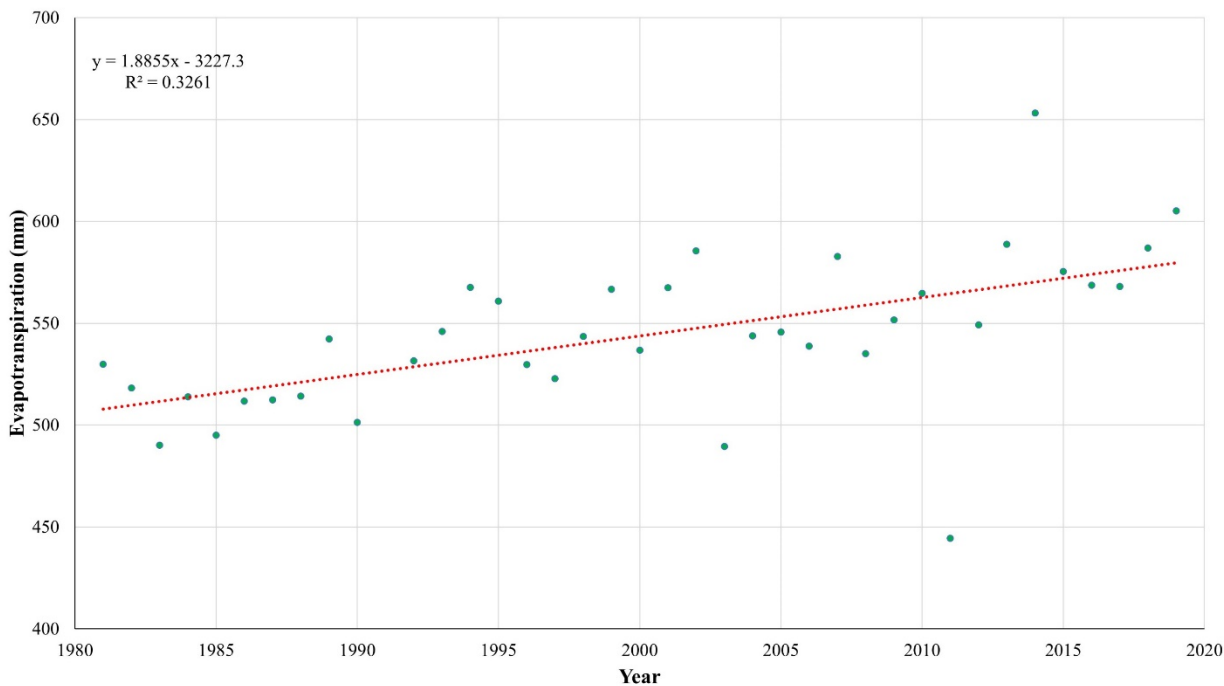


**Figure 21:** Trend of yearly evapotranspiration (modified according to **Bačeković, 2020**)
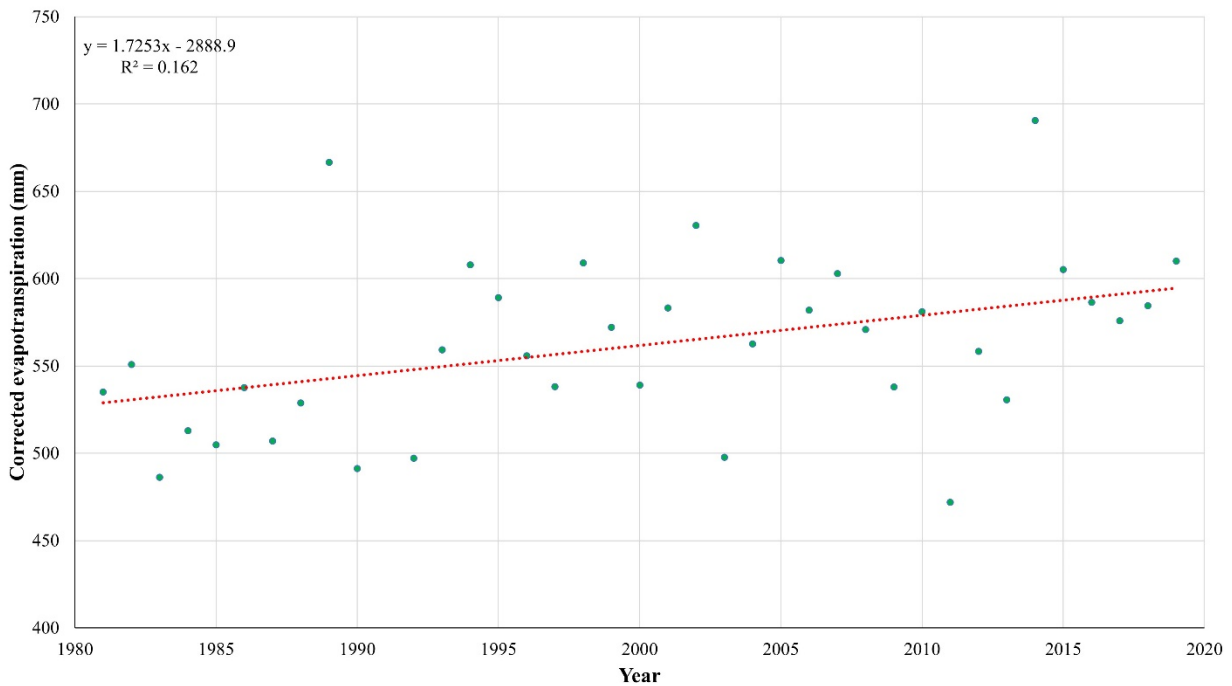
**Figure 22:** Trend of yearly corrected evapotranspiration (modified according to **Bačeković, 2020**)

**Table 3:** Results of statistical analysis for yearly trends of precipitation, average air temperature, evapotranspiration, corrected evapotranspiration and maximum water available for infiltration (modified according to **Bačeković, 2020**)

| Variable | p-value | N | statistically significant | trend |
|---|---|---|---|---|
| Precipitation | 2.14E-01 | 38 | - | - |
| Average air temperature | 5.88E-09 | 38 | + | Ascending |
| Evapotranspiration | 1.81E-04 | 38 | + | Ascending |
| Corrected evapotranspiration | 1.22E-02 | 38 | + | Ascending |
| Maximum water available for infiltration | 6.33E-01 | 38 | - | - |
| Maximum water available for infiltration (calculated with corrected evapotranspiration) | 5.68E-01 | 38 | - | - |

It can be seen that, when examining trends on a monthly and yearly basis, results are very similar. Trend of precipitation does not exist, neither in monthly or yearly calculation, while ascending trend of average air temperature in some months has generated the existence of yearly ascending trend in a whole examined period. Also, these results showed that evapotranspiration, and consequently maximum water available for infiltration, depends more on temperature than on precipitation, in a case when Turc`s formula is used for calculation. Although it`s not that obvious, if temperature continuous to grow, much less water for infiltration should be expected, especially in the summer months, where hydrological minimums occur in most cases. This suggests that in the future, part of the decrease in the seasonal groundwater reserves of the Zagreb aquifer, if observed, could be related with the climate change and warmer climate. However, this issue should be explored in detail in the future research.

### 3.2. Trends of river water level

Within the hydrological part of the trend analysis, trends have been calculated for the minimum, maximum and average values of Bregana River water level at hydrological station Koretići. Also, trends have been examined on a

monthly and yearly basis. Summary statistics for monthly and yearly trend analysis is shown in **Table 4**. Due to a lot of statistically significant trends, only trends calculated on a yearly basis have been graphically presented (**Figure 23 to 25**). It can be seen that only statistically ascending trend has been observed for the February when evaluating maximum water levels of the Bregana River. Although ascending trend for maximum values has been observed, it is not statistically significant, which is partly consistent with the previous research (**Ivezić et al., 2019)**, where more pronounced ascending trend has been observed after year 2000**.** All other statistically significant trends are descending, especially when observing minimum water levels, both on monthly and yearly basis. Results suggest that in the future low waters caused by dry periods will be more pronounced. Another question that arises is how will this affect flooding of the areas downstream. Although, in general, ascending trends have not been observed, results suggest that bigger differences between minimum and maximum, i.e. extremes, of the Bregana River water levels can be expected (**Figure 26**). When considering all selected time period (1980 to 2017), results show ascending, but not statistically significant trend, what coincides with the yearly statistically significant descending trend for minimum and ascending, but not statistically significant trend for maximum water levels. However, it is evident that these values are slowly growing. For example, in last seven years average difference in cm was 43.43 cm, while from the 1980 till 2010 it was 35.42 cm. Although occasionally Bregana River floods areas downstream, results suggest that in the future dry periods will appear more often. On the other hand, results show that more frequent flooding can be expected in February.

If all results are compared together, it is evident that increase in air temperature and evapotranspiration will generate more dry periods what is consistent with the results of trend analysis of the Bregana River water level, which showed that in general descending trend should be expected. All these points suggest that less water from the precipitation, as well as reduced inflow to the Sava River from the Bregana River, will result with the smaller recharge to the Zagreb aquifer in the future, i.e. the smaller seasonal groundwater reserves, which could be because of the climate change.

**Table 4:** Summary of trend analysis for Bregana River water levels (modified according to **Rukavina, 2020**)

| Month | N | Minimum | | | Maximum | | | Average | | |
|---|---|---|---|---|---|---|---|---|---|---|
| | | p-value | statistically significant | trend | p-value | statistically significant | trend | p-value | statistically significant | trend |
| January | 37 | 4.24E-04 | + | descending | 1.33E-01 | - | - | 2.68E-03 | + | descending |
| February | 37 | 8.30E-03 | + | descending | 1.30E-02 | + | ascending | 8.40E-01 | - | - |
| March | 37 | 1.52E-02 | + | descending | 1.58E-01 | - | - | 8.18E-02 | - | - |
| April | 37 | 1.09E-03 | + | descending | 2.12E-01 | - | - | 2.99E-02 | + | descending |
| May | 37 | 1.75E-03 | + | descending | 8.68E-01 | - | - | 1.72E-02 | + | descending |
| June | 37 | 6.00E-04 | + | descending | 1.84E-02 | + | descending | 1.55E-04 | + | descending |
| July | 37 | 1.60E-03 | + | descending | 1.05E-01 | - | - | 6.93E-04 | + | descending |
| August | 37 | 4.20E-02 | + | descending | 4.10E-01 | - | - | 6.25E-02 | - | - |
| September | 38 | 1.69E-04 | + | descending | 6.22E-01 | - | - | 1.90E-02 | + | descending |
| October | 38 | 3.44E-04 | + | descending | 8.71E-01 | - | - | 8.14E-03 | + | descending |
| November | 38 | 1.79E-02 | + | descending | 1.94E-01 | - | - | 3.53E-01 | - | - |
| December | 38 | 3.40E-03 | + | descending | 7.56E-02 | - | - | 7.90E-03 | + | descending |
| Yearly basis | 38 | 1.04E-02 | + | descending | 4.94E-01 | - | - | 2.46E-04 | + | descending |

**Minimum water level (1980-2017)**
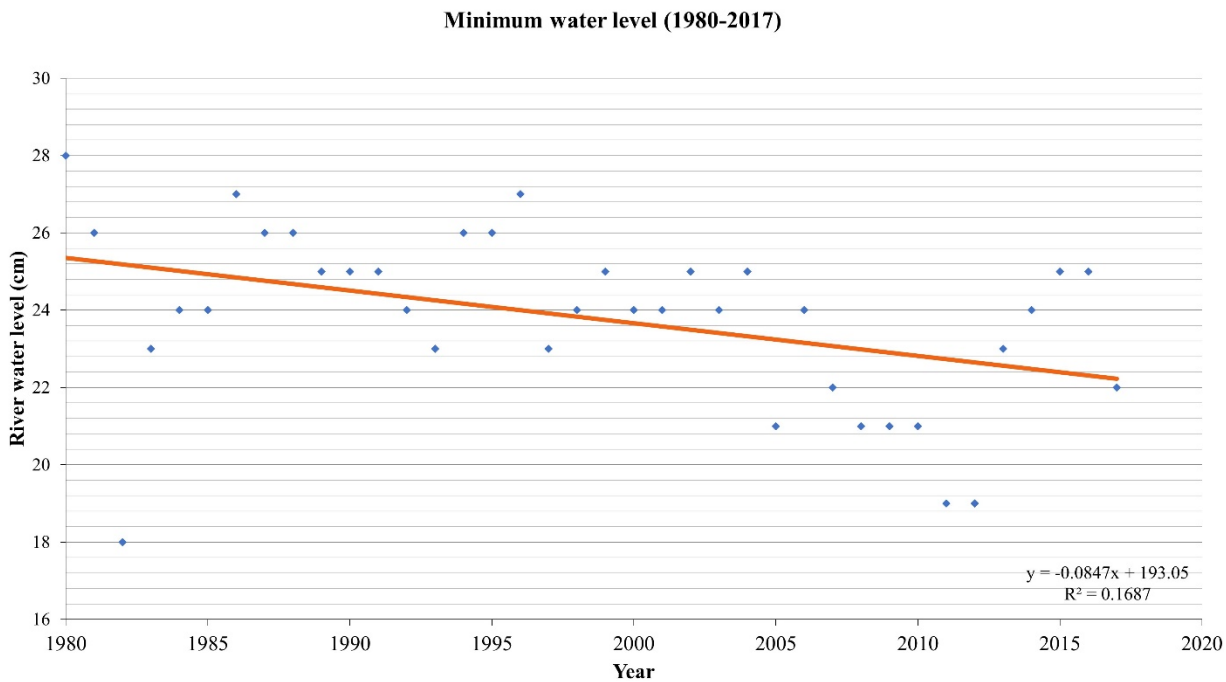


**Figure 23:** Trend of minimum water level of the Bregana River (modified according to **Rukavina, 2020**)
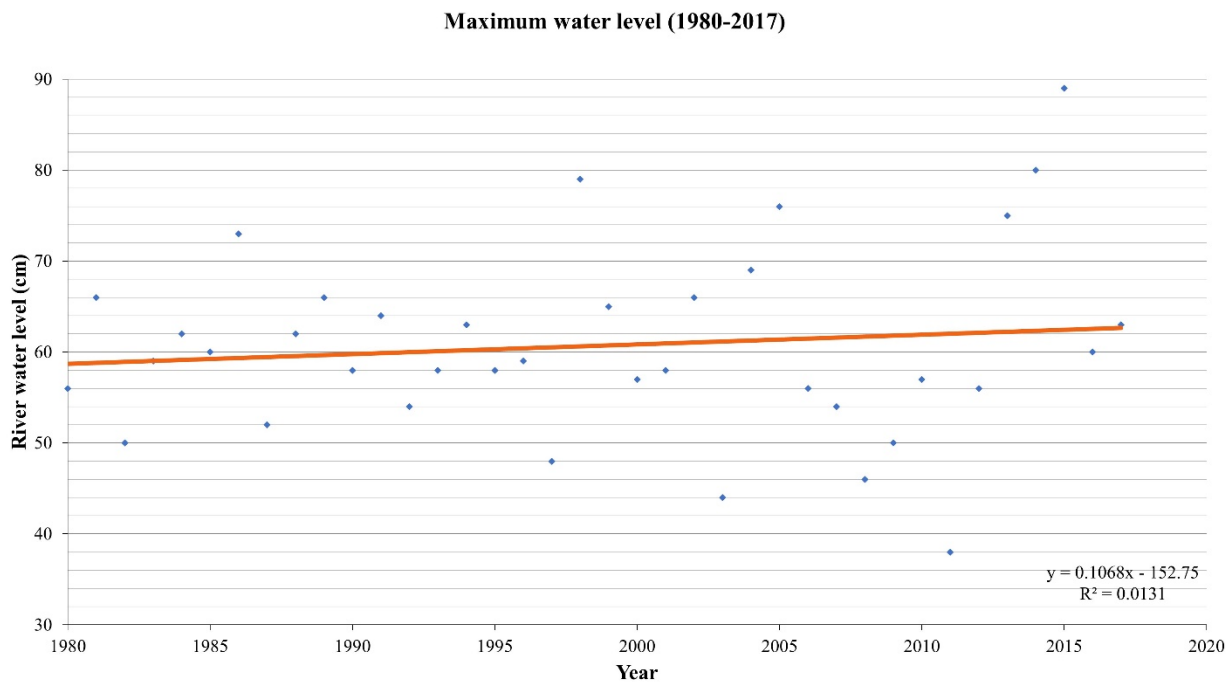
**Maximum water level (1980-2017)**



**Figure 24:** Trend of maximum water level of the Bregana River (modified according to **Rukavina, 2020**)
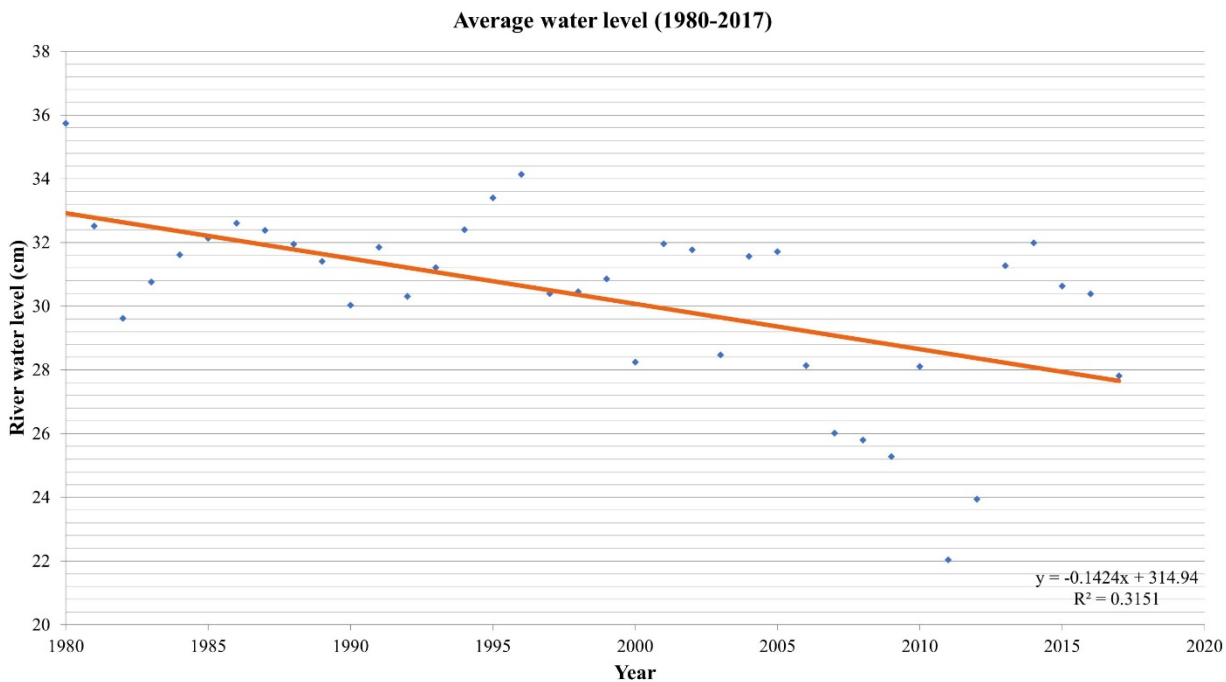
**Average water level (1980-2017)**



**Figure 25:** Trend of average water level of the Bregana River (modified according to **Rukavina, 2020**)

**Difference between maximum and minimum (1980-2017)**
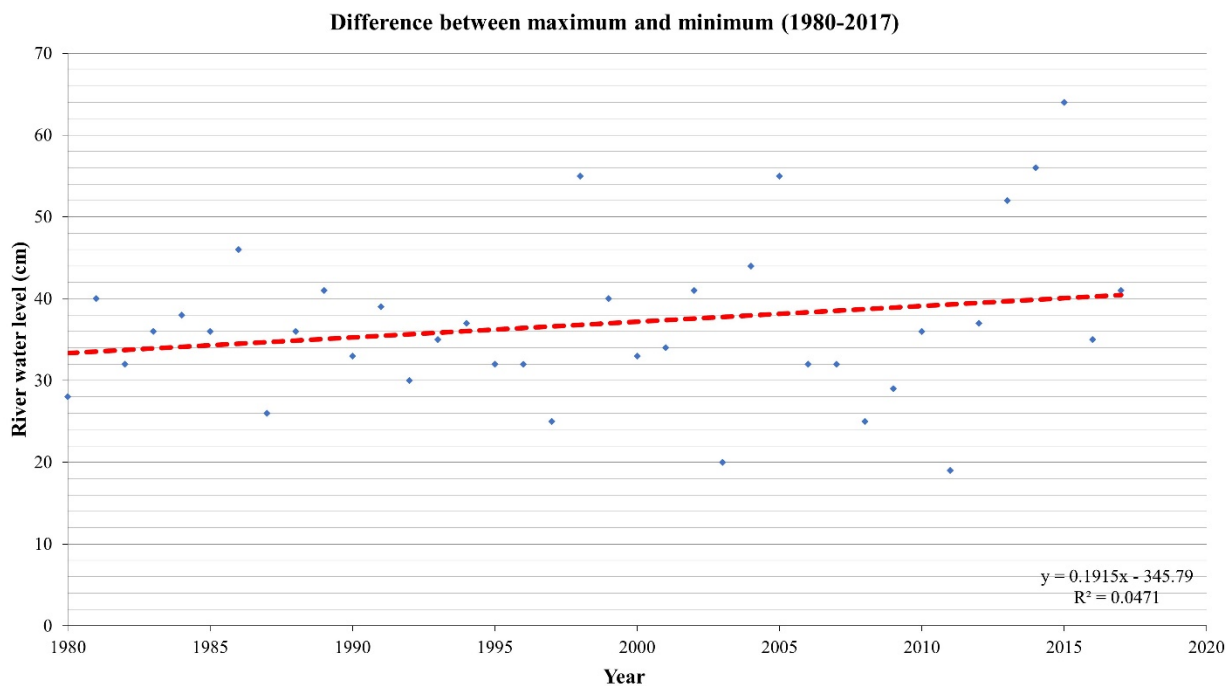


**Figure 26:** Trend of difference between minimum and maximum water levels of the Bregana River (modified according to **Rukavina, 2020**)

# 5. Conclusions

In this paper linear regression was used to estimate monthly and yearly trends of meteorological and hydrological variables. Statistical significance was tested with t-test ($\alpha$=0.05). Monthly trend analysis showed statistically significant ascending trends for air temperature and evapotranspiration (especially in the summer months), and descending trends for Bregana River water levels when observing minimum and average data. Statistically significant ascending trends of Bregana River maximum water levels are only observed for the February, which could indicate that more flooding can be expected in that month. Although yearly trends showed similar pattern in most cases as monthly trends, it was also shown that sometimes evaluation of trends on a yearly basis could hide potentially very important information. This suggests that trends of hydrometeorological variables should be evaluated in the different time scales. Most of the results suggest that more dry periods should be expected, as well as bigger difference between low and high water, i.e. extremes. It is evident that smaller infiltration from precipitation and reduced inflow from Bregana River to Sava River will probably result with the smaller recharge to the Zagreb aquifer. All this suggests that climate change is potentially occurring in the research area. However, to confirm this, it is necessary to conduct more detail research with more observation points and longer time period. Also, future research must include hydrological and hydrogeological analysis and variables, for example evaluation of river water level duration curves and trend of groundwater levels.

# 6. References

Bačeković, S. (2020): Izračun trendova oborina i temperatura na meteorološkoj postaji Pleso u Zagrebu (*Calculation of precipitation and temperature trends at the meteorological station Pleso*). Bachelor`s thesis, Faculty of Mining, Geology and Petroleum Engineering, University of Zagreb (*in Croatian*).

Barnett, T. P., Pierce, D. W., Hidalgo, H. G., Bonfils, C., Santer, B. D., Das, T., Bala, G., Wood, A. W., Nozawa, T., Mirin, A. A., Cayan, D. R. and Dettinger, M. D. (2008): Human-induced changes in the hydrology of the Western United States. Science, 319, 1080–1083. Doi: 10.1126/science.1152538.

Bonacci, O. and Roje-Bonacci, T. (2019): Analiza dnevnih, mjesečnih i godišnjih oborina Zagreb-Griča (1862-2017.) za potrebe inženjerske hidrologije (*Analysis of daily, monthly and annual precipitation at the Zagreb-Grič observatory (1862 -2017) for purposes of engineering hydrology*). Hrvatske vode 27 (107), 7-20 (*in Croatian*).

Diamantini, E., Lutz, S. R., Mallucci, S., Majone, B., Merz R. and Bellin, A. Driver detection of water quality trends in three large European river basins. Science of the Total Environment 2018, 612, 49-62. Doi: 10.1016/j.scitotenv.2017.08.172.

EU Water Framework Directive (2000/60/EC).

Gebremedhin, K., Shetty, A. and Nandagiri, L. Analysis of variability and trends in rainfall over northern Ethiopia. Arabian Journal of Geosciences, 9 (451). Doi 10.1007/s12517-016-2471-1.

Grath, J., Scheidleder, A., Uhlig, S., Weber, K., Kralik, M., Keimel, T. and Gruber, D. (2001): The EU Water Framework 372 Directive: Statistical aspects of the identification of groundwater pollution trends, and aggregation of 373 monitoring results. Final Report.

Groundwater Directive (2006/118/EC).

Groisman, P. Y., Knight, R. W., Easterling, D. R., Karl, T. R., Hegerl, G. C. and Razuvaev, V. N. (2005): Trends in intense precipitation in the climate record. Journal of Climate, 18, 1326–1350. Doi: 10.1175/JCLI3339.1.

Ivezić, V., Filipan, S. and Kadić, V. (2019): Hidrološki ekstremi na slivu rijeke Bregane (*Hydrological extremes in the Bregana River basin*). Hrvatske vode u zaštiti okoliša i prirode. 7. Hrvatska konferencija o vodama, Opatija, 30.5.-1.6.2019. (*in Croatian*).

Kendall, M.G. (1975): Rank Correlation Methods. Charles Griffin, London, UK.

Kovač, Z., Nakić, Z., Špoljarić, D., Stanek, D. and Bačani, A. (2018): Estimation of nitrate trends in the groundwater of the Zagreb aquifer. Geosciences 2018, 8, 5. Doi: 10.3390/geosciences8050159.

Lutz, S. R, Mallucci, S., Diamantini, E., Majone, B., Bellin, A. and Merz, R. (2016): Hydroclimatic and water quality trends across three Mediterranean river basins. Science of the Total Environment, 571, 1392-1406. Doi: 10.1016/j.scitotenv.2016.07.102.

Mann, H.B. (1945): Nonparametric tests against trend. Econometrica 13 (3), 245–259. Doi: 10.2307/1907187.

Murphy, C., Harrigan, S., Hall, J. and Wilby, R. L. (2013): Climate-driven trends in mean and high flows from a network of reference stations in Ireland. Hydrological Sciences Journal 58, 4, 755–772. Doi: 10.1080/02626667.2013.782407.

Pavlić, K., Kovač, Z. and Jurlina, T. (2017): Trend analysis of mean and high flows in response to climate warming. Evidence from karstic catchments in Croatia. Geofizika 34 (1), 157-174. Doi: 10.15233/gfz.2017.34.11.

Rukavina, D. (2020): Određivanje trendova vodostaja na hidrološkoj postaji "Koretići" (*Determination of river water level trends at hydrological station "Koretići"*). Bachelor`s thesis, Faculty of Mining, Geology and Petroleum Engineering, University of Zagreb (*in Croatian*).

Scott, D. W. (1979): On Optimal and Data-Based Histograms. Biometrika, 66, 605-610.

Yue, S., Pilon, P. and Cavadias, G. (2002): Power of the Mann-Kendall test and the Spearman's rho test for detecting monotonic trends in hydrological time series. Journal of Hydrology 259, 254–271. Doi: 10.1016/S0022-1694(01)00594-7.

# SAŽETAK

**Trendovi hidrometeoroloških varijabli na širem području zagrebačkog vodonosnika**

Cilj ovog rada bio je procijeniti trendove hidrometeoroloških varijabli u različitim vremenskim periodima kako bi se vidjelo hoće li rezultati generirati različite zaključke i postoje li naznake utjecaja klimatskih promjena na šire područje istraživanja. Trendovi su procijenjeni na mjesečnoj i godišnjoj razini za oborine, temperaturu zraka, evapotranspiraciju i maksimalnu vodu dostupnu za infiltraciju na meteorološkoj postaji Pleso, i za vodostaje rijeke Bregane na hidrološkoj postaji Koretići. Obje lokacije su važne jer mogu ukazati na obrasce koji bi mogli biti karakteristični za šire područje Zagreba, a povezani su sa napajanjem zagrebačkoga vodonosnika. Linearna regresija, zajedno s *t-testom*, korištena je za procjenu trenda. Mjesečna analiza trendova pokazala je rastuće trendove temperature zraka i evapotranspiracije, posebno u ljetnim mjesecima. Silazni trendovi vodostaja rijeke Bregane primijećeni su kada su uzete u obzir minimalne i prosječne vrijednosti, dok je statistički značajan uzlazni trend maksimalnih vodostaja uočen samo za veljaču. Općenito, godišnji trendovi pokazali su sličan obrazac. Također se pokazalo da evaluacija trendova samo na godišnjoj razini može ponekad sakriti važne informacije. Svi rezultati sugeriraju da bi trebalo očekivati više sušnih razdoblja, dok bi poplave mogle biti češće u veljači. Iako nije statistički značajna, primijećena je veća razlika između visokih i niskih voda, tj. ekstrema. Trendovi su pokazali kako se može očekivati manja infiltracija vode od oborina i smanjeni dotok rijeke Bregane u rijeku Savu, koji će vrlo vjerojatno rezultirati slabijim napajanjem zagrebačkoga vodonosnika, što potencijalno može biti posljedica klimatskih promjena.

**Ključne riječi:** trend; hidrometeorološka varijabla; zagrebački vodonosnik; linearna regresija

## Acknowledgment

## Author's contribution:

**Sara Bačeković (1)** (student) made the statistical analysis for meteorological variables, while **Dominik Rukavina** (2) (student) made it for hydrological variables. **Zoran Kovač (3)** (assistant professor) defined the concept and wrote first draft of the manuscript. All authors participated in the creation of figures and tables, and data interpretation.

# Scientometric Analysis of Journal of Marine Sciences and Engineering (JMSE) Regular and Special Issues – Opportunity for Publishing Quality Results in a Highly Visible Journal

**Jasenka Sremac[1]; Tony Clare[2]; Gary Wilson[3]**

[1] Faculty of Science, Department of Geology, University of Zagreb, 10000 Zagreb, Croatia; jsremac@geol.pmf.hr; http://orcid.org/0000-0002-4736-7497

[2] School of Natural and Environmental Sciences, Newcastle University, Newcastle upon Tyne NE1 7RU, UK, tony.clare@ncl.ac.uk; https://orcid.org/0000-0002-7692-9583

[3] GNS Science, PO Box 30368, Lower Hutt, Wellington, New Zealand and Department of Marine Science, University of Otago, Dunedin, New Zealand, gary.wilson@otago.ac.nz; https://orcid.org/0000-0003-0025-3641

**Abstract:** A *Journal of Marine Science and Engineering* is a widely recognized magazine, published monthly online by MDPI, as an open access and internationally peer-reviewed journal. Its high visibility and rapid publishing, together with well-recognized reviewers make it an interesting choice for a variety of natural scientists, including geologists. Journal statistics and its rapidly increasing rating are the topic of this study.

**Keywords**: JMSE journal; MDPI; open access; peer-review; statistics

## 1. Introduction

A *Journal of Marine Science and Engineering* (ISSN 2077-1312), published by a Swiss publisher MDPI, is an international, peer-reviewed open access journal which provides an advanced forum for studies related to marine science and engineering. It publishes reviews, research papers and communications. The journal aims to encourage scientists to publish the results of scholarly research on ocean and coastal engineering, chemical oceanography, physical oceanography, marine biology and marine geosciences (**URL 1**).

Journal was launched in 2013, following the vision of Professor Tony Clare (**Figure 1**), who, since then, acts as its Editor-in-chief. It was initially published as a quarterly journal. With widening of journal topics, since the year 2015, sections were established, with *Section Editors-in-Chief as follows:* Prof. Dr. Dong-Sheng Jeng for "Section Ocean Engineering"; Prof. Dr. Boris Peter Koch for "Section Chemical Oceanography"; Prof. Dr. Charitha Pattiaratchi for "Section Physical Oceanography" and Prof. Dr. Magnus Wahlberg for "Section Marine Biology". Since 2018, two new sections were established, with two new *Section Editors-in-Chief*: Prof. Dr. Gary Wilson for "Section Geological Oceanography" and Prof. Dr. Roshanka Ranasinghe for "Section Coastal Engineering" (**URL 2**). Alltogether eight volumes were published, followed by a variety of additional Special Issues (**URL 3**). For each Special Issue, a Guest Editor is engaged.

Sremac, J.; Clare, T.; Wilson, G.



**Figure 1:** Journal founder and Editor-in Chief, Prof. Dr. Tony Clare

Journal policy includes no restriction on the length of the papers, but the full experimental details must be provided so that the results can be reproduced. Electronic files and software regarding the full details of the calculation or experimental procedure, can be a part of the article, or can be deposited as supplementary electronic material.

Rapid publication (average: 33 days), with acceptance note within 3,5 days, are additional author benefits.
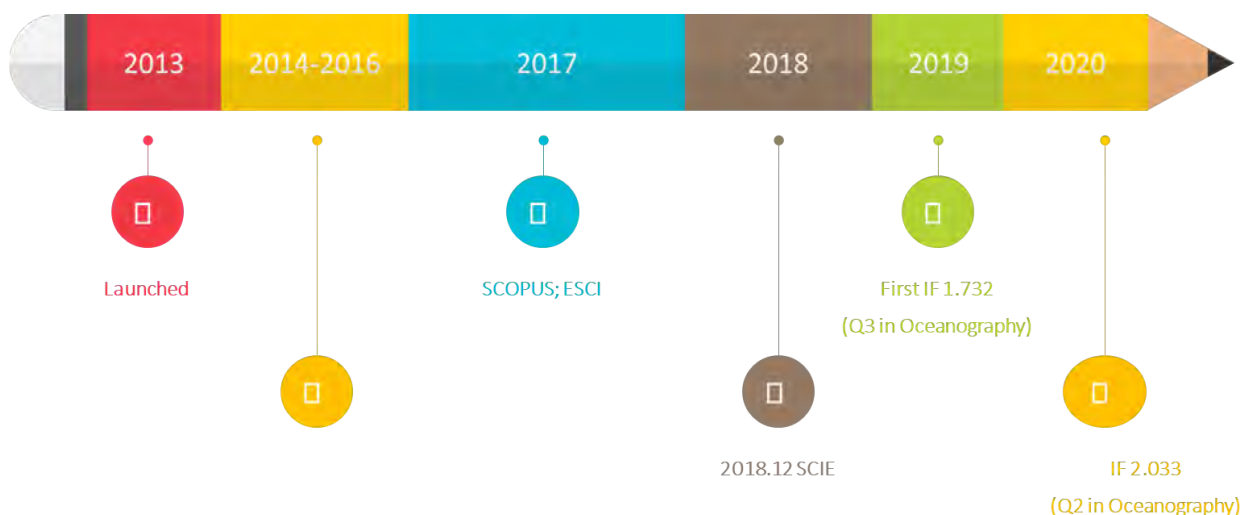


**Figure 2:** *Journal of Marine Science and Engineering* history (Publisher: Terry; AP: Natalie and Dalia)

Journal is indexed in the following bases: CAB Abstracts, Current Contents, Directory of Open Access Journals, Genamics Journal Seek, GeoRef, Inspec, Journal Citation Reports / Science Edition, Norwegian Register for Scientific Journals, Series and Publishers, Review of Agricultural Entomology, Science Citation Index Expanded, Scopus and Web of Science (Clarivate Analytics) (**URL 4**). History of indexing and some important citing scores are presented on **Figure 2**.

Publishers pay a lot of attention to promotion and availability of the Journal information, through a user-friendly web-site and journal/Special Issue flyers (**Figure 3**).

**Figure 3:** Front page of the official journal flyer (**URL1, September 2020**)

## 2. Journal Statistical Analysis, Methods and Results

Simple statistical methods were applied, taking into consideration total number of publications, sum of times cited (with and without self -citations), number of citing articles, h-index and average number of citations per item.

### 2.1. Journal Analytics

Journal analytics (**URL 5**) is based upon the studied 1,467 publications, presenting the abruptly increasing trends (**Figure 4**). Number is still increasing, and, in the moment of finishing this study, it was 1,639 articles published so far (**URL 5**). High visibility and accurate publishing of the relevant data lead to the large number of citations (3,335), which counts 2.27 per item for the moment (**Figure 4**). Ninety-six articles have been cited 10 times or more, and h-10 index is 18 (**Figure 4**) with Impact factor is 2,033 (WoS). Regarding Scopus Citecore is 1.8, h-index 17 and SJR 0.533 (2019; **Figures 5** and **6**).
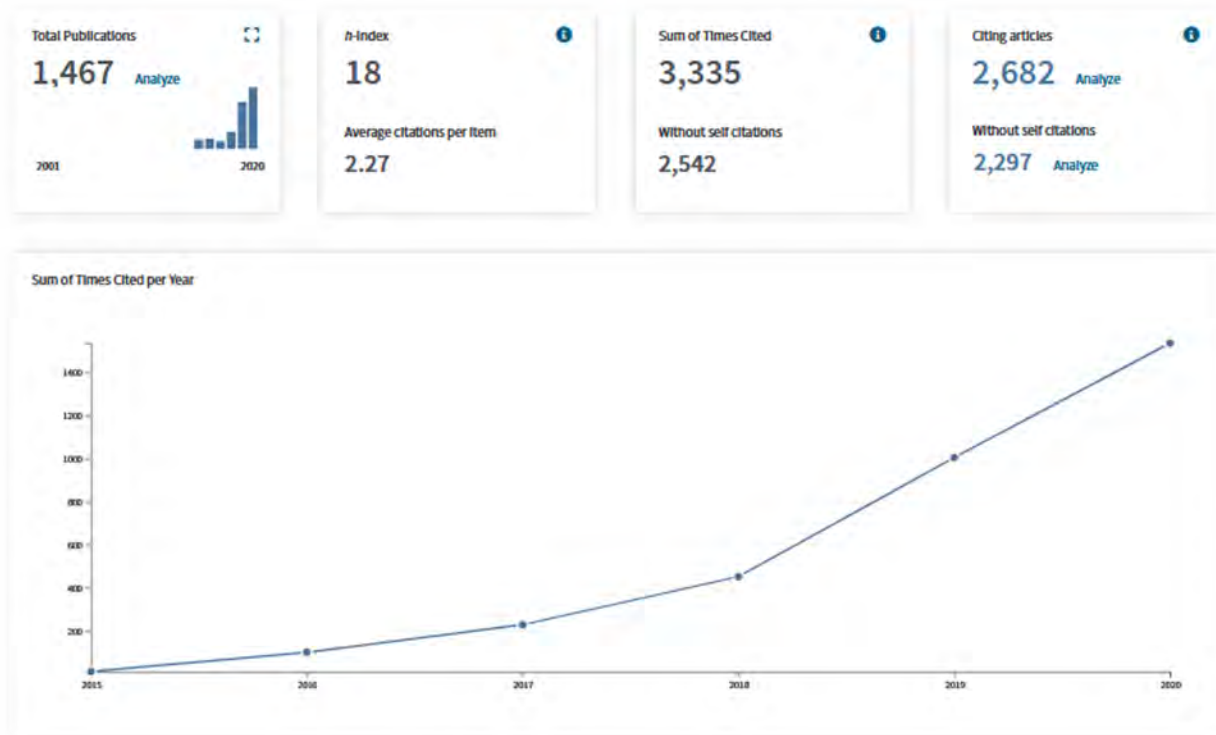
**Figure 4:** Journal analytics (**URL 5**, September 2020)
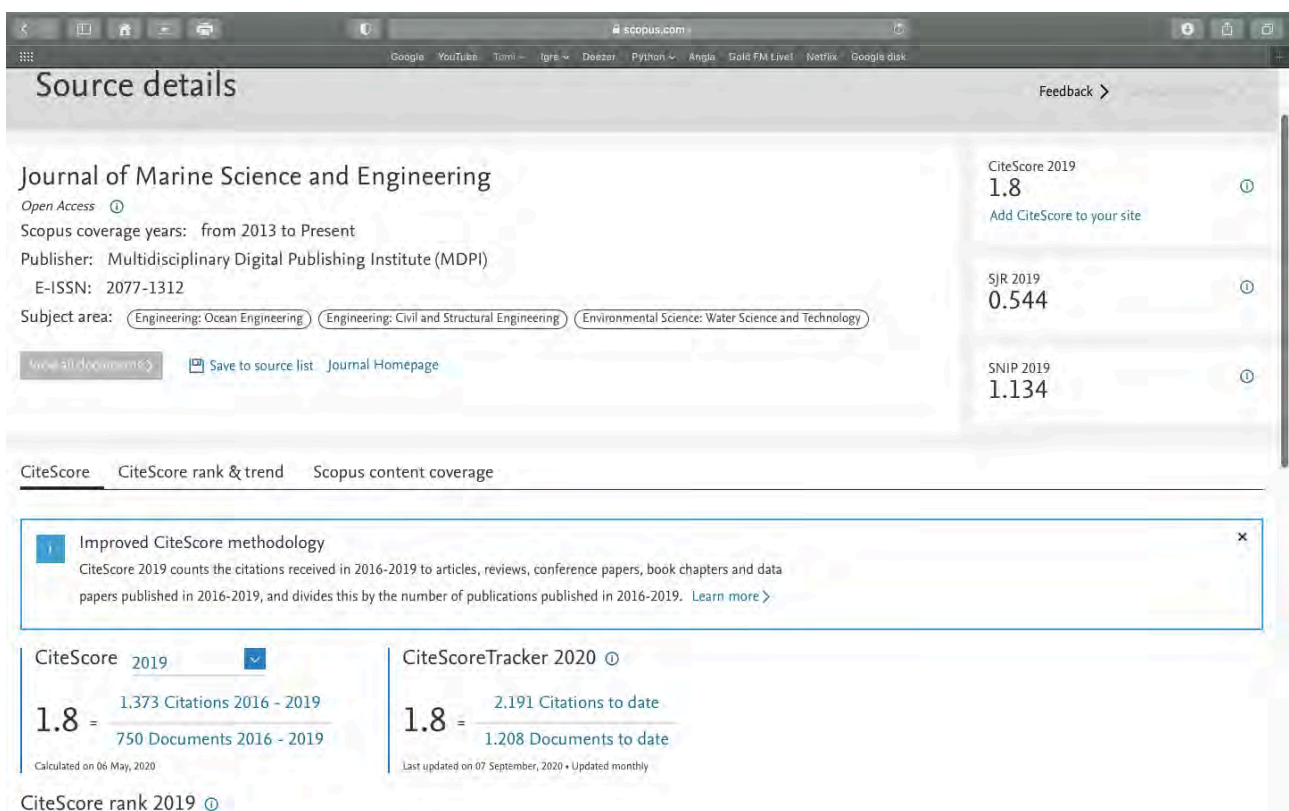


**Figure 5:** CiteScore values and trends (**URL 6**)
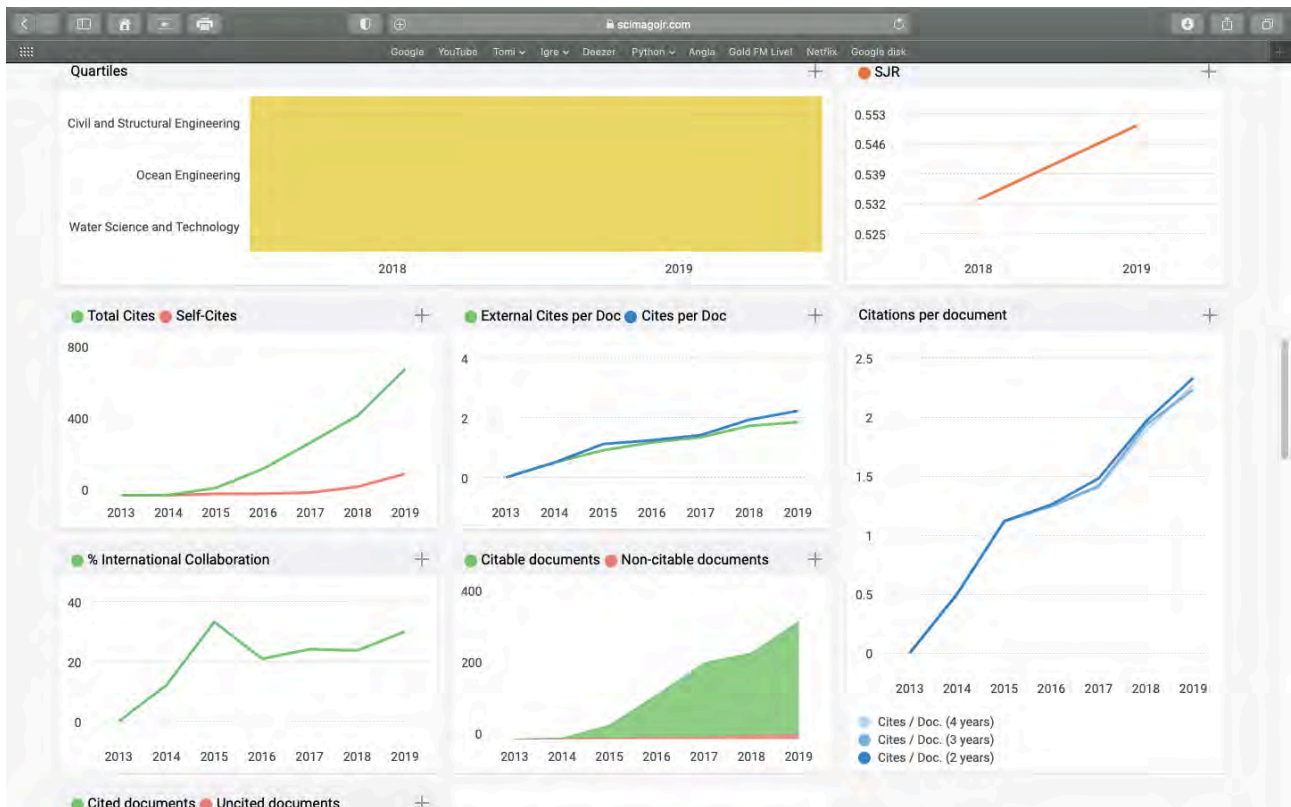
Sremac, J.; Clare, T.; Wilson, G.



**Figure 6:** SJR values and trends (**URL 7**)

Review process and firm and consequently rejection rate is high. In 2019 that value is 50 % (**Figure 7**).
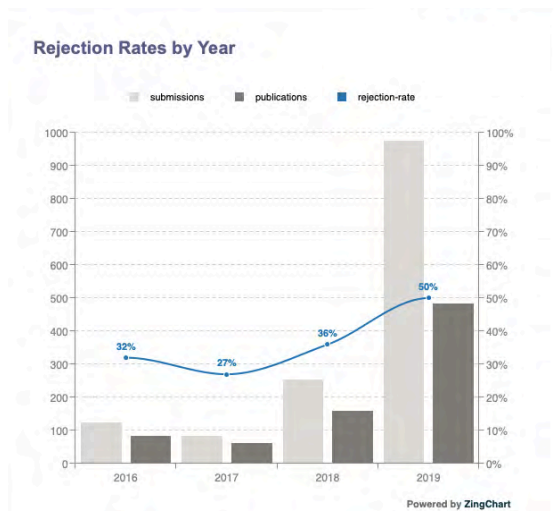


**Figure 7:** Rejection rate in the Journal of Marine Science and Engineering (**URL 5**, September 2020)

*2.2. Special Issue Paleoworld and Microbody Paleontological System Evolution*

This Special Issue belongs to the Section Geological Oceanography. It is dedicated to an interesting and highly specialized paleontological research field: microbody evolution. The proposed topic has been present in biological studies for less than seventy years, and more recently known from the palaeontological research. Such challenging research themes open new possibilities in paleontological studies and provide us with more colorful and realistic insights into the history of life (URL 8).

Sremac, J.; Clare, T.; Wilson, G.

The scope of this Special Issue is to encourage researchers to present their state-of-the-art microbody studies. Such efforts also help scientists to establish new contacts, collaborations, and networks and encourage young naturalists to explore new approaches to the study of fascinating Earth history.

Guest Editor of this issue is Prof. Dr. Jasenka Sremac, from the University of Zagreb. Submissions are welcome, by the 30 November 2020

## 3. Discussion and Conclusion

Scientific community today is highly sensible to the visibility of research results. Particularly in Natural and Technical Sciences, publishing dynamics, number of citations and Journal ranking can be of vital importance for scientists of all generations. JMSE is one of such journals, which can be a good choice in biology, chemistry and some branches of geology. Other journals from the same MDPI publisher have a very similar publishing policy, and deserve attention also from the Croatian geologists.

## 4. References

Internet sources:
URL 1: https://www.mdpi.com/journal/jmse
URL 2: https://www.mdpi.com/journal/jmse/history
URL 3: https://www.mdpi.com/journal/jmse/special_issues
URL 4: https://www.mdpi.com/journal/jmse/indexing
URL 5: https://www.mdpi.com/journal/jmse/stats
URL 6: https://www.scopus.com/sourceid/21100830140
URL 7: https://www.scimagojr.com/journalsearch.php?q=21100830140&tip=sid&clean=0
URL 8: https://www.mdpi.com/journal/jmse/special_issues/Jasenka_Paleoworld_Microbody_Paleontological_System_Evolution

**SAŽETAK (prošireni)**

**Scientometrijska analiza časopisa Journal of Marine Sciences and Engineering (JMSE) i njegovih posebnih izdanja – prigoda za objavljivanje kvalitetnih rezultata u časopisu visoke vidljivosti**

Časopis *Journal of Marine Science and Engineering* (ISSN 2077-1312), švicarskog izdavača MDPI, je međunarodni, časopis otvorenog pristupa, koji objavljuje radove iz znanosti o moru i inženjerstva. Od osnivanja, godine 2013., objavljeno je osam svezaka, s više od 1500 radova, koji redovito postižu visoku citiranost, koja prosječno iznosi 2,25 citata po radu. U prošloj, 2019. godini, impact factor časopisa bio je 2,033 te se ubraja u časopise druge kvartile (Q2). Među brojnim Posebnim izdanjima u tijeku je prikupljanje radova za naslov: *Paleoworld and Microbody Paleontological System Evolution*, čija je pridružena urednica prof.dr.sc. Jasenka Sremac. Ovaj i drugi specijalizirani časopisi izdavača MDPI svakako su jedan od dobrih izbora i za naše geologe, zbog kvalitetnih i brzih recenzija, visokog rangiranja i dinamike izlaženja.

**Ključne riječi**: časopis JMSE, MDPI, otvoreni pristup, recenzija, statistika

**Author's contribution**: **Jasenka Sremac** (1) (Dr, Full Professor, geology, palaeontology, palaeoenvironment) provided the conception and presentation of the results. **Tony Clare** (2) (Dr, Professor, marine chemical ecology) provided the general and historical data. **Gary Wilson** (3) (Dr, Professor, marine geology, palaeoclimatology, geophysics), took care of the data on the Section of Geological Oceanography.